

A gauge-invariant, symmetry-preserving truncation of JIMWLK

Mr Robert William MOERMAN

Supervisor: A/Prof. Heribert WEIGERT



Dissertation presented for the degree of
Master of Science in Theoretical Physics
in the

Department of Physics
Faculty of Science
University of Cape Town

January 2018

The copyright of this thesis vests in the author. No quotation from it or information derived from it is to be published without full acknowledgement of the source. The thesis is to be used for private study or non-commercial research purposes only.

Published by the University of Cape Town (UCT) in terms of the non-exclusive license granted to UCT by the author.

University of Cape Town

Abstract

Faculty of Science
Department of Physics

Master of Science in Theoretical Physics

A gauge-invariant, symmetry-preserving truncation of JIMWLK

by Mr Robert William MOERMAN

The colour glass condensate captures quantum chromodynamics in its application to high-energy collider experiments in the spirit of an effective field theory. In deeply inelastic lepton-hadron scattering experiments, as well as in hadron-hadron collisions, the internal degrees of freedom of in-state hadrons are dominated by a dense medium of gluonic matter called the colour glass condensate. Interactions with this medium by some (dilute) probe are most naturally described in terms of Wilson-lines and their correlators. The energy-dependence of these correlators is given by the JIMWLK (Jalilian-Marian+Iancu+McLerran+Weigert+Leonidov+Kovner) equation which, when applied to a correlator, generates an infinite tower of coupled Dyson-Schwinger-like equations referred to as a Balitsky Hierarchy.

In this thesis, I present a novel method for truncating, in a gauge-invariant and symmetry-preserving manner, the Balitsky hierarchy associated with matrices of Wilson-line correlators. This truncation is realized by parameterizing the energy-dependence of the symmetric and anti-symmetric parts of these matrices independently via energy-evolution operators which evolve initial conditions in a manner akin to the time-evolution of Hermitian operators in the Heisenberg picture of quantum mechanics. These energy-evolution operators are path-ordered exponentials whose exponents are expanded in terms of energy-dependent “colour structure functions”. I show how the properties of contributions to the expansion of these exponents (at each order in the expansion) are constrained by the group theory of $SU(N_c)$.

Declaration of Authorship

I know the meaning of plagiarism and declare that all of the work in the dissertation, save for that which is properly acknowledged, is my own.

Signed by candidate

Mr Robert William MOERMAN
Student Number: MRMROB003

2017-11-19

Date signed

Acknowledgements

Firstly, I wish to thank the two funding agencies that helped support me financially while I completed my MSc degree: the National Institute for Theoretical Physics (NITheP) for awarding me an MSc bursary and the Postgraduate Funding Office of the University of Cape Town (UCT) for awarding me the Myer Levinson Scholarship¹.

Thereafter, I would like to thank my supervisor, A/Prof. Heribert Weigert, for his expert guidance during the past two years, especially when I did not yet know what the big picture was and how the various puzzle pieces fitted together to construct it. I am thankful not only for the countless many conversations that he and I have had, but also for his engaging with me as a collaborator (as someone whom he solves problems with and not necessarily for). To him I owe my particular palate for mathematical physics as well as my current command of *Mathematica*. I wish to also thank him for reading and commenting on multiple drafts of my thesis which have helped immensely to improve its overall presentation. Finally, I would like to thank him for encouraging and sponsoring me to attend the [QCD Master Class 2017](#) in Saint-Jacut-de-la-Mer.

While attending the [QCD Master Class 2017](#), I had the opportunity to meet, among other world-renowned academics of the field, Dr Stefan Keppeler from the University of Tübingen. I wish to thank him for his excellent lectures on birdtracks. They helped me to better understand the subject and greatly influenced how I introduced the subject in this thesis. I am also thankful for his helping me one evening to solve a combinatorics problem; the result that we derived together is given in Sec. ?? of this thesis.

To my parents, Ewald and Marcia: thank you for your unwavering support; for listening to my lengthy layman explanations of what I do and for at least pretending to be interested (if not genuinely being interested); for telling me to take it easy at times and to push myself at other times; for loving me regardless and encouraging me to do what I love. Words cannot describe the debt I owe to my incredible parents. To *usisi wam*², Nicola: thank you for filling my life with laughs, panache and culture.

In addition, I would like to thank a number of postgraduate students of the UCT Physics Department for all the discussions and debates on matters of physics, mathematics, metaphysics, philosophy, faith and life. In no particular order, thank you Daniel Adamiak, Luke Lippstreu, Jonathan Rayner, William Grunow, Judy Alcock-Zelinger and Charlotte Hillebrand-Viljoen. I am also indebted to Charlotte Hillebrand-Viljoen for proof reading my introduction and conclusions, and for providing invaluable corrections to them.

¹The Myer Levinson Scholarship is “awarded every second year to a candidate who has obtained the BSc Hons. degree in the first class and who proposes to pursue further study” for a tenure of 2 years.

²which means *my sister* in Xhosa

To the people I live with in community: thank you for being quiet when I needed to sleep, for being my family away from home and for cooking supper for me. I am grateful also to Lauren Denny for encouraging me in the final stretch of writing up.

Lastly, but not least of all, I am eternally beholden to God who sustains me and enables me to marvel at and fathom the intricacies of His physical universe. In the words of Hebrews 11:3, “By faith we understand that the universe was created by the word of God, so that what is seen was not made out of things that are visible.”

Contents

Abstract	i
Declaration of Authorship	ii
Acknowledgements	iii
Contents	v
List of Figures	vii
1 Introduction	1
1.1 QCD at high energies and the CGC	1
1.2 How to read this thesis	4
2 Evidence of the CGC from DIS at small Bjorken x_{bj}	9
2.1 Structure Functions	13
2.2 The Bjorken limit: the parton model, PDFs and sum rules	14
2.3 The DGLAP equations	19
2.3.1 Motivation: collinear singularities	19
2.3.2 An outline of the systematic derivation of the DGLAP equations	23
2.4 The Regge-Gribov limit and the CGC formalism	31
3 Eikonalization at high energies	35
3.1 Perturbation theory in the presence of a large external field	35
3.1.1 Example: an interacting real-valued scalar field	35
3.1.1.1 The Dyson-Schwinger equations	37
3.1.1.2 A semi-classical truncation	39
3.2 Observables at small Bjorken x_{bj} , Wilson-lines and their correlators	43
4 Wilson-line correlators	49
4.1 Birdtracks, colour singlet states, and Wilson-line amplitude matrices	49
4.1.1 The Fierz Identity	55
4.1.2 Complex Conjugation	56
4.2 Colour structures	58
4.2.1 Pure adjoint colour singlet states and colour structures	59
4.2.2 The trace basis for colour structures	60
4.2.3 The Young basis for colour structures	62
4.2.4 Complex conjugating pure adjoint colour singlet states	69
4.3 Fierz bases for colour space	71

4.3.1	The Fierz property: simultaneous eigenstates of the Fierz projection operators	71
4.3.2	The Fierz-permutation basis	73
4.3.3	The Fierz-Young basis	75
4.3.4	The Fierz-Young basis and the swap operator	75
4.4	Embedding Wilson-line amplitude/correlator matrices	79
4.4.1	Fierz bases as embedding bases	79
4.4.2	Example: the $q^3\bar{q}^3$ amplitude matrix	81
5	The JIMWLK equation and the Balitsky hierarchy	85
5.1	A systematic derivation of the leading-log (LL) JIMWLK Hamiltonian	85
5.2	The JIMWLK equation and the Balitsky hierarchy	100
5.2.1	The JIMWLK evolution of the dipole operator and its associated Balitsky hierarchy	100
5.2.2	The JIMWLK equation for correlator matrices: coupling blocks in higher dimensional correlator matrices	103
6	The exponential parameterization	113
6.1	A systematic derivation of the exponential parameterization	113
6.2	Imprinting symmetries of Young colour structures onto Young colour structure functions	125
6.3	Properties of the exponentiating matrix	134
7	The 3-point truncation	139
7.1	JIMWLK evolution of the $q\bar{q}$ correlator: needing the 3-point truncation	139
7.2	The 3-point truncation of the full $q^2\bar{q}^2$ correlator matrix	142
7.3	Inconsistent JIMWLK evolution of the 3-point truncation: needing still higher order truncations	145
8	Conclusion	151
8.1	Thesis summary	151
8.2	Outlook	154
A	Standard pQFT results	159
A.1	Radiating a soft and co-linear, on-shell gluon from a hard quark	159
B	Propagators in the presence of a large background field	163
B.1	The Scalar Propagator	163
B.2	The Quark Propagator	166
B.3	The Gluon Propagator	168
C	The size of the Fierz-permutation basis	171
	Bibliography	173
	Turnitin Report	179

List of Figures

2.1	Amplitude for deeply inelastic electron-proton scattering. <i>Time runs from right to left.</i>	9
2.2	Cross-section for deeply inelastic electron-proton scattering. The dashed line through the middle of diagram denotes a Cutkosky cut. <i>Time runs from right to left.</i>	11
2.3	Hadronic tensor for deeply inelastic electron-proton scattering. The dashed line through the middle of diagram denotes a Cutkosky cut. <i>Time runs from right to left.</i>	12
2.4	Amplitude for $e^-q_f \rightarrow e^-X$ at tree-level, namely for $e^-q_f \rightarrow e^-q_f$. <i>Time runs from right to left.</i>	16
2.5	(Colour online) (Approximate) Bjorken scaling of the proton structure function $F_2(x_{\text{bj}}, Q^2) = \frac{Q^2}{8\pi x_{\text{bj}}} W_2(x_{\text{bj}}, Q^2)$ [1] measured in deeply inelastic electron-proton and positron-proton scattering (at the collider experiments H1 and ZEUS for $Q^2 \geq 2 \text{ GeV}^2$), and in the scattering of electrons (SLAC) and muons (BCDMS, E665, NMC) on a fixed target. The data are plotted as a function of Q^2 in bins of fixed x_{bj} where Q^2 and x_{bj} take on values in the kinematic domain of the HERA data. For ease of plotting, the vertical axis $F_2(x_{\text{bj}}, Q^2)$ is multiplied by $2^{i_{x_{\text{bj}}}}$ where $i_{x_{\text{bj}}}$ labels the number of the x_{bj} bin beginning at $i_{x_{\text{bj}}} = 1$ for $x_{\text{bj}} = 8.5 \times 10^{-1}$ and ending at $i_{x_{\text{bj}}} = 24$ for $x_{\text{bj}} = 5 \times 10^{-5}$. This plot is taken from [2].	18
2.6	The <i>handbag diagram</i> : the leading order contribution to the parton model prediction of the cross section for deeply inelastic electron-proton scattering coming from the partonic sub-process $e^-q_f \rightarrow e^-q_f$. The dashed line through the middle of diagram denotes a Cutkosky cut. <i>Time runs from right to left.</i>	20
2.7	(Colour online) One of several (naively) next-to-leading order contributions to parton model prediction of the cross-section for deeply inelastic electron-proton scattering coming from the partonic sub-process $e^-q_f \rightarrow e^-q_f g$. When the final state gluon is emitted collinearly to the initial state quark, the momentum of the intermediate (red-coloured) quark goes on-shell and the corresponding propagator produces a logarithm in Q^2 under the <i>Lorentz-invariant phase space</i> integral for the emitted final state gluon. The dashed line through the middle of diagram denotes a Cutkosky cut. <i>Time runs from right to left.</i>	20
2.8	(Colour online) The $q_f \rightarrow q_f g$ vertex in Fig. 2.7. The outgoing (red-coloured) quark line corresponds to the intermediate (red-coloured) quark line in Fig. 2.7. <i>Time runs from right to left.</i>	20

2.9	(Colour online) An example of a <i>ladder diagram</i> contribution to the parton model prediction of the cross section for DIS where multiple, <i>strongly-ordered</i> , colinear gluons are emitted into the final state. The red-coloured quark lines represent almost singular propagators which, under the product of <i>Lorentz-invariant phase space</i> integrals for each previously emitted final state gluon, generate logarithms in Q^2 . The dashed line through the middle of diagram denotes a Cutkosky cut. <i>Time runs from right to left.</i>	22
2.10	(Colour online) One of several (naively) next-to-leading order contributions to parton model prediction of the cross-section for deeply inelastic electron-proton scattering coming from the partonic sub-process $e^-g \rightarrow e^-gq_f\bar{q}_f$. When the final state anti-quark is emitted colinearly to the initial state gluon, the momentum of the intermediate (red-coloured) quark goes on-shell and the corresponding propagator produces a logarithm in Q^2 under the <i>Lorentz-invariant phase space</i> integral for the emitted final state anti-quark. The dashed line through the middle of diagram denotes a Cutkosky cut. <i>Time runs from right to left.</i>	23
2.11	Processes of the form $\gamma^*q_f \rightarrow X$ contributing to $\hat{W}_0(z, Q^2)$ at $\mathcal{O}(\alpha_s^0)$. <i>Time runs from right to left.</i>	24
2.12	Processes of the form $\gamma^*q_f \rightarrow X$ contributing to $\hat{W}_0(z, Q^2)$ at $\mathcal{O}(\alpha_s^1)$. <i>Time runs from right to left.</i>	26
2.13	Processes of the form $\gamma^*g \rightarrow X$ contributing to $\hat{W}_0(z, Q^2)$ at $\mathcal{O}(\alpha_s^1)$. <i>Time runs from right to left.</i>	29
2.14	(Colour online) PDFs from HERAPDF1.7 and HERAPDF1.5 at $Q^2 = 10^1\text{GeV}^2$ and $Q^2 = 10^4\text{GeV}^2$, respectively [3]. The gluon $x_{\text{bj}}g(x_{\text{bj}}, Q^2)$ and sea (or wee) quark $x_{\text{bj}}S(x_{\text{bj}}, Q^2)$ distribution functions have been reduced by a scale factor of 20. Both plots show enhanced gluon production at small Bjorken x_{bj} .	31
2.15	(Colour online) Kinematics for high-energy DIS. The world-lines of the electron (the projectile) and the proton (the target) lie almost along the light-cone directions and are separated by a large rapidity Y .	32
4.1	(Colour online) Explaining the notation of $[\mathfrak{M}_I^{(m)}]_{ii}$.	66
4.2	(Colour online) Explaining the notation of $\mathcal{C}^{(m;I;i;m_i)a_1\cdots a_m}$.	67
5.1	(Colour online) Fluctuations on top of the background field of the target which are subsumed into a redefinition of the target background field through Lorentz contraction as $Y = \ln(1/x_{\text{bj}})$ increases. The shaded regions denote perturbative corrections from fluctuations to the target average which are included via renormalization group flow.	86
6.1	The gauge-invariance property of a truncation.	116
8.1	A single gluon exchanged between an outgoing quark and anti-quark emanating from a common vertex. Time runs from right to left.	155
A.1	The factorized production (represented by the blob) of an outgoing hard quark with momentum p , spin s and colour i accompanied (right) and un-accompanied (left) by the emission of an on-shell gluon with momentum k , adjoint colour index a , and transverse polarization λ . Time runs from right to left.	159

To my incredible parents and sister.

Chapter 1

Introduction

1.1 QCD at high energies and the CGC

Protons and neutrons, the particles which form the nuclei of the atoms in your physical body, are examples of hadrons. In fact, it is claimed in [4] that 99% of all visible matter is composed of hadrons. Hadrons are bound configurations of quarks and/or anti-quarks. These bound states are held together by the strong nuclear force. The strong nuclear force/interaction is mediated by gluons and the mathematical description underpinning this interaction is a quantum field theory (QFT) called quantum chromodynamics (QCD). QCD is a sector of the standard model (SM) of particle physics and was first penned in 1973 [5]. It is a non-Abelian gauge theory with a local $SU(3)$ gauge symmetry. Quarks, anti-quarks and gluons, collectively called partons, all carry colour charge which means that they transform under non-trivial representations of $SU(3)$; quarks transform under the fundamental, anti-quarks under the anti-fundamental, and gluons under the adjoint representation. Although QCD has been known now for over 40 years, there is still much to be understood about the theory.

In particular, there is still much to learn about the high-energy asymptotic behaviour of QCD. Since the completion of the Tevatron in 1983, and with the subsequent construction of HERA, RHIC and LHC, and the proposed construction of EIC, understanding the high-energy asymptotic behaviour of QCD has become a hot topic of research. In these colliders all experiments involve at least one hadronic in-state (a QCD bound state) and are conducted at enormous centre-of-mass energies \sqrt{s} : the Tevatron conducted proton–anti-proton collisions at 1 TeV; at HERA, electrons/positrons and protons were collided at 318 GeV; collisions of gold nuclei are conducted at RHIC at 200 GeV/nucleon-pair; LHC collides lead ions at 2.76 TeV/nucleon-pair and protons with a centre-of-mass energy of 13 TeV.

Chief among the goals of high-energy QCD phenomenology is to calculate accurate predictions for observables associated with these high-energy collider experiments. These predictions are often calculated using perturbative QCD (pQCD). In pQCD, the observable of interest is expanded as a power series in the QCD coupling α_s . When this coupling is small, it is often sufficient to compute the contributions from only the first few terms in the expansion since (one anticipates that) higher-order terms are suppressed by powers of the small coupling. However, at energies as high as those quoted above, the emission of a single soft gluon leads to an enhancement of observables like the cross-section by a logarithm which increases with s ; this diverging contribution is called a single Sudakov logarithm (SSL) and it is discussed in Sec. A.1. For such a process, the smallness of α_s is compensated for by the largeness of $\ln(s)$ such that the combination $\alpha_s \ln(s) \sim \mathcal{O}(1)$. Consequently, the contribution to the cross-section from the emission of a single soft gluon cannot be neglected. But what about corrections due to multiple soft gluon emissions? The emission of multiple soft gluons again produces logarithmic enhancements which compensate the smallness of the coupling constant at each order in perturbation theory and, thus, one needs to sum over all these contributions.

One encounters a similar situation already in quantum electrodynamics (QED) — the sector of the SM governing the electromagnetic force — where large logarithms arise from the emission of multiple soft photons, the mediators of the electro-magnetic interaction. In this case, the large logarithms can be easily resummed (to all orders in perturbation theory) through Abelian exponentiation (see [6, 7] for reviews) which produces a damped exponential factor known as a Sudakov form factor. This damped exponential renders the observable of interest finite and restores the predictive power of the theory. For QCD, however, the situation is more complicated because gluons carry colour charge, which means that they can act as sources for further soft gluon emission. This provides an additional growth mechanism for observables, like the cross-section, that is not present in QED where photons cannot (directly) radiate additional soft photons. This growing cascade of multiple soft gluon emissions does not continue ad infinitum. Indeed it cannot since one of the consequences of unitarity in QCD, known as Froissart's theorem [8], is that the rate at which a cross-section may rise as a function of s is bounded asymptotically by $(\ln s)^2$. The physical mechanism responsible for ensuring that this unitarity bound is respected is the effect of recombination; after a sufficient number of soft gluon emissions into a given region of phase space, the gluons in that region begin to recombine. Eventually the rate of emission is balanced by the rate of recombination and a dynamic equilibrium is achieved. In this state of dynamic equilibrium, gluon numbers remain (approximately) fixed and this is known as gluon saturation. This phenomenon describes the dominant internal make-up of hadrons involved in the aforementioned high-energy collider experiments. In short, when hadrons are accelerated to ultra-relativistic speeds, they become densely populated by gluons.

In addition to becoming gluon saturated, these hadrons also experience severe relativistic effects. It is a simple back-of-the-envelope calculation in relativistic kinematics to show that given two colliding participants of equal mass¹, if in the center-of-mass frame they collide with energy \sqrt{s} , then in the rest frame of one of the participants the other has energy

$$E = \frac{s}{2mc^2} - mc^2. \quad (1.1)$$

Using Einstein's mass-energy equivalence formula

$$E = \gamma mc^2, \quad (1.2)$$

the boost factor γ is given in terms of s via

$$\gamma = \frac{s}{2(mc^2)^2} - 1 \xrightarrow{\sqrt{s} \gg mc^2} \frac{s}{2(mc^2)^2} \frac{\frac{mc^2}{\text{GeV}} \approx 1}{2} \frac{s}{\text{GeV}^2}, \quad (1.3)$$

where in the last equality we took the mass of a nucleon² to be approximately 1 GeV/ c^2 . Using the energies \sqrt{s} quoted for each of the colliders above, Eq. 1.3 implies that hadrons encounter boost factors of between $\sim 10^4$ and $\sim 10^8$. Consequently, in the rest-frame of one of the participants, the other participant appears hugely Lorentz contracted (in the direction of the collision axis) by $1/\gamma$ and its internal degrees of freedom are massively time dilated by γ .

These effects of Lorentz contraction and time dilation together with the phenomenon of gluon saturation lead to a description of in-state hadrons as pancake-thin sheets of a highly-dense, highly-correlated medium of gluons [9] referred to as the Colour Glass Condensate³ (CGC). “Colour” obviously refers to the fact that the medium is composed predominantly of gluons which, as discussed previously, are colour sources. Although these colour sources fluctuate stochastically due to emission and recombination effects, given the humongous boost factors involved, the dynamics of the colour field associated with the medium are essentially frozen in by time dilation on the natural time scales of the strong interaction. This property of a disordered system being solid-like on short timescales, but behaving as a liquid on long timescales is a property of silica, hence the moniker “glass”. Lastly, the word “Condensate” highlights the saturation of gluon numbers.

This discussion of CGC provides context for this thesis. The purpose of this thesis is to summarize some recent results that I have developed alone as well as together with my supervisor which extend the existing mathematical formalism used to describe interactions with the CGC. This determines the structure of the thesis as given in the following section.

¹Although this calculation excludes the electron/positron-proton collisions that were performed at HERA (since the colliding participants were not of equal masses), the sentiment expressed in the conclusion of this calculation is general and includes HERA collisions.

²The mass of a proton is ~ 0.938 GeV/ c^2 while the neutron weighs ~ 0.940 GeV/ c^2 .

³The term CGC was originally coined in [10].

1.2 How to read this thesis

In Chap. 2, I motivate the CGC in the context of deep inelastic scattering (DIS). In particular, I present the evidence for enhanced gluon production at small Bjorken x_{bj} obtained from HERA data for DIS. In order to explain the data I introduce a number of concepts. I begin by writing the cross-section for DIS (which to leading order in the electromagnetic coupling α_{em} is given by Fig. 2.2) in terms of a leptonic and a hadronic tensor following the treatments of [1, 11–13]. The leptonic tensor is easily and exactly calculated while the hadronic tensor given in Fig. 2.3 is non-perturbative and incalculable. However, the allowed form of the hadronic tensor is strictly constrained by symmetry considerations⁴ and this allows us to parameterize the hadronic tensor in terms of structure functions. The concept of structure functions plays an important role later in Chap. 6 where I present a parameterization for the JIMWLK evolution of Wilson-line correlators in the CGC in terms of “colour structure functions”. Another important idea which I purposefully highlight in this chapter is the idea that depending on how inclusive or exclusive the cross-section is, fewer or more structure functions in the hadronic tensor are probed: more or fewer degrees of freedom in the hadronic tensor are filtered out. I shall later comment on the extent to which this idea also applies to colour structure functions. I then present an alternative expression for the cross-section, as presented in [1, 6], in terms of parton distribution functions (PDFs) which is valid only in the Bjorken limit of QCD. This parton model description for the cross-section leads to two concrete predictions: the Callan-Gross relation and Bjorken scaling. Comparing to data, one sees that Bjorken scaling is only approximately true. Corrections to Bjorken scaling come from considering collinear emissions and these considerations inevitably lead to the DGLAP (Dokshitzer+Gribov+Lipatov+Altarelli+Parisi) equations. The DGLAP equations are the renormalization group (RG) equations for the PDFs and they serve as an instructive example of renormalization in the context of factorization. Using these two different expressions for the cross-section, one in terms of structure functions and one in terms of PDFs, I outline a derivation of the DGLAP equations which closely follows [1]. From the DGLAP equations, it is important to note that

- (i) PDFs mix under RG flow, and
- (ii) the splitting functions for a parton to a parton plus a gluon become singular at small Bjorken x_{bj} .

The first observation is emphasized because in Chap. 5 I show that Wilson-line correlators mix under JIMWLK evolution. The second observation suggests that gluon production is enhanced at small Bjorken x_{bj} . This is confirmed by fits of DGLAP evolution of PDFs to HERA data

⁴Our discussion is taken from [14]. We suspect that this is *not* the first reference to consider contributions to the Hadronic tensor beyond those that are probed by the total (inclusive) cross-section for DIS. However, this is the first such reference that we came across.

plotted in Fig. 2.14 and it is from these fits that one infers enhanced gluon production at small Bjorken x_{bj} .

In Chap. 3, I review perturbation theory in the presence of a large external field. As shall become evident later, this subject will become important when we want to do perturbation theory in the presence of the CGC. At the end of Chap. 2, I argue that in the regime of small Bjorken x_{bj} , known as the Regge-Gribov limit of QCD, it is natural to model the proton as a large background colour field b^μ with Dirac delta-function support in the direction of the collision axis (due to Lorentz contraction) and no “time” dependence (due to time dilation). By “large” I mean that $b^\mu \sim \mathcal{O}(\alpha_s^{-1})$. In the presence of such a large external field one needs to rewrite the perturbation theory for the gauge field A^μ which describes gluons in terms of fluctuations δA^μ on top of b^μ . In Sec. 3.1, I illustrate the consequences of performing perturbation theory about the vacuum in the presence of a large external field. Working explicitly in ϕ^4 -theory, I re-derive a diagrammatic version of the Dyson-Schwinger (DS) equations for the connected 1- and 2-point Green’s functions in the presence of a large external field J , inspired largely by [15–17]. These DS equations lead to an infinite tower of coupled integro-differential equations with characteristics similar to the Balitsky hierarchy to be encountered in Chap. 5. Like the Balitsky hierarchy, the DS equations need to be truncated in order to be solved. In the semi-classical limit — a truncation in which one ignores all loop diagrams and considers only tree-level diagrams — the tree-level connected Green’s functions can be solved iteratively. I show that the tree-level connected 1-point function, which I label $\varphi_c[J]$ (adopting the notation of [15]), is a non-perturbative object, but more importantly I show that in the iterative solution to the DS equation for the tree-level connected 2-point function (or propagator), each diagram contributes the same order in the coupling which means that all contributions must be resummed since each contribution is equally large. This resummation can be performed using the geometric series. The same resummed propagator can, however, be obtained directly from the Lagrangian density provided one re-expresses the scalar field ϕ as a fluctuation $\delta\varphi$ on top of $\varphi_c[J]$ and expand the Lagrangian density in $\delta\varphi$. This chapter is largely a compilation of (known) results which are seldom shown in standard QFT textbooks and which I learned from [17]. In the context of the CGC, since b^μ is large, the propagators for fermions and gluons needs to be re-derived to account of the presence of b^μ . They immediately encode all contributions from multiple interactions with the large external field — an insight gained from the toy ϕ^4 -theory example. These re-derived propagators are explicitly and exactly calculated following [18] in App. B and presented in Sec. 3.2. From them we see that the natural degrees of freedom for describing interactions with the CGC are Wilson-lines — path ordered colour rotations — which enter cross-sections like that of DIS through energy-dependent correlators. In fact, all cross-sections in the CGC context “factorize” into the convolution of some perturbatively calculable probability density and some linear combination of Wilson-line correlators. These Wilson-line correlators are the objects which capture interactions with the CGC and carry the energy-dependence of the cross-section.

In Chap. 4, I explain how to construct general Wilson-line amplitudes and correlators. I begin in Sec. 4.1 by introducing the birdtracks formalism, which is the group theory equivalent of Feynman diagrams for QFT. I introduce colour singlet states and use them to construct amplitudes and amplitude matrices. In Sec. 4.2.4, I prove an important and original lemma, Lemma 4.1, which I use throughout this thesis. In Sec. 4.3, I discuss a specific class of bases for colour singlet states called Fierz bases. In Sec. 4.3.1, I provide a canonical definition for any Fierz basis in terms of colour structures. This is an original definition which, to my knowledge, and the knowledge of my supervisor, has not appeared in the literature to date. Fierz bases are relevant for constructing amplitude/correlator matrices, specifically in the context of the CGC, because

- (i) they allow for lower dimensional amplitude/correlator matrices to be naturally embedded into high-dimensional ones which I demonstrate in Sec. 4.4, and
- (ii) this embedding is the natural language for writing down the JIMWLK evolution for correlator matrices which I show in Chap. 5.

I then observe, at least for the examples considered, that elements of a particular the Fierz basis possess the interesting property that they are either even or odd under the pair-wise interchange of quark and anti-quark labels. This is a new observation. This has a particular consequence for the behaviour of the real and imaginary parts of amplitude matrices constructed in the Fierz basis. I conclude the chapter by explicitly constructing the $q^3\bar{q}^3$ amplitude matrix in the Fierz Young basis which describes the colour transition probabilities between the different colour singlet channels for 3 quarks and 3 anti-quarks in the CGC formalism. This amplitude matrix contains lower dimensional amplitude matrices in particular coincidence limits and these amplitude matrices are used in Chap. 5 and Chap. 7.

In Chap. 5, I discuss the energy-dependence of correlators in the CGC formalism as determined by the JIMWLK functional RG equation. I re-derive the JIMWLK Hamiltonian at leading-logarithmic accuracy in Sec. 5.1. The derivation closely follows yet greatly expands on the one presented in [9]. In Sec. 5.2, I introduce the Balitsky hierarchy in the context of the $q\bar{q}$ correlator. The Balitsky hierarchy is the infinite tower of coupled integro-differential equations for a given correlator generated by the JIMWLK equation. The pattern of equations is similar to that of the DS equations encountered earlier. I derive the first two equations in the Balitsky hierarchy for the $q\bar{q}$ correlator. These two equations are in fact contained in the first equation in the Balitsky hierarchy for the $q^2\bar{q}^2$ correlator matrix. I show that the JIMWLK equation for any higher-dimensional correlator matrix captures multiple nested equations in the Balitsky hierarchy of lower-dimensional correlator matrices. To this end, I write down a novel expression for the JIMWLK equation for any correlator matrix constructed in a Fierz basis. This version of the equation is enormously useful as it highlights an important and overlooked property of the

equation: symmetric parts remain symmetric and anti-symmetric parts remain anti-symmetric under evolution. This (original) insight informs the truncation I present in Chap. 6. Solving the JIMWLK equation for a given correlator matrix is equivalent to simultaneously solving the associated Balitsky hierarchy which is only possible if one implements a truncation.

In Chap. 6, I motivate and present a gauge-invariant, symmetry-preserving truncation for any Balitsky hierarchy. The latter “symmetry-preserving” property is inspired by the discussion in the previous paragraph and is a novel contribution to an existing truncation that A/Prof. Heribert Weigert has been championing for some years now. This truncation extends the BK (Balitsky+Kovchegov) mean-field approximation and is necessary, specifically for situations where the latter truncation sets some correlators immediately to zero. Our truncation follows naturally from a particular parameterization for the energy-evolution of correlator matrices which shares a striking resemblance to the time-evolution of Hermitian operators in the Heisenberg picture of quantum mechanics. The form of the parameterization which I write down in this thesis generalizes the parameterizations given in [9,19,20] and reduces to the same thing for the examples considered in [9,20]. The energy-evolution is given by two path-ordered exponentials which are parameterized in terms of colour structures and colour structure functions. The colour structures can be chosen to have well-defined symmetry properties and I show how the symmetry properties of colour structures can be imprinted onto their associated colour structure functions. This result was obtained in collaboration with my supervisor and is written down for the first time here. I also present two original results, one of which determines whether a contribution to the truncation is symmetric or anti-symmetric. The proof for this result depends only on the symmetry properties of the colour structures and colour structure functions and not on any specific correlator matrix.

In Chap. 7, I specifically examine properties of the 3-point truncation. I express the $q^2\bar{q}^2$ correlator matrix in the 3-point truncation since it is the smallest correlator matrix which is able to access all available 3-point colour structure functions. I show that the 3-point truncation is not sufficient to consistently parameterize the evolution of $q^2\bar{q}^2$ correlator matrix by showing the JIMWLK equations for the $q\bar{q}$ correlator and the g^2 correlator expressed in the 3-point truncation are inconsistent. This is also an original result. The problem stems from the fact that there are too few degrees of freedom available; the correlators describe less inclusive observables and hence probe more colour structure functions. This inconsistency can be remedied by using a higher order truncation.

Finally, **in Chap. 8**, I summarize the aspects of the exponential parameterization which are not yet fully understood and the mathematical machinery which is being and still needs to be developed. I conclude with a brief outlook on possible links between the work presented in this thesis and recent work that has been done in the context of jet physics. Exploring the details of these links will be the topic of future research.

Chapter 2

Evidence of the CGC from DIS at small Bjorken x_{bj}

The simplest setting for extracting evidence of enhanced gluon production at small Bjorken x_{bj} (which is the theoretical point of departure for motivating the Colour Glass Condensate as a “dense medium of gluonic matter” [9]) is deep inelastic scattering (DIS). It is the “cleanest” means of experimentally accessing information about the multiplicity as well as the distribution of quarks and gluons, collectively called partons, inside hadrons (i.e. mesons, baryons, nuclei, etc.) [11]. In a deeply inelastic scattering experiment, a leptonic probe is impinged on a hadronic target. The incoming lepton ℓ scatters off one of the target nucleons N , producing an outgoing lepton ℓ' and any number of (hadronized) products labelled collectively by the symbol X . To lowest order in the electroweak interaction, but to all orders in the strong interaction, this interaction, denoted $\ell N \rightarrow \ell' X$, is mediated via the exchange of a single, (deeply) virtual gauge boson [21].

For the aforementioned purpose, it is sufficient to consider only the neutral current case where $\ell = \ell'$. To ground the subsequent discussion, suppose that the leptonic probe is an electron ($\ell = e^-$) with incoming momentum k , outgoing momentum k' , and spin vector r ; the target

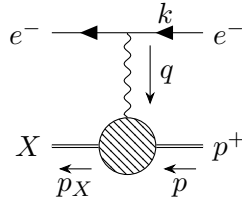


FIGURE 2.1: Amplitude for deeply inelastic electron-proton scattering. *Time runs from right to left.*

nucleon is a proton ($N = p^+$) with momentum p and spin vector s ; and the mediator is an off-mass-shell photon γ^* with momentum $q := k - k'$. The amplitude for this process is depicted in Fig. 2.1. For pedagogical reasons (to be justified later), the spin vectors associated with in-state participants are initially not averaged over; this is known as polarized DIS since the incoming electron and proton are polarized [13].

The reaction $e^- p^+ \rightarrow e^- X$ can be described in terms of the following Lorentz invariants¹:

$$s := (p + k)^2, \quad t := q^2 =: -Q^2, \quad x_{\text{bj}} := \frac{Q^2}{2p \cdot q}, \quad y := \frac{p \cdot q}{p \cdot k}. \quad (2.1)$$

where s is the centre-of-mass energy, Q^2 is the virtuality of the exchanged gauge boson, x_{bj} is the Bjorken scaling variable (whose interpretation shall be given soon) and y is the inelasticity variable which measures the fraction of the incoming electron's energy carried away by the exchanged virtual photon. Another useful Lorentz invariant is the invariant mass of the hadronic final state X , defined through

$$m_X^2 := (p + q)^2. \quad (2.2)$$

Since m_X has the interpretation of the centre-of-mass energy of the $\gamma^* p^+$ system, $m_X^2 \geq m_p^2$ [13] which implies that

$$x_{\text{bj}} = \frac{Q^2}{Q^2 + m_X^2 - m_p^2} \in [0, 1). \quad (2.3)$$

The phrase “deeply virtual” reflects the fact that the momentum of the exchanged gauge boson is large and space-like with $Q^2 \gg m_p^2$. Consequently, Q^2 sets the resolution or “hard” scale for the scattering experiment [9, 12]. In addition, we restrict our attention to the high-energy limit where the centre-of-mass energy $s \gg m_p^2$ and one may ignore the electron and proton masses as being effectively zero. A corollary of this zero mass limit is that the momenta of the in-state participants is approximately light-like [6]. In the high-energy limit, the Lorentz invariants of Eq. 2.1 satisfy [4]

$$x_{\text{bj}} y s = Q^2. \quad (2.4)$$

The invariant matrix element for DIS [1]

$$i\mathcal{M}(e^- p^+ \rightarrow e^- X) = \bar{u}^{r'}(k')(-ie\gamma^\mu)u^r(k)\frac{-ig_{\mu\nu}}{q^2 + i\varepsilon}i\mathcal{M}^\nu(\gamma^* p^+ \rightarrow X), \quad (2.5)$$

¹Note that these Lorentz invariants are not independent.

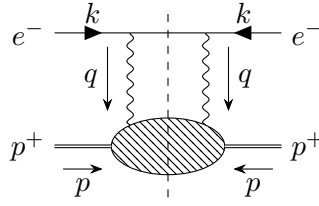


FIGURE 2.2: Cross-section for deeply inelastic electron-proton scattering. The dashed line through the middle of diagram denotes a Cutkosky cut. Time runs from right to left.

is written in terms of the invariant matrix element for the process $\gamma^* p^+ \rightarrow X$ which can be expressed formally in terms of hadronic in- and out-states as

$$i\mathcal{M}(\gamma^* p^+ \rightarrow X) = i\varepsilon_{\nu;\lambda}(q)\mathcal{M}^\nu(\gamma^* p^+ \rightarrow X) = \varepsilon_{\nu;\lambda}(q)\langle X | -ieJ^\nu(0) | p; s \rangle. \quad (2.6)$$

Here $J^\nu(0)$ is the *flavour neutral electro-magnetic current* to which the virtual photon couples [1]. Since the virtual photon carries no hadronic quantum numbers, X may be regarded as a virtual state of the proton realized by the absorption of a virtual photon [21].

The corresponding inclusive cross-section for polarized DIS, drawn in Fig. 2.2, is given in terms of Eq. 2.5 by [13]

$$\begin{aligned} d^3\sigma_{\text{pol}}(e^- p^+ \rightarrow e^- X) \\ = \frac{1}{4k \cdot p} \frac{d^3k'}{(2\pi)^3 2k'^0} \sum_{r'} \sum_X \int d\Pi_X (2\pi)^4 \delta^{(4)}(q + p - P_X) |\mathcal{M}(e^- p^+ \rightarrow e^- X)|^2, \end{aligned} \quad (2.7)$$

where $d\Pi_X = \frac{d^3P_X}{(2\pi)^3 2P_X^0}$ is the Lorentz invariant phase space measure. Note the explicit sum over the outgoing electron's spin in Eq. 2.7, but there is no average over the initial electron's spin nor the spin of the proton.

Eq. 2.7 naturally separates into contributions from the leptonic vertex $e^- \rightarrow e^- \gamma^*$ and the hadronic vertex $\gamma^* p^+ \rightarrow X$. It is instructive to distinguish these contributions by introducing two tensors: a leptonic tensor

$$L_{\mu\nu} := \sum_{r'} (\bar{u}^{r'}(k') \gamma^\mu u^r(k)) (\bar{u}^{r'}(k') \gamma^\nu u^r(k))^* = \text{Tr} \left((\not{k} + m_e) \frac{1}{2} (1 + \gamma_5 \not{r}) \gamma_\mu (\not{k}' + m_e) \gamma_\nu \right), \quad (2.8)$$

where the electron mass has been kept explicit for the time being and $\Sigma(r) := \frac{1}{2}(1 + \gamma_5 \not{r})$ is the spin projection operator associated with the spin vector r of the incoming electron [22]; and a

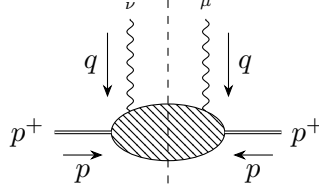


FIGURE 2.3: Hadronic tensor for deeply inelastic electron-proton scattering. The dashed line through the middle of diagram denotes a Cutkosky cut. Time runs from right to left.

hadronic tensor [1]

$$\begin{aligned}
e^2 \varepsilon_{\mu;\lambda}(q) \varepsilon_{\nu;\lambda}^*(q) W^{\mu\nu} &:= \sum_X \int d\Pi_X (2\pi)^4 \delta^{(4)}(q + p - P_X) |\mathcal{M}(\gamma^* p^+ \rightarrow X)|^2 \\
&= e^2 \varepsilon_{\mu;\lambda}(q) \varepsilon_{\nu;\lambda}^*(q) \sum_X \int d\Pi_X \int d^4\xi e^{i\xi \cdot (q+p-P_X)} \langle p, s | J^\mu(0) | X \rangle \langle X | J^\nu(0) | p, s \rangle \\
&= e^2 \varepsilon_{\mu;\lambda}(q) \varepsilon_{\nu;\lambda}^*(q) \sum_X \int d\Pi_X \int d^4\xi e^{i\xi \cdot (q+p-P_X)} \langle p, s | e^{-i\hat{P} \cdot \xi} J^\mu(\xi) e^{i\hat{P} \cdot \xi} | X \rangle \langle X | J^\nu(0) | p, s \rangle \\
&= e^2 \varepsilon_{\mu;\lambda}(q) \varepsilon_{\nu;\lambda}^*(q) \int d^4\xi e^{i\xi \cdot q} \langle p, s | J^\mu(\xi) J^\nu(0) | p, s \rangle,
\end{aligned} \tag{2.9}$$

where, in going to the second line the integral representation of the Dirac delta function and Eq. 2.6 were used, in the third line the translation operator $J^\mu(0) = e^{-i\hat{P} \cdot \xi} J^\mu(\xi) e^{i\hat{P} \cdot \xi}$ was used, and the last line follows from the completeness relation $\sum_X \int d\Pi_X |X\rangle \langle X| = \mathbb{1}$. The hadronic tensor is depicted visually in Fig. 2.3.

In terms of these two tensors, Eq. 2.7 can be written as

$$d^3\sigma_{\text{pol}}(e^- p^+ \rightarrow e^- X) = \frac{1}{2s} \frac{d^3k'}{(2\pi)^3 2k'^0} \frac{e^4}{Q^4} L_{\mu\nu} W^{\mu\nu}. \tag{2.10}$$

The leptonic tensor can be decomposed into its symmetric and anti-symmetric components [13] (demarcated by the round and square braces around the Lorentz indices, respectively)

$$L_{\mu\nu} = L_{(\mu\nu)} + L_{[\mu\nu]}, \tag{2.11}$$

where, evaluating the trace in Eq. 2.8, these components are given by

$$L_{(\mu\nu)} := 2[k_\mu k'_\nu + k_\nu k'_\mu - g_{\mu\nu}(k \cdot k' - m_e^2)], \tag{2.12a}$$

$$L_{[\mu\nu]} := 2i m_e \varepsilon_{\mu\nu\rho\sigma} r^\rho (k - k')^\sigma. \tag{2.12b}$$

If the incoming electron is longitudinally polarized with

$$r^\mu = \lambda_e \frac{k^\mu}{m_e}, \quad \lambda_e = \pm 1, \quad r^2 = 1 \tag{2.13}$$

then Eq. 2.12b becomes²

$$L_{[\mu\nu]} = -2i \varepsilon_{\mu\nu\rho\sigma} k^\rho k'^\sigma. \quad (2.14)$$

2.1 Structure Functions

Unlike the leptonic tensor, the hadronic tensor in Eq. 2.9 cannot be evaluated directly in perturbation theory because it is defined in terms of the proton wave-function which necessarily contains information about the non-perturbative physics responsible for the structure of the proton as a QCD bound state [6]. Its tensorial structure can, however, be completely constrained up to a finite set of coefficients called structure functions; these structure functions are parametrically independent degrees of freedom which track the hadronic tensor's dependence on the Lorentz invariants of Eq. 2.1. The tensorial structure can only come from the Lorentz structures available in the $\gamma^* p^+ \rightarrow X$ process (excluding those associated directly with the hadronic final state X which is inclusively summed over in Eq. 2.1): namely p^μ , s^μ , q^μ , the metric $g^{\mu\nu}$, and the Levi-Civita symbol $\varepsilon^{\mu\nu\rho\sigma}$ with two of its indices contracted. In addition, only particular combinations of these Lorentz structures may enter the parameterization of the hadronic tensor as determined by [14]

$$\text{Ward-Takahashi identity: } q_\mu W^{\mu\nu}(p, s, q) = 0 = W^{\mu\nu}(p, s, q) q_\nu, \quad (2.15a)$$

$$\text{Hermiticity: } W_{\mu\nu}^*(p, s, q) = W_{\nu\mu}(p, s, q), \quad (2.15b)$$

$$\text{Parity-reversal invariance: } \Lambda_\mu^\rho \Lambda_\nu^\sigma W_{\rho\sigma}(p, s, q) = W_{\mu\nu}(\tilde{p}, -\tilde{s}, \tilde{q}), \quad (2.15c)$$

$$\text{Time-reversal invariance: } \Lambda_\mu^\rho \Lambda_\nu^\sigma W_{\rho\sigma}^*(p, s, q) = W_{\mu\nu}(\tilde{p}, \tilde{s}, \tilde{q}), \quad (2.15d)$$

where $\Lambda^\mu{}_\nu = \text{diag}(1, -1, -1, -1)^\mu{}_\nu$ and $\tilde{V}^\mu = \Lambda^\mu{}_\nu V^\nu = \delta^{\mu 0} V^0 - \delta^{\mu i} V^i$ for any four vector V^μ . From these considerations, one concludes the following general parameterization of the polarized hadronic tensor

$$W^{\mu\nu} = W^{(\mu\nu)} + W^{[\mu\nu]}, \quad (2.16)$$

where³

$$W^{(\mu\nu)} = W_1(x_{\text{bj}}, Q^2) \left[-g^{\mu\nu} + \frac{q^\mu q^\nu}{q^2} \right] + W_2(x_{\text{bj}}, Q^2) \left[p^\mu - \frac{p \cdot q}{q^2} q^\mu \right] \left[p^\nu - \frac{p \cdot q}{q^2} q^\nu \right], \quad (2.17a)$$

$$W^{[\mu\nu]} = i 2m_p \varepsilon^{\mu\nu\rho\sigma} q^\rho \left[m_p s^\sigma G_1(x_{\text{bj}}, Q^2) + \frac{1}{m_p} (p \cdot q s^\sigma - s \cdot q p^\sigma) G_2(x_{\text{bj}}, Q^2) \right], \quad (2.17b)$$

and $W_{1,2}$ and $G_{1,2}$ are called structure functions.

² The electron mass drops automatically.

³ There exist many different conventions for the normalization of the structure functions $W_{1,2}$ and $G_{1,2}$ in the literature. Our convention for $W_{1,2}$ is taken from [1] while our convention for $G_{1,2}$ is taken from [13].

In terms of Eq. 2.11 and Eq. 2.16, Eq. 2.10 becomes

$$d^3\sigma_{\text{pol}}(e^-p^+ \rightarrow e^-X) = \frac{1}{2s} \frac{d^3k'}{(2\pi)^3 2k'^0} \frac{e^4}{Q^4} \left[L_{(\mu\nu)} W^{(\mu\nu)} + L_{[\mu\nu]} W^{[\mu\nu]} \right], \quad (2.18)$$

where separately the symmetric and anti-symmetric parts of the leptonic and hadronic tensors couple and, consequently, Eq. 2.18 is real. The cross-section for unpolarized DIS can be obtained from the polarized one by averaging Eq. 2.18 over the spin vectors of the incoming electron and proton:

$$\begin{aligned} d^3\sigma(e^-p^+ \rightarrow e^-X) &= \frac{1}{4} \sum_r \sum_s d^3\sigma_{\text{pol}}(e^-N \rightarrow e^-X) \\ &= \frac{1}{2s} \frac{d^3k'}{(2\pi)^3 2k'^0} \frac{e^4}{Q^4} L_{(\mu\nu)} W^{(\mu\nu)} \\ &= \frac{1}{2s} \frac{d^3k'}{(2\pi)^3 2k'^0} \frac{e^4}{Q^4} \left[2x_{\text{bj}}ys W_1(x, Q^2) + s^2(1-y) W_2(x_{\text{bj}}, Q^2) \right]. \end{aligned} \quad (2.19)$$

Eq. 2.19 is regarded as more inclusive than Eq. 2.18, because the initial-spin average includes more events. The net effect of the initial-spin average in Eq. 2.19 is the dropping of contributions from the anti-symmetric parts of the leptonic and hadronic tensors. As a consequence of this, Eq. 2.19 no longer depends on the structure functions $G_{1,2}$, only $W_{1,2}$. In general, for an observable describing a process with at least one hadronic vertex, the less inclusive the observable is, the greater the number of structure functions required to parameterize contributions from each hadronic vertex, and vice versa.

After an appropriate change of variables [6], Eq. 2.19 can be written solely in terms of the Lorentz invariants in Eq. 2.1

$$\frac{d^2\sigma}{dx_{\text{bj}}dy}(e^-p^+ \rightarrow e^-X) = \frac{1}{2} \frac{\alpha_{\text{em}}^2 y}{Q^4} \left[2x_{\text{bj}}ys W_1(x, Q^2) + s^2(1-y) W_2(x_{\text{bj}}, Q^2) \right], \quad (2.20)$$

where $\alpha_{\text{em}} = \frac{e^2}{4\pi}$ is the fine-structure constant. In the remainder of this section we shall restrict our discussion to unpolarized DIS.

2.2 The Bjorken limit: the parton model, PDFs and sum rules

In order to further probe the QCD content of the proton wave function (in the high-energy limit) or, equivalently, to say something more about the structure functions $W_{1,2}$ in Eq. 2.20, it is instructive, for fixed y , to consider two asymptotic limits of Eq. 2.4: the Bjorken limit, where x_{bj} is fixed while $Q^2, s \rightarrow \infty$, and the Regge-Gribov limit, where Q^2 is fixed while $x_{\text{bj}} \rightarrow 0$ and $s \rightarrow \infty$ [4]. Although the Colour Glass Condensate exists as a state of QCD matter in the latter limit, first evidence for its existence came from results of the former limit at small Bjorken x_{bj} .

In the Bjorken limit, the proton can be viewed in the infinite momentum frame as a dilute system of valence quarks and “wee” (to borrow terminology from Feynman) partons [4]. In addition, the strong coupling $\alpha_s(Q^2)$ at large Q^2 is small [6]. Consequently, to leading order (LO) in $\alpha_s(Q^2)$, the reaction $e^- p^+ \rightarrow e^- X$ can be expressed as the scattering of the incoming electron with an individual quark (valence or wee) inside the proton known as the impulse approximation [4]. The possibility of scattering with a wee gluon is excluded at LO in $\alpha_s(Q^2)$, because the exchanged virtual photon can only couple to a gluon via a quark propagator. This picture of the proton wave-function was originally postulated by Feynman [23, 24] and is called the parton model.

Consider a quark of flavour f , labelled q_f , inside the proton with some momentum p_f . As mentioned previously, in the high-energy limit where masses can be ignored, the proton’s momentum is approximately light-like and so are the momenta of its constituents (since their masses are smaller than the mass of the proton). *In addition to being light-like, p_f is approximately colinear with the proton’s momentum because the only mechanism available for acquiring a significant transverse momentum is through the emission or absorption of a hard gluon which is (naively) suppressed by the smallness of the QCD coupling $\alpha_s(Q^2)$.* Therefore, to lowest order in pQCD, one may write

$$p_f^\mu = \xi p^\mu, \quad (2.21)$$

where $\xi \in [0, 1]$ is the (longitudinal) momentum fraction of the struck quark.

In the parton model, the cross-section for deep inelastic electron-proton scattering, is given as the cross-section for electron-quark scattering at a specific momentum fraction ξ , denoted $\hat{\sigma}(e^- q_f \rightarrow e^- X)$, convolved with the classical probability $f_f(\xi) d\xi$ of finding a quark with such a momentum fraction inside the proton:

$$\sigma(e^- p^+ \rightarrow e^- X) = \sum_f \int_0^1 d\xi f_f(\xi) \hat{\sigma}(e^- q_f \rightarrow e^- X), \quad (2.22)$$

where the sum over f incorporates both quark and anti-quark flavours⁴, but not gluon contributions as explained earlier. The function $f_f(\xi)$ is called a parton distribution function (PDF) for quarks of flavour f . These parton distribution functions cannot be computed using pQCD since they are non-perturbative objects [6]. Their physical justification is that the characteristic timescales over which the proton is probed $\sim Q^{-1}$ is much slower than the characteristic timescales over which momentum sloshes amongst the partons $\sim m_p^{-1} \gg Q^{-1}$ [1]. It is conventional to denote partonic quantities by a circumflex (hat). The leading order contribution to the partonic process $e^- q_f \rightarrow e^- X$ is the tree-level scattering process $e^- q_f \rightarrow e^- q_f$ whose

⁴Anti-quark flavours are typically denoted by a bar: e.g. \bar{u} , \bar{d} and \bar{s} for anti-up, anti-down and anti-strange, respectively.

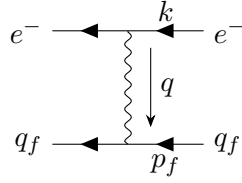


FIGURE 2.4: Amplitude for $e^-q_f \rightarrow e^-X$ at tree-level, namely for $e^-q_f \rightarrow e^-q_f$. Time runs from right to left.

amplitude is drawn in Fig. 2.4 and whose differential cross-section is computed as [6]

$$\frac{d\hat{\sigma}}{d\hat{t}}(e^-q_f \rightarrow e^-q_f) = \frac{2\pi\alpha_{\text{em}}^2}{\hat{t}^2} Q_f^2 \left[1 + \frac{\hat{u}^2}{\hat{s}^2} \right], \quad (2.23)$$

where Q_f (not to be confused with $Q^2 = -q^2$, the virtuality of the photon) is the elementary charge fraction of the struck quark. The hatted Mandelstam variables $\hat{t}, \hat{s}, \hat{u}$ of the partonic process need to be written in terms of the Lorentz invariants of Eq. 2.1 which are experimentally accessible. In the massless limit,

$$\hat{t} := t, \quad \hat{s} = (p_f + k)^2 = 2p_f \cdot k = \xi 2p \cdot k = \xi s, \quad \hat{u} = -\hat{t} - \hat{s}. \quad (2.24)$$

Since the out-going quark mass is approximately zero, one has that

$$0 = (p_f + q)^2 = 2p_f \cdot q + q^2 = \xi 2p \cdot q - Q^2 \implies \xi = \frac{Q^2}{2p \cdot q} = x, \quad (2.25)$$

which implies that x_{bj} may be interpreted, to leading order in $\alpha_s(Q^2)$, as the (longitudinal) momentum fraction of the struck constituent.

It follows that the cross-section for deep inelastic electron-proton scattering at fixed Q^2 is given by [6]

$$\frac{d\sigma}{dQ^2}(e^-p^+ \rightarrow e^-X) = \int_0^1 d\xi \sum_f f_f(\xi) Q_f^2 \frac{2\pi\alpha_{\text{em}}^2}{Q^2} \left[1 + (1-y)^2 \right] \theta(\xi s - Q^2) \quad (2.26)$$

up to order $\alpha_s(Q^2)$ corrections. The Heaviside function in Eq. 2.26 enforces the kinematic constraint $\hat{s} \geq |\hat{t}|$. Since $0 \leq k'^0 \leq k^0$ (the probe electron cannot gain energy through scattering), in the proton's rest frame

$$y = \frac{2p \cdot q}{2p \cdot k} = \frac{q^0}{k^0} = 1 - \frac{k'^0}{k^0} \in [0, 1], \quad (2.27)$$

which means that the Heaviside function in Eq. 2.26 is trivially satisfied and can be omitted. Using the change of variables [6]

$$d\xi dQ^2 = dx_{bj} dQ^2 = dx_{bj} \frac{dQ^2}{dy} dy = x_{bj} s dx_{bj} dy, \quad (2.28)$$

Eq. 2.26 becomes

$$\frac{d\sigma}{dx_{bj} dy}(e^- p^+ \rightarrow e^- X) = \left(\sum_f x_{bj} f_f(x_{bj}) Q_f^2 \right) \frac{2\pi\alpha_{em}^2 s}{Q^2} [1 + (1-y)^2]. \quad (2.29)$$

Comparing Eq. 2.29 with Eq. 2.20, one may read off

$$W_1(x_{bj}, Q^2) = 2\pi \sum_f Q_f^2 f_f(x_{bj}), \quad W_2(x_{bj}, Q^2) = 8\pi \frac{x_{bj}^2}{Q^2} \sum_f Q_f^2 f_f(x_{bj}). \quad (2.30)$$

Eq. 2.30 provides two concrete predictions. Firstly,

$$W_1(x_{bj}, Q^2) = \frac{Q^2}{4x_{bj}^2} W_2(x_{bj}, Q^2), \quad (2.31)$$

known as the Callan-Gross relation. Secondly, at fixed x_{bj} , $W_1(x_{bj}, Q^2)$ is a constant function in Q^2 : this is known as Bjorken scaling. In Fig. 2.5 one observes approximate Bjorken scaling; there exists a weak (and we shall show) logarithmic dependence of the structure functions and, consequently, the PDFs on Q^2 . To account for this violation of the Bjorken scaling prediction, one needs to consider processes that are (naively) next-to-leading order (NLO) in $\alpha_s(Q^2)$. Doing so inevitably leads to the DGLAP equations: a set of coupled renormalization group (RG) equations which govern the Q^2 dependence of PDFs. The derivation of the DGLAP equations is briefly discussed in the next section.

In order for the PDFs to have an interpretation as classical probabilities, they need to satisfy a set of constraints called sum rules. For example, a proton is composed of two valence up quarks and one valence down quark. In addition to these valence quarks, there are also virtual quark-anti-quark pairs which fluctuate into and out of existence within the proton. However, in QED and QCD there is a number conservation law for each quark flavour which means that

$$\int_0^1 d\xi [f_u(\xi) - f_{\bar{u}}(\xi)] = 2, \quad \int_0^1 d\xi [f_d(\xi) - f_{\bar{d}}(\xi)] = 1, \quad (2.32)$$

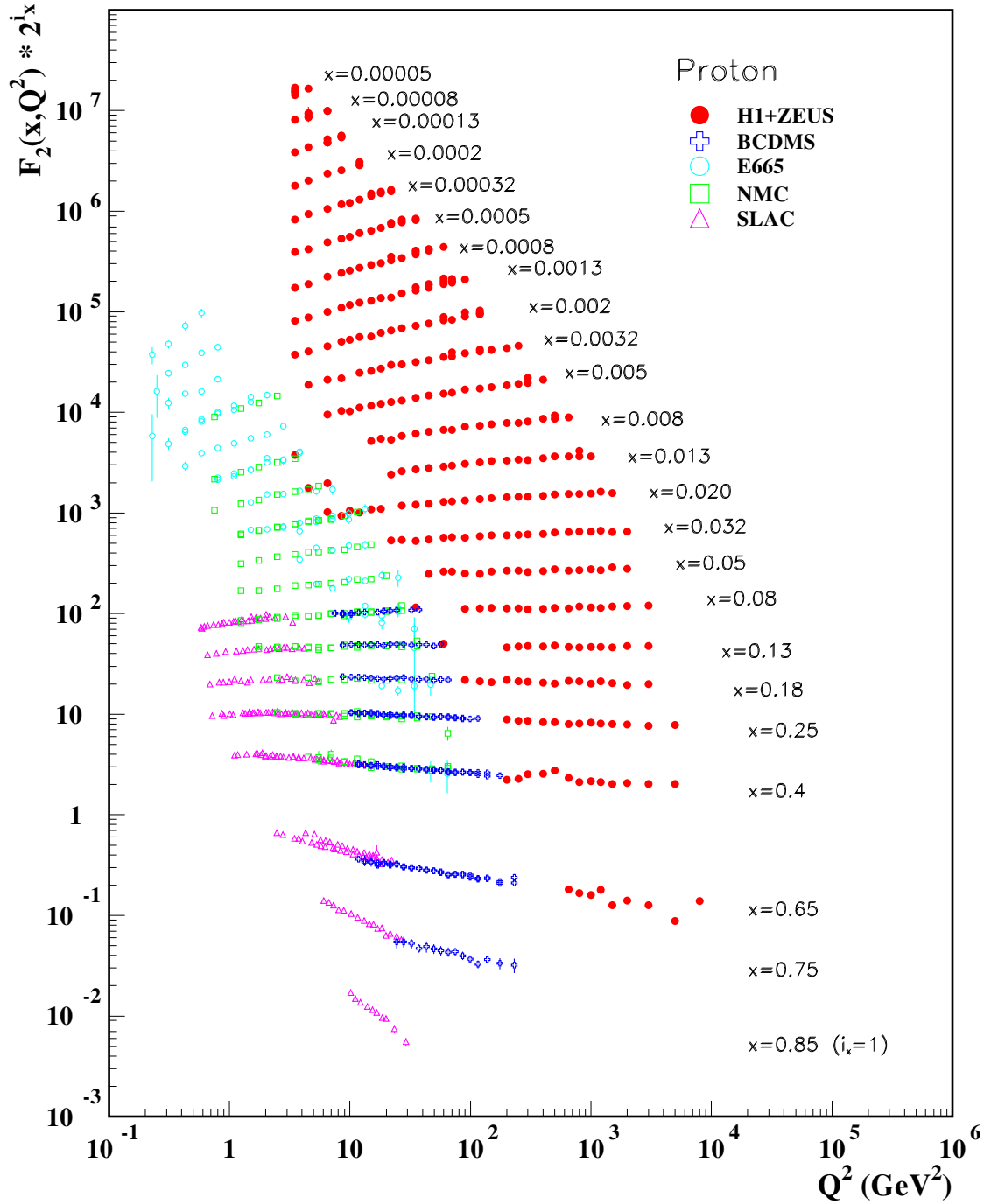


FIGURE 2.5: (Colour online) (Approximate) Bjorken scaling of the proton structure function $F_2(x_{bj}, Q^2) = \frac{Q^2}{8\pi x_{bj}} W_2(x_{bj}, Q^2)$ [1] measured in deeply inelastic electron-proton and positron-proton scattering (at the collider experiments H1 and ZEUS for $Q^2 \geq 2$ GeV²), and in the scattering of electrons (SLAC) and muons (BCDMS, E665, NMC) on a fixed target. The data are plotted as a function of Q^2 in bins of fixed x_{bj} where Q^2 and x_{bj} take on values in the kinematic domain of the HERA data. For ease of plotting, the vertical axis $F_2(x_{bj}, Q^2)$ is multiplied by $2^{i_{x_{bj}}}$ where $i_{x_{bj}}$ labels the number of the x_{bj} bin beginning at $i_{x_{bj}} = 1$ for $x_{bj} = 8.5 \times 10^{-1}$ and ending at $i_{x_{bj}} = 24$ for $x_{bj} = 5 \times 10^{-5}$. This plot is taken from [2].

and for $f = s, c, b, t$

$$\int_0^1 d\xi [f_f(\xi) - f_{\bar{f}}(\xi)] = 0. \quad (2.33)$$

Since there is no number conservation law for gluons, there is no associated sum rule for the gluon distribution function $f_g(\xi)$. There is also a sum rule associated with momentum conservation which reads

$$\sum_i \int_0^1 d\xi \xi f_i(\xi) = 1, \quad (2.34)$$

where i sum over all quark and anti-quark flavours as well as gluons.

Since the sum over f , appearing in the parton model description and predictions of deeply inelastic electron-proton scattering, does not include contributions from gluons, the gluon distribution function $f_g(\xi)$ cannot be measured directly in a DIS experiment. However, since it enters the DGLAP evolution for the quark distributions, it can be extracted⁵ from fits of the DGLAP evolution of the quark distributions to DIS data [6].

2.3 The DGLAP equations

In this section, we consider corrections to our parton model prediction of the cross section for DIS; we consider partonic processes which are (naively) next-to-leading order (NLO) in $\alpha_s(Q^2)$. Our analysis inevitably leads to the derivation of a set of coupled renormalization group (RG) equations, called the DGLAP equations. These equations govern the Q^2 dependence of PDFs and correctly account for the violation of Bjorken scaling encountered earlier.

2.3.1 Motivation: collinear singularities

Hitherto, we have only considered the leading order (LO) partonic contribution to the parton model prediction of the cross-section for DIS, namely the contribution from $e^- q_f \rightarrow e^- q_f$ where q_f is the struck quark of flavour f inside the proton. This contribution corresponds to the so-called *handbag diagram* which is drawn in Fig. 2.6.

Let us now suppose that this struck quark emits a gluon into the final state. This contribution to the parton model prediction of the cross section for DIS is depicted in Fig. 2.7. Previously, we argued that such a process is “(naively) suppressed by the smallness of the QCD coupling $\alpha_s(Q^2)$.” In order to understand in what sense this argument is naive, let us examine the

⁵A more direct process for extracting $f_g(\xi)$ is direct-photon production [25].

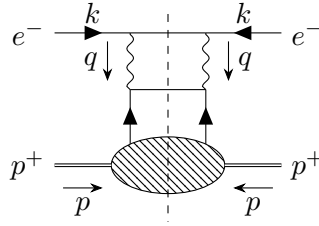


FIGURE 2.6: The *handbag diagram*: the leading order contribution to the parton model prediction of the cross section for deeply inelastic electron-proton scattering coming from the partonic sub-process $e^- q_f \rightarrow e^- q_f$. The dashed line through the middle of diagram denotes a Cutkosky cut. *Time runs from right to left.*

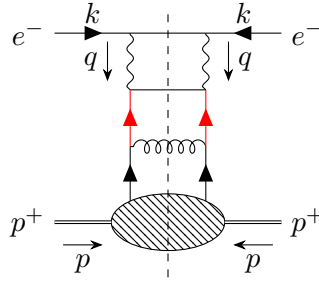


FIGURE 2.7: (Colour online) One of several (naively) next-to-leading order contributions to parton model prediction of the cross-section for deeply inelastic electron-proton scattering coming from the partonic sub-process $e^- q_f \rightarrow e^- q_f g$. When the final state gluon is emitted collinearly to the initial state quark, the momentum of the intermediate (red-coloured) quark goes on-shell and the corresponding propagator produces a logarithm in Q^2 under the *Lorentz-invariant phase space* integral for the emitted final state gluon. The dashed line through the middle of diagram denotes a Cutkosky cut. *Time runs from right to left.*

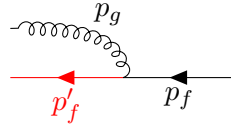


FIGURE 2.8: (Colour online) The $q_f \rightarrow q_f g$ vertex in Fig. 2.7. The outgoing (red-coloured) quark line corresponds to the intermediate (red-coloured) quark line in Fig. 2.7. *Time runs from right to left.*

$q_f \rightarrow q_f g$ vertex in Fig. 2.7 which is redrawn in Fig. 2.8. Without loss of generality, suppose that the struck quark, before emitting the gluon, is moving only in the $\hat{3}$ -direction with momentum⁶

$$p_f^\mu = (p, \mathbf{0}, p)^\mu, \quad (2.35a)$$

and that after emitting the gluon, the struck quark recoils, acquiring a transverse momentum

⁶Remember that in the high-energy limit, all masses are taken to be approximately zero.

\mathbf{p}_T and retaining a fraction $1 - z$ (where $z \in [0, 1]$) of its original energy. In this case, the momenta of the emitted gluon and recoiling struck quark are given by

$$p_g^\mu = \left(zp, -\mathbf{p}_T, \sqrt{z^2 p^2 - p_T^2} \right)^\mu, \quad (2.35b)$$

$$p_f'^\mu = \left((1 - z)p, \mathbf{p}_T, p - \sqrt{z^2 p^2 - p_T^2} \right)^\mu, \quad (2.35c)$$

respectively, where the components of p_g^μ and $p_f'^\mu$ were fixed by requiring $p_f^\mu = p_f'^\mu + p_g^\mu$ (energy-momentum conservation) and $p_g^2 = 0$ (on-shellness of the final-state gluon). Now, notice that for $p_T^2 = |\mathbf{p}_T|^2 \ll p^2$

$$p_f'^2 = -2zp^2 \left[1 - \sqrt{1 - \frac{p_T^2}{z^2 p^2}} \right] \frac{p_T^2 \ll p^2}{z^2 p^2} - \frac{p_T^2}{z} + \mathcal{O}(p_T^4/p^4), \quad (2.36)$$

which means that the momentum of the outgoing quark in Fig. 2.8 (which is the intermediate quark in Fig. 2.7) goes on-shell and the corresponding propagator is said to have a collinear singularity. Following the analysis of [6, 26] (which I shall not repeat here for the sake of brevity), one can show that in the regime where $p_T^2 \ll p^2$, the collinear singularity of the intermediate (red-coloured) quark leads to a logarithmically divergent integral contribution to the cross section depicted in Fig. 2.7 of the form

$$\alpha_s(Q^2) \int \frac{dp_T^2}{p_T^2}. \quad (2.37)$$

This integral comes from the *Lorentz-invariant phase space* integral over the momentum of the final state gluon. Furthermore, this integral is regularized by physical cut-offs: the lower integration bound is given by the mass of the proton m_p (the momentum scale at which the effects of non-perturbative QCD become important [6]) while the hard scale of the partonic interaction Q^2 is taken to be the upper limit of integration [26]. Therefore, the collinear emission of a gluon by the struck quark into the final state contributes (in addition to the single factor of $\alpha_s(Q^2)$ already present at LO) a factor of

$$\alpha_s(Q^2) \ln(Q^2/m_p^2). \quad (2.38)$$

Using the one-loop expression for the running coupling, given by [1]

$$\alpha_s(Q^2) = \frac{4\pi}{\beta_0 \ln(Q^2/\Lambda_{\text{QCD}}^2)}, \quad (2.39)$$

where $\beta_0 = 11 - \frac{2}{3}n_f$ is the coefficient of the one-loop contribution to the QCD β -function, n_f is the number of quark flavours and $\Lambda_{\text{QCD}} \approx 217$ MeV, for $Q^2 \gg m_p^2$ one finds that Eq. 2.38 is

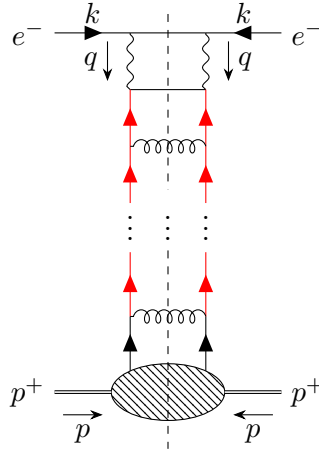


FIGURE 2.9: (Colour online) An example of a *ladder diagram* contribution to the parton model prediction of the cross section for DIS where multiple, *strongly-ordered*, colinear gluons are emitted into the final state. The red-coloured quark lines represent almost singular propagators which, under the product of *Lorentz-invariant phase space* integrals for each previously emitted final state gluon, generate logarithms in Q^2 . The dashed line through the middle of diagram denotes a Cutkosky cut. *Time runs from right to left*.

an order one contribution; i.e.

$$\alpha_s(Q^2) \ln(Q^2/m_p^2) = \frac{4\pi}{\beta_0} \frac{\ln(Q^2/m_p^2)}{\ln(Q^2/m_p^2) + \ln(m_p^2/\Lambda_{\text{QCD}}^2)} \underbrace{\frac{Q^2 \gg m_p^2}{\sim \mathcal{O}(1)}}_{\sim \mathcal{O}(1)} 4\pi/\beta + \mathcal{O}\left(\frac{1}{\ln(Q^2/m_p^2)}\right),$$

where $4\pi/\beta$ is numerically between 1 and 2 for $n_f \in \mathbb{N} \cap [1, 6]$. Since Eq. 2.38 is $\mathcal{O}(1)$, one needs to include the contribution of Eq. 2.7 from the colinear region to the LO parton model prediction of the cross section for DIS since its size is comparable to the contribution of Eq. 2.6.

What about multiple colinear gluon emissions? The emission of $n \in \mathbb{N}^+ \geq 2$ gluons into the final state produces a so-called *ladder diagram* of the form displayed in Eq. 2.9. It can be shown [6, 26] (but I shall not show this here for the sake of brevity) that the most singular contribution to Eq. 2.9 is obtained when the emitted gluons are *strongly-ordered*: when their transverse momenta satisfy $m_p^2 \ll p_{1,T}^2 \ll \dots \ll p_{n,T}^2 \ll Q^2$ (where the labels $1, \dots, n$ on the transverse momenta denote the order of emission). In this case, one obtains

$$\alpha_s^n(Q^2) \int_{m_p^2}^{Q^2} \frac{dp_{n,T}^2}{p_{n,T}^2} \int_{m_p^2}^{p_{n,T}^2} \frac{dp_{n-1,T}^2}{p_{n-1,T}^2} \dots \int_{m_p^2}^{p_{2,T}^2} \frac{dp_{1,T}^2}{p_{1,T}^2} = \frac{1}{n!} \underbrace{\alpha_s^n(Q^2) \ln^n(Q^2/m_p^2)}_{\substack{Q^2 \gg m_p^2 \\ \mathcal{O}(1)}}. \quad (2.40)$$

Since Eq. 2.40 is also of order one (for all $n \in \mathbb{N}^+ \geq 2$), it too needs to be included to the LO parton model prediction of the cross section for DIS.

In addition to the emission of colinear gluons into the final state, one also needs to take into account the colinear emission of real quarks and anti-quarks. For example, in Fig. 2.10 a gluon

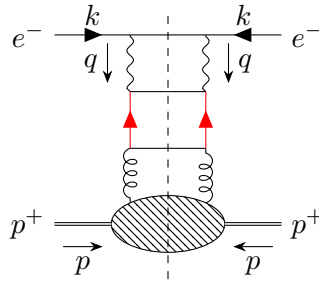


FIGURE 2.10: (Colour online) One of several (naively) next-to-leading order contributions to parton model prediction of the cross-section for deeply inelastic electron-proton scattering coming from the partonic sub-process $e^-g \rightarrow e^-gq_f\bar{q}_f$. When the final state anti-quark is emitted collinearly to the initial state gluon, the momentum of the intermediate (red-coloured) quark goes on-shell and the corresponding propagator produces a logarithm in Q^2 under the *Lorentz-invariant phase space* integral for the emitted final state anti-quark. The dashed line through the middle of diagram denotes a Cutkosky cut. *Time runs from right to left.*

from the proton splits into a quark–anti-quark pair where the quark then scatters with the electron via the exchange of a deeply virtual photon and the anti-quark is simply emitted into the final state. If the anti-quark is emitted collinearly to the quark, the quark propagator develops a collinear singularity as before. Through this mechanism, one can produce an infinite number of ladder diagrams with gluons, quarks and anti-quarks being emitted with infinitely many combinations and ratios into the final state.

Consequently, resumming all possible ladder diagrams, although necessary, is a non-trivial task. The most efficient manner of encoding this resummation is in a set of coupled integro-differential equations known as the DGLAP equations. I briefly outline the systematic derivation of the DGLAP equations in the following subsection.

2.3.2 An outline of the systematic derivation of the DGLAP equations

The parton model enables hadronic quantities to be expressed in terms of partonic quantities where the latter can be computed directly in perturbation theory. For example, the hadronic tensor $W^{\mu\nu}(x_{bj}, Q^2)$, defined in Eq. 2.9, can be expressed in terms of a partonic version of the hadronic tensor, denoted $\hat{W}^{\mu\nu}(z, Q^2)$. $\hat{W}^{\mu\nu}(z, Q^2)$ is defined as in Eq. 2.9, but with $|\mathcal{M}(\gamma^*q_f \rightarrow X)|^2$ instead of $|\mathcal{M}(\gamma^*p^+ \rightarrow X)|^2$, where q_f is a quark of flavour f with momentum p_f and z is the partonic version of the Bjorken scaling variable x_{bj}

$$z := \frac{Q^2}{2p_f \cdot q}. \quad (2.41)$$

Writing (as has been done previously) $p_f = \xi p$, one obtains from Eq. 2.41 the constraint equation $z\xi = x_{bj}$. This constraint can be enforced with a Dirac delta-function $\delta(z\xi - x_{bj})$ which must be integrated over $z \in [0, 1]$. The resultant formula for expressing $W^{\mu\nu}(x_{bj}, Q^2)$ in terms of

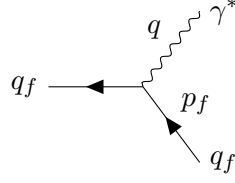


FIGURE 2.11: Processes of the form $\gamma^* q_f \rightarrow X$ contributing to $\hat{W}_0(z, Q^2)$ at $\mathcal{O}(\alpha_s^0)$. Time runs from right to left.

$\hat{W}^{\mu\nu}(z, Q^2)$ is given by

$$W^{\mu\nu}(x_{\text{bj}}, Q^2) = \sum_f \int_0^1 d\xi f_f(\xi) \int_0^1 dz \hat{W}^{\mu\nu}(z, Q^2) \delta(x_{\text{bj}} - z\xi) = \sum_f \int_x^1 \frac{d\xi}{\xi} f_f(\xi) \hat{W}^{\mu\nu}\left(\frac{x_{\text{bj}}}{\xi}, Q^2\right), \quad (2.42)$$

Let us define the (scalar) form factor

$$W_0(x_{\text{bj}}, Q^2) := -g_{\mu\nu} W^{\mu\nu}(x_{\text{bj}}, Q^2), \quad (2.43)$$

the quantity of interest in our derivation of the DGLAP equations. Since a sum over polarizations λ in Eq. 2.9 is equivalent to the replacement⁷ [6]

$$\sum_{\lambda} \varepsilon_{\mu;\lambda}(q) \varepsilon_{\nu;\lambda}^*(q) \rightarrow -g_{\mu\nu}, \quad (2.45)$$

Eq. 2.43 is proportional to the inclusive, unpolarized cross-section for $\gamma^* p^+ \rightarrow X$ [1]. $W_0(x_{\text{bj}}, Q^2)$ can be evaluated either using Eq. 2.17a and Eq. 2.30 which yields

$$W_0(x_{\text{bj}}, Q^2) = 4\pi \sum_f Q_f^2 f_f(x_{\text{bj}}), \quad (2.46)$$

or using Eq. 2.42, yielding

$$W_0(x_{\text{bj}}, Q^2) = \sum_f \int_x^1 \frac{d\xi}{\xi} f_f(\xi) \hat{W}_0\left(\frac{x_{\text{bj}}}{\xi}, Q^2\right), \quad \hat{W}_0(z, Q^2) = -g_{\mu\nu} \hat{W}^{\mu\nu}(z, Q^2). \quad (2.47)$$

The only process contributing to $\hat{W}_0(z, Q^2)$ of the form $\gamma^* q_f \rightarrow X$ at $\mathcal{O}(\alpha_s^0)$ is $\gamma^* q_f \rightarrow q_f$ as displayed in Fig. 2.11. Here, one may (correctly) guess that

⁷Technically speaking, the sum over polarizations is given by [1, 27]

$$\sum_{\lambda} \varepsilon_{\mu;\lambda}(q) \varepsilon_{\nu;\lambda}^*(q) = -g_{\mu\nu} + \frac{q_{\mu} \bar{q}_{\nu} + q_{\nu} \bar{q}_{\mu}}{q \cdot \bar{q}}, \quad (2.44)$$

where $\bar{q}^{\mu} = 2(n \cdot q)n^{\mu} - q^{\mu}$ and n^{μ} is some fixed timelike four-vector. However, due to the Ward-Takahashi identity, the terms in Eq. 2.44 proportional to q^{μ} do not contribute to physical quantities which allows one to drop these terms from the right-hand-side of Eq. 2.44 and use Eq. 2.45 instead.

$$\hat{W}_0^{\text{LO}}(z, Q^2) = 4\pi Q_f^2 \delta(z - 1). \quad (2.48)$$

By comparing with Eq. 2.46, this ansatz follows from the fact that the probability of the quark carrying a momentum fraction z of its original momentum at lowest order in α_s is 1 if $z = 1$ and zero otherwise, and this information is captured mathematically by the distribution $\delta(z - 1)$. Substituting Eq. 2.48 into Eq. 2.47 reproduces⁸ Eq. 2.46 as expected. In order to confirm Eq. 2.48, consider the invariant matrix element for the process $\gamma^* q_f \rightarrow q_f$

$$i\mathcal{M}(\gamma^* q_f \rightarrow q_f) = \varepsilon_{\mu;\lambda}(q) \bar{u}^{s'_f}(p'_f) (ieQ_f \gamma^\mu) u^{s_f}(p_f), \quad (2.49)$$

where s_f and s'_f are the spins of the incoming and outgoing quark, respectively, and $\hat{W}^{\mu\nu}(z, Q^2)$ is given by

$$\begin{aligned} \hat{W}^{\mu\nu}(z, Q^2) &= \frac{Q_f^2}{2} \int \frac{d^3 p'_f}{(2\pi)^3 2p'_f{}^0} \text{Tr} \left(\gamma^\mu \not{p}_f \gamma^\nu \not{p}'_f \right) (2\pi)^4 \delta^{(4)}(p_f + q - p'_f) \\ &= \frac{Q_f^2}{2} \int \frac{d^3 p'_f}{(2\pi)^3 2p'_f{}^0} 4(p_f^\mu p'_f{}^\nu + p'_f{}^\mu p_f^\nu - g^{\mu\nu} p_f \cdot p'_f) (2\pi)^4 \delta^{(4)}(p_f + q - p'_f) \\ &= 2\pi Q_f^2 (p_f^\mu (p_f^\nu + q^\nu) + p_f^\nu (p_f^\mu + q^\mu) - g^{\mu\nu} p_f \cdot (p_f + q)) \frac{\delta(|\mathbf{p}_f| + \sqrt{\mathbf{q}^2 - Q^2} - |\mathbf{p}_f + \mathbf{q}|)}{|\mathbf{p}_f + \mathbf{q}|}. \end{aligned} \quad (2.50)$$

Eq. 2.50 can be further simplified by rewriting Eq. 2.41 as

$$2\mathbf{p}_f \cdot \mathbf{q} = 2|\mathbf{p}_f| \sqrt{\mathbf{q}^2 - Q^2} - \frac{Q^2}{z}, \quad (2.51)$$

from which one can show that

$$\frac{\delta(|\mathbf{p}_f| + \sqrt{\mathbf{q}^2 - Q^2} - |\mathbf{p}_f + \mathbf{q}|)}{|\mathbf{p}_f + \mathbf{q}|} = \frac{2}{Q^2} \delta(z - 1). \quad (2.52)$$

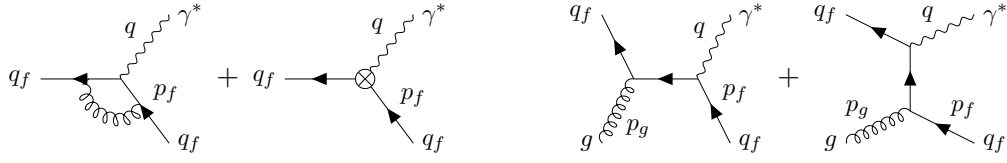
Substituting Eq. 2.52 into Eq. 2.50 yields

$$\begin{aligned} \hat{W}^{\mu\nu}(z, Q^2) &= 2\pi Q_f^2 \left(\frac{4}{Q^2} p_f^\mu p_f^\nu + \frac{2}{Q^2} (p_f^\mu q^\nu + p_f^\nu q^\mu) - g^{\mu\nu} \right) \delta(z - 1) \\ &= 2\pi Q_f^2 \left[\left(-g^{\mu\nu} + \frac{q^\mu q^\nu}{q^2} \right) + \frac{4z^2}{Q^2} \left(p_f^\mu - \frac{p_f \cdot q}{q^2} q^\mu \right) \left(p_f^\nu - \frac{p_f \cdot q}{q^2} q^\nu \right) \right] \delta(1 - z), \end{aligned} \quad (2.53)$$

where the constraint enforced by the Dirac delta-function has been used. Comparing Eq. 2.53 with Eq. 2.17a, one can read off the partonic structure functions

$$\hat{W}_1(z, Q^2) = 2\pi Q_f^2 \delta(z - 1) = \frac{Q^2}{4z^2} \hat{W}_2(z, Q^2), \quad (2.54)$$

⁸Here we assume the right-continuous definition of the Heaviside step function such that $\theta(0) = 1$.



(A) Vertex correction graphs: single virtual (B) Real emission graphs: s -channel (left) and gluon correction (left) and counter-term (right) t -channel (right) diagrams for $\gamma^* q_f \rightarrow q_f g$. for $\gamma^* q_f \rightarrow q_f$.

FIGURE 2.12: Processes of the form $\gamma^* q_f \rightarrow X$ contributing to $\hat{W}_0(z, Q^2)$ at $\mathcal{O}(\alpha_s^1)$. Time runs from right to left.

which is the partonic version of the Callan-Gross relation. Finally, contracting $-g_{\mu\nu}$ with Eq. 2.53, one obtains Eq. 2.48.

Given that we are able to reproduce the leading order in α_s prediction of the parton model for $W_0(x_{bj}, Q^2)$ as expressed in Eq. 2.46, we wish to compute the next-to-leading order in α_s corrections to this prediction. In order to determine these corrections, consider the following formal expansion for $i\mathcal{M}(\gamma^* q_f \rightarrow X)$ in powers of the strong coupling g

$$i\mathcal{M}(\gamma^* q_f \rightarrow X) = i\mathcal{M}_0(\gamma^* q_f \rightarrow X) + i\mathcal{M}_1(\gamma^* q_f \rightarrow X) + i\mathcal{M}_2(\gamma^* q_f \rightarrow X) + \mathcal{O}(g^3), \quad (2.55)$$

where the subscript labels the power of g . The first term in Eq. 2.55 is precisely Eq. 2.49 while the next two terms in Eq. 2.55 are the invariant matrix elements

$$i\mathcal{M}_1(\gamma^* q_f \rightarrow X) =: i\mathcal{M}(\gamma^* q_f \rightarrow q_f g) = \varepsilon_{\mu;\lambda}(q) \varepsilon_{\nu;\lambda'}^*(p_g) (ig) (ieQ_f) \\ \times \bar{u}_j^{s_f'}(p_f') t_{ji}^a \left[\gamma^\nu \frac{(\not{p}_f + \not{q}) + m_{q_f}}{(p_f + q)^2 - m_{q_f}^2 + i\varepsilon} \gamma^\mu + \gamma^\mu \frac{(\not{p}_f' - \not{q}) + m_{q_f}}{(p_f' - q)^2 - m_{q_f}^2 + i\varepsilon} \gamma^\nu \right] u_i^{s_f}(p_f), \quad (2.56)$$

describing the process depicted in Fig. 2.12b and

$$i\mathcal{M}_2(\gamma^* q_f \rightarrow X) =: i\mathcal{M}(\gamma^* q_f \rightarrow q_f(+g)) = \varepsilon_{\mu;\lambda}(q) \bar{u}^{s_f'}(p_f') (ieQ_f \Gamma_2^\mu(p_f')) u^{s_f}(p_f), \quad (2.57)$$

describing the process depicted in Fig. 2.12a where the first graph is the $\mathcal{O}(\alpha_s^1)$ virtual (loop) correction to the $\gamma^* q_f \rightarrow q_f$ vertex while the second graph is the counter-term responsible for cancelling the ultraviolet (UV) divergence associated with the loop in the first graph.

The square of the modulus of Eq. 2.55 is given by

$$|\mathcal{M}(\gamma^* q_f \rightarrow X)|^2 = |\mathcal{M}_0(\gamma^* q_f \rightarrow X)|^2 + 2\text{Re} \left[\mathcal{M}_0(\gamma^* q_f \rightarrow X) \mathcal{M}_2(\gamma^* q_f \rightarrow X)^\dagger \right] \\ + |\mathcal{M}_1(\gamma^* q_f \rightarrow X)|^2 + \mathcal{O}(\alpha_s^2), \quad (2.58)$$

where the latter two terms are $\mathcal{O}(\alpha_s^1)$. For the sake of parameterizing the infrared (IR) singularities in these $\mathcal{O}(\alpha_s^1)$ corrections, we shall work in $d = 4 - \varepsilon$ dimensions and use dimensional regularization.

The contribution to $\hat{W}_0(z, Q^2)$ from the second term in Eq. 2.58, the interference between the leading-order graph in Eq. 2.49 and the vertex correction graphs in Eq. 2.57, is given in [1] as

$$\hat{W}_0^V(z, Q^2) = 4\pi Q_f^2 \frac{\alpha_s}{2\pi} C_f \left(\frac{4\pi\mu^2}{Q^2} \right)^{\frac{\varepsilon}{2}} \frac{\Gamma(1 - \frac{\varepsilon}{2})}{\Gamma(1 - \varepsilon)} \left[-\frac{8}{\varepsilon^2} - \frac{6}{\varepsilon} - 8 - \frac{\pi^2}{3} \right] \delta(z - 1). \quad (2.59)$$

up to terms in $\mathcal{O}(\varepsilon)$. The result of the calculation for the contribution to $\hat{W}_0(z, Q^2)$ from the third term in Eq. 2.58 which comes from the real emission graphs in Eq. 2.56, is also given in [1] up to terms in $\mathcal{O}(\varepsilon)$ as

$$\begin{aligned} \hat{W}_0^R(z, Q^2) &= 4\pi Q_f^2 \frac{\alpha_s}{2\pi} C_f \left(\frac{4\pi\mu^2}{Q^2} \right)^{\frac{\varepsilon}{2}} \frac{\Gamma(1 - \frac{\varepsilon}{2})}{\Gamma(1 - \varepsilon)} \\ &\times \left[3z + z^{\frac{\varepsilon}{2}} (1 - z)^{-\frac{\varepsilon}{2}} \left(-\frac{2}{\varepsilon} \frac{1 + z^2}{1 - z} + 3 - z - \frac{3}{2} \frac{1}{1 - z} - \frac{7}{4} \frac{\varepsilon}{1 - z} \right) \right]. \end{aligned} \quad (2.60)$$

In order to make explicit the $\frac{1}{\varepsilon^2}$ pole in Eq. 2.60, one needs to expand $\frac{1}{1-z}(1-z)^{-\frac{\varepsilon}{2}}$ around $\varepsilon = 0$ which yields a distribution over the interval $[0, 1]$. To this end, consider⁹

$$\begin{aligned} \int_0^1 dz \frac{1}{(1-z)^{1-\varepsilon}} f(z) &= f(1) \int_0^1 dz \frac{1}{(1-z)^{1-\varepsilon}} + \int_0^1 dz \frac{1}{1-z} e^{\varepsilon \ln(1-z)} (f(z) - f(1)) \\ &= \frac{1}{\varepsilon} f(1) + \sum_{n=0}^{\infty} \frac{\varepsilon^n}{n!} \int_0^1 dz \frac{\ln^n(1-z)}{1-z} (f(z) - f(1)) \\ &= \frac{1}{\varepsilon} \int_0^1 \delta(1-z) f(z) + \sum_{n=0}^{\infty} \frac{\varepsilon^n}{n!} \int_0^1 dz \left[\frac{\ln^n(1-z)}{1-z} \right]_+ f(z), \\ \implies \frac{1}{(1-z)^{1-\varepsilon}} &= \frac{1}{\varepsilon} \delta(1-z) + \sum_{n=0}^{\infty} \frac{\varepsilon^n}{n!} \left[\frac{\ln^n(1-z)}{1-z} \right]_+, \end{aligned} \quad (2.61)$$

where the plus distribution is defined through the identity

$$\int_0^1 dz \left[\frac{\ln^n(1-z)}{1-z} \right]_+ f(z) = \int_0^1 dz \frac{\ln^n(1-z)}{1-z} (f(z) - f(1)). \quad (2.62)$$

⁹Here we assume the right-continuous definition of the Heaviside step function such that $\theta(0) = 1$.

Analytically continuing Eq. 2.61 to negative values of ε , replacing ε with $-\frac{\varepsilon}{2}$ and inserting Eq. 2.61 into Eq. 2.60 we obtain

$$\begin{aligned} \hat{W}_0^R(z, Q^2) = & 4\pi Q_f^2 \frac{\alpha_s}{2\pi} C_f \left(\frac{4\pi\mu^2}{Q^2} \right)^{\frac{\varepsilon}{2}} \frac{\Gamma(1 - \frac{\varepsilon}{2})}{\Gamma(1 - \varepsilon)} \left[3 + 2z - \frac{1+z^2}{1-z} \ln z + (1+z^2) \left[\frac{\ln(1-z)}{1-z} \right]_+ \right. \\ & \left. + \left(\frac{8}{\varepsilon^2} + \frac{3}{\varepsilon} + \frac{7}{2} \right) \delta(1-z) - \left(\frac{2(1+z^2)}{\varepsilon} + \frac{3}{2} \right) \left[\frac{1}{1-z} \right]_+ \right], \end{aligned} \quad (2.63)$$

where $\mathcal{O}(\varepsilon)$ terms have been dropped. Adding Eq. 2.59 and Eq. 2.63 to Eq. 2.48 we obtain

$$\begin{aligned} \hat{W}_0^{\text{NLO}}(z, Q^2) = & \hat{W}_0^{\text{LO}}(z, Q^2) + \hat{W}_0^V(z, Q^2) + \hat{W}_0^R(z, Q^2) \\ = & 4\pi Q_f^2 \left[\delta(1-z) - \frac{1}{\varepsilon} \frac{\alpha_s}{\pi} P_{q \rightarrow q}(z) \left(\frac{4\pi\mu^2}{Q^2} \right)^{\frac{\varepsilon}{2}} \frac{\Gamma(1 - \frac{\varepsilon}{2})}{\Gamma(1 - \varepsilon)} + \frac{\alpha_2}{2\pi} C_f \left\{ 3 + 2z - \frac{1+z^2}{1-z} \ln z \right. \right. \\ & \left. \left. + (1+z^2) \left[\frac{\ln(1-z)}{1-z} \right]_+ - \left(\frac{9}{2} + \frac{\pi^2}{3} \right) \delta(1-z) - \frac{3}{2} \left[\frac{1}{1-z} \right]_+ \right\} \right], \end{aligned} \quad (2.64)$$

where

$$P_{q \rightarrow q}(z) := C_f \left[(1+z^2) \left[\frac{1}{1-z} \right]_+ + \frac{3}{2} \delta(1-z) \right], \quad (2.65)$$

is known as a DGLAP splitting function. Notice that the addition of Eq. 2.63 to Eq. 2.48 cancels the $\frac{1}{\varepsilon^2}$ pole, but not the $\frac{1}{\varepsilon}$ pole. The latter infrared singularity is already present in the high-energy limit of Compton scattering which is precisely the process shown in Fig. 2.12b. One can expand the terms multiplying the splitting function around $\varepsilon = 0$ which yields

$$\begin{aligned} \frac{1}{\varepsilon} \frac{\alpha_s}{\pi} \left(\frac{4\pi\mu^2}{Q^2} \right)^{\frac{\varepsilon}{2}} \frac{\Gamma(1 - \frac{\varepsilon}{2})}{\Gamma(1 - \varepsilon)} &= \frac{\alpha_s}{2\pi} \frac{2}{\varepsilon} \left[1 + \frac{\varepsilon}{2} \ln \left(\frac{4\pi\mu^2}{Q^2} \right) + \mathcal{O}(\varepsilon^2) \right] \left[1 - \frac{\varepsilon}{2} \gamma_E + \mathcal{O}(\varepsilon^2) \right] \\ &= \frac{\alpha_s}{2\pi} \left[\frac{2}{\varepsilon} + \ln \left(\frac{4\pi\mu^2}{Q^2} \right) - \gamma_E \right] + \mathcal{O}(\varepsilon) = \frac{\alpha_s}{2\pi} \left[\frac{2}{\varepsilon} + \ln \left(\frac{\tilde{\mu}^2}{Q^2} \right) \right] + \mathcal{O}(\varepsilon), \end{aligned} \quad (2.66)$$

where γ_E is the Euler-Mascheroni constant and $\tilde{\mu}^2 = 4\pi\mu^2 e^{-\gamma_E}$. Substituting Eq. 2.64 into Eq. 2.47 and using Eq. 2.66 we obtain

$$\begin{aligned} W_0(x_{bj}, Q^2) &= 4\pi \sum_f Q_f^2 \int_x^1 \frac{d\xi}{\xi} f_f(\xi, Q^2) \left[\delta \left(1 - \frac{x_{bj}}{\xi} \right) - \frac{\alpha_s}{2\pi} P_{q \rightarrow q} \left(\frac{x_{bj}}{\xi} \right) \left(\frac{2}{\varepsilon} + \ln \left(\frac{\tilde{\mu}^2}{Q^2} \right) \right) + \dots \right]. \end{aligned} \quad (2.67)$$

Although the precise physical origin of the logarithm in Q^2 is obscured in dimensional regularization, the logarithm in Q^2 is due to the colinear emission of a real gluon into the final state as

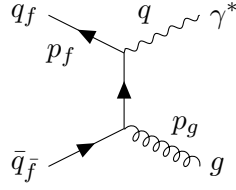


FIGURE 2.13: Processes of the form $\gamma^* g \rightarrow X$ contributing to $\hat{W}_0(z, Q^2)$ at $\mathcal{O}(\alpha_s^1)$. Time runs from right to left.

discussed in the previous subsection. Taking the difference in Eq. 2.67 at fixed x_{bj} but different hard scales Q^2 and Q_0^2 leads to the finite difference equation

$$W_0(x_{bj}, Q^2) - W_0(x_{bj}, Q_0^2) = 4\pi \sum_f Q_f^2 \int_x^1 \frac{d\xi}{\xi} f_f(\xi, Q^2) \left[\frac{\alpha_s}{2\pi} P_{q \rightarrow q} \left(\frac{x_{bj}}{\xi} \right) \ln \left(\frac{Q^2}{Q_0^2} \right) \right], \quad (2.68)$$

which is infrared finite. Substituting Eq. 2.46 into the left hand side, moving $\ln(Q^2/Q_0^2)$ to the left hand side and taking the limit $|Q^2 - Q_0^2| \rightarrow 0$ leads to an integro-differential equation for the quark distribution functions

$$\frac{\partial}{\partial \ln(Q^2)} f_f(x_{bj}, Q^2) = \frac{\alpha_s}{2\pi} \int_x^1 \frac{d\xi}{\xi} f_f(\xi, Q^2) P_{q \rightarrow q} \left(\frac{x_{bj}}{\xi} \right). \quad (2.69)$$

However, Eq. 2.69 is only one component of the DGLAP equation for the quark distribution functions. At $\mathcal{O}(\alpha_s^1)$, there is also a contribution to $\hat{W}_0(z, Q^2)$ from the process $\gamma^* g \rightarrow q\bar{q}$ which is displayed in Fig. 2.13. Consequently, there is an additional contribution to the DGLAP evolution for the quark distribution functions from the gluon distribution function. One says that the parton distribution functions mix under RG evolution. In fact, the DGLAP equations for the parton distribution functions are a set of coupled integro-differential equations.

In order to write the DGLAP equations compactly, we introduce the following notation: we define the vectors $\mathbf{q}(x_{bj}, Q^2)$ and $\bar{\mathbf{q}}(x_{bj}, Q^2)$ whose components consist of all the different flavour quark and anti-quark distribution functions, respectively, given by

$$[\mathbf{q}(x_{bj}, Q^2)]_f = f_f(x_{bj}, Q^2), \quad [\bar{\mathbf{q}}(x_{bj}, Q^2)]_{\bar{f}} = f_{\bar{f}}(x_{bj}, Q^2). \quad (2.70)$$

It is also conventional to write the gluon distribution function $f_g(x_{bj}, Q^2)$ as $g(x_{bj}, Q^2)$. In this notation, the DGLAP equations are given (to all-orders) by [28]

$$\frac{\partial}{\partial \ln(Q^2)} \begin{bmatrix} \mathbf{q}(x_{bj}, Q^2) \\ \bar{\mathbf{q}}(x_{bj}, Q^2) \\ g(x_{bj}, Q^2) \end{bmatrix} = \frac{\alpha_s}{2\pi} \int_{x_{bj}}^1 \frac{d\xi}{\xi} \begin{bmatrix} \tilde{P}_{qq}(x_{bj}/\xi) & \tilde{P}_{q\bar{q}}(x_{bj}/\xi) & \tilde{P}_{qg}(x_{bj}/\xi) \\ \tilde{P}_{\bar{q}q}(x_{bj}/\xi) & \tilde{P}_{\bar{q}\bar{q}}(x_{bj}/\xi) & \tilde{P}_{\bar{q}g}(x_{bj}/\xi) \\ \tilde{P}_{gq}(x_{bj}/\xi) & \tilde{P}_{g\bar{q}}(x_{bj}/\xi) & \tilde{P}_{gg}(x_{bj}/\xi) \end{bmatrix} \begin{bmatrix} \mathbf{q}(\xi, Q^2) \\ \bar{\mathbf{q}}(\xi, Q^2) \\ g(\xi, Q^2) \end{bmatrix}, \quad (2.71)$$

where

- $\tilde{P}_{qq}(x_{bj}/\xi)$, $\tilde{P}_{q\bar{q}}(x_{bj}/\xi)$, $\tilde{P}_{\bar{q}q}(x_{bj}/\xi)$ and $\tilde{P}_{\bar{q}\bar{q}}(x_{bj}/\xi)$ are n_f -by- n_f matrices,
- $\tilde{P}_{qg}(x_{bj}/\xi)$ and $\tilde{P}_{\bar{q}g}(x_{bj}/\xi)$ are n_f -by-1 column vectors,
- $\tilde{P}_{gq}(x_{bj}/\xi)$ and $\tilde{P}_{g\bar{q}}(x_{bj}/\xi)$ are 1-by- n_f row vectors,
- $\tilde{P}_{gg}(x_{bj}/\xi)$ is a 1-by-1 matrix,

and n_f is the number of quark flavours inside the proton. At leading-logarithmic (LL) accuracy, these matrices are given by

$$[\tilde{P}_{qq}(x_{bj}/\xi)]_{ij} = [\tilde{P}_{\bar{q}\bar{q}}(x_{bj}/\xi)]_{ij} = \delta_{ij} P_{q \rightarrow q}(x_{bj}/\xi), \quad (2.72a)$$

$$[\tilde{P}_{q\bar{q}}(x_{bj}/\xi)]_{ij} = [\tilde{P}_{\bar{q}q}(x_{bj}/\xi)]_{ij} = 0, \quad (2.72b)$$

$$[\tilde{P}_{qg}(x_{bj}/\xi)]_i = [\tilde{P}_{\bar{q}g}(x_{bj}/\xi)]_i = P_{g \rightarrow q}(x_{bj}/\xi), \quad (2.72c)$$

$$[\tilde{P}_{gq}(x_{bj}/\xi)]_i = [\tilde{P}_{g\bar{q}}(x_{bj}/\xi)]_i = P_{q \rightarrow g}(x_{bj}/\xi), \quad (2.72d)$$

$$\tilde{P}_{gg}(x_{bj}/\xi) = P_{g \rightarrow g}(x_{bj}/\xi). \quad (2.72e)$$

Beyond LL, the n_f -by- n_f matrices $\tilde{P}_{\bar{q}\bar{q}}(x_{bj}/\xi)$ and $\tilde{P}_{q\bar{q}}(x_{bj}/\xi)$ are no longer zero [28]. The splitting function $P_{q \rightarrow q}(x_{bj}/\xi)$ in Eq. 2.72a is given in Eq. 2.65 while the remaining splitting functions are given below [1]

$$P_{g \rightarrow q}(z) := \frac{1}{2}(z^2 + (1-z)^2), \quad (2.73a)$$

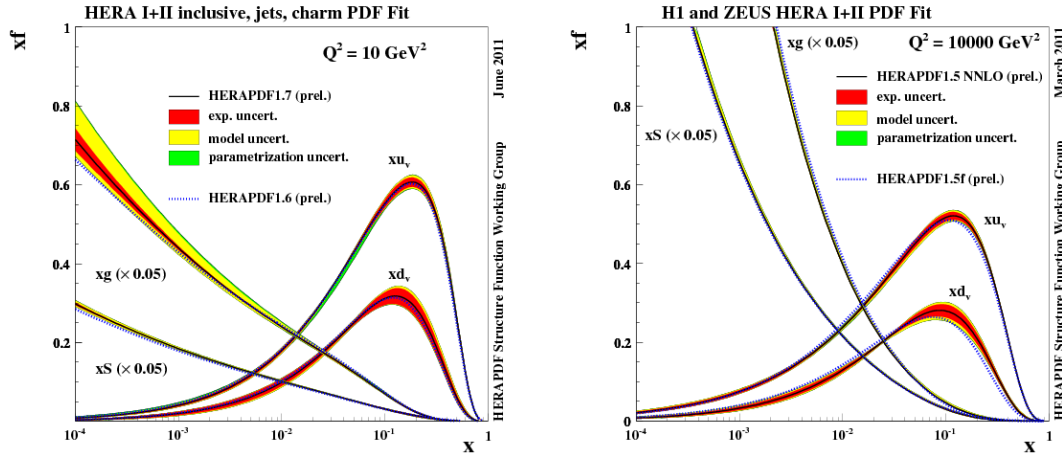
$$P_{q \rightarrow g}(z) := C_f \left(\frac{1 + (1-z)^2}{z} \right), \quad (2.73b)$$

$$P_{g \rightarrow g}(z) := 2C_A \left(z \left[\frac{1}{1-z} \right]_+ + \frac{1-z}{z} + z(1-z) \right) + \frac{\beta_0}{2} \delta(1-z), \quad (2.73c)$$

where, $C_f = \frac{N_c^2 - 1}{2N_c}$ and $C_A = N_c$ are the quadratic Casimirs in the fundamental and adjoint representations, respectively, and $\beta_0 = \frac{11}{3}C_A - \frac{2}{3}n_f$ is the coefficient of the one-loop contribution to the QCD β -function with n_f being the number of quark flavours. A similar analysis to that presented in this subsection allows one to compute the remaining DGLAP splitting functions, given in Eq. 2.73.

With the gluon distribution function being a flavour singlet density, and by defining the *flavour singlet quark density* [28]

$$\Sigma(x_{bj}, Q^2) := \sum_{i=1}^{n_f} [q_i(x_{bj}, Q^2) + \bar{q}_i(x_{bj}, Q^2)], \quad (2.74)$$



(A) (Colour online) PDFs from HERAPDF1.7 at $Q^2 = 10^1 \text{ GeV}^2$. (B) (Colour online) PDFs from HERAPDF1.5 at $Q^2 = 10^4 \text{ GeV}^2$.

FIGURE 2.14: (Colour online) PDFs from HERAPDF1.7 and HERAPDF1.5 at $Q^2 = 10^1 \text{ GeV}^2$ and $Q^2 = 10^4 \text{ GeV}^2$, respectively [3]. The gluon $x_{bj}g(x_{bj}, Q^2)$ and sea (or wee) quark $x_{bj}S(x_{bj}, Q^2)$ distribution functions have been reduced by a scale factor of 20. Both plots show enhanced gluon production at small Bjorken x_{bj} .

one can immediately write down the LL DGLAP equations for the flavour singlet densities

$$\frac{\partial}{\partial \ln(Q^2)} \begin{bmatrix} \Sigma(x_{bj}, Q^2) \\ g(x_{bj}, Q^2) \end{bmatrix} = \frac{\alpha_s}{2\pi} \int_{x_{bj}}^1 \frac{d\xi}{\xi} \begin{bmatrix} P_{q \rightarrow q}(x_{bj}/\xi) & 2n_f P_{g \rightarrow q}(x_{bj}/\xi) \\ P_{q \rightarrow g}(x_{bj}/\xi) & P_{g \rightarrow g}(x_{bj}/\xi) \end{bmatrix} \begin{bmatrix} \Sigma(\xi, Q^2) \\ g(\xi, Q^2) \end{bmatrix}. \quad (2.75)$$

Returning to Eq. 2.71, notice that in Eq. 2.71 the ξ integral which convolves the PDFs with the DGLAP splitting functions is over the interval $[x_{bj}, 1]$ which means that only partons with (longitudinal) momentum fractions larger than x_{bj} “feed” the DGLAP evolution of the PDFs.

In the limit that $x_{bj} \rightarrow 0$, the DGLAP splitting functions $P_{q \rightarrow g}(x_{bj}/\xi)$ and $P_{g \rightarrow g}(x_{bj}/\xi)$ contributing to the DGLAP evolution of the gluon distribution function in Eq. 2.71 become singular with a pole in $\frac{1}{x_{bj}}$. Consequently, we expect that for small Bjorken x_{bj} , the Q^2 evolution of gluon distribution function is significantly enhanced. This expectation is confirmed in Fig. 2.14. Moreover, Fig. 2.14 shows that at small Bjorken x_{bj} the gluon distribution function, plotted $x_{bj}g(x_{bj}, Q^2) = x_{bj}f_g(x_{bj}, Q^2)$, dominates all other PDFs. From this behaviour of the PDFs at small Bjorken x_{bj} , one motivates the existence of the Colour Glass Condensate in the Regge-Gribov limit of QCD.

2.4 The Regge-Gribov limit and the CGC formalism

Recall that the Regge-Gribov limit of QCD is the limit in which $s \rightarrow \infty$ and $x_{bj} \rightarrow 0$ while y and Q^2 remain fixed. In the preceding section we presented the evidence for large gluon occupation

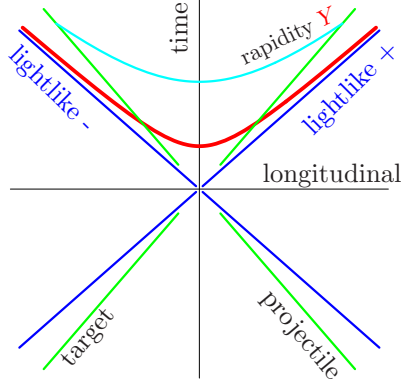


FIGURE 2.15: (Colour online) Kinematics for high-energy DIS. The world-lines of the electron (the projectile) and the proton (the target) lie almost along the light-cone directions and are separated by a large rapidity Y .

numbers in this limit. In order for these gluons to be probed by the virtual photon exchanged between the electron (the projectile) and the proton (the target), the colourless virtual photon needs to fluctuate into colour singlet degrees of freedom which to lowest order in pQCD is a $q\bar{q}$ -pair. Since the target consists mostly of gluons in this limit, one can describe interaction of this $q\bar{q}$ -pair with the target as the propagation of quarks and anti-quarks in the presence of a large background gauge field b^μ where b^μ represents the gluonic field of the target. By large we mean that $b^\mu \sim \mathcal{O}(1/\alpha_s)$ [4]. Consequently, we split A^μ up into

$$A^\mu = b^\mu + \delta A^\mu, \quad (2.76)$$

where δA^μ describes perturbative or kinematically suppressed gluons on top of b^μ .

Since b^μ captures the kinematically enhanced contributions to A^μ , its form is constrained by relativistic effects. In order to see this, let us again consider the experimental setup of DIS and, without loss of generality, let us orient our coordinate system such that both the projectile (the electron) and the target are traveling along the z -axis. Their momenta are given by

$$p^\mu = (p^0, \mathbf{0}, p^3)^\mu, \quad p^2 = m_p^2 > 0, \quad p^3 \geq 0, \quad (2.77a)$$

$$k^\mu = (k^0, \mathbf{0}, k^3)^\mu, \quad k^2 = m_e^2 > 0, \quad k^3 \leq 0. \quad (2.77b)$$

Since these momenta are both time-like, their directions are related (as depicted in Fig. 2.15) through a Lorentz boost

$$\frac{1}{m_p} \begin{bmatrix} p^0 \\ p^3 \end{bmatrix} = \begin{bmatrix} \cosh(Y) & \sinh(Y) \\ \sinh(Y) & \cosh(Y) \end{bmatrix} \frac{1}{m_e} \begin{bmatrix} k^0 \\ k^3 \end{bmatrix}, \quad (2.78)$$

where Y is called the rapidity separation or Minkowski boost angle between the two directions. Note that we have omitted the zero transverse components of the momenta in Eq. 2.78 for

simplicity. In order to compute Y it is convenient to choose a particular frame like the rest frame of the projectile (the electron) where $k^0 = m_e$ and $k^3 = 0$. With this choice, from Eq. 2.78 one obtains

$$\frac{p^0}{m_p} = \cosh(Y). \quad (2.79)$$

p^0 can be written in terms of some of the Lorentz invariants defined in Eq. 2.1 as follows

$$x_{\text{bj}} = \frac{Q^2}{2p \cdot q} = \frac{Q^2}{2(p \cdot k)y} = \frac{Q^2}{2p^0 m_e y} \iff p^0 = \frac{Q^2}{2x_{\text{bj}} m_e y}. \quad (2.80)$$

Substituting Eq. 2.80 into Eq. 2.79 and solving for Y yields

$$Y = \cosh^{-1} \left(\frac{Q^2}{2x_{\text{bj}} m_e m_p y} \right) \stackrel{x_{\text{bj}} \rightarrow 0}{=} \ln(1/x_{\text{bj}}) + \ln \left(\frac{Q^2}{2m_e m_p y} \right) + \mathcal{O}(x_{\text{bj}}^2), \quad (2.81)$$

where in the last equality we took the limit of small Bjorken x_{bj} . Since y and Q^2 are kept constant in this Regge-Gribov limit of QCD, Eq. 2.81 tells us that decreasing x_{bj} is directly related to increasing the rapidity separation between the projectile and the target¹⁰. Note that at leading order in x_{bj} , a change in Y is given solely by a change in x_{bj} where the latter variable is defined in terms of the momenta of the target and the exchanged virtual photon and not projectile. Many textbooks and papers often give the impression that the rapidity separation is between the target and the exchange virtual photon because only those momenta are needed to define x_{bj} and correspondingly Y , but such an impression is nonsensical because q^μ is a space-like momentum which cannot be related to a time-like momentum p^μ via a Lorentz boost.

Writing Eq. 2.78 in light-cone coordinates

$$\frac{1}{m_p} \begin{bmatrix} p^+ \\ p^- \end{bmatrix} = \begin{bmatrix} e^Y & 0 \\ 0 & e^{-Y} \end{bmatrix} \frac{1}{m_e} \begin{bmatrix} k^+ \\ k^- \end{bmatrix}, \quad (2.82)$$

where

$$p^\pm := \frac{1}{\sqrt{2}}(p^0 \pm p^3), \quad p^\pm := \frac{1}{\sqrt{2}}(k^0 \pm k^3), \quad (2.83)$$

one sees that in the rest frame of the projectile, the plus-component of the target's momentum is enhanced by a factor of e^Y while its minus-component is suppressed by a factor of e^{-Y} . Consequently, the target effectively lies along the x^+ -axis (at $x^- = 0$). In this frame, x^+ takes on the role of time and x^- becomes the longitudinal coordinate. Since it lies effectively along the x^+ -axis, the target is effectively Lorentz contracted to a Dirac delta function in the longitudinal

¹⁰The relation in Eq. 2.81 is written in many textbooks and papers as $Y = \ln(1/x_{\text{bj}})$ without any or much justification, and without mention of the constant logarithm.

direction and the stochastic dynamics (due to emission and recombination effects) of the gluons in the target are effectively frozen-in due to time dilation. From these considerations, the background field strength tensor can be written as

$$F^{\mu\nu}[b](x^+, x^-, \mathbf{x}) = \delta(x^-) F^{\mu\nu}[b](\mathbf{x}). \quad (2.84)$$

We consider the associated field strength tensor of the background field and not the background field directly because the field strength tensor is gauge covariant. Using Eq. 2.82, one finds that for large Y only

$$F^{+i}[b](x^+, x^-, \mathbf{x}) = \delta(x^-) \partial^i F^{+i}[b](\mathbf{x}) =: \delta(x^-) \partial^i \beta(\mathbf{x}), \quad (2.85)$$

is boost enhanced [9] by e^Y where $\beta(\mathbf{x}) = \beta^a(\mathbf{x}) t^a$ is an as-yet-unspecified $\mathfrak{su}(N_c)$ -valued function describing the distribution of gluons in the transverse plane and t^a are the generators of $\mathfrak{su}(N_c)$. Since Eq. 2.85 carries the dominant contribution, one may choose the background field to be [9]

$$b^\mu(x^+, x^-, \mathbf{x}) = g_+^\mu \delta(x^-) \beta(\mathbf{x}). \quad (2.86)$$

As mentioned earlier, this background field is large being of the order of α_s^{-1} . In the presence of a large background field, one needs to rewrite the perturbation theory as an expansion around b^μ instead of the vacuum; this is the topic of the next chapter.

Chapter 3

Eikonalization at high energies

3.1 Perturbation theory in the presence of a large external field

In this section, we shall demonstrate the downfall of using vacuum perturbation theory for an interacting theory in the presence of a large external source with the aid of a toy example¹. In particular, we shall show that in the iterative solution to the tree-level Dyson-Schwinger equation for the connected 1-point Green's function in the presence of a large external source, each term contributes the same order. Since each diagram contributes equally, one needs to sum every term in the perturbative expansion which renders the expansion meaningless and computationally intractable. This problem can be side-stepped by expanding the interacting theory not around the vacuum but around the tree-level connected 1-point Green's function.

3.1.1 Example: an interacting real-valued scalar field

To this end, consider a theory for an interacting real-valued scalar field on Minkowski space $\phi : \mathbb{R}^{1,3} \rightarrow \mathbb{R}$ of mass m coupled to an external source $J : \mathbb{R}^{1,3} \rightarrow \mathbb{R}$ described by the Lagrangian

$$\mathcal{L}[\phi, J](x) = \mathcal{L}[\phi](x) + J(x)\phi(x) = \mathcal{L}_0[\phi](x) + \mathcal{L}_{\text{int}}[\phi](x) + J(x)\phi(x), \quad (3.1)$$

where the “free” Lagrangian $\mathcal{L}_0[\phi]$, which governs the dynamics of the scalar field in the absence of self-interactions, is the Klein-Gordon Lagrangian

$$\mathcal{L}_0[\phi](x) = -\frac{1}{2}\phi(x)(\Box_x + m^2)\phi(x), \quad (3.2)$$

¹For a review of the path integral formulation of QFT which we shall use below, read chapters 2 through 4 of [16].

and $\mathcal{L}_{\text{int}}[\phi]$ describes the interaction of the scalar field with itself. Unlike in most textbooks, we shall regard the external source to be a physical entity. Here the dynamics of the external source are assumed to be known and unmodified by the presence of the scalar field. The converse, however, is not true and we are interested in understanding the dynamics of the scalar field in reaction to the external source.

The following definitions are necessary for our derivation and discussion of the Dyson-Schwinger (DS) equations in the next subsection. The n -point Green's functions *in the presence of the external source* J (or n -point functions for short) are defined by

$$G^{(n)}[J](x_1, \dots, x_n) := \langle \Omega | T \{ \phi(x_1) \cdots \phi(x_n) \} | \Omega \rangle_J, \quad (3.3)$$

where

$$\langle \Omega | T \{ \phi(x_1) \cdots \phi(x_n) \} | \Omega \rangle_J := \frac{1}{N} \int D[\phi] \phi(x_1) \cdots \phi(x_n) \exp \left[i \int d^4x \mathcal{L}[\phi, J](x) \right]. \quad (3.4)$$

is the expectation value of the time-ordered product of n scalar field insertions at n space-time positions computed in the vacuum $|\Omega\rangle$ of interacting theory in the presence of the external source J . Let us introduce the generating functional for the n -point functions

$$Z[J] = \frac{1}{N} \int D[\phi] \exp \left[i \int d^4x \mathcal{L}[\phi, J](x) \right], \quad (3.5)$$

where N is an overall normalization constant defined such that $Z[0] = 1$. Then the n -point function in Eq. 3.3 can be obtained from $Z[J]$ via

$$G^{(n)}[J](x_1, \dots, x_n) = \frac{\delta^n Z[J]}{\delta i J(x_1) \cdots \delta i J(x_n)}, \quad (3.6)$$

justifying the name “generating functional”. $Z[J]$ can be rewritten as

$$Z[J] = \exp \left[i \int d^4x \mathcal{L}_{\text{int}} \left[\frac{\delta}{\delta(iJ)} \right] (x) \right] Z_0[J], \quad (3.7)$$

where

$$Z_0[J] = \frac{1}{N} \int D[\phi] \exp \left[i \int d^4x (\mathcal{L}_0[\phi](x) + J(x)\phi(x)) \right], \quad (3.8)$$

is the generating functional in the free theory. In fact, $Z_0[J]$ is a functional Gaussian integral which can be computed by completing the square in the argument of the exponential (see Chapter 1 of [16]). The result of this functional Gaussian integral is

$$Z_0[J] = \exp \left[-\frac{i}{2} \int d^4x d^4x' J(x) \Delta_F(x - x') J(x') \right], \quad (3.9)$$

where

$$i\Delta_F(x - x') =: \bullet \xrightarrow{x \quad x'} \bullet, \quad (3.10)$$

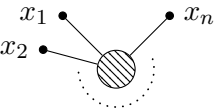
is the Feynman propagator in the free theory; the propagator is the functional inverse of the differential operator $(\square + m^2)$ appearing in the term quadratic in ϕ in $\mathcal{L}_0[\phi]$ in Eq. 3.1. The free Feynman propagator satisfies the differential equation

$$(\square_x + m^2)i\Delta_F(x - x') = -i\delta^{(4)}(x - x'). \quad (3.11)$$

$Z[J]$ can also be written in terms of the generating functional $W[J]$ for the connected n -point functions via

$$Z[J] = e^{iW[J]}, \quad (3.12)$$

where the interpretation of $W[J]$ can be shown using the replica trick from statistical physics [29]. The connected n -point functions are defined by

$$G_{\text{con}}^{(n)}[J](x_1, \dots, x_n) := \frac{\delta^n iW[J]}{\delta iJ(x_1) \cdots \delta iJ(x_n)} =: \begin{array}{c} x_1 \bullet \\ \diagdown \\ \text{---} \bullet \text{---} \\ \diagup \\ x_2 \bullet \end{array} \begin{array}{c} \bullet x_n \\ \diagup \\ \text{---} \bullet \text{---} \\ \diagdown \\ \bullet x_2 \end{array} \quad (3.13)$$


3.1.1.1 The Dyson-Schwinger equations

The Dyson-Schwinger equations are the quantum equations of motion for the n -point functions. These equations can be derived using the Symanzik construction (see Chapter 1.3 of [15]) which does not rely on the path integral formulation of QFT, but we shall not take this route. Instead, consider the following one-parameter family of local variations

$$\phi(x) \mapsto \phi_s(x; x_0) := \phi(x) + s\delta^{(4)}(x - x_0), \quad (3.14)$$

which leaves the functional measure in Eq. 3.5 invariant. Substituting Eq. 3.14 into $Z[J]$ in Eq. 3.5 yields

$$\begin{aligned} Z[J] &= \frac{1}{N} \int D[\phi] \exp \left[i \int d^4x (\mathcal{L}[\phi_s](x; x_0) + J(x)\phi_s(x; x_0)) \right] \\ &= \frac{1}{N} \int D[\phi] \exp \left[\int d^4y s \delta^{(4)}(y - x_0) \frac{\delta}{\delta \phi(y)} \right] \exp \left[i \int d^4x (\mathcal{L}[\phi](x) + J(x)\phi(x)) \right] \\ &= \frac{1}{N} \int D[\phi] \exp \left[s \frac{\delta}{\delta \phi(x_0)} \right] \exp \left[i \int d^4x (\mathcal{L}[\phi](x) + J(x)\phi(x)) \right]. \end{aligned} \quad (3.15)$$

where in the second line we introduced the translation operator². Differentiating both sides of Eq. 3.15 with respect to s at $s = 0$ we obtain

$$0 = \frac{1}{N} \int D[\phi] \frac{\delta}{\delta \phi(x_0)} \exp \left[i \int d^4x (\mathcal{L}[\phi](x) + J(x)\phi(x)) \right], \quad (3.16)$$

which leads to first Dyson-Schwinger equation

$$(\square_{x_0} + m^2) \frac{\delta Z[J]}{\delta iJ(x_0)} = \left[\mathcal{L}'_{\text{int}} \left[\frac{\delta}{\delta iJ} \right] (x_0) + J(x_0) \right] Z[J]. \quad (3.17)$$

For concreteness, let us restrict our attention to ϕ^4 theory where the interaction Lagrangian is given by

$$\mathcal{L}_{\text{int}}[\phi](x) = -\frac{g^2}{4!} \phi^4(x). \quad (3.18)$$

Then using Eq. 3.12 to write $Z[J] = e^{iW[J]}$, Eq. 3.17 becomes

$$(\square_{x_0} + m^2) \frac{\delta iW[J]}{\delta iJ(x_0)} = -\frac{g^2}{3!} \left[\left(\frac{\delta iW[J]}{\delta iJ(x_0)} \right)^3 + 3 \frac{\delta^2 iW[J]}{\delta (iJ(x_0))^2} \frac{\delta iW[J]}{\delta iJ(x_0)} + \frac{\delta^3 iW[J]}{\delta (iJ(x_0))^3} \right] + J(x_0). \quad (3.19)$$

Multiplying both sides of Eq. 3.19 by $i\Delta_F(x - x_0)$ and integrating over $x_0 \in \mathbb{R}^{1,3}$ we obtain

$$\begin{aligned} \frac{\delta iW[J]}{\delta iJ(x)} &= -i \frac{g^2}{3!} \int d^4x_0 i\Delta_F(x - x_0) \left[\left(\frac{\delta iW[J]}{\delta iJ(x_0)} \right)^3 + 3 \frac{\delta^2 iW[J]}{\delta (iJ(x_0))^2} \frac{\delta iW[J]}{\delta iJ(x_0)} + i \frac{\delta^3 iW[J]}{\delta (iJ(x_0))^3} \right] \\ &\quad + i \int d^4x_0 i\Delta_F(x - x_0) J(x_0). \end{aligned} \quad (3.20)$$

Using the Feynman rules defined in Eq. 3.10 and Eq. 3.13 as well as those defined below

$$i \int d^4x_0 i\Delta_F(x - x_0) J(x_0) =: \begin{array}{c} x \\ \bullet \text{---} \bigcirc(J) \end{array}, \quad ig^2 \int d^4x_0 =: \begin{array}{c} x_0 \\ | \\ \bullet \end{array}, \quad (3.21a)$$

Eq. 3.19 can be expressed diagrammatically as

$$\begin{array}{c} x \\ \bullet \text{---} \text{shaded circle} \end{array} = \begin{array}{c} x \\ \bullet \text{---} \bigcirc(J) \end{array} - \frac{1}{3!} \left[\begin{array}{c} \text{shaded circle} \quad \text{shaded circle} \\ \diagup \quad \diagdown \\ x \text{---} \bullet \text{---} \text{shaded circle} \end{array} + 3 \begin{array}{c} \text{shaded circle} \\ \text{loop} \\ x \text{---} \bullet \text{---} \text{shaded circle} \end{array} + \begin{array}{c} x \text{---} \bullet \text{---} \text{shaded circle} \\ \text{loop} \end{array} \right]. \quad (3.22)$$

Notice that the Dyson-Schwinger equation for the connected 1-point function depends on itself as well as the connected 2- and 3-point functions. Taking a functional derivative of Eq. 3.19 with

² $e^{a \frac{d}{dx}} f(x) = \sum_{n=0}^{\infty} \frac{a^n}{n!} f^{(n)}(x) = f(x + a)$.

respect to $iJ(y)$, we obtain the Dyson-Schwinger equation for the connected 2-point function

$$\begin{aligned}
 x \text{---} \textcircled{\bullet} \text{---} y &= x \text{---} y - \frac{1}{3!} \left[3 \left(x \text{---} \textcircled{\bullet} \text{---} y \right) + 3 \left(x \text{---} \textcircled{\bullet} \text{---} y \right) \right. \\
 &\quad \left. + x \text{---} \textcircled{\bullet} \text{---} y \right] + x \text{---} \textcircled{\bullet} \text{---} y. \tag{3.23}
 \end{aligned}$$

which depends on itself and the connected 1-pt function as well as the connected 3- and 4-point functions. This process continues ad infinitum, generating an infinite hierarchy of equations where the Dyson-Schwinger equation for the connected n -point function depends on itself and all preceding lower order connected functions as well as the connected $(n+1)$ - and $(n+2)$ -point functions.

3.1.1.2 A semi-classical truncation

In order to solve the infinite hierarchy of Dyson-Schwinger equations, we need to introduce a truncation that renders the system in some sense “finite”. Clearly if we were to a first-approximation ignore the loop diagrams (cf. Eq. 3.22 and Eq. 3.23), then the hierarchy would close; the Dyson-Schwinger equation for the connected n -point function would depend only on itself and all preceding lower-order connected functions. It turns out that such a loop expansion (zero loops, 1 loop, 2-loops, etc.) is equivalent to an expansion in \hbar ; the number of loops in a Feynman diagram counts the power of \hbar .

Before proving this equivalence, it is useful to derive a formula for the number of loops n_L in a Feynman diagram in terms of the the number of vertices n_V and the number of internal propagators n_I (excluding those connected to the external source). Consider an arbitrary Feynman diagram in ϕ^4 theory with n_V vertices. Each vertex has four legs which need to be saturated. Each internal propagator saturate two legs, each external propagator saturates one leg, and each external source term saturates one leg. Consequently,

$$4n_V = 2n_I + n_E + n_J, \tag{3.24}$$

where n_E counts the number of external legs and n_J counts the number of external source terms. The maximum number of loops that can be contained in a connected Feynman diagram in ϕ^4 theory with n_V vertices is

$$n_{L,\max} = n_V + 1, \tag{3.25}$$

where each vertex contains a single loop constructed by saturating two of the four legs with an internal propagator, and then the remaining two legs on each vertex are used to connect the vertex to other vertices such that the diagram is connected. For every internal propagator that is cut, there are the two newly created free legs that can be saturated either by two external propagators, two external source terms or one of each. From this consideration, one can also write down

$$n_{L,\max} = n_L + \frac{1}{2}(n_E + n_J). \quad (3.26)$$

Equating Eq. 3.25 and Eq. 3.26, one obtains

$$n_V + 1 = n_L + \frac{1}{2}(n_E + n_J). \quad (3.27)$$

Using Eq. 3.24, one can eliminate n_E and n_J from Eq. 3.27 to produce

$$n_L = n_I - n_V + 1. \quad (3.28)$$

In order to count the power of \hbar associated with a connected Feynman diagram, one needs to reintroduce a factor of \hbar into the exponent of $Z[J]$ in 3.5 since we had been working in natural units where $\hbar = 1$. The factor of \hbar is reintroduced by multiplying the Lagrangian by \hbar^{-1} . The net result of reintroducing \hbar is that each vertex carries a factor of \hbar^{-1} while each propagator (both internal and external) carries a factor of \hbar . Vertex legs which are connected to an external source term via a propagator do not contribute to the counting of the power of \hbar because the \hbar from the propagator is compensated by the \hbar^{-1} from the external source term. Consequently, the power of \hbar associated with a connected Feynman diagram is

$$\text{pow}(\hbar) = n_I - n_V + n_E = n_L + n_E - 1, \quad (3.29)$$

where the second equality follows from Eq. 3.28. The implication of Eq. 3.29 is that for a fixed number of external propagators, the number of loops in a connected Feynman diagram determines the associated power of \hbar , and vice versa. One refers to leading order in \hbar as “classical” and higher orders as “quantum”. The fact that loops are a quantum effect is not surprising since loops represent the interaction of the scalar field with itself and self-interaction is an inherently quantum phenomenon.

$$x \text{---} \textcircled{\times}_T = x \text{---} \textcircled{J} - \frac{1}{3!} x \begin{array}{c} \diagup \textcircled{\times}_T \\ \bullet \\ \diagdown \textcircled{\times}_T \end{array} \text{---} \textcircled{\times}_T, \quad (3.30)$$
$$x \text{---} \textcircled{\text{shaded}}_{\text{T}} = x \text{---} (J) - \frac{1}{6} x \text{---} \textcircled{J} + \frac{1}{12} x \text{---} \textcircled{J} \text{---} \textcircled{J} + \frac{1}{12} x \text{---} \textcircled{J} \text{---} \textcircled{J} \text{---} \textcircled{J} + \dots \quad (3.31)$$
$$\begin{array}{c}
\text{---} \bullet \text{---} \text{---} \bullet \text{---} \\
\text{---} \bullet \text{---} \bullet \text{---}
\end{array}
= \frac{1}{2} \begin{array}{c}
\text{---} \bullet \text{---} \bullet \text{---} \\
\text{---} \bullet \text{---} \bullet \text{---}
\end{array}
\quad (3.32)$$
$$\begin{array}{c} \text{\scriptsize x} \\ \bullet \end{array} \text{\scriptsize y} \begin{array}{c} \diagdown \\ \text{\scriptsize T} \\ \diagup \end{array} \bullet = \begin{array}{c} \text{\scriptsize x} \\ \bullet \end{array} \begin{array}{c} \text{\scriptsize y} \\ \bullet \end{array} - \frac{1}{2} \begin{array}{c} \text{\scriptsize x} \\ \bullet \end{array} \begin{array}{c} \diagdown \\ \text{\scriptsize T} \\ \diagup \end{array} \begin{array}{c} \text{\scriptsize y} \\ \bullet \end{array} + \frac{1}{4} \begin{array}{c} \text{\scriptsize x} \\ \bullet \end{array} \begin{array}{c} \diagdown \\ \text{\scriptsize T} \\ \diagup \end{array} \begin{array}{c} \text{\scriptsize y} \\ \bullet \end{array} + \dots . \quad (3.33)$$

Since the connected 1-point function is $\mathcal{O}(g^{-1})$, each term in Eq. 3.33 is $\mathcal{O}(g^0)$. Since each diagram contributes the same order of the coupling, again one needs to sum all diagrams in order to iteratively solve Eq. 3.32. Eq. 3.33 can, however, be formally summed using the operator

version of the geometric series. To this end, we define the following additional Feynman rules

$$\left[\begin{array}{c} \text{diagram with two shaded circles labeled T connected to a central vertex, which is connected to a horizontal line segment} \end{array} \right]_{xy} = \begin{array}{c} \text{diagram with two shaded circles labeled T connected to a central vertex, which is connected to a horizontal line segment} \\ x \qquad y \end{array} = i \int d^4 z \left(\frac{\delta i W[J]}{\delta i J(x)} \right)^2 \delta^{(4)}(x-z) i \Delta_F(z-y), \quad (3.34a)$$

$$\left[\begin{array}{c} \text{diagram with two shaded circles labeled T connected to a central vertex, which is connected to a horizontal line segment} \end{array} \right]_{xy}^0 = [1]_{xy} = \delta^{(4)}(x-y) \quad (3.34b)$$

$$\begin{aligned} \left[\begin{array}{c} \text{diagram with two shaded circles labeled T connected to a central vertex, which is connected to a horizontal line segment} \end{array} \right]_{xy}^2 &= \left[\begin{array}{c} \text{diagram with two shaded circles labeled T connected to a central vertex, which is connected to a horizontal line segment} \end{array} \right]_{xz} \times \left[\begin{array}{c} \text{diagram with two shaded circles labeled T connected to a central vertex, which is connected to a horizontal line segment} \end{array} \right]_{zy} \\ &= \int d^4 z \left[\begin{array}{c} \text{diagram with two shaded circles labeled T connected to a central vertex, which is connected to a horizontal line segment} \end{array} \right]_{xz} \left[\begin{array}{c} \text{diagram with two shaded circles labeled T connected to a central vertex, which is connected to a horizontal line segment} \end{array} \right]_{zy} = \begin{array}{c} \text{diagram with two shaded circles labeled T connected to a central vertex, which is connected to a horizontal line segment} \\ x \qquad y \end{array} \end{aligned} \quad (3.34c)$$

where in analogy to the summation over repeated indices in matrix multiplication, we defined the product of two Feynman diagram nodes by the integral over a dummy space-time variable

$$\text{---} \times \text{---} = \int d^4 z \text{---}^z \text{---} . \quad (3.35)$$

Using Eq. 3.34, we write down a formal solution for the tree-level connected 2-point function as

$$\begin{aligned} x \text{---} \text{---} y &= \left[\text{---} \times \sum_{n=0}^{\infty} \frac{(-g^2)^n}{2^n} \left[\begin{array}{c} \text{diagram with two shaded circles labeled T connected to a central vertex, which is connected to a horizontal line segment} \end{array} \right]^n \right]_{xy} \\ &= \left[\text{---} \times \left[1 + \frac{g^2}{2} \begin{array}{c} \text{diagram with two shaded circles labeled T connected to a central vertex, which is connected to a horizontal line segment} \end{array} \right]^{-1} \right]_{xy} . \end{aligned} \quad (3.36)$$

Our above analysis of the tree-level connected 1-point function shows that standard (vacuum) perturbation theory in the presence of a large external source is no longer a useful calculational tool, because the relevant dynamical degrees of freedom are not fluctuations around the vacuum, but fluctuations around the tree-level connected 1-point function. The correct approach in such a situation is to expand the Lagrangian around the tree-level connected 1-point function which we shall do shortly. For notational brevity, we introduce the following mathematical symbol for

the tree-level connected 1-point function (also called the “classical field” [16])

$$\varphi_c[J](x) := \frac{\delta iW[J]}{\delta iJ(x)} = \text{diagram: a dot labeled } x \text{ connected to a shaded circle labeled } T, \quad (3.37)$$

which satisfies the classical equations of motion (cf. Eq. 3.19 and Eq. 3.30)

$$(\square_x + m^2)\varphi_c[J](x) + \frac{g^2}{3!}\varphi_c^3[J](x) = J(x). \quad (3.38)$$

Consider the following expansion of $\mathcal{L}[\varphi_c[J] + \delta\varphi, J]$ around the classical field $\varphi_c[J]$

$$\begin{aligned} \mathcal{L}[\varphi_c[J] + \delta\varphi, J](x) &= \sum_{n=0}^{\infty} \frac{1}{n!} \int d^4x_1 \cdots d^4x_n \delta\varphi(x_1) \cdots \delta\varphi(x_n) \left. \frac{\delta^n \mathcal{L}[\phi, J](x)}{\delta\phi(x_1) \cdots \delta\phi(x_n)} \right|_{\phi=\varphi_c[J]} \\ &= \mathcal{L}[\varphi_c[J], J](x) - \frac{1}{2} \delta\varphi(x) \left[\square_x + m^2 + \frac{g^2}{2} \varphi_c^2[J](x) \right] \delta\varphi(x) - \frac{g^2}{3!} \delta\varphi^3(x) \varphi_c[J](x) - \frac{g^2}{4!} \delta\varphi^4(x). \end{aligned} \quad (3.39)$$

The term linear in $\delta\varphi$ in Eq. 3.39 vanishes due to the equations of motion for classical field given in Eq. 3.38. The inverse of the differential operator in the term quadratic in $\delta\varphi$ is precisely the propagator in the presence of the external source J given in Eq. 3.36; the tree-level connected 2-point function is the propagator for ϕ^4 theory expanded about the classical field.

3.2 Observables at small Bjorken x_{bj} , Wilson-lines and their correlators

One of the goals of the previous section was to show that in the presence of a large external source, vacuum perturbation theory breaks down because the smallness of the coupling constant is compensated for by the largeness of the external source. This breakdown was shown in the iterative solution to the DS equation for the tree-level propagator where each diagram in the series contributed the same order in the coupling. Consequently, the entire series needed to be resummed. The resummed propagator, which encoded the multiple interactions with the external source, was also shown to be precisely the propagator for fluctuations $\delta\varphi$ on top of the large tree-level 1-point function $\varphi_c[J] \sim \mathcal{O}(g^{-1})$.

An analogous resummation occurs in the CGC formalism. Recall that the gauge field A^μ can be split into fluctuations δA^μ on top of the large background field b^μ where the latter describes the kinematically enhanced gluonic contributions in the target at small Bjorken x_{bj} . This split is given in Eq. 2.76. One can think of b^μ , whose most constrained form is given in Eq. 2.86, as analogous to the large tree-level 1-point function of the previous section. In this case, since $b^\mu \sim \mathcal{O}(\alpha_s^{-1})$ one needs to expand the QCD Lagrangian density around b^μ and derive modified

where t^c are the generators of the fundamental representation.

For a propagator corresponding to a given parton, the Wilson-lines encode multiple eikonal interactions of the parton with b^μ along the (approximately) light-like trajectory of the parton [14]. In this sense the propagator is analogous to the resummed propagator derived in the previous section, encoding multiple interactions with the external source through the tree-level connected 1-point function. In the absence of the background field, one would expect the above propagators to reduce to the standard propagators for quarks and gluons and indeed this is the case. However, since the background field has Dirac delta function support in the x^- -direction, the Wilson-lines are only “triggered” when the parton passes through the background field which means that in general the parton propagates freely and upon passing the background field picks up a colour rotation before propagating freely again.

Although the expressions for the Wilson-lines given in Eq. 3.40d and Eq. 3.41b are mathematically correct, they become cumbersome when computing integrals where these Wilson-lines appear in the integrand. For the moment let me write down a light-like Wilson-line in a general representation R as

$$U_{z;y^-,x^-}^R = P \exp \left[ig \int_{x^-}^{y^-} dz^- \delta(z^-) \beta^c(z) t^c \right], \quad (3.42)$$

where t^c are generators of the R representation. Provided Eq. 3.42 is not being differentiated, if it appears under an integral over the longitudinal coordinates x^- and y^- , then given the Dirac delta function support of the background field one can replace the right-hand-side of Eq. 3.42 by the expression

$$U_{z;x^-,y^-}^R = \theta(-x^-)\theta(y^-)U_z^R + \theta(x^-)\theta(-y^-)U_z^{\dagger R} + [\theta(x^-)\theta(y^-) + \theta(-x^-)\theta(-y^-)]\mathbb{1}, \quad (3.43)$$

where

$$U_z^R := U_{z;-\infty,\infty}^R, \quad U_z^{\dagger R} := U_{z;\infty,-\infty}^R, \quad (3.44)$$

are infinite light-like Wilson-lines in the representation R . Clearly Eq. 3.43 can be applied to the Wilson-lines in Eq. 3.40d and Eq. 3.41b. Consequently, we expect that observables calculated using the propagators for quarks and gluons should contain infinite light-like Wilson-lines in the fundamental and the adjoint representations, respectively.

These Wilson-lines always enter observables through Y dependent averages called correlators. To see why, recall that the background field although constrained by kinematics is still undetermined; it is expressed in terms of an as-yet-unspecified $\mathfrak{su}(N_c)$ -valued function $\beta(\mathbf{x}) = \beta^a(\mathbf{x})t^a$

(see Eq. 2.86). Consequently, when computing any observable, one needs to average over all possible background field configurations. But the separation of the gauge field into fluctuations on top of the background field (see Eq. 2.76) is a resolution dependent one: as Bjorken x_{bj} is lowered or, correspondingly, the rapidity separation Y is increased, additional modes which were previously contained in δA^μ will begin to take on the features of b^μ through Lorentz contraction and time dilation. Accordingly, one writes the averaging procedure over the background field as Y dependent

$$\langle \cdots \rangle (Y) = \int D[b^+] \cdots W_Y[b^+], \quad (3.45)$$

where $W_Y[b^+]$ is a Y dependent functional distribution. However, since the only place where the background field can enter an observable is through Wilson-lines, we can just as easily perform the average over Wilson-lines instead of the background field, in which case Eq. 3.45 becomes

$$\langle \cdots \rangle (Y) = \int_{\text{SU}(N_c)} D[U] \cdots Z_Y[U], \quad (3.46)$$

where $D[U]$ is the unimodular Haar measure on $\text{SU}(N_c)$. The functional distributions are such that the averaging procedure is normalized to 1; i.e. $\langle 1 \rangle (Y) = 1$.

Putting the above discussion into action, one can compute the total cross-section for DIS at small Bjorken x_{bj} using the optical theorem and standard perturbation theory except with the quark propagator given by Eq. 3.41a [9] and the result is

$$\sigma_{\text{DIS}}(Y, Q^2) = \sum_{\lambda=T,L} \int d^2r \int_0^1 d\alpha |\psi_\lambda(\alpha, r^2, Q^2)|^2 \int d^2b \, 2 \left(1 - \text{Re} \left\langle \frac{1}{N_c} \text{Tr} (U_x U_y^\dagger) \right\rangle (Y) \right). \quad (3.47)$$

The sum over λ is a sum over both the transverse (T) and the longitudinal (L) polarizations of the virtual photon. The squared absolute value of the $q\bar{q}$ component of the virtual photon wave function, $|\psi_\lambda(\alpha, r^2, Q^2)|^2$, describes the probability for a virtual photon of polarization λ and virtuality Q^2 to split into a $q\bar{q}$ -pair of size r where the quark carries a fraction α of the incoming momentum q and the anti-quark carries the remaining $(1-\alpha)$ fraction. This contribution is given by

$$|\psi_\lambda(\alpha, r^2, Q^2)|^2 = \frac{3\alpha_{\text{em}}}{2\pi^2} \sum_f Q_f^2 \begin{cases} [\alpha^2 + (1-\alpha)^2] \bar{Q}^2 K_1^2(\bar{Q}r) + m_f^2 K_0^2(\bar{Q}r), & \text{if } \lambda = T \\ 4Q^2 \alpha^2 (1-\alpha)^2 K_0^2(\bar{Q}r), & \text{if } \lambda = L \end{cases}, \quad (3.48)$$

where there is a sum over quark flavors f , Q_f is the elementary charge fraction of the quark flavor (in units of e), m_f is the quark flavor's mass and $\bar{Q}^2 = \alpha(1-\alpha)Q^2 + m_f^2$.

The Y dependence of the total cross-section for DIS is given by the real part of a Wilson line correlator, the so-called dipole correlator or $q\bar{q}$ correlator

$$\langle \mathcal{A}_{xy}^{(1)} \rangle(Y) = \left\langle \frac{1}{N_c} \text{Tr} \left(U_x U_y^\dagger \right) \right\rangle(Y). \quad (3.49)$$

But this is by no means the only observable for which this is true. In general, observables computed within the CGC formalism are written in terms of Wilson-line correlators and these Wilson-line correlators carry the Y dependence of the observable. Other examples include inclusive vector-meson production [19], dijet production [30], medium-induced soft gluon radiation in hard forward parton scattering [31], and Single Transverse Spin Asymmetry (STSA) [32].

Chapter 4

Wilson-line correlators

In the previous chapter, it was argued that Wilson-line correlators appear ubiquitously in the saturation formalism description of observables. This chapter is dedicated to the construction and properties of Wilson-line correlators. In this chapter, I also introduce (relevant aspects of) the birdtrack formalism — a diagrammatic notation that is to group theory what Feynman diagrams are to perturbation theory — which I shall use extensively throughout the remainder of this thesis.

4.1 Birdtracks, colour singlet states, and Wilson-line amplitude matrices

This section collects a number of important definitions and establishes the notation that is used throughout the remainder of this thesis.

Let V be a complex vector space carrying the *fundamental representation* of $\mathrm{SU}(N_c)$, the group of special unitary $N_c \times N_c$ matrices. Since the dimension of V is

$$\dim(V) = N_c =: d_f, \tag{4.1}$$

V is isomorphic to \mathbb{C}^{N_c} and, without loss of generality, we can take $V = \mathbb{C}^{N_c}$. We endow V with the scalar product

$$\langle \cdot, \cdot \rangle : V \times V \rightarrow \mathbb{C}; (v_1, v_2) \mapsto \langle v_1, v_2 \rangle = v_1^\dagger v_2, \tag{4.2}$$

which is inherited from the canonical scalar product on \mathbb{C} . Here the dagger symbol † means the transposed conjugate.

The identity map on V , denoted $i_V : V \rightarrow V$, is a linear transformation on V whose matrix representation always has components $[i_V]^i_j = \delta^i_j$ (regardless of the choice of basis for V) where δ^i_j is the Kronecker delta symbol and the indices i, j run over $1, \dots, \dim(V)$. One can represent the identity map i_V and its matrix components $[i_V]^i_j$ in birdtrack notation [33] as

$$i_V := \longrightarrow, \quad [i_V]^i_j := i \longrightarrow_j = \delta^i_j, \quad (4.3)$$

respectively. Let \bar{V} be the dual space of V (the space of all linear functionals on V) which carries the anti-fundamental representation of $\mathrm{SU}(N_c)$. In general, we shall use left-pointing lines, as in Eq. 4.3, to denote lineal maps of the form $V \rightarrow V$ while right-pointing lines represent linear maps of the form $\bar{V} \rightarrow \bar{V}$.

Fundamental and anti-fundamental Wilson-lines are represented graphically by

$$\begin{aligned} U_x &:= \text{---} \triangleleft_x, & [U_x]^i_j &:= i \text{---} \triangleleft_x \text{---} j, \\ U_y^\dagger &:= \text{---} \triangleright_y = [U_y^*]^t, & [U_y^\dagger]^j_i &:= i \text{---} \triangleright_y \text{---} j = [U_y^*]^j_i, \end{aligned} \quad (4.4)$$

respectively, where the right-hand column denotes the matrix components (in some basis) of the Wilson-lines.

In birdtrack notation, contracting indices is depicted simply by connecting two birdtrack lines. For example, the dimension of the (anti-)fundamental representation may be depicted diagrammatically as

$$d_f, d_{\bar{f}} = \mathrm{Tr}(\mathbb{1}) = \delta^j_i \delta^i_j = \text{---} \triangleleft_i \triangleright_j = \bigcirc. \quad (4.5)$$

As another example, the dipole operator (which I shall write as $\mathcal{A}_{x;y}^{(1)}$) can be depicted in birdtrack notation as

$$\mathcal{A}_{x;y}^{(1)} = \frac{1}{d_f} \mathrm{Tr}(U_x U_y^\dagger) = \frac{1}{d_f} \delta^l_i [U_x]^i_j [U_y^\dagger]^j_k \delta^j_k = \frac{1}{d_f} \text{---} \triangleleft_i \triangleright_j \text{---} = \frac{1}{d_f} \bigcirc. \quad (4.6)$$

In the limit that the transverse coordinates x and y become coincident (i.e. $y \mapsto x$), then Eq. 4.6 reduces to

$$\mathcal{A}_{x;x}^{(1)} = \frac{1}{d_f} \mathrm{Tr}(U_x U_x^\dagger) = \frac{1}{d_f} \mathrm{Tr}(\mathbb{1}) = 1, \quad (4.7)$$

or in birdtrack notation

$$\mathcal{A}_{x;x}^{(1)} = \frac{1}{d_f} \bigcirc \text{---} \bigcirc = \frac{1}{d_f} \bigcirc = 1, \quad (4.8)$$

where we have distinguished the Wilson-lines with identified coordinates by a black-coloured arrow. As a matter of convention, whenever there is only one coincidence limit being taken

Wilson-lines with identified coordinates will be denoted by black-coloured arrows.

The tensor product space with m copies of V followed by \bar{m} copies of \bar{V} (for $m, \bar{m} \in \mathbb{N}$) is given by $V^{\otimes m} \otimes \bar{V}^{\otimes \bar{m}}$. Any element of $V^{\otimes m} \otimes \bar{V}^{\otimes \bar{m}}$ can be regarded as a (complex) multi-linear map of the form $\bar{V}^{\otimes m} \otimes V^{\otimes \bar{m}} \rightarrow \mathbb{C}$. The tensor product of m fundamental and \bar{m} anti-fundamental Wilson-lines, written

$$U_{x_1} \otimes \cdots \otimes U_{x_m} \otimes U_{y_1}^\dagger \otimes \cdots \otimes U_{y_{\bar{m}}}^\dagger, \quad (4.9)$$

is an element in the tensor-product representation of $SU(N_c)$ on $V^{\otimes m} \otimes \bar{V}^{\otimes \bar{m}}$. A *Wilson-line amplitude*¹ (of which Eq. 4.6 is the simplest example) is a complex-valued function of transverse coordinates formed by “sandwiching” a tensor product of Wilson-lines of the form given in Eq. 4.9 between two colour singlet states. A *colour singlet state* $|s\rangle \in V^{\otimes m} \otimes \bar{V}^{\otimes \bar{m}}$ is a tensor

$$|s\rangle = s^{i_1 \cdots i_m}_{\bar{i}_1 \cdots \bar{i}_{\bar{m}}} e_{i_1} \otimes \cdots \otimes e_{i_m} \otimes e^{\bar{i}_1} \otimes \cdots \otimes e^{\bar{i}_{\bar{m}}}, \quad (4.10)$$

(where $s^{i_1 \cdots i_m}_{\bar{i}_1 \cdots \bar{i}_{\bar{m}}}$ are the coefficients of $|s\rangle$ in some basis $e_{i_1} \otimes \cdots \otimes e_{i_m} \otimes e^{\bar{i}_1} \otimes \cdots \otimes e^{\bar{i}_{\bar{m}}}$ for $V^{\otimes m} \otimes \bar{V}^{\otimes \bar{m}}$) which, for all $U \in SU(N_c)$, satisfies

$$[U]^{i_1}_{j_1} \cdots [U]^{i_m}_{j_m} [U^\dagger]^{\bar{j}_1}_{\bar{i}_1} \cdots [U^\dagger]^{\bar{j}_{\bar{m}}}_{\bar{i}_{\bar{m}}} s^{i_1 \cdots i_m}_{\bar{i}_1 \cdots \bar{i}_{\bar{m}}} = s^{i_1 \cdots i_m}_{\bar{i}_1 \cdots \bar{i}_{\bar{m}}}, \quad (4.11)$$

or more compactly,

$$\underbrace{U \otimes \cdots \otimes U}_m \otimes \underbrace{U^\dagger \otimes \cdots \otimes U^\dagger}_{\bar{m}} |s\rangle = |s\rangle. \quad (4.12)$$

In other words, $|s\rangle$ is an invariant under *global* $SU(N_c)$ transformations. It is important to note that the group elements U appearing in Eq. 4.11 and Eq. 4.12 are all the *same* group element. One may replace these group elements with Wilson-lines U_x , provided that every Wilson-line is evaluated at the same transverse coordinate x .

We shall refer to the linear space of colour singlet states in $V^{\otimes m} \otimes \bar{V}^{\otimes \bar{m}}$ as the colour space of $V^{\otimes m} \otimes \bar{V}^{\otimes \bar{m}}$ and we shall denote this space by $\mathfrak{C}(SU(N_c); V^{\otimes m} \otimes \bar{V}^{\otimes \bar{m}})$ or more simply $\mathfrak{C}(V^{\otimes m} \otimes \bar{V}^{\otimes \bar{m}})$. If it is clear which tensor-product (base) space we are working with, we shall simply write *colour space* without explicit reference to the base space. For $\bar{m} \neq m$, there exists an $|s\rangle \in V^{\otimes m} \otimes \bar{V}^{\otimes \bar{m}}$ satisfying Eq. 4.12 if and only if there exist positive integers $a, b \in \mathbb{N}^+$ such that $m - a N_c = n - b N_c =: k$, in which case $|s\rangle$ can be mapped onto an equivalent colour singlet state on the base space $V^{\otimes k} \otimes \bar{V}^{\otimes k}$ which has the same number of quark and anti-quark legs [34]. Therefore, it is sufficient to only study colour space for $\bar{m} = m$. We shall restrict our attention to this case for the remainder of this thesis.

¹We shall distinguish Wilson-line amplitudes from Wilson-line correlators with the latter being the target average of the former.

Having argued that it is sufficient to consider only the case when the number of quarks equals the number of anti-quarks ($m = \bar{m}$), for ease of adding quark–anti-quark pairs (which we shall want to do a little later) it is more natural to work with the following tensor-product space

$$W^{\otimes m}, \quad W = V \otimes \bar{V}, \quad (4.13)$$

as opposed to $V^{\otimes m} \otimes \bar{V}^{\otimes m}$ even though the two tensor-product spaces are canonically isomorphic. The tensor-product representation of $\text{SU}(N_c)$ on $W^{\otimes m}$ (which is canonically isomorphic to Eq. 4.9 for $m = \bar{m}$) can be depicted in birdtrack notation as

$$(U_{\mathbf{x}_1} \otimes U_{\mathbf{y}_1}^\dagger) \otimes \cdots \otimes (U_{\mathbf{x}_m} \otimes U_{\mathbf{y}_m}^\dagger) =: \left. \begin{array}{c} \text{---} \text{---} \text{---} \\ \text{---} \text{---} \text{---} \\ \vdots \\ \text{---} \text{---} \text{---} \\ \text{---} \text{---} \text{---} \end{array} \right\} m \text{ pairs}, \quad (4.14)$$

where the Wilson-line symbols are labeled from top to bottom $\mathbf{x}_1, \mathbf{y}_1, \dots, \mathbf{x}_m, \mathbf{y}_m$. The advantage of using $W^{\otimes m}$ instead of $V^{\otimes m} \otimes \bar{V}^{\otimes m}$ is that one can easily add a quark–anti-quark pair (represented by the tensor product of a fundamental with an anti-fundamental Wilson-line) to Eq. 4.14 by appending the pair to the bottom of the diagram

$$\left. \begin{array}{c} \text{---} \text{---} \text{---} \\ \vdots \\ \text{---} \text{---} \text{---} \end{array} \right\} m \text{ pairs} \xrightarrow{\text{add a } q\bar{q} \text{ pair}} \left. \begin{array}{c} \text{---} \text{---} \text{---} \\ \vdots \\ \text{---} \text{---} \text{---} \\ \text{---} \text{---} \text{---} \\ \text{---} \text{---} \text{---} \end{array} \right\} (m+1) \text{ pairs} . \quad (4.15)$$

In birdtrack notation, $|s\rangle \in \mathfrak{C}(W^{\otimes m})$ is written

$$|s\rangle =: m \text{ pairs} \left\{ \begin{array}{c} \text{---} \text{---} \text{---} \\ \vdots \\ \text{---} \text{---} \text{---} \end{array} \right\} s, \quad (4.16)$$

and the analogue of Eq. 4.11 is represented by

$$\begin{array}{c} i_1 \text{---} j_1 \text{---} \\ \bar{i}_1 \text{---} \bar{j}_1 \text{---} \\ \vdots \\ i_m \text{---} j_m \text{---} \\ \bar{i}_m \text{---} \bar{j}_m \text{---} \end{array} \left\{ \begin{array}{c} \text{---} \text{---} \text{---} \\ \vdots \\ \text{---} \text{---} \text{---} \end{array} \right\} s = \begin{array}{c} i_1 \text{---} \\ \bar{i}_1 \text{---} \\ \vdots \\ i_m \text{---} \\ \bar{i}_m \text{---} \end{array} \left\{ \begin{array}{c} \text{---} \text{---} \text{---} \\ \vdots \\ \text{---} \text{---} \text{---} \end{array} \right\} s = \begin{array}{c} i_1 \text{---} \\ \bar{i}_1 \text{---} \\ \vdots \\ i_m \text{---} \\ \bar{i}_m \text{---} \end{array} \left\{ \begin{array}{c} \text{---} \text{---} \text{---} \\ \vdots \\ \text{---} \text{---} \text{---} \end{array} \right\} s, \quad (4.17)$$

where the black-coloured Wilson-line symbols all share the same transverse coordinate.

Let $\mathfrak{B}_{\text{ON}}(\text{SU}(N_c); W^{\otimes m})$ or more simply $\mathfrak{B}_{\text{ON}}(W^{\otimes m})$ denote an orthonormal (ON) basis for colour space, where the i^{th} basis element is labeled $|m; i\rangle$. For $|m; i\rangle, |m; j\rangle \in \mathfrak{B}_{\text{ON}}(W^{\otimes m})$, the probability for the colour singlet state $|m; j\rangle$ representing a colour component of the wave function for m quarks and m anti-quarks in the asymptotic “past” (with respect to the minus light-cone direction) to transition into the colour singlet state $|m; i\rangle$ in the asymptotic “future”

in the presence of the shock-wave background field of the target is given by the square of the amplitude

$$\langle m; i | U_{x_1} \otimes \cdots \otimes U_{x_m} \otimes U_{y_1}^\dagger \otimes \cdots \otimes U_{y_m}^\dagger | m; j \rangle = \text{Diagram}, \quad (4.18)$$

where the “time” evolution operator sandwiched between the in and out basis states is precisely the tensor-product given in Eq. 4.14. We shall label the amplitude in Eq. 4.18 by

$$(4.18) = \mathcal{A}_{ij}^{(m)}[U_{x_1}, \dots, U_{x_m}; U_{y_1}^\dagger, \dots, U_{y_m}^\dagger] = [\mathcal{A}_{x_1 \dots x_m; y_1 \dots y_m}^{(m)}]_{ij} = [\mathcal{A}_{\vec{x}; \vec{y}}^{(m)}]_{ij}, \quad (4.19)$$

where \vec{x} and \vec{y} (seen in the last equality above) are compact notation for

$$\vec{x} = \begin{pmatrix} x_1 \\ \vdots \\ x_m \end{pmatrix}, \quad \vec{y} = \begin{pmatrix} y_1 \\ \vdots \\ y_m \end{pmatrix}. \quad (4.20)$$

Eq. 4.18 may be regarded as the i^{th} row and j^{th} column of the $q^m \bar{q}^m$ Wilson-line amplitude matrix. For $m \leq N_c$, the dimension of colour space is $m!$ [34] which means that the $q^m \bar{q}^m$ amplitude matrix is a matrix in $\text{Mat}_m!(\mathbb{C})$. With Eq. 4.18 computed as an expectation value in a basis of colour singlet states, any amplitude consisting of m fundamental and m anti-fundamental Wilson-lines can be expressed as a linear combination of elements from this $q^m \bar{q}^m$ amplitude matrix. In the limit that all transverse coordinates become coincident (i.e. the same) Eq. 4.18 reduces to

$$[\mathcal{A}_{x_1 \dots x_1; x_1 \dots x_1}^{(m)}]_{ij} := \text{Diagram} = \text{Diagram} = \delta_{ij}. \quad (4.21)$$

The second equality in Eq. 4.21 follows from Eq. 4.17 and the third one from the orthonormality of the basis colour singlet states. As mentioned previously in this section, the dipole operator or $q\bar{q}$ amplitude matrix given in Eq. 4.6 is the simplest example of an amplitude matrix which is computed by sandwiching the Wilson-line tensor product

$$U_x \otimes U_y^\dagger =: \text{Diagram}, \quad (4.22)$$

between the only normalized element in $\mathfrak{C}(W)$, namely

$$|1\rangle := |1; 1\rangle = \frac{1}{\sqrt{d_f}} \mathfrak{D}. \quad (4.23)$$

Let us pause briefly to discuss two specific (types of) bases for colour space.

respectively, (where t^a is some generator) and differentiating both sides with respect to s at $s = 0$ produces

$$\begin{array}{c} \leftarrow \\ \text{---} \\ \text{---} \\ \vdots \\ \text{---} \\ \text{---} \\ \rightarrow \end{array} \begin{array}{c} \nearrow \\ s \\ \searrow \end{array} + \cdots + \begin{array}{c} \leftarrow \\ \text{---} \\ \text{---} \\ \vdots \\ \text{---} \\ \text{---} \\ \rightarrow \end{array} \begin{array}{c} \nwarrow \\ s \\ \swarrow \end{array} - \begin{array}{c} \leftarrow \\ \text{---} \\ \text{---} \\ \vdots \\ \text{---} \\ \text{---} \\ \rightarrow \end{array} \begin{array}{c} \nwarrow \\ s \\ \swarrow \end{array} - \cdots - \begin{array}{c} \leftarrow \\ \text{---} \\ \text{---} \\ \vdots \\ \text{---} \\ \text{---} \\ \rightarrow \end{array} \begin{array}{c} \nwarrow \\ s \\ \swarrow \end{array} = 0. \quad (4.27)$$

This relation will be useful later. It can also be used to prove the infrared finiteness of the JIMWLK equation for colour singlet channels [17].

We shall find it useful to think of generators as *Clebsches* (*Clebsch-Gordan coefficients*): states which take a pair of (anti-)fundamental indices into an adjoint index, or vice versa, which we write as

$$\sqrt{2}|t^a\rangle =: \mathfrak{A}^a, \quad \sqrt{2}\langle t^a| =: {}_a\mathfrak{C}. \quad (4.28)$$

An adjoint Wilson-line \tilde{U}_z can be expressed in terms of (anti-)fundamental Wilson-lines $U_z^{(\dagger)}$ through

$$[\tilde{U}_z]^{ab} := 2 \operatorname{Tr} \left(t^a U_z t^b U_z^\dagger \right) = 2 \langle t^a | U_z \otimes U_z^\dagger | t^b \rangle, \quad (4.29)$$

which in birdtracks reads

$$a \cdots \text{---} \begin{array}{c} \blacktriangleleft \\ z \end{array} \cdots b := a \cdots \text{---} \begin{array}{c} \circlearrowright \\ z \end{array} \cdots b . \quad (4.30)$$

4.1.1 The Fierz Identity

We can always decompose $W = V \otimes \bar{V}$ into a direct sum over *irreducible representations* (also known as *irreps* or *multiplets*). This decomposition is performed with the aid of the following two projection operators $P_\bullet, P_A : W \rightarrow W$ defined as

$$P_{\bullet} := |1\rangle\langle 1| = \frac{1}{d_f} \mathfrak{D} \mathfrak{C}, \quad (4.31a)$$

$$P_A := 2|t^a\rangle\langle t^a| = \mathfrak{A} \cdot \mathfrak{A}. \quad (4.31b)$$

Clearly these projection operators are orthonormal and their ranks² (which can be computed by taking the trace of each projection operator) are given by

$$\text{rank}(P_\bullet) = \langle 1|1 \rangle = \frac{1}{d_f} \text{Tr}(\mathbb{1}) = 1, \quad (4.32a)$$

$$\text{rank}(P_A) = 2\langle t^a|t^a \rangle = 2\text{Tr}(t^a t^a) = \delta^{aa} = N_c^2 - 1. \quad (4.32b)$$

Notice that the sum of their ranks is N_c^2 which is precisely the dimension of W . P_\bullet projects onto the singlet representation of W , denoted \bullet , while P_A projects onto the adjoint representation A . This allows us to write

$$W = \bullet \oplus A, \quad (4.33)$$

which is precisely the decomposition of W into multiplets. The above projection operators sum to the identity map on W :

$$i_W = P_\bullet + P_A, \quad (4.34a)$$

or in birdtrack notation

$$\begin{array}{c} \longrightarrow \\ \longleftarrow \end{array} = \frac{1}{d_f} \begin{array}{c} \curvearrowright \\ \curvearrowleft \end{array} \begin{array}{c} \text{---} \\ \text{---} \end{array} \begin{array}{c} \curvearrowleft \\ \curvearrowright \end{array} + \begin{array}{c} \curvearrowright \\ \curvearrowleft \end{array} \begin{array}{c} \text{---} \\ \text{---} \end{array} \begin{array}{c} \curvearrowright \\ \curvearrowleft \end{array}. \quad (4.34b)$$

Rearranging the above equation gives us the *Fierz identity*

$$\begin{array}{c} \curvearrowright \\ \curvearrowleft \end{array} \begin{array}{c} \text{---} \\ \text{---} \end{array} \begin{array}{c} \curvearrowleft \\ \curvearrowright \end{array} = \begin{array}{c} \longrightarrow \\ \longleftarrow \end{array} - \frac{1}{d_f} \begin{array}{c} \curvearrowright \\ \curvearrowleft \end{array} \begin{array}{c} \text{---} \\ \text{---} \end{array} \begin{array}{c} \curvearrowright \\ \curvearrowleft \end{array}. \quad (4.35)$$

4.1.2 Complex Conjugation

It is necessary for subsequent discussions to derive the birdtrack rules associated with complex conjugation. Firstly, the complex conjugate of the identity map is $(i_V)^* = i_{\bar{V}}$ which is the identity map on \bar{V} ; the action of complex conjugation can be depicted diagrammatically by

$$i_{\bar{V}} = (i_V)^* = (\longrightarrow)^* = \longleftarrow, \quad [i_{\bar{V}}]_i^j = i \longrightarrow_j = \delta_i^j. \quad (4.36)$$

Note that as linear maps, $i_V \neq i_{\bar{V}}$ because each linear map operates on a different linear space, but the components of their respective matrix representations are equal. We shall denote this equality of matrix components by the symbol \cong where

$$i_V \cong i_{\bar{V}} \iff ([i_V]_j^i \text{ is equal to } [i_{\bar{V}}]_i^j \text{ for any pair of indices } i, j), \quad (4.37)$$

²The rank of a linear map is the dimension of its image.

or in birdtracks

$$\longrightarrow \cong \longleftarrow \iff (i \longleftarrow_j \text{ is equal to } i \longrightarrow_j \text{ for any pair of indices } i, j). \quad (4.38)$$

One can easily check that \cong is an equivalence relation. Comparing Eq. 4.36 with Eq. 4.3, specifically the columns on the right-hand side, one can conclude that the action of complex conjugation on a birdtracks diagram representing a linear transformation is to reverse the direction of each arrow while leaving the position of each index label unchanged. This diagrammatic rule is true in general: it holds for Wilson-lines, colour singlet states and generators. In order to clarify this birdtrack rule for complex conjugation, we shall examine two examples. The first example is

$$\text{Tr} \left(U_{x_1} U_{y_1}^\dagger U_{x_2} U_{y_2}^\dagger \right) = \text{Tr} \left(\text{Diagram} \right). \quad (4.39)$$

The complex conjugate of the left-hand side of the equality in Eq. 4.39 is computed as

$$\left[\text{Tr} \left(U_{x_1} U_{y_1}^\dagger U_{x_2} U_{y_2}^\dagger \right) \right]^* = \text{Tr} \left(\left[U_{x_1} U_{y_1}^\dagger U_{x_2} U_{y_2}^\dagger \right]^\dagger \right) = \text{Tr} \left(U_{x_1}^\dagger U_{y_2} U_{x_2}^\dagger U_{y_1} \right) = \text{Tr} \left(\text{Diagram} \right). \quad (4.40)$$

The diagrammatic manipulations required to map Eq. 4.40 into Eq. 4.39 are

$$\left[\text{Diagram} \right]^* = \left[\text{Diagram} \right]^* = \left[\begin{matrix} i_1 & j_1 \\ \bar{i}_1 & \bar{j}_1 \\ i_2 & j_2 \\ \bar{i}_2 & \bar{j}_2 \end{matrix} \right]^* = \left[\begin{matrix} i_1 & j_1 \\ \bar{i}_1 & \bar{j}_1 \\ i_2 & j_2 \\ \bar{i}_2 & \bar{j}_2 \end{matrix} \right] = \text{Diagram}, \quad (4.41)$$

which implies the following:

- For fundamental and anti-fundamental Wilson-lines

$$\begin{aligned} (i \longleftarrow_x j)^* &= [(U_x)^*]_j^i = [U_x^\dagger]_j^i =: i \longrightarrow_x j, \\ (\bar{i} \longrightarrow_y \bar{j})^* &= [(U_y^\dagger)^*]_{\bar{i}}^{\bar{j}} = [U_y]_{\bar{i}}^{\bar{j}} =: \bar{i} \longleftarrow_y \bar{j}. \end{aligned} \quad (4.42)$$

The operation of complex conjugation for Wilson-lines may seem somewhat “unnatural”, since the complex conjugate of a unitary linear map is equal to the transpose of its adjoint which is not necessarily anything useful. However, later we shall find that these diagrammatic rules for complex conjugating Wilson-lines become immensely useful when we consider real and imaginary parts of Wilson-line amplitudes/correlators.

- For tensor-product representations of Wilson-lines acting on $W^{\otimes m}$

$$\left[\begin{matrix} i_1 & j_1 \\ \bar{i}_1 & \bar{j}_1 \\ \vdots & \vdots \\ i_m & j_m \\ \bar{i}_m & \bar{j}_m \end{matrix} \right]^* = \begin{matrix} i_1 & j_1 \\ \bar{i}_1 & \bar{j}_1 \\ \vdots & \vdots \\ i_m & j_m \\ \bar{i}_m & \bar{j}_m \end{matrix}. \quad (4.43)$$

- For colour singlet states on $W^{\otimes m}$

$$\left[\begin{array}{c} \overleftarrow{j_1} \\ \overleftarrow{j_1} \\ \vdots \\ \overleftarrow{j_m} \\ \overleftarrow{j_m} \end{array} \right]^{*} = \begin{array}{c} \overleftarrow{j_1} \\ \overleftarrow{j_1} \\ \vdots \\ \overleftarrow{j_m} \\ \overleftarrow{j_m} \end{array} \left[\begin{array}{c} \overrightarrow{j} \\ \overrightarrow{j} \\ \vdots \\ \overrightarrow{j} \\ \overrightarrow{j} \end{array} \right], \quad \left[\begin{array}{c} \overleftarrow{i_1} \\ \overleftarrow{i_1} \\ \vdots \\ \overleftarrow{i_m} \\ \overleftarrow{i_m} \end{array} \right]^{*} = \begin{array}{c} \overleftarrow{i_1} \\ \overleftarrow{i_1} \\ \vdots \\ \overleftarrow{i_m} \\ \overleftarrow{i_m} \end{array} \left[\begin{array}{c} \overrightarrow{i^*} \\ \overrightarrow{i^*} \\ \vdots \\ \overrightarrow{i^*} \\ \overrightarrow{i^*} \end{array} \right], \quad (4.44)$$

where the labels i^* and j^* are a shorthand reminder that, when writing the colour singlet states as complex linear combinations of Kronecker delta symbols, the complex coefficients need to be complex conjugated. For real colour singlet states

$$\begin{array}{c} \overleftarrow{j_1} \\ \overleftarrow{j_1} \\ \vdots \\ \overleftarrow{j_m} \\ \overleftarrow{j_m} \end{array} \left[\begin{array}{c} \overrightarrow{j^*} \\ \overrightarrow{j^*} \\ \vdots \\ \overrightarrow{j^*} \\ \overrightarrow{j^*} \end{array} \right] = \begin{array}{c} \overleftarrow{j_1} \\ \overleftarrow{j_1} \\ \vdots \\ \overleftarrow{j_m} \\ \overleftarrow{j_m} \end{array} \left[\begin{array}{c} \overrightarrow{j} \\ \overrightarrow{j} \\ \vdots \\ \overrightarrow{j} \\ \overrightarrow{j} \end{array} \right] = \begin{array}{c} \overleftarrow{j_1} \\ \overleftarrow{j_1} \\ \vdots \\ \overleftarrow{j_m} \\ \overleftarrow{j_m} \end{array} \left[\begin{array}{c} \overrightarrow{j} \\ \overrightarrow{j} \\ \vdots \\ \overrightarrow{j} \\ \overrightarrow{j} \end{array} \right], \quad \begin{array}{c} \overleftarrow{i_1} \\ \overleftarrow{i_1} \\ \vdots \\ \overleftarrow{i_m} \\ \overleftarrow{i_m} \end{array} \left[\begin{array}{c} \overrightarrow{i^*} \\ \overrightarrow{i^*} \\ \vdots \\ \overrightarrow{i^*} \\ \overrightarrow{i^*} \end{array} \right] = \begin{array}{c} \overleftarrow{i_1} \\ \overleftarrow{i_1} \\ \vdots \\ \overleftarrow{i_m} \\ \overleftarrow{i_m} \end{array} \left[\begin{array}{c} \overrightarrow{i} \\ \overrightarrow{i} \\ \vdots \\ \overrightarrow{i} \\ \overrightarrow{i} \end{array} \right] = \begin{array}{c} \overleftarrow{i_1} \\ \overleftarrow{i_1} \\ \vdots \\ \overleftarrow{i_m} \\ \overleftarrow{i_m} \end{array} \left[\begin{array}{c} \overrightarrow{i} \\ \overrightarrow{i} \\ \vdots \\ \overrightarrow{i} \\ \overrightarrow{i} \end{array} \right], \quad (4.45)$$

where we again note that although the complex conjugate of colour singlet states are tensors living in different tensor-product spaces, their tensor components are real linear combinations of Kronecker delta symbols and, consequently, are equal.

The second example is the adjoint Wilson-line \tilde{U}_z seen earlier:

$$[\tilde{U}_z]^{ab} = 2\text{Tr} \left(t^a U_z t^b U_z^\dagger \right) = a \cdots \begin{array}{c} \overleftarrow{\quad} \quad \overrightarrow{\quad} \\ \text{z} \end{array} \cdots b = a \cdots \begin{array}{c} \overleftarrow{\quad} \\ \text{z} \end{array} \cdots b. \quad (4.46)$$

The complex conjugate of Eq. 4.46 is

$$[\tilde{U}_z^*]^{ab} = [\tilde{U}_z^\dagger]^{ab} = 2\text{Tr} \left(t^a U_z^\dagger t^b U_z \right) = a \cdots \begin{array}{c} \overleftarrow{\quad} \quad \overrightarrow{\quad} \\ \text{z} \end{array} \cdots b = a \cdots \begin{array}{c} \overrightarrow{\quad} \\ \text{z} \end{array} \cdots b = [\tilde{U}_z]^{ba}, \quad (4.47)$$

from which we have that

$$\begin{aligned} \left[\begin{array}{c} \overleftarrow{i} \\ \overleftarrow{j} \end{array} \right]^{*} &= \sqrt{2} [(t^a)^*]_j^i = \sqrt{2} [t^a]_j^i = \begin{array}{c} \overleftarrow{i} \\ \overleftarrow{j} \end{array}, \\ \left[\begin{array}{c} \overleftarrow{a} \\ \overleftarrow{i} \end{array} \right]^{*} &= \sqrt{2} [(t^a)^*]_j^i = \sqrt{2} [t^a]_j^i = \begin{array}{c} \overleftarrow{a} \\ \overleftarrow{i} \end{array}. \end{aligned} \quad (4.48)$$

4.2 Colour structures

Before introducing the Fierz property (as promised earlier), in this section I introduce the notion of colour structures. Colour structures are colour singlets states of $A^{\otimes m}$ (where A is a real vector space carrying the adjoint representation of $\text{SU}(N_c)$ and $m \in \mathbb{N}^+ \geq 2$). They are important because:

- (i) they are used to canonically construct Fierz bases for the colour space of $W^{\otimes m}$;

- **For $m = 4$,** one can form nine trace basis elements: three of the nine elements consist of products of two traces of pairs of generators

$$\text{Tr}(t^{a_1}t^{a_2})\text{Tr}(t^{a_3}t^{a_4}) = \frac{1}{4}\delta^{a_1a_2}\delta^{a_3a_4} = \frac{1}{4} \begin{array}{c} a_1 \\ a_2 \\ a_3 \\ a_4 \end{array} \bigg) \bigg), \quad (4.56a)$$

$$\text{Tr}(t^{a_1}t^{a_3})\text{Tr}(t^{a_2}t^{a_4}) = \frac{1}{4}\delta^{a_1a_3}\delta^{a_2a_4} = \frac{1}{4} \begin{array}{c} a_1 \\ a_2 \\ a_3 \\ a_4 \end{array} \bigg) \bigg), \quad (4.56b)$$

$$\text{Tr}(t^{a_1}t^{a_4})\text{Tr}(t^{a_2}t^{a_3}) = \frac{1}{4}\delta^{a_1a_4}\delta^{a_2a_3} = \frac{1}{4} \begin{array}{c} a_1 \\ a_2 \\ a_3 \\ a_4 \end{array} \bigg) \bigg), \quad (4.56c)$$

while the remaining four elements consist of a single trace of four generators

$$\text{Tr}(t^{a_1}t^{a_2}t^{a_3}t^{a_4}) = \frac{1}{4} \begin{array}{c} a_1 \\ a_2 \\ a_3 \\ a_4 \end{array} \bigcirc, \quad (4.56d)$$

$$\text{Tr}(t^{a_1}t^{a_2}t^{a_4}t^{a_3}) = \frac{1}{4} \begin{array}{c} a_1 \\ a_2 \\ a_3 \\ a_4 \end{array} \bigcirc, \quad (4.56e)$$

$$\text{Tr}(t^{a_1}t^{a_3}t^{a_2}t^{a_4}) = \frac{1}{4} \begin{array}{c} a_1 \\ a_2 \\ a_3 \\ a_4 \end{array} \bigcirc, \quad (4.56f)$$

$$\text{Tr}(t^{a_1}t^{a_3}t^{a_4}t^{a_2}) = \frac{1}{4} \begin{array}{c} a_1 \\ a_2 \\ a_3 \\ a_4 \end{array} \bigcirc, \quad (4.56g)$$

$$\text{Tr}(t^{a_1}t^{a_4}t^{a_2}t^{a_3}) = \frac{1}{4} \begin{array}{c} a_1 \\ a_2 \\ a_3 \\ a_4 \end{array} \bigcirc, \quad (4.56h)$$

$$\text{Tr}(t^{a_1}t^{a_4}t^{a_3}t^{a_2}) = \frac{1}{4} \begin{array}{c} a_1 \\ a_2 \\ a_3 \\ a_4 \end{array} \bigcirc. \quad (4.56i)$$

Consider the function $f : \mathfrak{B}_{\text{Tr}}(A^{\otimes m}) \rightarrow S_m$ which (for a given trace basis element consisting of a product of traces) maps each trace over say $n \in \mathbb{N}^+ \geq 2$ generators with free adjoint indices a_1, \dots, a_n into a cycle in n symbols $1, \dots, n$:

$$f(\text{Tr}(t^{a_1} \dots t^{a_n})) = (1, \dots, n). \quad (4.57)$$

Then f maps each trace basis element in $\mathfrak{B}_{\text{Tr}}(A^{\otimes m})$ into a distinct product of *disjoint cycles*. This product of disjoint cycles represents a permutation on the symbols $1, \dots, m$, but since all m symbols are present and there are no disjoint 1-cycles⁵ the permutation does not have any fixed points and, hence, is a derangement⁶ on the symbols $1, \dots, m$. One can easily convince oneself that f is 1-to-1 and, hence, a bijection between $\mathfrak{B}_{\text{Tr}}(A^{\otimes m})$ and the set of all derangements in S_m .

⁵A disjoint 1-cycle would correspond to a trace over a single generator which is zero since the generators are traceless.

⁶A derangement on m symbols is any permutation in the permutation group S_m on m symbols without a fixed point.

For example, the trace basis elements in Eq. 4.55 are mapped onto the derangements

$$\text{Tr}(t^{a_1} t^{a_2} t^{a_3}) \xrightarrow{f} (1, 2, 3), \quad (4.58a)$$

$$\text{Tr}(t^{a_1} t^{a_3} t^{a_2}) \xrightarrow{f} (1, 3, 2), \quad (4.58b)$$

in S_3 . These are the only derangements in S_3 ; the other $3! - 2 = 4$ elements in S_3 are given by $(1, 2)$, $(1, 3)$, $(2, 3)$ and the identity map, all of which have at least one fixed point.

Thus, the total number of derangements in m letters counts the total number of trace basis elements in $\mathfrak{B}_{\text{Tr.}}(A^{\otimes m})$. The former is given by $!m$ — the sub-factorial of m — which can be calculated using⁷ [36, 37]

$$!m = m! \sum_{k=0}^m \frac{(-1)^k}{k!}. \quad (4.59)$$

For $N_c \geq m$, Eq. 4.59 counts the dimension of the linear space of colour structures [35]

$$\dim(\mathfrak{C}(A^{\otimes m})) \stackrel{N_c \geq m}{=} |\mathfrak{B}_{\text{Tr.}}(A^{\otimes m})| = !m. \quad (4.60)$$

4.2.3 The Young basis for colour structures

The trace basis is problematic for two reasons:

- (i) Firstly, the trace basis is, in general, not orthogonal. This problem can be rectified using Gram-Schmidt orthogonalization since there exists a natural inner-product for the colour space of colour structures. However, the Gram-Schmidt algorithm leaves something to be desired in that the output of the algorithm is dependent on the order in which one chooses to label the basis elements before applying the algorithm. Independent of this problem, Gram-Schmidt orthogonalization does not help to address the second problem.
- (ii) For $N_c < m \in \mathbb{N}^+$, the trace basis for the colour space of $A^{\otimes m}$ becomes over-complete; its elements are no longer linearly-independent which means that the trace basis is no longer a basis, only a spanning set.

This second problem is already seen in the trace basis given in Eq. 4.55 for the colour space of $A^{\otimes 3}$. For $N_c = 2$, the generators of $\text{SU}(N_c)$ are proportional to the Pauli-spin matrices which satisfy the anti-commutation relation

$$\{t^{a_1}, t^{a_2}\} \stackrel{N_c=2}{=} \frac{1}{2} \delta^{a_1 a_2} \mathbb{1}_{2 \times 2}, \quad (4.61)$$

⁷For all $m \in \mathbb{N}$, $!m \in \mathbb{N}$ as can be seen from Eq. 4.59 since for all $k \in \mathbb{N} \leq m$, $\frac{m!}{k!} \in \mathbb{N}^+$.

from which one can easily derive the well know result

$$d^{a_1 a_2 a_3} = 2\text{Tr}(\{t^{a_1}, t^{a_2}\}t^{a_3}) \xrightarrow{N_c=2} \delta^{a_1 a_2} \text{Tr}(t^{a_3}) = 0. \quad (4.62)$$

Eq. 4.62 implies that two trace basis elements in Eq. 4.55 are linearly dependent when $N_c = 2$, related to one another through

$$(4.55a) \xrightarrow{N_c=2} \frac{1}{4} \begin{smallmatrix} a_1 \\ a_2 \\ a_3 \end{smallmatrix} \rightarrow \xrightarrow{N_c=2} -(4.55b). \quad (4.63)$$

Clearly a better choice of basis for the colour space of $A^{\otimes 3}$ are the normalized states $d^{a_1 a_2 a_3}$ and $if^{a_1 a_2 a_3}$ since they are orthogonal and they are *sensitive to dimensional zeros*.

*A basis for the colour space of $A^{\otimes m}$ is said to be **sensitive to dimensional zeros**, if for $N_c < m$ certain basis elements automatically drop/become zero such that the remaining basis elements are still linearly independent and they still span the colour space of $A^{\otimes m}$.*

In summary, we do not like the trace basis because we want a basis for the colour space of $A^{\otimes m}$ which is orthonormal and which remains linearly independent (and, hence, a basis) for all $N_c \in \mathbb{N}^+ \geq 2$. Furthermore, we want a construction which produces a unique basis. There exists an algorithm in the literature [35] which can be used to construct such a basis. However, this algorithm is inefficient, listing possibilities that need to be systematically checked. Recently, an alternative construction for an orthonormal basis for the colour space of $A^{\otimes m}$ has been proposed in [38]. This construction is also not quite fully developed, but for the examples considered (for $m = 2, 3, 4$) it fulfills both the requirements of orthogonality and sensitivity to dimensional zeros. In addition, this construction produces basis colour structures with definite symmetry properties; they are simultaneous eigenstates (in the trace basis) of *Hermitian Young projection operators* on $A^{\otimes m}$.

By Hermitian Young projection operators on $A^{\otimes m}$ I am referring to the natural action of the standard Hermitian Young projection operators on $A^{\otimes m}$ where the standard Hermitian Young projection operators are formally elements of the permutation algebra

$$\mathbb{R}[S_m] := \left\{ \sum_{\sigma \in S_m} \alpha_\sigma \sigma \mid \alpha_\sigma \in \mathbb{R}, \sigma \in S_m \right\}. \quad (4.64)$$

When viewed as projection operators on $V^{\otimes m}$ they are mutually orthogonal and they project onto irreducible representations of $V^{\otimes m}$. However, as projection operators on $A^{\otimes m}$, they do not project onto irreducible representations of $A^{\otimes m}$. A review of standard Hermitian Young projection operators and transition operators is outside the scope of this thesis. Instead I shall introduce only the definitions necessary for our purposes and refer the interested reader

to [38–40] for the rest of the details.

I shall call the basis of colour structures produced by the following construction as the *Young colour structures*, and I shall denote this basis by $\mathfrak{B}_{\text{Young}}(A^{\otimes m})$.

An outline of the construction for Young colour structures

Let us use the symbol \mathbf{Y}_m to denote the set of all Young diagrams with m boxes where each Young diagram is labeled $\hat{\Theta}_I^{(m)}$ for $I = 1, \dots, |\mathbf{Y}_m|$. For a given Young diagram $\hat{\Theta}_I^{(m)} \in \mathbf{Y}_m$, let us denote the set of all Young tableau corresponding to the Young diagram $\hat{\Theta}_I^{(m)}$ by $\mathcal{Y}_I^{(m)}$. We shall label elements of $\mathcal{Y}_I^{(m)}$ by $\Theta_{I;i}^{(m)}$ where i runs from 1 to $|\mathcal{Y}_I^{(m)}|$. For example:

- **For $m = 2$** , there are only 2 Young diagrams

$$\mathbf{Y}_2 = \left\{ \overset{\hat{\Theta}_1^{(2)}}{\begin{array}{|c|c|} \hline \square & \square \\ \hline \end{array}}, \overset{\hat{\Theta}_2^{(2)}}{\begin{array}{|c|} \hline \square \\ \hline \square \\ \hline \end{array}} \right\}, \quad (4.65)$$

with corresponding Young tableaux

$$\mathcal{Y}_1^{(2)} = \left\{ \overset{\Theta_{1;1}^{(2)}}{\begin{array}{|c|c|} \hline 1 & 2 \\ \hline \end{array}} \right\}, \quad \mathcal{Y}_2^{(2)} = \left\{ \overset{\Theta_{2;1}^{(2)}}{\begin{array}{|c|} \hline 1 \\ \hline 2 \\ \hline \end{array}} \right\}. \quad (4.66)$$

- **For $m = 3$** , there are 3 Young diagrams

$$\mathbf{Y}_3 = \left\{ \overset{\hat{\Theta}_1^{(3)}}{\begin{array}{|c|c|c|} \hline \square & \square & \square \\ \hline \end{array}}, \overset{\hat{\Theta}_2^{(3)}}{\begin{array}{|c|c|} \hline \square & \square \\ \hline \square & \square \\ \hline \end{array}}, \overset{\hat{\Theta}_3^{(3)}}{\begin{array}{|c|} \hline \square \\ \hline \square \\ \hline \square \\ \hline \end{array}} \right\}, \quad (4.67)$$

with corresponding Young tableaux

$$\mathcal{Y}_1^{(3)} = \left\{ \overset{\Theta_{1;1}^{(3)}}{\begin{array}{|c|c|c|} \hline 1 & 2 & 3 \\ \hline \end{array}} \right\}, \quad \mathcal{Y}_2^{(3)} = \left\{ \overset{\Theta_{2;1}^{(3)}}{\begin{array}{|c|c|} \hline 1 & 2 \\ \hline 3 & \end{array}}, \overset{\Theta_{2;2}^{(3)}}{\begin{array}{|c|c|} \hline 1 & 3 \\ \hline 2 & \end{array}} \right\}, \quad \mathcal{Y}_3^{(3)} = \left\{ \overset{\Theta_{3;1}^{(3)}}{\begin{array}{|c|} \hline 1 \\ \hline 2 \\ \hline 3 \\ \hline \end{array}} \right\}. \quad (4.68)$$

Take any Young diagram $\hat{\Theta}_I^{(m)} \in \mathbf{Y}_m$. Then one can define a $|\mathcal{Y}_I^{(m)}| \times |\mathcal{Y}_I^{(m)}|$ matrix $\mathfrak{M}_I^{(m)}$ whose components are elements of the permutation algebra $\mathbb{R}[S_m]$ and are defined through

$$[\mathfrak{M}_I^{(m)}]_{ij} = \begin{cases} P[\Theta_{I;i}^{(m)}] & \text{if } i = j \\ T[\Theta_{I;i}^{(m)}, \Theta_{I;j}^{(m)}] & \text{otherwise} \end{cases}, \quad (4.69)$$

where $P[\Theta_{I;i}^{(m)}]$ is the Hermitian Young projection operator associated with the Young tableau $\Theta_{I;i}^{(m)}$ as defined in [39] and $T[\Theta_{I;i}^{(m)}, \Theta_{I;j}^{(m)}]$ is the transition operator from image of $P[\Theta_{I;i}^{(m)}]$ to the image of $P[\Theta_{I;j}^{(m)}]$ as defined in [40]. These matrices $\mathfrak{M}_I^{(m)}$ for $I = 1, \dots, |\mathbf{Y}_m|$ can be embedded in a larger block diagonal matrix

$$\mathfrak{M}^{(m)} = \begin{bmatrix} \mathfrak{M}_1^{(m)} & 0_{1,2} & \cdots & 0_{1,|\mathbf{Y}_m|} \\ 0_{2,1} & \mathfrak{M}_2^{(m)} & \cdots & 0_{2,|\mathbf{Y}_m|} \\ \vdots & \vdots & \ddots & \vdots \\ 0_{|\mathbf{Y}_m|,1} & 0_{|\mathbf{Y}_m|,2} & \cdots & \mathfrak{M}_{|\mathbf{Y}_m|}^{(m)} \end{bmatrix}, \quad (4.70)$$

where $0_{I,J}$ denotes a $|\mathcal{Y}_I^{(m)}| \times |\mathcal{Y}_J^{(m)}|$ matrix of zeros. Below are examples of $\mathfrak{M}^{(m)}$ for $m = 2, 3$:

- For $m = 2$,

$$\mathfrak{M}^{(2)} = \begin{bmatrix} \mathfrak{M}_1^{(2)} & 0_{1,2} \\ 0_{2,1} & \mathfrak{M}_2^{(2)} \end{bmatrix}, \quad (4.71a)$$

where

$$\mathfrak{M}_1^{(2)} = \begin{bmatrix} \text{---} \square \text{---} \end{bmatrix}, \quad \mathfrak{M}_2^{(2)} = \begin{bmatrix} \text{---} \blacksquare \text{---} \end{bmatrix}. \quad (4.71b)$$

- For $m = 3$,

$$\mathfrak{M}^{(3)} = \begin{bmatrix} \mathfrak{M}_1^{(3)} & 0_{1,2} & 0_{1,3} \\ 0_{2,1} & \mathfrak{M}_2^{(3)} & 0_{2,3} \\ 0_{3,1} & 0_{3,2} & \mathfrak{M}_3^{(3)} \end{bmatrix}, \quad (4.72a)$$

where

$$\mathfrak{M}_1^{(3)} = \begin{bmatrix} \text{---} \square \text{---} \\ \text{---} \square \text{---} \end{bmatrix}, \quad \mathfrak{M}_2^{(3)} = \begin{bmatrix} \frac{4}{3} \text{---} \square \blacksquare \text{---} & \sqrt{\frac{4}{3}} \text{---} \square \blacksquare \text{---} \\ \sqrt{\frac{4}{3}} \text{---} \blacksquare \square \text{---} & \frac{4}{3} \text{---} \blacksquare \square \text{---} \end{bmatrix}, \quad \mathfrak{M}_3^{(3)} = \begin{bmatrix} \text{---} \blacksquare \text{---} \end{bmatrix}. \quad (4.72b)$$

For future convenience we shall write

$$\text{HYPO}_m = \bigcup_{I=1}^{|\mathbf{Y}_m|} \bigcup_{i=1}^{|\mathcal{Y}_I^{(m)}|} \{[\mathfrak{M}_I^{(m)}]_{ii}\} \subseteq \mathbb{R}[S_m], \quad (4.73)$$

to denote the set of all *Hermitian Young projection operators*.

To re-iterate, $[\mathfrak{M}_I^{(m)}]_{ii} := P[\Theta_{I;i}^{(m)}]$ (see Eq. 4.69) is the Hermitian Young projection operator associated with the Young tableau $\Theta_{I;i}^{(m)}$ where $\Theta_{I;i}^{(m)}$ is the i^{th} Young tableau corresponding to the I^{th} Young diagram with m boxes; this is summarized in Fig. 4.1.

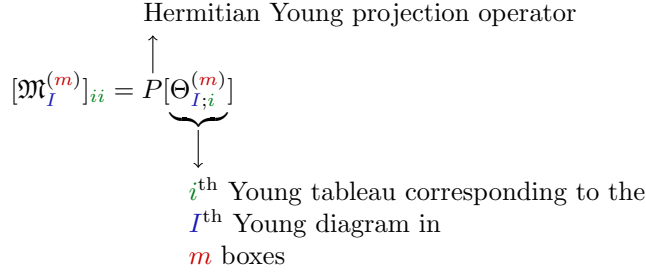


FIGURE 4.1: (Colour online) Explaining the notation of $[\mathfrak{M}_I^{(m)}]_{ii}$.

At this stage, the notation $[\mathfrak{M}_I^{(m)}]_{ii}$ feels unnecessarily cumbersome. Unfortunately, the notation is necessary, but this only becomes apparent Sec. 6.2.

In order to act with these projectors on the colour space of $A^{\otimes m}$, one needs to define an action of the permutation algebra $\mathbb{R}[S_m]$ on the base space $A^{\otimes m}$. We define our action

$$\circ_m : \mathbb{R}[S_m] \times A^{\otimes m} \rightarrow A^{\otimes m} \quad (4.74a)$$

such that $\forall \sigma \in S_m$ and $\forall T^{a_1 \cdots a_m} \in A^{\otimes m}$

$$\sigma \circ_m T^{a_1 \cdots a_m} := T^{a_{\sigma(1)} \cdots a_{\sigma(m)}}, \quad (4.74b)$$

and then we extend by linearity; i.e. $\forall \alpha_1, \alpha_2 \in \mathbb{R}$, $\forall \sigma_1, \sigma_2 \in S_m$, and $\forall T^{a_1 \cdots a_m} \in A^{\otimes m}$

$$(\alpha_1 \sigma_1 + \alpha_2 \sigma_2) \circ_m T^{a_1 \cdots a_m} := \alpha_1 (\sigma_1 \circ_m T^{a_1 \cdots a_m}) + \alpha_2 (\sigma_2 \circ_m T^{a_1 \cdots a_m}). \quad (4.74c)$$

In what follows, we shall simply write \circ instead of \circ_m for the sake of brevity.

Let $\mathfrak{B}_{\text{Tr}}(A^{\otimes m}) = \{\tilde{\mathcal{C}}^{(m;k)a_1 \cdots a_m}\}_{k=1}^{\text{!}m}$ denote the trace basis for the colour space of $A^{\otimes m}$. Consider an arbitrary vector in $\mathcal{C}^{a_1 \cdots a_m} \in \mathfrak{C}(A^{\otimes m})$ expanded in the trace basis

$$\mathcal{C}^{a_1 \cdots a_m} = \sum_{k=1}^{\text{!}m} \alpha_k \tilde{\mathcal{C}}^{(m;k)a_1 \cdots a_m}. \quad (4.75)$$

where $\alpha_k \in \mathbb{R}$ for all $k = 1, \dots, \text{!}m$. Now, $\mathcal{C}^{a_1 \cdots a_m}$ in Eq. 4.75 is a simultaneous eigenstate of the projection operators in HYPO_m if $\mathcal{C}^{a_1 \cdots a_m}$ is non-zero and for all $I = 1, \dots, |\mathbf{Y}_m|$, $i =$

$1, \dots, |\mathcal{Y}_I^{(m)}|$ there exists $\lambda^{(m;I;i)} \in \mathbb{R}$ such that

$$[\mathfrak{M}_I^{(m)}]_{ii} \circ \mathcal{C}^{a_1 \dots a_m} = \lambda^{(m;I;i)} \mathcal{C}^{a_1 \dots a_m}, \quad (4.76)$$

where the composition \circ is the action defined in Eq. 4.74. Since HYPO_m forms a complete set of mutually orthogonal projection operators [39], for all $I = 1, \dots, |\mathbf{Y}_m|$ and for all $i = 1, \dots, |\mathcal{Y}_I^{(m)}|$ the following is true for Eq. 4.76:

- (i) $\lambda^{(m;I;i)}$ can only be 0 or 1, since $[\mathfrak{M}_I^{(m)}]_{ii}$ is idempotent;
- (ii) $\lambda^{(m;I;i)}$ can be 1 for at most one pair (I, i) since the projection operators are mutually orthogonal;
- (iii) $\lambda^{(m;I;i)}$ must be 1 for at least one pair (I, i) since the projection operators decompose unity, otherwise $\mathcal{C}^{a_1 \dots a_m} = 0$.

Consequently, in order to find all simultaneous eigenstates of HYPO_m in $\mathfrak{C}(A^{\otimes m})$, it is sufficient to find the eigenstates of each projection operator with eigenvalue 1. We shall use the notation $\mathcal{C}^{(m;I;i;m_i)_{a_1 \dots a_m}}$ to denote the m_i^{th} eigenstate of the projection operator $[\mathfrak{M}_I^{(m)}]_{ii}$ with eigenvalue 1 in $\mathfrak{C}(A^{\otimes m})$. Here m_i is a degeneracy label; i.e. for all $m_i = 1, \dots, d(m; I; i)$

$$[\mathfrak{M}_I^{(m)}]_{ii} \mathcal{C}^{(m;I;i;m_i)_{a_1 \dots a_m}} = \mathcal{C}^{(m;I;i;m_i)_{a_1 \dots a_m}}. \quad (4.77)$$

The above notation is summarized below in Fig. 4.2.

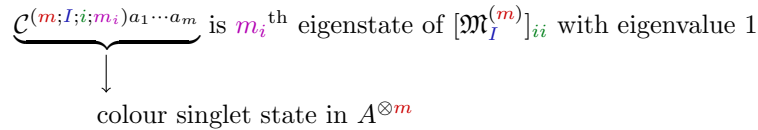


FIGURE 4.2: (Colour online) Explaining the notation of $\mathcal{C}^{(m;I;i;m_i)_{a_1 \dots a_m}}$.

In the case where $d(m; I; i) > 1$ one needs additional criteria in order to uniquely orthogonalize $\{\mathcal{C}^{(m;I;i;m_i)_{a_1 \dots a_m}}\}_{m_i=1}^{d(m;I;i)}$ in such a way that dimensional zeros are made manifest. This is a topic of ongoing investigation [41].

Let us consider, as examples, the Young colour structures of $A^{\otimes m}$ for $m = 2, 3$:

- **For $m = 2$,** since there is only one trace basis element (c.f. Eq. 4.54), namely

$$\text{Tr}(t^{a_1} t^{a_2}) = \frac{1}{2} \delta^{a_1 a_2} = \frac{1}{2} \begin{smallmatrix} a_1 \\ a_2 \end{smallmatrix} \triangleright,$$

which spans $\mathfrak{C}(A^{\otimes 2})$, it must be the case that $\text{Tr}(t^{a_1}t^{a_2})$ is automatically a simultaneous eigenstate of the projection operators in Eq. 4.71. Indeed this is the case. It is easy to show that

$$[\mathfrak{M}_1^{(2)}]_{11} \circ 2\text{Tr}(t^{a_1}t^{a_2}) = \begin{smallmatrix} a_1 \\ a_2 \end{smallmatrix} \begin{array}{c} \text{---} \text{---} \text{---} \\ \text{---} \text{---} \end{array} \begin{smallmatrix} a_1 \\ a_2 \end{smallmatrix} \supset = 2\text{Tr}(t^{a_1}t^{a_2}), \quad (4.78a)$$

$$[\mathfrak{M}_2^{(2)}]_{11} \circ 2\text{Tr}(t^{a_1}t^{a_2}) = \begin{smallmatrix} a_1 \\ a_2 \end{smallmatrix} \begin{array}{c} \text{---} \text{---} \text{---} \\ \text{---} \text{---} \end{array} \begin{smallmatrix} a_1 \\ a_2 \end{smallmatrix} \supset = 0. \quad (4.78b)$$

Consequently, the only Young color structure in $A^{\otimes 2}$ is

$$\mathcal{C}^{(2;1;1;1)a_1a_2} = \mathcal{N}_{2;1;1;1}^{(A)} \delta^{a_1a_2} = \mathcal{N}_{2;1;1;1}^{(A)} \begin{smallmatrix} a_1 \\ a_2 \end{smallmatrix} \supset, \quad (4.79)$$

where the normalization constant is given by

$$\mathcal{N}_{2;1;1;1}^{(A)} = \frac{1}{\sqrt{d_A}}, \quad (4.80)$$

with $d_A = \dim(A) = N_c^2 - 1$ such that the inner-product of Eq. 4.79 with itself is unity

$$\langle \mathcal{C}^{(2;1;1;1)} | \mathcal{C}^{(2;1;1;1)} \rangle = (\mathcal{C}^{(2;1;1;1)a_1a_2})^* \mathcal{C}^{(2;1;1;1)a_1a_2} = 1. \quad (4.81)$$

- **For $\mathbf{m} = \mathbf{3}$,** there are two trace basis elements (see Eq. 4.55)

$$\begin{aligned} \text{Tr}(t^{a_1}t^{a_2}t^{a_3}) &= \frac{1}{2\sqrt{2}} \begin{smallmatrix} a_1 \\ a_2 \\ a_3 \end{smallmatrix} \begin{array}{c} \text{---} \text{---} \text{---} \\ \text{---} \text{---} \end{array} \begin{smallmatrix} a_1 \\ a_2 \\ a_3 \end{smallmatrix}, \\ \text{Tr}(t^{a_1}t^{a_3}t^{a_2}) &= \frac{1}{2\sqrt{2}} \begin{smallmatrix} a_1 \\ a_2 \\ a_3 \end{smallmatrix} \begin{array}{c} \text{---} \text{---} \text{---} \\ \text{---} \text{---} \end{array} \begin{smallmatrix} a_1 \\ a_2 \\ a_3 \end{smallmatrix}, \end{aligned}$$

which span $\mathfrak{C}(A^{\otimes 3})$. Let us compute explicitly compute the eigenstate of

$$[\mathfrak{M}_1^{(3)}]_{11} = \begin{array}{c} \text{---} \text{---} \text{---} \\ \text{---} \text{---} \end{array}, \quad (4.82)$$

with eigenvalue 1 in $\mathfrak{C}(A^{\otimes 3})$. To this end, we write

$$\mathcal{C}^{(3;1;1;1)a_1a_2a_3} = \alpha_1 \text{Tr}(t^{a_1}t^{a_2}t^{a_3}) + \alpha_2 \text{Tr}(t^{a_1}t^{a_3}t^{a_2}) \quad (4.83)$$

where $\alpha_1, \alpha_2 \in \mathbb{R}$ are as yet undetermined, and we require that

$$[\mathfrak{M}_1^{(3)}]_{11} \circ \mathcal{C}^{(3;1;1;1)a_1a_2a_3} = \mathcal{C}^{(3;1;1;1)a_1a_2a_3} \quad (4.84a)$$

$$\begin{aligned} \iff \frac{\alpha_1 + \alpha_2}{2} [\text{Tr}(t^{a_1}t^{a_2}t^{a_3}) + \text{Tr}(t^{a_1}t^{a_3}t^{a_2})] &= \alpha_1 \text{Tr}(t^{a_1}t^{a_2}t^{a_3}) + \alpha_2 \text{Tr}(t^{a_1}t^{a_3}t^{a_2}) \\ \implies \alpha_1 &= \alpha_2. \end{aligned} \quad (4.84b)$$

Consequently, we have that

$$\mathcal{C}^{(3;1;1;1)a_1a_2a_3} = \alpha_1 \text{Tr}(t^{a_1}\{t^{a_2}, t^{a_3}\}) = \frac{\alpha_1}{2} d^{a_1a_2a_3}. \quad (4.85)$$

The overall normalization constant α_1 is then fixed by requiring that

$$\langle \mathcal{C}^{(3;1;1;1)} | \mathcal{C}^{(3;1;1;1)} \rangle = (\mathcal{C}^{(3;1;1;1)a_1a_2a_3})^* \mathcal{C}^{(3;1;1;1)a_1a_2a_3} = 1. \quad (4.86)$$

Repeating this process for the other elements of HYPO_3 , we find that the Young colour structures in $A^{\otimes 3}$ are unique⁸ and are given by

$$\mathcal{C}^{(3;1;1;1)a_1a_2a_3} := \mathcal{N}_{3;1;1;1}^{(A)} d^{a_1a_2a_3} =: \mathcal{N}_{3;1;1;1}^{(A)} \begin{array}{c} a_1 \\ a_2 \\ a_3 \end{array} \begin{array}{c} \curvearrowright \end{array}, \quad (4.87a)$$

$$\mathcal{C}^{(3;3;1;1)a_1a_2a_3} := \mathcal{N}_{3;3;1;1}^{(A)} i f^{a_1a_2a_3} =: \mathcal{N}_{3;3;1;1}^{(A)} \begin{array}{c} a_1 \\ a_2 \\ a_3 \end{array} \begin{array}{c} \bullet \end{array}, \quad (4.87b)$$

where $d^{a_1a_2a_3}$ and $i f^{a_1a_2a_3}$ are the structures constants of $\text{su}(N_c)$ and the normalizations in Eq. 4.87 are given by

$$\mathcal{N}_{3;1;1;1}^{(A)} = \frac{1}{\sqrt{d_A C_d}}, \quad (4.88a)$$

$$\mathcal{N}_{3;3;1;1}^{(A)} = \frac{1}{\sqrt{d_f d_A}}. \quad (4.88b)$$

The quadratic Casimir $d^{ac_1c_2} d^{bc_1c_2} = C_d \delta^{ab}$ is given by $C_d = \frac{N_c^2 - 4}{N_c}$.

4.2.4 Complex conjugating pure adjoint colour singlet states

We now turn our attention to a simple but important result, Lemma 4.1, which pertains to the complex conjugation of pure adjoint colour singlet states: a result which follows from the statement that the projection operator $P_A = \mathfrak{D} \text{---} \mathfrak{C}$ is real; i.e.

$$(\mathfrak{D} \text{---} \mathfrak{C})^* = \mathfrak{D} \text{---} \mathfrak{C} \cong \mathfrak{D} \text{---} \mathfrak{C}. \quad (4.89)$$

As we shall see, we shall need to use Lemma 4.1 on more than one occasion.

Recall from Eq. 4.35, that the Fierz identity is given by

$$P_A = i_W - P_\bullet, \quad (4.90a)$$

⁸Up to an overall sign.

or diagrammatically

The diagram shows two triangles. The left triangle has external lines labeled i_1, j_1 at the top and i_m, j_m at the bottom, with vertical dots between j_1 and i_m . The internal line is labeled s . The right triangle is identical but the internal line is labeled s^* . The two triangles are separated by an equals sign. The equation is labeled (4.95b) on the right.

Proof. Recall that a colour structure $\mathcal{C}^{(s)a_1 \dots a_m} \in \mathfrak{C}(A^{\otimes m})$ (where $m \in \mathbb{N}^+ \geq 2$) can always be expanded in the trace basis as a real linear combination of products of traces containing products of generators t^{a_1}, \dots, t^{a_m} . Therefore, it is sufficient to show that for all $m \in \mathbb{N}^+ \geq 2$

$$|(t^{a_1})^*\rangle \otimes \dots \otimes |(t^{a_m})^*\rangle \text{Tr}(t^{a_1} \dots t^{a_m}) \cong |t^{a_1}\rangle \otimes \dots \otimes |t^{a_m}\rangle \text{Tr}(t^{a_1} \dots t^{a_m})^*, \quad (4.96)$$

where $\text{Tr}(t^{a_1} \dots t^{a_m})^* = \text{Tr}((t^{a_1} \dots t^{a_m})^*) = \text{Tr}((t^{a_1} \dots t^{a_m})^\dagger) = \text{Tr}((t^{a_1})^\dagger \dots (t^{a_m})^\dagger) = \text{Tr}(t^{a_m} \dots t^{a_1})$; i.e. complex conjugation of a trace of generators reverses the order of the trace. In birdtrack notation, Eq. 4.96 reads

The diagram shows two birdtrack diagrams. The left diagram has two vertical lines with arrows pointing upwards. The right diagram is identical but the arrows point downwards. The two diagrams are separated by an equals sign. The equation is labeled (4.97) on the right.

where the second diagram is related to the first one by flipping the directions of the generator arrows on both the external and the internal lines. But Eq. 4.97 follows immediately from Eq. 4.93. This concludes the proof of Lemma 4.1. \blacksquare

4.3 Fierz bases for colour space

Having introduced colour structures in the previous section, we are now in a position to properly define the Fierz property and write down the set of all bases for colour space that posses this property. This is the topic of the following section.

4.3.1 The Fierz property: simultaneous eigenstates of the Fierz projection operators

Recall that we can decompose W into multiplets

$$W = \bullet \oplus A, \quad (4.98)$$

where the projection operators onto each multiplet are given by

$$\frac{1}{d_f} \overset{P_\bullet}{\curvearrowright} \curvearrowleft, \quad \overset{P_A}{\curvearrowright} \curvearrowleft. \quad (4.99)$$

These projection operators are mutually orthogonal and they are complete: they sum to the identity map on W (see Eq. 4.34). Using Eq. 4.98 one obtains the following decompositions

$$W^{\otimes 2} = W \otimes (\bullet \oplus A) = \bullet^{\otimes 2} \oplus (A \otimes \bullet) \oplus (\bullet \otimes A) \oplus A^{\otimes 2}, \quad (4.100)$$

$$\begin{aligned} W^{\otimes 3} = W^{\otimes 2} \otimes (\bullet \oplus A) = & \bullet^{\otimes 3} \oplus (A \otimes \bullet^{\otimes 2}) \oplus (\bullet \otimes A \otimes \bullet) \oplus (A^{\otimes 2} \otimes \bullet) \\ & \oplus (\bullet^{\otimes 2} \otimes A) \oplus (A \otimes \bullet \otimes A) \oplus (\bullet \otimes A^{\otimes 2}) \oplus A^{\otimes 3}, \end{aligned} \quad (4.101)$$

and so on, with the projection operators onto each factor in the direct sum after the last equality in Eq. 4.100 and Eq. 4.101 given by

$$\begin{aligned} & \overset{P_\bullet^{\otimes 2}}{\frac{1}{d_f^2} \curvearrowright \curvearrowleft}, \quad \overset{P_A \otimes P_\bullet}{\frac{1}{d_f} \curvearrowright \curvearrowleft}, \quad \overset{P_\bullet \otimes P_A}{\frac{1}{d_f} \curvearrowright \curvearrowleft}, \quad \overset{P_A^{\otimes 2}}{\curvearrowright \curvearrowleft}, \\ & \overset{P_\bullet^{\otimes 2}}{\frac{1}{d_f^2} \curvearrowright \curvearrowleft}, \quad \overset{P_A \otimes P_\bullet}{\frac{1}{d_f} \curvearrowright \curvearrowleft}, \quad \overset{P_\bullet \otimes P_A}{\frac{1}{d_f} \curvearrowright \curvearrowleft}, \quad \overset{P_A^{\otimes 2}}{\curvearrowright \curvearrowleft}, \end{aligned} \quad (4.102)$$

$$\begin{aligned} & \overset{P_\bullet^{\otimes 3}}{\frac{1}{d_f^3} \curvearrowright \curvearrowleft}, \quad \overset{P_A \otimes P_\bullet^{\otimes 2}}{\frac{1}{d_f^2} \curvearrowright \curvearrowleft}, \quad \overset{P_\bullet \otimes P_A \otimes P_\bullet}{\frac{1}{d_f^2} \curvearrowright \curvearrowleft}, \quad \overset{P_A^{\otimes 2} \otimes P_\bullet}{\frac{1}{d_f} \curvearrowright \curvearrowleft}, \quad \overset{P_\bullet^{\otimes 2} \otimes P_A}{\frac{1}{d_f^2} \curvearrowright \curvearrowleft}, \\ & \overset{P_A \otimes P_\bullet \otimes P_A}{\frac{1}{d_f} \curvearrowright \curvearrowleft}, \quad \overset{P_\bullet \otimes P_A^{\otimes 2}}{\frac{1}{d_f} \curvearrowright \curvearrowleft}, \quad \overset{P_A^{\otimes 3}}{\frac{1}{d_f} \curvearrowright \curvearrowleft}, \end{aligned} \quad (4.103)$$

These projection operators are also mutually orthogonal and complete.

In general, one can always choose to decompose $W^{\otimes m}$ according to the above procedure, producing

$$W^{\otimes m} = \oplus_{i=0}^m \oplus_{\sigma \in S_{m-i,i}} (\bullet_{\sigma(1)} \otimes \cdots \otimes \bullet_{\sigma(m-i)} \otimes A_{\sigma(m-i+1)} \otimes \cdots \otimes A_{\sigma(m)}), \quad (4.104)$$

where for each $i = 0, \dots, m$ in the direct sum, $S_{m-i,i}$ is the set of $(m-i, i)$ shuffles⁹, and the subscript on the multiplets \bullet and A labels their positions in the m -long tensor product. It is understood that the contributions to the direct sum over i from $i = 0$ and $i = m$ are $\bullet^{\otimes m}$ and $A^{\otimes m}$, respectively. The projection operators onto each term in the double direct sum in

⁹A (k, l) shuffle, where $k, l \in \mathbb{N}$ and $k + l \geq 1$, is a permutation $\sigma \in S_{k+l}$ in the permutation group on $k + l$ symbols which satisfies [14]

$$\sigma(1) < \cdots < \sigma(k), \quad \text{and} \quad \sigma(k+1) < \cdots < \sigma(k+l). \quad (4.105)$$

The set of (k, l) shuffles is denoted as $S_{k,l}$. The size of $S_{k,l}$ is given by

$$|S_{k,l}| = \binom{k+l}{k}. \quad (4.106)$$

For $k = 0$ or $l = 0$, $S_{k,l}$ contains only the identity element of S_{k+l} which is in agreement with the formula for the size of $S_{k,l}$ which is 1 in this case.

Eq. 4.104 is given by the set

$$\text{FPO}(W^{\otimes m}) = \bigcup_{i=0}^m \bigcup_{\sigma \in S_{m-i,i}} \{(P_{\bullet})_{\sigma(1)} \otimes \cdots \otimes (P_{\bullet})_{\sigma(m-i)} \otimes (P_A)_{\sigma(m-i+1)} \otimes \cdots \otimes (P_A)_{\sigma(m)}\}, \quad (4.107)$$

which we shall refer as the set of *Fierz projection operators*. The number of Fierz projection operators can be counted as

$$\text{number of Fierz projection operators} = \sum_{i=0}^m |S_{m-i,i}| = \sum_{i=0}^m \binom{m}{i} = (1+1)^m = 2^m, \quad (4.108)$$

as expected.

Finally, we are able to provide a definition for the Fierz property: a definition which, to my knowledge, and the knowledge of my supervisor, has not appeared in the literature to date. A basis for the colour space of $W^{\otimes m}$ is said to be a *Fierz basis* or, equivalently, possess the *Fierz property* if it simultaneously diagonalizes the Fierz projection operators given in Eq. 4.107. Having already introduced pure adjoint colour singlet states and colour structures in the previous section, we can immediately write down a canonical definition for all Fierz bases. Any Fierz basis for the colour space of $W^{\otimes m}$ is given by

$$\bigcup_{i=0}^m \bigcup_{\sigma \in S_{i,m-i}} \bigcup_k \{\sqrt{2^i} |1\rangle_{\sigma(1)} \otimes \cdots \otimes |1\rangle_{\sigma(m-i)} \otimes |t^{a_1}\rangle_{\sigma(m-i+1)} \otimes \cdots \otimes |t^{a_i}\rangle_{\sigma(m)} \mathcal{C}^{(i;k)a_1 \cdots a_i}\}. \quad (4.109)$$

where for each $i \in \mathbb{N} \cap [2, m]$, $\mathfrak{B}(A^{\otimes i}) = \{\mathcal{C}^{(i;k)a_1 \cdots a_i}\}_k$ is some basis for the colour space of $A^{\otimes i}$ and the state $|t^a\rangle$ is defined in Eq. 4.28 as $\sqrt{2}|t^a\rangle =: \mathfrak{D}^a$. The definition in Eq. 4.109 is canonical in the sense that it is independent of the choice of basis colour structures.

For $m = 1$, there is only one basis element, namely

$$\begin{aligned} &|1;1\rangle = |1\rangle \\ &\mathcal{N}_{1;1} \mathfrak{D}. \end{aligned} \quad (4.110)$$

where

$$\mathcal{N}_{1;1} = \frac{1}{\sqrt{d_f}}. \quad (4.111)$$

4.3.2 The Fierz-permutation basis

The *Fierz-permutation basis* is a spanning set for $\mathfrak{C}(W^{\otimes m})$ possessing the Fierz property which is uniquely constructed from the set of permutations on m symbols S_m . The “basis” elements

are written as m -long tensor-products as in Eq. 4.109 according to the following procedure:

- (i) Label each element by a permutation $\sigma \in S_m$ where we choose to decompose σ as a product of disjoint cycles, keeping disjoint 1-cycles explicit.
- (ii) For each disjoint 1-cycle (j) (where $j \in \mathbb{N} \cap [1, m]$) in σ , assign the colour singlet state $|1\rangle$ to the j^{th} position of the m -long tensor-product.
- (iii) For each disjoint n -cycle (j_1, \dots, j_n) (where $n \in \mathbb{N} \cap [2, m]$ and $\{j_1, \dots, j_n\} \subseteq \mathbb{N} \cap [1, m]$) include

$$\frac{1}{\sqrt{\text{Tr}(t^{b_1} \dots t^{b_n}) \text{Tr}(t^{b_1} \dots t^{b_n})}} \underbrace{\sqrt{2^n} |t^{a_1}\rangle_{j_1} \otimes \dots \otimes |t^{a_n}\rangle_{j_n} \text{Tr}(t^{a_1} \dots t^{a_n})}_{= \left[\begin{array}{c} \text{---} \text{---} \text{---} \text{---} \text{---} \text{---} \\ \text{---} \text{---} \text{---} \text{---} \text{---} \text{---} \\ \text{---} \text{---} \text{---} \text{---} \text{---} \text{---} \\ \text{---} \text{---} \text{---} \text{---} \text{---} \text{---} \end{array} \right]^{-1/2}}$$

in the m -factor tensor-product where $|t^a\rangle_j$ means assign the state $|t^a\rangle$ (defined in Eq. 4.28 as $\sqrt{2}|t^a\rangle =: \text{---}^a$) to the j^{th} position in the m -long tensor-product.

The $m!$ “basis” elements produced by the above procedure are already normalized but not necessarily orthogonal and they are only linearly independent for $m \leq N_c$. The result of the above procedure is identical to the spanning set given by Eq. 4.109 where the colour structures are given by the normalized trace basis. The Fierz-permutation basis for $m = 2, 3$ are given below.

- **For $m = 2$,** the Fierz-permutation basis is given by

$$\begin{array}{cc} |(1)(2)\rangle & |(12)\rangle \\ \tilde{\mathcal{N}}_{2;1} \text{---} & \tilde{\mathcal{N}}_{2;2} \text{---} \end{array}, \quad (4.112)$$

where

$$\tilde{\mathcal{N}}_{2;1} = \frac{1}{d_f}, \quad \tilde{\mathcal{N}}_{2;2} = \frac{1}{\sqrt{d_A}}. \quad (4.113)$$

Eq. 4.112 is an ON basis for all N_c .

- **For $m = 3$,** the Fierz-permutation basis is given by

$$\begin{array}{cccccc} |(1)(2)(3)\rangle & |(12)(3)\rangle & |(13)(2)\rangle & |(1)(23)\rangle & |(123)\rangle & |(132)\rangle \\ \tilde{\mathcal{N}}_{3;1} \text{---} & \tilde{\mathcal{N}}_{3;2} \text{---} & \tilde{\mathcal{N}}_{3;3} \text{---} & \tilde{\mathcal{N}}_{3;4} \text{---} & \tilde{\mathcal{N}}_{3;5} \text{---} & \tilde{\mathcal{N}}_{3;6} \text{---} \end{array}, \quad (4.114)$$

where

$$\tilde{\mathcal{N}}_{3;1} = \frac{1}{\sqrt{d_f^3}}, \quad \tilde{\mathcal{N}}_{3;2} = \tilde{\mathcal{N}}_{3;3} = \tilde{\mathcal{N}}_{3;4} = \frac{\tilde{\mathcal{N}}_{2;1}}{\sqrt{d_f}}, \quad \tilde{\mathcal{N}}_{3;5} = \tilde{\mathcal{N}}_{3;6} = \sqrt{\frac{4N_c}{d_A(N_c^2 - 5)}}. \quad (4.115)$$

Eq. 4.114 is linearly independent for $N_c \geq 3$ but is over-complete for $N_c < 3$. Eq. 4.114 is not orthogonal because the last two elements have a non-zero inner-product with each other.

4.3.3 The Fierz-Young basis

The *Fierz-Young basis* is the Fierz basis given by Eq. 4.109 where the colour structures are given by the Young colour structures. For the Young colour structures listed in Eq. 4.79 and Eq. 4.87, the Fierz-Young basis for $m = 2$ and $m = 3$ are given below.

- **For $m = 2$** , the Fierz-Young basis is given by

$$\begin{array}{cc} |2;1\rangle & |2;2\rangle \\ \mathcal{N}_{2;1} \begin{array}{c} \curvearrowright \\ \curvearrowleft \end{array} & \mathcal{N}_{2;2} \begin{array}{c} \curvearrowright \\ \curvearrowleft \end{array} \end{array}, \quad (4.116)$$

where

$$\mathcal{N}_{2;1} = \frac{1}{d_f}, \quad \mathcal{N}_{2;2} = \mathcal{N}_{2;1;1;1}^{(A)}. \quad (4.117)$$

- **For $m = 3$** , the Fierz-Young basis is given by

$$\begin{array}{cccccc} |3;1\rangle & |3;2\rangle & |3;3\rangle & |3;4\rangle & |3;5\rangle & |3;6\rangle \\ \mathcal{N}_{3;1} \begin{array}{c} \curvearrowright \\ \curvearrowleft \end{array} & \mathcal{N}_{3;2} \begin{array}{c} \curvearrowright \\ \curvearrowleft \end{array} & \mathcal{N}_{3;3} \begin{array}{c} \curvearrowright \\ \curvearrowleft \end{array} & \mathcal{N}_{3;4} \begin{array}{c} \curvearrowright \\ \curvearrowleft \end{array} & \mathcal{N}_{3;5} \begin{array}{c} \curvearrowright \\ \curvearrowleft \end{array} & \mathcal{N}_{3;6} \begin{array}{c} \curvearrowright \\ \curvearrowleft \end{array} \end{array}, \quad (4.118)$$

where

$$\mathcal{N}_{3;1} = \frac{1}{\sqrt{d_f^3}}, \quad \mathcal{N}_{3;2} = \mathcal{N}_{3;3} = \mathcal{N}_{3;4} = \frac{\mathcal{N}_{2;2}}{\sqrt{d_f}}, \quad \mathcal{N}_{3;5} = \mathcal{N}_{3;3;1;1}^{(A)}, \quad \mathcal{N}_{3;6} = \mathcal{N}_{3;1;1;1}^{(A)}. \quad (4.119)$$

4.3.4 The Fierz-Young basis and the swap operator

In this subsection, I generalize the discussion presented in [32] regarding the real and imaginary parts of the dipole operator being even and odd, respectively, under the interchange of quark and anti-quark coordinate labels. To this end, I introduce an operator I dub the swap operator and observe an interesting transformation property of the Fierz-Young basis under the action

of it. This transformation property has important implications for the real and imaginary parts of amplitude/correlator matrices (constructed in the Fierz-Young basis) under a simultaneous pairwise interchange of quark and anti-quark coordinate labels. The content of this section is entirely original.

Consider the swap operator defined as $S : W \rightarrow \bar{W}; (v, \bar{v}) \mapsto (\bar{v}, v)$ which in birdtracks is given by

$$S = \text{X}, \quad (4.120)$$

where $W = V \otimes \bar{V}$ and $\bar{W} = \bar{V} \otimes V$. Notice that

$$S|1\rangle = \text{X} = \text{J} \cong \text{J} = |1\rangle, \quad (4.121)$$

where the equivalence relation \cong in the second last step follows from Eq. 4.38. We say that $|1\rangle$ is an eigenstate of S with respect to \cong with eigenvalue 1. Raising the swap operator to some tensor power $\otimes m$ where $m \in \mathbb{N}^+$ defines the swap operator $S^{\otimes m} : W^{\otimes m} \rightarrow \bar{W}^{\otimes m}$ where

$$S^{\otimes m} = \left. \begin{array}{c} \text{X} \\ \vdots \\ \text{X} \end{array} \right\} m \text{ pairs}. \quad (4.122)$$

Consider the application of $S^{\otimes m}$ on some pure adjoint colour singlet state $|m; s\rangle_A \in \mathfrak{C}^{(A)}(W^{\otimes m})$ as given in Eq. 4.50,

$$S^{\otimes m}|m; s\rangle_A = \left. \begin{array}{c} \text{X} \\ \vdots \\ \text{X} \end{array} \right\} \text{X} = \left. \begin{array}{c} \text{J} \\ \vdots \\ \text{J} \end{array} \right\} \text{X} \cong \left. \begin{array}{c} \text{J} \\ \vdots \\ \text{J} \end{array} \right\} \text{X}^* = |m; s^*\rangle_A. \quad (4.123)$$

The equivalence relation \cong in the second last step follows from Lemma 4.1. Eq. 4.123 says that the action of $S^{\otimes m}$ on $|m; s\rangle_A$ is equivalent to complex conjugating the colour structure (the coefficient tensor of $|m; s\rangle_A$ in the basis $\sqrt{2^m}|t^{a_1}\rangle \otimes \cdots \otimes |t^{a_m}\rangle$) used to construct $|m; s\rangle_A$. For the Young colour structures given in Eq. 4.79 and Eq. 4.87 we see that

$$\left(\mathcal{C}^{(2;1;1;1)a_1 a_2} \right)^* \stackrel{\text{Eq. 4.79}}{=} \left(\frac{1}{\sqrt{d_A}} \delta^{a_1 a_2} \right)^* = \frac{1}{\sqrt{d_A}} \delta^{a_1 a_2} \stackrel{\text{Eq. 4.79}}{=} \mathcal{C}^{(2;1;1;1)a_1 a_2}, \quad (4.124a)$$

- For fundamental and anti-fundamental Wilson-lines

$$\begin{aligned} (i \text{---} \text{---} j)^* &= [(U_x)^*]_j^i = [U_x^\dagger]_j^i =: i \text{---} \text{---} j, \\ (\bar{i} \text{---} \text{---} \bar{j})^* &= [(U_y^\dagger)^*]_{\bar{i}}^{\bar{j}} = [U_y]_{\bar{i}}^{\bar{j}} =: \bar{i} \text{---} \text{---} \bar{j}. \end{aligned} \quad (4.130)$$

- For tensor-product representations of Wilson-lines acting on $W^{\otimes m}$

$$\left[\begin{array}{c} i_1 \text{---} \text{---} j_1 \\ \bar{i}_1 \text{---} \text{---} \bar{j}_1 \\ \vdots \\ i_m \text{---} \text{---} j_m \\ \bar{i}_m \text{---} \text{---} \bar{j}_m \end{array} \right]^* = \begin{array}{c} i_1 \text{---} \text{---} j_1 \\ \bar{i}_1 \text{---} \text{---} \bar{j}_1 \\ \vdots \\ i_m \text{---} \text{---} j_m \\ \bar{i}_m \text{---} \text{---} \bar{j}_m \end{array}. \quad (4.131)$$

- For colour singlet states on $W^{\otimes m}$

$$\left[\begin{array}{c} j_1 \text{---} \text{---} j \\ \bar{j}_1 \text{---} \text{---} \bar{j} \\ \vdots \\ j_m \text{---} \text{---} j \\ \bar{j}_m \text{---} \text{---} \bar{j} \end{array} \right]^* = \begin{array}{c} j_1 \text{---} \text{---} j \\ \bar{j}_1 \text{---} \text{---} \bar{j} \\ \vdots \\ j_m \text{---} \text{---} j \\ \bar{j}_m \text{---} \text{---} \bar{j} \end{array}, \quad \left[\begin{array}{c} i_1 \text{---} \text{---} i \\ \bar{i}_1 \text{---} \text{---} \bar{i} \\ \vdots \\ i_m \text{---} \text{---} i \\ \bar{i}_m \text{---} \text{---} \bar{i} \end{array} \right]^* = \begin{array}{c} i_1 \text{---} \text{---} i \\ \bar{i}_1 \text{---} \text{---} \bar{i} \\ \vdots \\ i_m \text{---} \text{---} i \\ \bar{i}_m \text{---} \text{---} \bar{i} \end{array}, \quad (4.132)$$

where the labels i^* and j^* are a shorthand reminder that, when writing the colour singlet states as complex linear combinations of Kronecker delta symbols, the complex coefficients need to be complex conjugated. For real colour singlet states

$$\begin{array}{c} j_1 \text{---} \text{---} j^* \\ \bar{j}_1 \text{---} \text{---} \bar{j}^* \\ \vdots \\ j_m \text{---} \text{---} j^* \\ \bar{j}_m \text{---} \text{---} \bar{j}^* \end{array} = \begin{array}{c} j_1 \text{---} \text{---} j \\ \bar{j}_1 \text{---} \text{---} \bar{j} \\ \vdots \\ j_m \text{---} \text{---} j \\ \bar{j}_m \text{---} \text{---} \bar{j} \end{array} = \begin{array}{c} j_1 \text{---} \text{---} j \\ \bar{j}_1 \text{---} \text{---} \bar{j} \\ \vdots \\ j_m \text{---} \text{---} j \\ \bar{j}_m \text{---} \text{---} \bar{j} \end{array}, \quad \begin{array}{c} i_1 \text{---} \text{---} i^* \\ \bar{i}_1 \text{---} \text{---} \bar{i}^* \\ \vdots \\ i_m \text{---} \text{---} i^* \\ \bar{i}_m \text{---} \text{---} \bar{i}^* \end{array} = \begin{array}{c} i_1 \text{---} \text{---} i \\ \bar{i}_1 \text{---} \text{---} \bar{i} \\ \vdots \\ i_m \text{---} \text{---} i \\ \bar{i}_m \text{---} \text{---} \bar{i} \end{array} = \begin{array}{c} i_1 \text{---} \text{---} i \\ \bar{i}_1 \text{---} \text{---} \bar{i} \\ \vdots \\ i_m \text{---} \text{---} i \\ \bar{i}_m \text{---} \text{---} \bar{i} \end{array}, \quad (4.133)$$

where we again note that although the complex conjugate of colour singlet states are tensors living in different tensor-product spaces, their tensor components are real linear combinations of Kronecker delta symbols and, consequently, are equal.

With the above diagrammatic rules for complex conjugation at hand, consider the operator \tilde{S} whose action on a general amplitude matrix $\mathcal{A}^{(m)}$ is given by

$$\tilde{S} \circ \mathcal{A}_{x_1 \dots x_m; y_1 \dots y_m}^{(m)} = \mathcal{A}_{y_1 \dots y_m; x_1 \dots x_m}^{(m)}; \quad (4.134)$$

i.e. \tilde{S} implements a pair-wise swap of all quark and anti-quarks coordinate labels on the Wilson-lines in the amplitude matrix. Suppose this amplitude matrix is constructed from an orthonormal basis of colour singlet states for $\mathfrak{C}(W^{\otimes m})$ which satisfy Eq. 4.129a. Then, in birdtracks, the i^{th} row and j^{th} column of Eq. 4.134 becomes

$$\tilde{S} \circ \left[\begin{array}{c} i \text{---} \text{---} j \\ \vdots \\ i \text{---} \text{---} j \end{array} \right] \xrightarrow{\text{Eq. 4.129b}} \left[\begin{array}{c} i \text{---} \text{---} j \\ \vdots \\ i \text{---} \text{---} j \end{array} \right] = s_i s_j \left[\begin{array}{c} i \text{---} \text{---} j \\ \vdots \\ i \text{---} \text{---} j \end{array} \right] \xrightarrow[\text{Eq. 4.133}]{\text{Eq. 4.131}} s_i s_j \left[\begin{array}{c} i \text{---} \text{---} j \\ \vdots \\ i \text{---} \text{---} j \end{array} \right]^*, \quad (4.135)$$

or

$$\tilde{S} \circ [\mathcal{A}_{x_1 \dots x_m; y_1 \dots y_m}^{(m)}]_{ij} = s_i s_j [\mathcal{A}_{x_1 \dots x_m; y_1 \dots y_m}^{(m)}]_{ij}^*, \quad (4.136)$$

where for each diagram in Eq. 4.135 the Wilson-lines are drawn such that they are labelled from top to bottom by the coordinates $x_1, y_1, \dots, x_m, y_m$. Eq. 4.136 implies that the real and imaginary parts of such an amplitude matrix satisfy

$$\tilde{S} \circ \text{Re} [\mathcal{A}_{x_1 \dots x_m; y_1 \dots y_m}^{(m)}]_{ij} = s_i s_j \text{Re} [\mathcal{A}_{x_1 \dots x_m; y_1 \dots y_m}^{(m)}]_{ij}, \quad (4.137a)$$

$$\tilde{S} \circ \text{Im} [\mathcal{A}_{x_1 \dots x_m; y_1 \dots y_m}^{(m)}]_{ij} = -s_i s_j \text{Im} [\mathcal{A}_{x_1 \dots x_m; y_1 \dots y_m}^{(m)}]_{ij}, \quad (4.137b)$$

This operator \tilde{S} provides a natural generalization of the parity operator implicit in [32] which implements the exchange of the quark and anti-quark coordinate labels in the $q\bar{q}$ amplitude.

4.4 Embedding Wilson-line amplitude/correlator matrices

In this section, I show how a general Wilson-line amplitude/correlator matrix can be embedded into a larger one. Following a single pairwise quark–anti-quark coincidence limit, the larger matrix block diagonalizes into two blocks with one of them being the original matrix. An explicit example of this embedding is given in Eq. 4.151, where the $q^2\bar{q}^2$ amplitude matrix is contained as one of two blocks in the $q^3\bar{q}^3$ amplitude matrix following the coincidence limit that $y_3 \mapsto x_3$. The motivation for considering the embedding of Wilson-line correlator/amplitude matrices into larger ones is given by JIMWLK evolution; in Eq. 5.94 I show how JIMWLK evolution couples the aforementioned disjoint blocks, from which one learns that this embedding framework is the most appropriate language for expressing the JIMWLK equation of general Wilson-line correlator matrices. The general discussion regarding how one embeds a general amplitude/correlator matrix into a larger one is new.

4.4.1 Fierz bases as embedding bases

Fierz bases, by virtue of the Fierz property, are examples of embedding bases. Notice that the basis element in Eq. 4.110, the only normalized colour singlet state in W , is embedded in the top half of the first basis element of Eq. 4.112 (the first element of the Fierz-permutation basis) as well as Eq. 4.116 (the first element of the Fierz-Young basis). Similarly, the basis elements of Eq. 4.112 are embedded in the top half of the first two elements of Eq. 4.114 and the basis elements of Eq. 4.116 are embedded in the top half of the first two elements of Eq. 4.118. This embedding of a given Fierz basis for $\mathfrak{C}(W^{\otimes m})$ into the associated Fierz basis for $\mathfrak{C}(W^{\otimes(m+1)})$ is a feature for all $m \in \mathbb{N}^+$ by construction.

The advantage of this embedding property is that for amplitude matrices constructed in a Fierz basis, the $q^m \bar{q}^m$ amplitude matrix can be naturally embedded in the amplitude matrix describing $(m+1)$ quarks and anti-quarks. This is possible because any Fierz basis for $\mathfrak{C}(W^{\otimes(m+1)})$ simultaneously diagonalizes the following complete pair of mutually orthogonal projection operators

$$i_{W^{\otimes m}} \otimes P_{\bullet} = \frac{1}{d_f} \left\{ \begin{array}{c} \overrightarrow{\hspace{1cm}} \\ \overrightarrow{\hspace{1cm}} \\ \vdots \\ \overrightarrow{\hspace{1cm}} \\ \overrightarrow{\hspace{1cm}} \end{array} \right\} i_{W^{\otimes m}}, \quad i_{W^{\otimes m}} \otimes P_A = \left\{ \begin{array}{c} \overrightarrow{\hspace{1cm}} \\ \overrightarrow{\hspace{1cm}} \\ \vdots \\ \overrightarrow{\hspace{1cm}} \\ \overrightarrow{\hspace{1cm}} \end{array} \right\} i_{W^{\otimes m}}, \quad (4.138a)$$

where $i_{W^{\otimes m}}$ is the identity map on $W^{\otimes m}$ and P_{\bullet}, P_A are given in Eq. 4.31. Let $\mathfrak{B}_{\text{Fierz}}(W^{\otimes(m+1)})$ be some Fierz basis for $\mathfrak{C}(W^{\otimes(m+1)})$. Then $\mathfrak{B}_{\text{Fierz}}(W^{\otimes(m+1)})$ partitions into the union of two bases: one for $\mathfrak{C}(W^{\otimes m} \otimes \bullet)$ and one for $\mathfrak{C}(W^{\otimes m} \otimes A)$

$$\mathfrak{B}_{\text{Fierz}}(W^{\otimes(m+1)}) = \mathfrak{B}_{\text{Fierz}}(W^{\otimes m} \otimes \bullet) \cup \mathfrak{B}_{\text{Fierz}}(W^{\otimes m} \otimes A), \quad (4.139)$$

where the former partition is given by

$$\mathfrak{B}_{\text{Fierz}}(W^{\otimes m} \otimes \bullet) = \mathfrak{B}_{\text{Fierz}}(W^{\otimes m}) \otimes \{|1\rangle\}, \quad (4.140)$$

where $\mathfrak{B}_{\text{Fierz}}(W^{\otimes m})$ is the associated Fierz basis for $\mathfrak{C}(W^{\otimes m})$ which can be used to construct the $q^m \bar{q}^m$ amplitude matrix and $|1\rangle$ is given in Eq. 4.23. We may draw the i^{th} basis state in Eq. 4.140 as

$$|m+1; i\rangle = |m; i\rangle \otimes |1\rangle = \frac{1}{d_f} \left\{ \begin{array}{c} \overrightarrow{\hspace{1cm}} \\ \overrightarrow{\hspace{1cm}} \\ \vdots \\ \overrightarrow{\hspace{1cm}} \\ \overrightarrow{\hspace{1cm}} \end{array} \right\} i, \quad (4.141)$$

where $|m; i\rangle$ is the i^{th} element in $\mathfrak{B}_{\text{Fierz}}(W^{\otimes m})$. Diagrammatically, it is immediately obvious that Eq. 4.141 is an eigenstate of $i_{W^{\otimes m}} \otimes P_{\bullet}$. The i^{th} basis state in the latter partition of Eq. 4.139 may be drawn as

$$|m+1; i\rangle = \left\{ \begin{array}{c} \overrightarrow{\hspace{1cm}} \\ \overrightarrow{\hspace{1cm}} \\ \vdots \\ \overrightarrow{\hspace{1cm}} \\ \overrightarrow{\hspace{1cm}} \end{array} \right\} i, \quad (4.142)$$

which is clearly an eigenstate of $i_{W^{\otimes m}} \otimes P_A$.

The amplitude matrix for $(m+1)$ quarks and anti-quarks constructed $\mathfrak{B}_{\text{Fierz}}(W^{\otimes(m+1)})$ is given by

$$\left[\mathcal{A}_{x_1 \dots x_m x_{m+1}; y_1 \dots y_m y_{m+1}}^{(m+1)} \right]_{ij} = \text{Diagram} \quad (4.143)$$

In the limit that x_{m+1} and y_{m+1} become coincident (i.e. $y_{m+1} \mapsto x_{m+1} = z$), Eq. 4.143 block diagonalizes because the overlap between basis states from different partitions in Eq. 4.139 vanishes;

$$\text{Diagram} = 0, \quad (4.144)$$

because

$$\text{Diagram} = \sqrt{2d_f} \langle 1 | U_z \otimes U_z^\dagger | t^a \rangle = \sqrt{2} \text{Tr} (U_z t^a U_z^\dagger) = \sqrt{2} \text{Tr} (t^a) = 0. \quad (4.145)$$

Consequently, in this coincidence limit, the amplitude matrix in Eq. 4.143 expanded in this basis becomes block diagonal

$$\mathcal{A}_{x_1 \dots x_m z; y_1 \dots y_m z}^{(m+1)} = \begin{bmatrix} \mathcal{A}_{x_1 \dots x_m; y_1 \dots y_m}^{(m)} & 0_{m! \times m \cdot m!} \\ 0_{m \cdot m! \times m!} & \mathcal{A}_{x_1 \dots x_m; y_1 \dots y_m; z}^{(m;g)} \end{bmatrix}, \quad (4.146)$$

where the upper left block is the original $q^m \bar{q}^m$ amplitude matrix

$$\left[\mathcal{A}_{x_1 \dots x_m; y_1 \dots y_m}^{(m)} \right]_{ij} = \text{Diagram}, \quad (4.147)$$

and the lower right block is the $q^m \bar{q}^m g$ amplitude matrix which we define to be

$$\left[\mathcal{A}_{x_1 \dots x_m; y_1 \dots y_m; z}^{(m;g)} \right]_{ij} = \text{Diagram} \quad (4.148)$$

4.4.2 Example: the $q^3 \bar{q}^3$ amplitude matrix

An important example (specifically for this thesis) which demonstrates the embedding of Wilson-line amplitude matrices in higher dimensional ones is the $q^3 \bar{q}^3$ amplitude matrix, constructed using the Fierz-Young basis given in Eq. 4.118 for $\mathfrak{C}(W^{\otimes 3})$. The full $q^3 \bar{q}^3$ amplitude matrix is

given by

$$\left[\begin{array}{cccccc}
 A_{11}^{(3)} & A_{12}^{(3)} & A_{13}^{(3)} & A_{14}^{(3)} & A_{15}^{(3)} & A_{16}^{(3)} \\
 A_{21}^{(3)} & A_{22}^{(3)} & A_{23}^{(3)} & A_{24}^{(3)} & A_{25}^{(3)} & A_{26}^{(3)} \\
 A_{31}^{(3)} & A_{32}^{(3)} & A_{33}^{(3)} & A_{34}^{(3)} & A_{35}^{(3)} & A_{36}^{(3)} \\
 A_{41}^{(3)} & A_{42}^{(3)} & A_{43}^{(3)} & A_{44}^{(3)} & A_{45}^{(3)} & A_{46}^{(3)} \\
 A_{51}^{(3)} & A_{52}^{(3)} & A_{53}^{(3)} & A_{54}^{(3)} & A_{55}^{(3)} & A_{56}^{(3)} \\
 A_{61}^{(3)} & A_{62}^{(3)} & A_{63}^{(3)} & A_{64}^{(3)} & A_{65}^{(3)} & A_{66}^{(3)}
 \end{array} \right], \quad (4.149)$$

$q^3 \bar{q}^3$

where the normalization constants $A_{ij}^{(3)}$ (for $i, j = 1, \dots, 6$) are given in terms of the normalization constants of the Fierz basis elements from Eq. 4.119 as

$$A_{ij}^{(3)} = \mathcal{N}_{3;i} \mathcal{N}_{3;j}. \quad (4.150)$$

The entries of Eq. 4.149 without a shaded background are those whose real parts are even and whose imaginary parts are odd under the action of \tilde{S} . The entries with shaded backgrounds have the opposite behaviour; the real parts are odd while the imaginary parts are even.

In the limit that the last quark–anti-quark pair becomes coincident (i.e. $\mathbf{y}_3 \mapsto \mathbf{x}_3$) the $q^3\bar{q}^3$ amplitude matrix block diagonalizes as follows

$$\left[\begin{array}{cccccc}
 A_{11}^{(3)} \text{ (diagram)} & A_{12}^{(3)} \text{ (diagram)} & 0 & 0 & 0 & 0 \\
 A_{21}^{(3)} \text{ (diagram)} & A_{22}^{(3)} \text{ (diagram)} & 0 & 0 & 0 & 0 \\
 0 & 0 & A_{33}^{(3)} \text{ (diagram)} & A_{34}^{(3)} \text{ (diagram)} & A_{35}^{(3)} \text{ (diagram)} & A_{36}^{(3)} \text{ (diagram)} \\
 0 & 0 & A_{43}^{(3)} \text{ (diagram)} & A_{44}^{(3)} \text{ (diagram)} & A_{45}^{(3)} \text{ (diagram)} & A_{46}^{(3)} \text{ (diagram)} \\
 0 & 0 & A_{53}^{(3)} \text{ (diagram)} & A_{54}^{(3)} \text{ (diagram)} & A_{55}^{(3)} \text{ (diagram)} & A_{56}^{(3)} \text{ (diagram)} \\
 0 & 0 & A_{63}^{(3)} \text{ (diagram)} & A_{64}^{(3)} \text{ (diagram)} & A_{65}^{(3)} \text{ (diagram)} & A_{66}^{(3)} \text{ (diagram)}
 \end{array} \right] \cdot \quad (4.151)$$

$q^2\bar{q}^2 \oplus q^2\bar{q}^2 g$

The top left block in Eq. 4.151 is precisely the $q^2\bar{q}^2$ amplitude matrix constructed using the Fierz-Young basis given in Eq. 4.116 for $\mathfrak{C}(W^{\otimes 2})$. Notice that the entire $q^2\bar{q}^2$ amplitude matrix possesses the property that its real part is even and its imaginary part is odd under the action of \tilde{S} . Just as the $q^2\bar{q}^2$ amplitude matrix was embedded in the $q^3\bar{q}^3$ amplitude matrix, if we take a further coincidence limit with $\mathbf{y}_2 \mapsto \mathbf{x}_2$, the top left $q^2\bar{q}^2$ block in Eq. 4.151 itself will block diagonalize producing the $q\bar{q}$ amplitude in upper left corner and the $q\bar{q}g$ amplitude matrix in the lower right corner. This coincidence limit is demonstrated below:

$$\begin{bmatrix}
A_{11}^{(3)} \text{ (diagram)} & 0 & 0 & 0 & 0 & 0 \\
0 & A_{22}^{(3)} \text{ (diagram)} & 0 & 0 & 0 & 0 \\
0 & 0 & A_{33}^{(3)} \text{ (diagram)} & 0 & 0 & 0 \\
0 & 0 & 0 & A_{44}^{(3)} \text{ (diagram)} & A_{45}^{(3)} \text{ (diagram)} & A_{46}^{(3)} \text{ (diagram)} \\
0 & 0 & 0 & A_{54}^{(3)} \text{ (diagram)} & A_{55}^{(3)} \text{ (diagram)} & A_{56}^{(3)} \text{ (diagram)} \\
0 & 0 & 0 & A_{64}^{(3)} \text{ (diagram)} & A_{65}^{(3)} \text{ (diagram)} & A_{66}^{(3)} \text{ (diagram)}
\end{bmatrix} \cdot \quad (4.152)$$

$q\bar{q} \oplus (q\bar{q}g)^{\oplus 2} \oplus q\bar{q}g^2$

For completeness as well as for later use, we also give a further coincidence limit where $\mathbf{y}_1 \mapsto \mathbf{x}_1$

$$\begin{bmatrix}
A_{11}^{(3)} \text{ (diagram)} & 0 & 0 & 0 & 0 & 0 \\
0 & A_{22}^{(3)} \text{ (diagram)} & 0 & 0 & 0 & 0 \\
0 & 0 & A_{33}^{(3)} \text{ (diagram)} & 0 & 0 & 0 \\
0 & 0 & 0 & A_{44}^{(3)} \text{ (diagram)} & 0 & 0 \\
0 & 0 & 0 & 0 & A_{55}^{(3)} \text{ (diagram)} & A_{56}^{(3)} \text{ (diagram)} \\
0 & 0 & 0 & 0 & A_{65}^{(3)} \text{ (diagram)} & A_{66}^{(3)} \text{ (diagram)}
\end{bmatrix} \cdot \quad (4.153)$$

$1 \oplus (g^2)^{\oplus 3} \oplus g^3$

Chapter 5

The JIMWLK equation and the Balitsky hierarchy

5.1 A systematic derivation of the leading-log (LL) JIMWLK Hamiltonian

In the preceding chapters, it was argued that the appropriate objects for describing scattering in the Regge-Gribov limit of QCD are Wilson-lines and their correlators. Wilson-line correlators latter are defined through a (functional) target average with respect to b^+ or, equivalently, U (since b^+ only features in observables through U). However, the definition of b^+ as the kinematically-enhanced, dominant contribution to the background field of the target is a resolution- dependent definition: as the rapidity separation Y between the projectile and the target increases, modes which were previously considered fluctuations δA^+ on top of b^+ become Lorentz contracted into a redefinition of b^+ (see Fig. 5.1). Consequently, the target average becomes Y dependent and one writes

$$\langle \cdots \rangle_b(Y) = \int D[b^+] \cdots W_Y[b^+], \text{ or, equivalently, } \langle \cdots \rangle_U(Y) = \int \hat{D}[U] \cdots \hat{Z}_Y[U], \quad (5.1)$$

where $W_Y[b^+]$ and $\hat{Z}_Y[U]$ are Y dependent distributions which encode information about the QCD action and the target wave-function relevant at large Y [9]. The evolution of Eq. 5.1 in Y is governed by a functional renormalization group equation called the JIMWLK equation named after its authors Jalilian-Marian+Iancu+McLerran+Weigert+Leonidov+Kovner¹. In this section, we re-derive of the JIMWLK equation (at leading logarithmic accuracy) at the level of the generating functional for Wilson-line correlators following [42].

¹The order of names was chosen by Al Mueller to give rise to the acronym JIMWLK, pronounced “gym walk”.

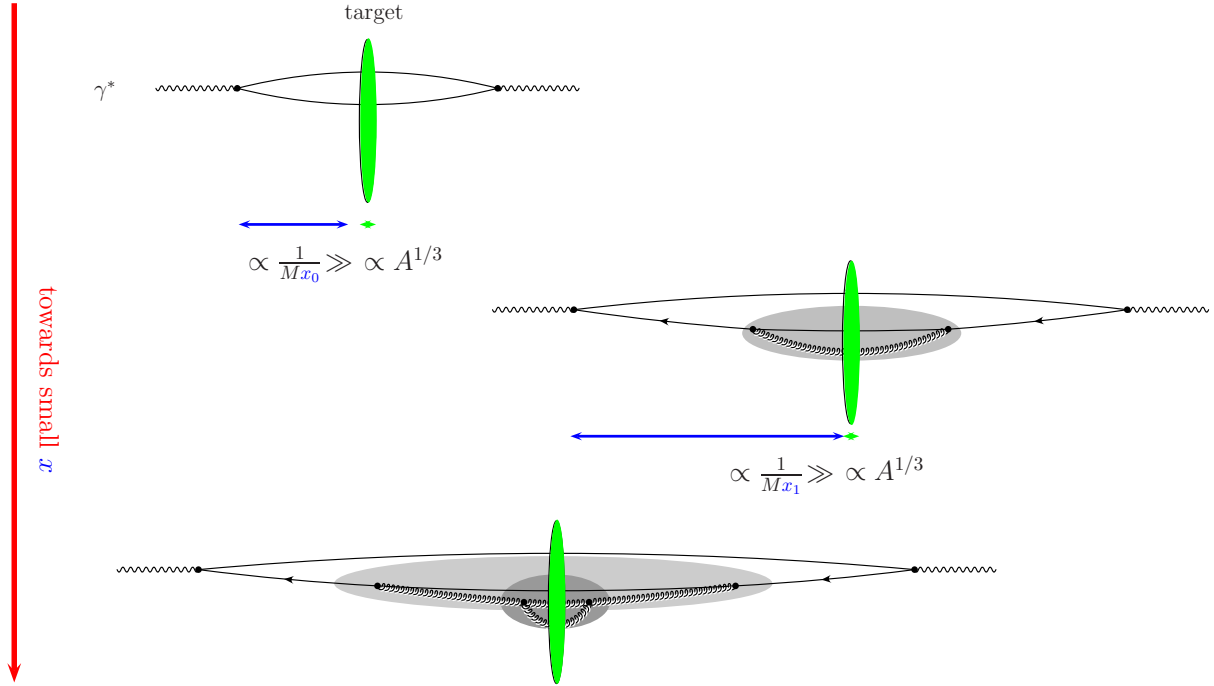


FIGURE 5.1: (Colour online) Fluctuations on top of the background field of the target which are subsumed into a redefinition of the target background field through Lorentz contraction as $Y = \ln(1/x_{bj})$ increases. The shaded regions denote perturbative corrections from fluctuations to the target average which are included via renormalization group flow.

This generating functional is defined as

$$\bar{\mathcal{Z}}_Y[J^\dagger, J] := \left\langle e^{\mathcal{S}_{\text{ext}}^{q\bar{q}}[b, J^\dagger, J]} \right\rangle_b(Y), \quad (5.2)$$

where

$$\mathcal{S}_{\text{ext}}^{q\bar{q}}[A, J^\dagger, J] := \int_x \left\{ \text{Tr} \left((J_x^\dagger)^t U_x[A] \right) + \text{Tr} \left((J_x)^t U_x^\dagger[A] \right) \right\}, \quad (5.3)$$

is the action which couples Wilson-lines in the fundamental and anti-fundamental representations to external sources J^\dagger and J , respectively. Since one can always express adjoint Wilson-lines (which describe gluons) in terms of the fundamental and anti-fundamental ones (which describe quarks and anti-quarks, respectively), Eq. 5.3 is sufficient for generating all Wilson-lines correlators of interest in QCD. In Eq. 5.3 we have chosen to subscript the coordinate dependence of functions as well as the integration measure, a convention which we shall adopt throughout this section.

The correlator of the tensor product of m fundamental and \bar{m} anti-fundamental Wilson-lines (where $m, \bar{m} \in \mathbb{N}^+$) is obtained from Eq. 5.2 via

$$\langle U_{x_1} \otimes \cdots \otimes U_{x_m} \otimes U_{y_1}^\dagger \otimes \cdots \otimes U_{y_{\bar{m}}}^\dagger \rangle_b(Y) = \frac{\delta}{\delta J_{x_1}^\dagger} \cdots \frac{\delta}{\delta J_{x_m}^\dagger} \frac{\delta}{\delta J_{y_1}} \cdots \frac{\delta}{\delta J_{y_{\bar{m}}}} \bigg|_{J^{(\dagger)}=0} \bar{\mathcal{Z}}_Y[J^\dagger, J]. \quad (5.4)$$

The logarithmically enhanced perturbative corrections to the target average which arise from Lorentz contracted (and time dilated) modes previously contained in δA^+ are most easily computed as perturbative corrections to the Wilson-lines describing the interaction of the projectile with the target. Once computed, these perturbative corrections can be subsumed into the target average via a functional integration by parts. In order to uncover these perturbative corrections, consider the generating functional in Eq. 5.2 where the average is performed with respect to $A^+ = b^+ + \delta A^+$ and let us expand around b^+ , isolating contributions of order $\alpha_s \ln(1/x_{\text{bj}}) = \alpha_s Y$. To this end, it is sufficient to expand Eq. 5.2 to quadratic order in δA^+ [9]:

$$\begin{aligned}
\left\langle e^{\mathcal{S}_{\text{ext}}^{q\bar{q}}[b+\delta A, J^\dagger, J]} \right\rangle_{b, \delta A}(Y) &= \left\langle \left[1 + \int_x \delta A_x^{a+} \frac{\delta}{\delta b_x^{a+}} + \frac{1}{2} \int_{xy} \delta A_x^{a+} \delta A_y^{b+} \frac{\delta}{\delta b_x^{a+}} \frac{\delta}{\delta b_y^{b+}} \right. \right. \\
&\quad \left. \left. + \mathcal{O}(\delta A^3) \right] e^{\mathcal{S}_{\text{ext}}^{q\bar{q}}[b, J^\dagger, J]} \right\rangle_{b, \delta A}(Y_0) \\
&= \left\langle e^{\mathcal{S}_{\text{ext}}^{q\bar{q}}[b, J^\dagger, J]} \right\rangle_b(Y_0) + \frac{1}{2} \int_{xy} \left\langle \langle \delta A_x^{a+} \delta A_y^{b+} \rangle_{\delta A}[b] \left[\left(\frac{\delta}{\delta b_x^{a+}} \mathcal{S}_{\text{ext}}^{q\bar{q}}[b, J^\dagger, J] \right) \left(\frac{\delta}{\delta b_y^{b+}} \mathcal{S}_{\text{ext}}^{q\bar{q}}[b, J^\dagger, J] \right) \right. \right. \\
&\quad \left. \left. + \frac{\delta}{\delta b_x^{a+}} \frac{\delta}{\delta b_y^{b+}} \mathcal{S}_{\text{ext}}^{q\bar{q}}[b, J^\dagger, J] \right] e^{\mathcal{S}_{\text{ext}}^{q\bar{q}}[b, J^\dagger, J]} \right\rangle_b(Y_0) + \mathcal{O}(\delta A^3), \tag{5.5}
\end{aligned}$$

where we have assumed the vacuum expectation value of the fluctuations $\langle \delta A_x^{a+} \rangle_{\delta A}[b]$ to be zero. In order to evaluate the $\mathcal{O}(\delta A^2)$ contribution in Eq. 5.5, we need to know what the functional derivative of fundamental and anti-fundamental Wilson-lines with respect to the background field is. This is computed as

$$\frac{\delta}{\delta b_x^{a+}} U_z = ig \delta_{x+0} \delta_{xz}^{(2)} U_{z; \infty, x^-}[b] t^a U_{z; x^-, -\infty}[b], \tag{5.6a}$$

$$\frac{\delta}{\delta b_x^{a+}} U_z^\dagger = -ig \delta_{x+0} \delta_{xz}^{(2)} U_{z; x^-, -\infty}^\dagger[b] t^a U_{z; \infty, x^-}^\dagger[b], \tag{5.6b}$$

respectively. The partial Wilson-lines on the right-hand-side expression of Eq. 5.6, although correct, are computationally cumbersome. Given the specific form of the background field b^+ , as long as we are not interested in taking derivatives of Eq. 5.6 with respect to x^- and for the purpose of evaluating their contributions to the integral in Eq. 5.5, we can represent the right-hand-side expressions of Eq. 5.6 by

$$\frac{\delta}{\delta b_x^{a+}} U_z = ig \delta_{x+0} \delta_{xz}^{(2)} (\theta_{x^-, 0} t^a U_z + \theta_{0, x^-} U_z t^a), \tag{5.7a}$$

$$\frac{\delta}{\delta b_x^{a+}} U_z^\dagger = -ig \delta_{x+0} \delta_{xz}^{(2)} (\theta_{x^-, 0} U_z^\dagger t^a + \theta_{0, x^-} t^a U_z^\dagger). \tag{5.7b}$$

The second term in Eq. 5.5, the calculable perturbative correction to the generating functional, consists of two contributions: one quadratic in the external sources

$$\begin{aligned} & \left(\frac{\delta}{\delta b_x^{a+}} \mathcal{S}_{\text{ext}}^{q\bar{q}}[b, J^\dagger, J] \right) \left(\frac{\delta}{\delta b_y^{b+}} \mathcal{S}_{\text{ext}}^{q\bar{q}}[b, J^\dagger, J] \right) = (ig)^2 \delta_{x+,0} \delta_{y+,0} \\ & \times \left[\theta_{x-,0} \left([J_x^\dagger]_{ij} [t^a U_x]_{ij} - [J_x]_{ij} [U_x^\dagger t^a]_{ij} \right) + \theta_{0,x-} \left([J_x^\dagger]_{ij} [U_x t^a]_{ij} - [J_x]_{ij} [t^a U_x^\dagger]_{ij} \right) \right] \\ & \times \left[\theta_{y-,0} \left([J_y^\dagger]_{ij} [t^b U_y]_{ij} - [J_y]_{ij} [U_y^\dagger t^b]_{ij} \right) + \theta_{0,y-} \left([J_y^\dagger]_{ij} [U_y t^b]_{ij} - [J_y]_{ij} [t^b U_y^\dagger]_{ij} \right) \right], \quad (5.8) \end{aligned}$$

and the other linear in them

$$\begin{aligned} & \frac{\delta}{\delta b_x^{a+}} \frac{\delta}{\delta b_y^{b+}} \mathcal{S}_{\text{ext}}^{q\bar{q}}[b, J^\dagger, J] = (ig)^2 \delta_{x+,0} \delta_{y+,0} \delta_{x,y}^{(2)} \\ & \times \left[[J_x^\dagger]_{ij} \left\{ \theta_{x-,y-} \left(\theta_{x-,0} \theta_{y-,0} t^a t^b U_x + \theta_{x-,0} \theta_{0,y-} t^a U_x t^b + \theta_{0,x-} \theta_{0,y-} U_x t^a t^b \right) \right. \right. \\ & \quad \left. \left. + \theta_{y-,x-} \left(\theta_{y-,0} \theta_{x-,0} t^b t^a U_x + \theta_{y-,0} \theta_{0,x-} t^b U_x t^a + \theta_{0,y-} \theta_{0,x-} U_x t^b t^a \right) \right\}_{ij} \right. \\ & \quad \left. + [J_x]_{ij} \left\{ \theta_{x-,y-} \left(\theta_{x-,0} \theta_{y-,0} U_x^\dagger t^b t^a + \theta_{x-,0} \theta_{0,y-} t^b U_x^\dagger t^a + \theta_{0,x-} \theta_{0,y-} t^b t^a U_x^\dagger \right) \right. \right. \\ & \quad \left. \left. + \theta_{y-,x-} \left(\theta_{y-,0} \theta_{x-,0} U_x^\dagger t^a t^b + \theta_{y-,0} \theta_{0,x-} t^a U_x^\dagger t^b + \theta_{0,y-} \theta_{0,x-} t^a t^b U_x^\dagger \right) \right\}_{ij} \right]. \quad (5.9) \end{aligned}$$

Eq. 5.8 represents contributions due to a gluon-exchange between two quarks, two anti-quarks, or a quark and an anti-quark. Eq. 5.9 represents pure self-energy corrections dressing quark and anti-quark lines. Since Eq. 5.8 and Eq. 5.9 are quadratic and linear, respectively, in the external sources, it is sufficient to compute

$$\frac{\delta}{\delta J_x^{(\dagger)}} \frac{\delta}{\delta J_y^{(\dagger)}} \frac{1}{2} \int_{uv} \langle \delta A_u^{a+} \delta A_u^{b+} \rangle_{\delta A} [b] \left(\frac{\delta}{\delta b_u^{a+}} \mathcal{S}_{\text{ext}}^{q\bar{q}}[b, J^\dagger, J] \right) \left(\frac{\delta}{\delta b_v^{b+}} \mathcal{S}_{\text{ext}}^{q\bar{q}}[b, J^\dagger, J] \right), \quad (5.10)$$

and

$$\frac{\delta}{\delta J_x^{(\dagger)}} \frac{1}{2} \int_{uv} \langle \delta A_u^{a+} \delta A_u^{b+} \rangle_{\delta A} [b] \left(\frac{\delta}{\delta b_u^{a+}} \frac{\delta}{\delta b_v^{b+}} \mathcal{S}_{\text{ext}}^{q\bar{q}}[b, J^\dagger, J] \right), \quad (5.11)$$

in order to reconstruct Eq. 5.8 and Eq. 5.9, and therefore Eq. 5.5. To keep track of different contributions to Eq. 5.8 and Eq. 5.9, it is useful to define a few objects which admit a definite physical interpretation. Consider

$$\begin{aligned} & \ln(x_{\text{bj}0}/x_{\text{bj}}) [\bar{\chi}_{x,y}^{q\bar{q}}]_{ij\,kl} := \frac{\delta}{\delta [J_x^\dagger]_{ij}} \frac{\delta}{\delta [J_y]_{kl}} \frac{1}{2} \int_{uv} \langle \delta A_u^{a+} \delta A_u^{b+} \rangle_{\delta A} [b] \\ & \times \left(\frac{\delta}{\delta b_u^{a+}} \mathcal{S}_{\text{ext}}^{q\bar{q}}[b, J^\dagger, J] \right) \left(\frac{\delta}{\delta b_v^{b+}} \mathcal{S}_{\text{ext}}^{q\bar{q}}[b, J^\dagger, J] \right) \\ & = -\frac{1}{2} (ig)^2 \int_{uv} \langle \delta A_u^{a+} \delta A_v^{b+} \rangle_{\delta A} [b] \delta_{u+,0} \delta_{v+,0} \\ & \times \left[\delta_{x,u}^{(2)} \delta_{y,v}^{(2)} [W_{x,y;u^-,v^-}]_{ij\,kl}^{ab} + \delta_{x,v}^{(2)} \delta_{y,u}^{(2)} [W_{x,y;v^-,u^-}]_{ij\,kl}^{ba} \right], \quad (5.12) \end{aligned}$$

where

$$[W_{x,y;u^-,v^-}]_{ij\,kl}^{ab} := \delta_{x,u}^{(2)} \delta_{y,v}^{(2)} \left(\theta_{u^-,0} [t^a U_x]_{ij} + \theta_{0,u^-} [U_x t^a]_{ij} \right) \left(\theta_{v^-,0} [U_y^\dagger t^b]_{kl} + \theta_{0,v^-} [t^b U_y^\dagger]_{kl} \right), \quad (5.13)$$

and we have already factored out the anticipated logarithmic enhancement $\ln(x_{bj0}/x_{bj}) = Y - Y_0$ which we shall see is the regulated result of a semi-infinite, logarithmically-divergent momentum integral. Eq. 5.12 describes the exchange of a gluon, represented by the gluon propagator $\langle \delta A_u^{a+} \delta A_v^{b+} \rangle_{\delta A[b]}$ in the presence of the background field b^+ , between a quark and an anti-quark, represented by the fundamental and anti-fundamental Wilson-lines U_x and U_y^\dagger , respectively, where the gluon propagator attaches to the quark and anti-quark lines through the gauge generators. Eq. 5.12 can be represented diagrammatically by

$$\ln(x_{bj0}/x_{bj}) \bar{\chi}_{x,y}^{q\bar{q}} := \text{diagram} = \text{diagram}_1 + \text{diagram}_2 + \text{diagram}_3 + \text{diagram}_4, \quad (5.14)$$

where the diagrams after the second equality correspond to the four unique Heaviside function combinations present in Eq. 5.12. Similarly one defines $\bar{\chi}_{x,y}^{q\bar{q}}$, $\bar{\chi}_{x,y}^{qq}$ and $\bar{\chi}_{x,y}^{\bar{q}\bar{q}}$ ². Calculationally, these diagrams differ only in the order of the product of Wilson-lines and gauge generators which are independent of the internal space-time coordinates u, v . The self-energy correction dressing the quark line is defined as

$$\begin{aligned} \ln(x_{bj0}/x_{bj}) \cdot [\bar{\sigma}_x^q]_{ij} &:= \frac{\delta}{\delta[J_x^\dagger]_{ij}} \frac{1}{2} \int_{uv} \langle \delta A_u^{a+} \delta A_v^{b+} \rangle_{\delta A[b]} \left(\frac{\delta}{\delta b_u^{a+}} \frac{\delta}{\delta b_v^{b+}} \mathcal{S}_{\text{ext}}^{q\bar{q}}[b, J^\dagger, J] \right) \\ &= \frac{1}{2} (ig)^2 \int_{uv} \langle \delta A_u^{a+} \delta A_v^{b+} \rangle_{\delta A[b]} \delta_{x,u}^{(2)} \delta_{y,v}^{(2)} \delta_{u^+,0} \delta_{v^+,0} [W_{x;u^-,v^-}]_{ij}^{ab} \end{aligned} \quad (5.15)$$

where

$$\begin{aligned} [W_{x;u^-,v^-}]_{ij}^{ab} &:= \left[\theta_{u^-,v^-} \left(\theta_{u^-,0} \theta_{v^-,0} t^a t^b U_x + \theta_{u^-,0} \theta_{0,v^-} t^a U_x t^b + \theta_{0,u^-} \theta_{0,v^-} U_x t^a t^b \right) \right. \\ &\quad \left. + \theta_{v^-,u^-} \left(\theta_{v^-,0} \theta_{u^-,0} t^b t^a U_x + \theta_{v^-,0} \theta_{0,u^-} t^b U_x t^a + \theta_{0,v^-} \theta_{0,u^-} U_x t^b t^a \right) \right]_{ij}, \end{aligned} \quad (5.16)$$

with an analogous definition for $\bar{\sigma}_x^{\bar{q}}$. Diagrammatically, Eq. 5.15 reads

$$\ln(x_{bj0}/x_{bj}) [\bar{\sigma}_x^q]_{ij} := \text{diagram} = \text{diagram}_1 + \text{diagram}_2 + \text{diagram}_3 + \text{diagram}_4, \quad (5.17)$$

²Diagrammatically, these are drawn by reversing (anti-)quark lines in Eq. 5.14 accordingly.

while the Feynman diagram describing $\bar{\sigma}_x^q$ is obtained by reversing the direction of the arrows in Eq. 5.17 which represents the replacement of the fundamental Wilson-line U_x in Eq. 5.15 with the anti-fundamental Wilson-line U_x^\dagger . The propagator for the gluon in the presence of the background field of the target, computed in Sec. B.3, is given by

$$\begin{aligned} \langle \delta A_u^{a+} \delta A_u^{b+} \rangle_{\delta A[b]} &= \delta^{ab} \left[\frac{i}{-(\partial^-)^2} \right]_{uv} \\ &- \int_{u'v'} (i\partial_u^-) \left[\frac{i}{-(\partial^-)^2} \right]_{uu'} (i\partial_v^-) \left[\frac{i}{-(\partial^-)^2} \right]_{vv'} (i\partial_{u'}^i)(i\partial_{v'}^i) \left[\frac{i}{-D[b]^2} \right]_{u'v'}^{ab}, \end{aligned} \quad (5.18a)$$

where

$$\left[\frac{i}{-(\partial^-)^2} \right]_{uv} = \delta_{u^-,v^-} \delta_{u,v}^{(2)} \int \frac{dk^-}{2\pi} \frac{i}{(k^-)^2 + i\varepsilon} e^{-ik^-(u^+-v^+)}, \quad (5.18b)$$

$$\begin{aligned} \left[\frac{i}{-D[b]^2} \right]_{uv}^{ab} &= \int \frac{dk^-}{(2\pi)^3 (2k^-)} [\theta_{u^-,v^-} \theta_{k^-,0} - \theta_{v^-,u^-} \theta_{0,k^-}] \int d^2p_\perp d^2q_\perp e^{-i(p \cdot u - q \cdot v)} \\ &\times \int \frac{d^2z_\perp}{(2\pi)^2} e^{-i(p-q) \cdot z} [\tilde{U}_{z;u^-,v^-}]^{ab}, \end{aligned} \quad (5.18c)$$

and the partial Wilson-line from v^- to u^- in the adjoint representation is defined as

$$[\tilde{U}_{z;u^-,v^-}]^{ab} = P \exp \left[ig \int_{v^-}^{u^-} dz^- \delta(z^-) \beta^c(z) \tilde{t}^c \right]^{ab}, \quad (5.18d)$$

where $[\tilde{t}^c]^{ab} = if^{abc}$. Borrowing the discussion below Eq. 5.6, we shall represent Eq. 5.18d by

$$[\tilde{U}_{z;u^-,v^-}]^{ab} = [\theta_{u^-,0} \theta_{v^-,0} + \theta_{0,u^-} \theta_{0,v^-}] \delta^{ab} + \theta_{u^-,0} \theta_{0,v^-} [\tilde{U}_z]^{ab} + \theta_{0,u^-} \theta_{v^-,0} [\tilde{U}_z^\dagger]^{ab}. \quad (5.19)$$

The contributions³ to Eq. 5.8 coming from the second term in Eq. 5.18a which are present in each gluon-exchange diagram are given by

$$\begin{aligned} &\frac{1}{2} (ig)^2 \int_{uv} \left\{ \int_{u'v'} \delta_{u^-,u'^-} \delta_{v^-,v'^-} \delta_{u,u'}^{(2)} \delta_{v,v'}^{(2)} \int \frac{dk^-}{(2\pi)^3 (2k^-)} [\theta_{u'^-,v'^-} \theta_{k^-,0} - \theta_{v'^-,u'^-} \theta_{0,k^-}] \right. \\ &\times \int \frac{dk_1^-}{2\pi} \frac{1}{k_1^-} e^{-ik_1^-(u^+-u'^+)} \int \frac{dk_2^-}{2\pi} \frac{1}{k_2^-} e^{-ik_2^-(v^+-v'^+)} \int d^2p_\perp d^2q_\perp p^i q^i e^{-i(p \cdot u' - q \cdot v')} \\ &\times \int \frac{d^2z_\perp}{(2\pi)^2} e^{-i(p-q) \cdot z} [\tilde{U}_{z;u^-,v^-}]^{ab} \left. \right\} \delta_{u^+,0} \delta_{v^+,0} \\ &\times [\delta_{x,u}^{(2)} \delta_{y,v}^{(2)} [W_{x,y;u^-,v^-}]_{ij\,kl}^{ab} + \delta_{x,v}^{(2)} \delta_{y,u}^{(2)} [W_{x,y;v^-,u^-}]_{ij\,kl}^{ba}] \\ &= -\frac{1}{4} (ig)^2 \int du^- dv^- d^2u_\perp d^2v_\perp \int \frac{dk^-}{(2\pi k^-)^3} [\theta_{u^-,v^-} \theta_{k^-,0} - \theta_{v^-,u^-} \theta_{0,k^-}] \int d^2p_\perp d^2q_\perp p^i q^i \end{aligned}$$

³The contributions to Eq. 5.8 coming from the first term in Eq. 5.18a are finite and do not produce a logarithm in $\ln(x_{bj0}/x_{bj})$. Consequently, these contributions drop out of the finite difference equation which leads to the JIMWLK equation.

$$\begin{aligned}
& \times \exp \left[-i \left(\frac{\mathbf{p}^2 u^-}{2k^-} - \frac{\mathbf{p}^2 v^-}{2k^-} \right) \right] e^{i(\mathbf{p} \cdot \mathbf{u} - \mathbf{q} \cdot \mathbf{v})} \int \frac{d^2 z_\perp}{(2\pi)^2} e^{-i(\mathbf{p} - \mathbf{q}) \cdot \mathbf{z}} [\tilde{U}_{\mathbf{z}; u^-, v^-}]^{ab} \\
& \times \left[\delta_{\mathbf{x}, \mathbf{u}}^{(2)} \delta_{\mathbf{y}, \mathbf{v}}^{(2)} [W_{\mathbf{x}, \mathbf{y}; u^-, v^-}]_{ij kl}^{ab} + \delta_{\mathbf{x}, \mathbf{v}}^{(2)} \delta_{\mathbf{y}, \mathbf{u}}^{(2)} [W_{\mathbf{x}, \mathbf{y}; v^-, u^-}]_{ij kl}^{ba} \right].
\end{aligned} \tag{5.20}$$

The integrals in u^- and v^- can be easily evaluated. Since there are four different combinations of products of Heaviside functions in u^- and v^- in Eq. 5.19, there are four different integrals in u^- and v^- contributing to Eq. 5.20; the results of these four different integrals are

$$\begin{aligned}
& \int du^- dv^- \int \frac{dk^-}{(2\pi k^-)^3} [\theta_{u^-, v^-} \theta_{k^-, 0} - \theta_{v^-, u^-} \theta_{0, k^-}] \exp \left[-i \left(\frac{\mathbf{p}^2 u^-}{2k^-} - \frac{\mathbf{p}^2 v^-}{2k^-} \right) \right] \\
& \times \theta_{s_u u^-, 0} \theta_{s_v v^-, 0} = -s_u s_v \frac{4}{(2\pi)^3} \frac{1}{\mathbf{p}^2 \mathbf{q}^2} \int_0^\infty \frac{dk^-}{k^-},
\end{aligned} \tag{5.21}$$

where $s_u, s_v = \pm 1$. The result of the k^- integral in Eq. 5.21 is logarithmically divergent in the ultraviolet and the infrared. Regulating this k^- integral, Eq. 5.21 becomes

$$(5.21) = -s_u s_v \frac{4}{(2\pi)^3} \frac{1}{\mathbf{p}^2 \mathbf{q}^2} \ln(x_{b j 0}/x_{b j}). \tag{5.22}$$

The integrals over the transverse coordinates \mathbf{u} and \mathbf{v} sets \mathbf{u}, \mathbf{v} to either \mathbf{x}, \mathbf{y} or \mathbf{y}, \mathbf{x} while the transverse momentum integrals in \mathbf{p} and \mathbf{q} produce the JIMWLK kernel (up to a minus sign)

$$\begin{aligned}
& - \int \frac{d^2 p_\perp}{2\pi} \frac{d^2 q_\perp}{2\pi} \frac{p^i q^j}{\mathbf{p}^2 \mathbf{q}^2} e^{i\mathbf{p} \cdot (\mathbf{u} - \mathbf{z})} e^{i\mathbf{q} \cdot (\mathbf{z} - \mathbf{v})} = - \left(\partial_z^i \int \frac{d^2 p_\perp}{2\pi} e^{i\mathbf{p} \cdot (\mathbf{u} - \mathbf{z})} \right) \left(\partial_z^j \int \frac{d^2 q_\perp}{2\pi} e^{i\mathbf{q} \cdot (\mathbf{z} - \mathbf{v})} \right) \\
& = \frac{(\mathbf{u} - \mathbf{z})^i (\mathbf{z} - \mathbf{v})^j}{(\mathbf{u} - \mathbf{z})^2 (\mathbf{z} - \mathbf{v})^2} =: \mathcal{K}_{uzv}.
\end{aligned} \tag{5.23}$$

Substituting Eq. 5.22 and Eq. 5.23 back into Eq. 5.20 yields

$$\begin{aligned}
(5.20) &= \frac{\alpha_s}{2\pi^2} \ln(x_{b j 0}/x_{b j}) \int d^2 z_\perp \mathcal{K}_{xzy} \left[\left\{ [\tilde{U}_z]^{ab} [t^a U_x]_{ij} [t^b U_y^\dagger]_{kl} + [\tilde{U}_z^\dagger]^{ab} [U_x t^a]_{ij} [U_y^\dagger t^b]_{kl} \right. \right. \\
& - [t^a U_x]_{ij} [U_y^\dagger t^a]_{kl} - [U_x t^a]_{ij} [t^a U_y^\dagger]_{kl} \left. \right\} + \left\{ [\tilde{U}_z]^{ab} [t^a U_y]_{ij} [t^b U_x^\dagger]_{kl} + [\tilde{U}_z^\dagger]^{ab} [U_y t^a]_{ij} [U_x^\dagger t^b]_{kl} \right. \\
& \left. \left. - [t^a U_y]_{ij} [U_x^\dagger t^a]_{kl} - [U_y t^a]_{ij} [t^a U_x^\dagger]_{kl} \right\} \right].
\end{aligned} \tag{5.24}$$

After applying the Fierz identity one finally obtains

$$\begin{aligned}
[\bar{\chi}_{\mathbf{x}, \mathbf{y}}^{q\bar{q}}]_{ij kl} &:= \frac{\alpha_s}{2\pi^2} \int d^2 z_\perp \mathcal{K}_{xzy} \left[[U_z U_y^\dagger]_{il} [U_z^\dagger U_x]_{kj} + [U_x U_z^\dagger]_{il} [U_y^\dagger U_z]_{kj} \right. \\
& \left. - [U_x U_y^\dagger]_{il} \delta_{kj} - \delta_{il} [U_y^\dagger U_x]_{kj} \right],
\end{aligned} \tag{5.25a}$$

The remaining three gluon-exchange diagrams differ from Eq. 5.24 only in the order of the product of the Wilson-lines and gauge generators, and sometimes by an overall sign; they are

given by

$$[\bar{\chi}_{x,y}^{\bar{q}q}]_{ij\,kl} := \frac{\alpha_s}{2\pi^2} \int d^2 z_\perp \mathcal{K}_{xzy} \left[[U_z^\dagger U_y]_{il} [U_z U_x^\dagger]_{kj} + [U_x^\dagger U_z]_{il} [U_y U_z^\dagger]_{kj} \right. \\ \left. - \delta_{il} [U_y U_x^\dagger]_{kj} - [U_x^\dagger U_y]_{il} \delta_{kj} \right], \quad (5.25b)$$

$$[\bar{\chi}_{x,y}^{qq}]_{ij\,kl} := -\frac{\alpha_s}{2\pi^2} \int d^2 z_\perp \mathcal{K}_{xzy} \left[[U_z]_{il} [U_y U_z^\dagger U_x]_{kj} + [U_x U_z^\dagger U_y]_{il} [U_z]_{kj} \right. \\ \left. - [U_x]_{il} [U_y]_{kj} - [U_y]_{il} [U_x]_{kj} \right], \quad (5.25c)$$

$$[\bar{\chi}_{x,y}^{\bar{q}\bar{q}}]_{ij\,kl} := -\frac{\alpha_s}{2\pi^2} \int d^2 z_\perp \mathcal{K}_{xzy} \left[[U_z^\dagger]_{il} [U_y^\dagger U_z U_x^\dagger]_{kj} + [U_x^\dagger U_z U_y^\dagger]_{il} [U_z^\dagger]_{kj} \right. \\ \left. - [U_x^\dagger]_{il} [U_y^\dagger]_{kj} - [U_y^\dagger]_{il} [U_x^\dagger]_{kj} \right]. \quad (5.25d)$$

In order to compute the quark self-energy diagram, examine the contributions to Eq. 5.9 from the second term in the gluon propagator which involves the scalar propagator in the adjoint representation:

$$-\frac{1}{2}(ig)^2 \int_{uv} \left\{ \int_{u'v'} \delta_{u^-,u'} \delta_{v^-,v'} \delta_{u,u'}^{(2)} \delta_{v,v'}^{(2)} \int \frac{dk^-}{(2\pi)^3(2k^-)} [\theta_{u'^-,v'} \theta_{k^-,0} - \theta_{v'^-,u'} \theta_{0,k^-}] \right. \\ \times \int \frac{dk_1^-}{2\pi} \frac{1}{k_1^-} e^{-ik_1^-(u^+-u'^+)} \int \frac{dk_2^-}{2\pi} \frac{1}{k_2^-} e^{-ik_2^-(v^+-v'^+)} \int d^2 p_\perp d^2 q_\perp p^i q^i e^{-i(p \cdot u' - q \cdot v')} \\ \times \int \frac{d^2 z_\perp}{(2\pi)^2} e^{-i(p-q) \cdot z} [\tilde{U}_{z;u'^-,v'^-}]^{ab} \left. \right\} \delta_{u^+,0} \delta_{v^+,0} \delta_{x,u}^{(2)} \delta_{u,v}^{(2)} [W_{x;u^-,v^-}]_{ij}^{ab} \\ = \frac{1}{4}(ig)^2 \int du^- dv^- \int \frac{dk^-}{(2\pi k^-)^3} [\theta_{u^-,v^-} \theta_{k^-,0} - \theta_{v^-,u^-} \theta_{0,k^-}] \int d^2 p_\perp d^2 q_\perp p^i q^i \\ \times \exp \left[-i \left(\frac{p^2 x u^-}{2k^-} - \frac{q^2 x v^-}{2k^-} \right) \right] e^{i(p-q) \cdot x} \int \frac{d^2 z_\perp}{(2\pi)^2} e^{-i(p-q) \cdot z} [\tilde{U}_{z;u^-,v^-}]^{ab} [W_{x;u^-,v^-}]_{ij}^{ab}. \quad (5.26)$$

Evaluating the contributions to the integrals in u^- and v^- produces Eq. 5.22, and from Eq. 5.26 one obtains

$$[\bar{\sigma}_x^q]_{ij} := -\frac{\alpha_s}{2\pi^2} \int d^2 z_\perp \mathcal{K}_{xzy} [[U_z]_{ij} \text{tr}(U_x U_z^\dagger) - N_c [U_x]_{ij}]. \quad (5.27a)$$

Similarly the anti-quark self-energy diagram can be calculated and yields

$$[\bar{\sigma}_x^{\bar{q}}]_{ij} := -\frac{\alpha_s}{2\pi^2} \int d^2 z_\perp \mathcal{K}_{xzy} [[U_z^\dagger]_{ij} \text{tr}(U_x^\dagger U_z) - N_c [U_x^\dagger]_{ij}]. \quad (5.27b)$$

With the results shown in Eq. 5.25 and Eq. 5.27, one can finally write down the finite difference equation

$$\begin{aligned}
& \left\langle e^{\mathcal{S}_{\text{ext}}^{q\bar{q}}[b+\delta A, J^\dagger, J]} \right\rangle_{b, \delta A}(Y) - \left\langle e^{\mathcal{S}_{\text{ext}}^{q\bar{q}}[b, J^\dagger, J]} \right\rangle_b(Y_0) \\
&= \frac{1}{2} \int_{xy} \left\langle \langle \delta A_x^{a+} \delta A_y^{b+} \rangle_{\delta A}[b] \left(\left(\frac{\delta}{\delta b_x^{a+}} \mathcal{S}_{\text{ext}}^{q\bar{q}}[b, J^\dagger, J] \right) \left(\frac{\delta}{\delta b_y^{b+}} \mathcal{S}_{\text{ext}}^{q\bar{q}}[b, J^\dagger, J] \right) \right. \right. \\
&\quad \left. \left. + \frac{\delta}{\delta b_x^{a+}} \frac{\delta}{\delta b_y^{b+}} \mathcal{S}_{\text{ext}}^{q\bar{q}}[b, J^\dagger, J] \right) e^{\mathcal{S}_{\text{ext}}^{q\bar{q}}[b, J^\dagger, J]} \right\rangle_b(x_{\text{bj}0}) + \mathcal{O}(\delta A^3) \\
&= \ln(x_{\text{bj}0}/x_{\text{bj}}) \left\langle \left\{ \frac{1}{2} \int_{xy} J_x^\alpha J_y^\beta \bar{\chi}_{x,y}^{\alpha\beta}[\vec{U}] + \int_x J_x^\alpha \bar{\sigma}_x^\alpha[\vec{U}] \right\} e^{\mathcal{S}_{\text{ext}}^{q\bar{q}}[b, \vec{J}]} \right\rangle_b(Y) + \mathcal{O}(\delta A^3) \\
&= \ln(x_{\text{bj}0}/x_{\text{bj}}) \left\{ \frac{1}{2} \int_{xy} J_x^\alpha J_y^\beta \bar{\chi}_{x,y}^{\alpha\beta} \left[\frac{\delta}{\delta \vec{J}} \right] + \int_x J_x^\alpha \bar{\sigma}_x^\alpha \left[\frac{\delta}{\delta \vec{J}} \right] \right\} \left\langle e^{\mathcal{S}_{\text{ext}}^{q\bar{q}}[b, \vec{J}]} \right\rangle_b(Y) + \mathcal{O}(\delta A^3). \quad (5.28)
\end{aligned}$$

In the second last line of Eq. 5.28 we introduced the vectors $\vec{J} := (J^\dagger, J)^t$ and $\vec{U} := (U, U^\dagger)^t$ as well as the dummy summation indices α, β which run from 1 to 2 and in the last line we used

$$\frac{\delta}{\delta J^\alpha} \mathcal{S}_{\text{ext}}^{q\bar{q}}[b, \vec{J}] = U^\alpha \mathcal{S}_{\text{ext}}^{q\bar{q}}[b, \vec{J}], \quad (5.29)$$

to pull the evolution operator (in the curly braces) outside of the target average. The finite difference equation in Eq. 5.28 becomes a differential equation in the limit that $|\ln(x_{\text{bj}0}/x_{\text{bj}})| = |Y - Y_0| \rightarrow 0$:

$$\frac{d}{dY} \bar{\mathcal{Z}}[\vec{J}](Y) = \left\{ \frac{1}{2} \int_{xy} J_x^\alpha J_y^\beta \bar{\chi}_{x,y}^{\alpha\beta} \left[\frac{\delta}{\delta \vec{J}} \right] + \int_x J_x^\alpha \bar{\sigma}_x^\alpha \left[\frac{\delta}{\delta \vec{J}} \right] \right\} \bar{\mathcal{Z}}[\vec{J}](Y). \quad (5.30)$$

As a *functional renormalization group (RG) equation* — an RG equation for the generating functional — Eq. 5.30 represents an infinite set of RG equations for all possible Wilson-line correlators. This infinite set is known as the *Balitsky hierarchy*.

Eq. 5.30 being at most quadratic in derivatives $\delta/\delta \vec{J}$ admits a statistical interpretation as a Fokker-Planck equation. In order to expose its Fokker-Planck nature one needs to perform functional Fourier transformation from \vec{J} to \vec{U} , but this in turn requires that $U^{(\dagger)}$ be taken to be independent variables (elements of $\text{Mat}(N_c; \mathbb{C})$ as opposed to $\text{SU}(N_c)$). (Eventually we shall find that the particular form of the evolution operator constrains $U^{(\dagger)}$ to the manifold of $\text{SU}(N_c)$ almost auto-magically.) From Eq. 5.3 we have that $\mathcal{S}_{\text{ext}}^{q\bar{q}}[b^+, \vec{J}] = \mathcal{S}_{\text{ext}}^{q\bar{q}}[\vec{U}, \vec{J}]$ is really a functional of $U^{(\dagger)}$ (with b^+ present through the definition of the Wilson-lines). Since we are regarding $U^{(\dagger)}$ as independent variables, let us write the target average in Eq. 5.1 as

$$\langle \cdots \rangle_{\vec{U}}(Y) = \int \bar{D}[\vec{U}] \cdots \bar{Z}_Y[\vec{U}], \quad (5.31)$$

for some statistical weight functional $\bar{Z}_Y[\vec{U}]$ which we shall later relate to the original $\hat{Z}_Y[U]$ written in Eq. 5.1. Writing the generating functional as

$$\bar{\mathcal{Z}}[\vec{J}](Y) = \langle e^{S_{\text{ext}}^{q\bar{q}}[\vec{U}, \vec{J}]} \rangle_{\vec{U}}(Y), \quad (5.32)$$

Eq. 5.30 may be cast as an equation for $\bar{Z}_Y[\vec{U}]$

$$\frac{d}{dY} \int \bar{D}[\vec{U}] \bar{Z}_Y[\vec{U}] e^{S_{\text{ext}}^{q\bar{q}}[\vec{U}, \vec{J}]} = \int \bar{D}[\vec{U}] \bar{Z}_Y[\vec{U}] \left\{ \frac{1}{2} \int_{xy} J_x^\alpha J_y^\beta \bar{\chi}_{x,y}^{\alpha\beta}[\vec{U}] + \int_x J_x^\alpha \bar{\sigma}_x^\alpha[\vec{U}] \right\} e^{S_{\text{ext}}^{q\bar{q}}[\vec{U}, \vec{J}]}, \quad (5.33)$$

where we have used Eq. 5.29 to turn $\bar{\chi}_{x,y}^{\alpha\beta}[\delta/\delta\vec{J}]$ and $\bar{\sigma}_x^\alpha[\delta/\delta\vec{J}]$ into $\bar{\chi}_{x,y}^{\alpha\beta}[\vec{U}]$ and $\bar{\sigma}_x^\alpha[\vec{U}]$, respectively. We now use the fact that $U^{(\dagger)}$ are independent variables in order to write the conjugate version of Eq. 5.29

$$\frac{\delta}{\delta U^\alpha} e^{S_{\text{ext}}^{q\bar{q}}[\vec{U}, \vec{J}]} = J^\alpha e^{S_{\text{ext}}^{q\bar{q}}[\vec{U}, \vec{J}]}. \quad (5.34)$$

Using Eq. 5.34 in Eq. 5.33 and performing a functional integration by parts one obtains

$$\frac{d}{dY} \bar{Z}_Y[\vec{U}] = \left\{ \frac{1}{2} \int_{xy} \frac{\delta}{\delta U_x^\alpha} \frac{\delta}{\delta U_y^\beta} \bar{\chi}_{x,y}^{\alpha\beta}[\vec{U}] - \int_x \frac{\delta}{\delta U_x^\alpha} \bar{\sigma}_x^\alpha[\vec{U}] \right\} \bar{Z}_Y[\vec{U}]. \quad (5.35)$$

As a final step towards writing Eq. 5.35 in the canonical form of a Fokker-Planck equation, observe that

$$\begin{aligned} \frac{1}{2} \left[\frac{\delta}{\delta U_x^\alpha} \bar{\chi}_{x,y}^{\alpha q}[\vec{U}] \right]_{kl} &= \frac{1}{2} \int_u \delta_{im} \delta_{jn} \delta_{x,u}^{(2)} \left\{ \frac{\delta}{\delta [U_u]_{mn}} [\bar{\chi}_{x,y}^{qq}[\vec{U}]]_{ij kl} + \frac{\delta}{\delta [U_x^\dagger]_{mn}} [\bar{\chi}_{x,y}^{q\bar{q}}[\vec{U}]]_{ij kl} \right\} \\ &= -\frac{\alpha_s}{4\pi^2} \int_{uz} \mathcal{K}_{xzy} \delta_{im} \delta_{jn} \delta_{x,u}^{(2)} \\ &\quad \times \left\{ \delta_{z,u}^{(2)} \delta_{im} \delta_{ln} [U_y U_z^\dagger U_x]_{kj} + \delta_{y,u}^{(2)} \delta_{km} \delta_{pn} [U_z]_{il} [U_z^\dagger U_x]_{pj} + \delta_{x,u}^{(2)} \delta_{pm} \delta_{jn} [U_z]_{il} [U_y U_z^\dagger]_{kp} \right. \\ &\quad + \delta_{z,u}^{(2)} \delta_{km} \delta_{jn} [U_x U_z^\dagger U_y]_{il} + \delta_{y,u}^{(2)} \delta_{pm} \delta_{ln} [U_x U_z^\dagger]_{ip} [U_z]_{kj} + \delta_{x,u}^{(2)} \delta_{im} \delta_{pn} [U_z^\dagger U_y]_{pl} [U_z]_{kj} \\ &\quad - \delta_{x,u}^{(2)} \delta_{im} \delta_{ln} [U_y]_{kj} - \delta_{y,u}^{(2)} \delta_{km} \delta_{jn} [U_x]_{il} - \delta_{y,u}^{(2)} \delta_{im} \delta_{ln} [U_x]_{kj} - \delta_{x,u}^{(2)} \delta_{km} \delta_{jn} [U_y]_{il} \\ &\quad + \delta_{x,u}^{(2)} \delta_{pm} \delta_{jn} \delta_{il} [U_y]_{kp} - \delta_{x,u}^{(2)} \delta_{pm} \delta_{jn} [U_z^\dagger U_y]_{il} [U_z]_{kp} - \delta_{z,u}^{(2)} \delta_{im} \delta_{pn} [U_y]_{pl} [U_z U_x^\dagger]_{kj} \\ &\quad \left. + \delta_{x,u}^{(2)} \delta_{im} \delta_{pn} \delta_{kj} [U_y]_{pl} - \delta_{x,u}^{(2)} \delta_{im} \delta_{pn} [U_z]_{pl} [U_y U_z^\dagger]_{kj} - \delta_{z,u}^{(2)} \delta_{pm} \delta_{jn} [U_x^\dagger U_z]_{il} [U_y]_{kp} \right\} \\ &= -\frac{\alpha_s}{4\pi^2} \int_{uz} \mathcal{K}_{xzy} \delta_{x,u}^{(2)} \left\{ 2\delta_{y,u}^{(2)} [U_z]_{kl} \text{Tr} \left(U_x U_z^\dagger \right) - 2\delta_{y,u}^{(2)} N_c [U_x]_{kl} \right. \\ &\quad \left. + \delta_{z,u}^{(2)} N_c [U_y U_z^\dagger U_x]_{kl} + \delta_{z,u}^{(2)} N_c [U_x U_z^\dagger U_y]_{kl} - \delta_{z,u}^{(2)} N_c [U_z U_x^\dagger U_y]_{kl} - \delta_{z,u}^{(2)} N_c [U_y U_x^\dagger U_z]_{kl} \right\} \\ &= -\frac{\alpha_s}{2\pi^2} \int_z \mathcal{K}_{yzy} \left[[U_z]_{kl} \text{tr}(U_y U_z^\dagger) - N_c [U_y]_{kl} \right] = [\bar{\sigma}_y^q]_{kl}. \quad (5.36a) \end{aligned}$$

Similarly, one can show that

$$\frac{1}{2} \left[\frac{\delta}{\delta U_x^\alpha} \bar{\chi}_{x,y}^{\alpha\bar{q}}[\vec{U}] \right]_{kl} = [\bar{\sigma}_y^{\bar{q}}]_{kl}. \quad (5.36b)$$

Together, Eq. 5.36 gives that

$$\frac{1}{2} \int_x \frac{\delta}{\delta U_x^\alpha} \bar{\chi}_{x,y}^{\alpha\beta}[\vec{U}] - \bar{\sigma}_y^\beta[\vec{U}] = 0. \quad (5.37)$$

and, consequently, Eq. 5.35 takes the canonical form of a Fokker-Planck equation in a non-trivial geometry

$$\frac{d}{dY} \bar{Z}_Y[\vec{U}] = \frac{1}{2} \int_{xy} \frac{\delta}{\delta U_x^\alpha} \bar{\chi}_{x,y}^{\alpha\beta}[\vec{U}] \frac{\delta}{\delta U_y^\beta} \bar{Z}_Y[\vec{U}]. \quad (5.38)$$

We now need to re-impose the group constraint. This amounts to showing that for physical distributions

$$\bar{Z}_Y^{(\text{phys.})}[\vec{U}] = \delta(UU^\dagger - \mathbb{1}) \delta(\det(U) - 1) \hat{Z}_Y[U], \quad (5.39)$$

the evolution operator in Eq. 5.38 leaves the constraint factor $\delta(UU^\dagger - \mathbb{1}) \delta(\det(U) - 1)$ invariant. If this can be shown, then the constraint factor can be absorbed into the measure $\bar{D}[\vec{U}]$ and produce the unimodular Haar measure

$$\hat{D}[U] = \bar{D}[\vec{U}] \delta(UU^\dagger - \mathbb{1}) \delta(\det(U) - 1). \quad (5.40)$$

To this end, it will prove invaluable to replace the functional derivatives present in Eq. 5.38 by the following set of $2N_c^2$ functional derivatives

$$\frac{\delta}{\delta U_x^\alpha} \mapsto [i\nabla_x^a]^\alpha := \begin{cases} [U_x t^a]_{ij} \frac{\delta}{\delta [U_x]_{ij}}, & \text{if } \alpha = 1, \\ -[t^a U_x^\dagger]_{ij} \frac{\delta}{\delta [U_x^\dagger]_{ij}}, & \text{if } \alpha = 2, \end{cases} \quad (5.41)$$

Here the index \mathbf{a} runs over $0, 1, \dots, d_A = N_c^2 - 1$. For $\mathbf{a} = a = 1, \dots, d_A$, t^a are the (Hermitian) generators of $\text{SU}(N_c)$ while $t^0 = \mathbb{1}/\sqrt{2N_c}$. The set $\{t^a\}_{a=0}^{d_A}$ is orthonormalized with

$$\text{Tr} \left((t^a)^\dagger t^b \right) = \frac{1}{2} \delta^{ab}, \quad (5.42)$$

and forms a basis for $\text{Mat}(N_c; \mathbb{C})$. Since $U_x^{(\dagger)} \in \text{Mat}(N_c; \mathbb{C})$, the sets $\{U_x t^a\}_{a=0}^{d_A}$ and $\{-t^a U_x^\dagger\}_{a=0}^{d_A}$ are also bases for $\text{Mat}(N_c; \mathbb{C})$. Consequently, the new functional derivatives given in Eq. 5.41 still probe all the component of \vec{U} as was probed by the old functional derivatives $\delta/\delta \vec{U}$.

But why are these new functional derivatives better than the old ones? We shall show that the evolution operator

$$\frac{1}{2} \int_{\mathbf{x}\mathbf{y}} \frac{\delta}{\delta U_{\mathbf{x}}^{\alpha}} \bar{\chi}_{\mathbf{x},\mathbf{y}}^{\alpha\beta}[\vec{U}] \frac{\delta}{\delta U_{\mathbf{y}}^{\beta}}, \quad (5.43)$$

on the right-hand-side of the equality in Eq. 5.38 can be rewritten as

$$\frac{1}{2} \int_{\mathbf{x}\mathbf{y}} i \nabla_{\mathbf{x}}^a \hat{\chi}_{\mathbf{x},\mathbf{y}}^{ab}[U] i \nabla_{\mathbf{y}}^b, \quad (5.44)$$

where $\hat{\chi}_{\mathbf{x},\mathbf{y}}^{ab}[U]$ will be given shortly and

$$i \nabla_{\mathbf{x}}^a := \sum_{\alpha=1}^2 [i \nabla_{\mathbf{x}}^a]^{\alpha} = [U_{\mathbf{x}} t^a]_{ij} \frac{\delta}{\delta [U_{\mathbf{x}}]_{ij}} - [t^a U_{\mathbf{x}}^{\dagger}]_{ij} \frac{\delta}{\delta [U_{\mathbf{x}}^{\dagger}]_{ij}}, \quad (5.45)$$

with a running over $1, \dots, d_A$. The upshot is that Eq. 5.45 immediately preserves the group constraints of $\text{SU}(N_c)$:

- **Unitarity:** Firstly, $i \nabla_{\mathbf{x}}^a \delta(U U^{\dagger} - \mathbb{1}) = 0$. This follows immediately from

$$\begin{aligned} i \nabla_{\mathbf{x}}^a (U_{\mathbf{y}} U_{\mathbf{y}}^{\dagger}) &= (i \nabla_{\mathbf{x}}^a U_{\mathbf{y}}) U_{\mathbf{y}}^{\dagger} + U_{\mathbf{y}} (i \nabla_{\mathbf{x}}^a U_{\mathbf{y}}^{\dagger}) \\ &= \delta_{\mathbf{x}\mathbf{y}}^{(2)} (U_{\mathbf{x}} t^a U_{\mathbf{y}}^{\dagger} - U_{\mathbf{y}} t^a U_{\mathbf{x}}^{\dagger}) \\ &= \delta_{\mathbf{x}\mathbf{y}}^{(2)} (U_{\mathbf{x}} t^a U_{\mathbf{x}}^{\dagger} - U_{\mathbf{x}} t^a U_{\mathbf{x}}^{\dagger}) = 0 = i \nabla_{\mathbf{x}}^a \mathbb{1}. \end{aligned} \quad (5.46)$$

- **Determinant equals 1:** Secondly, $i \nabla_{\mathbf{x}}^a \delta(\det(U) - 1) = 0$. To show this, we use the Leibniz formula for $\det(U_{\mathbf{y}})$ which is given by

$$\det(U_{\mathbf{y}}) = \frac{1}{N!} \varepsilon^{i_1 \dots i_N} \varepsilon^{j_1 \dots j_N} [U_{\mathbf{y}}]_{i_1 j_1} \dots [U_{\mathbf{y}}]_{i_N j_N}, \quad (5.47)$$

where I have written N as shorthand for N_c and $\varepsilon^{i_1 \dots i_N}$ is the Levi-Civita symbol in N indices. Applying $i \nabla_{\mathbf{x}}^a$ to Eq. 5.47 yields

$$\begin{aligned} i \nabla_{\mathbf{x}}^a \det(U_{\mathbf{y}}) &= \delta_{\mathbf{x}\mathbf{y}}^{(2)} \frac{1}{N!} \varepsilon^{i_1 \dots i_N} \varepsilon^{j_1 \dots j_N} \sum_{k=1}^N [U_{\mathbf{y}} t^a]_{i_k j_k} \prod_{\substack{l=1 \\ l \neq k}}^N [U_{\mathbf{y}}]_{i_l j_l} \\ &= \delta_{\mathbf{x}\mathbf{y}}^{(2)} \frac{N}{N!} \varepsilon^{i_1 i_2 \dots i_N} \varepsilon^{j_1 j_2 \dots j_N} [U_{\mathbf{y}} t^a]_{i_1 j_1} [U_{\mathbf{y}}]_{i_2 j_2} \dots [U_{\mathbf{y}}]_{i_N j_N} \\ &= \delta_{\mathbf{x}\mathbf{y}}^{(2)} \frac{N}{N!} \varepsilon^{j_1 j_2 \dots j_N} \underbrace{\varepsilon^{i_1 i_2 \dots i_N} [U_{\mathbf{y}}]_{i_1 j_1} [U_{\mathbf{y}}]_{i_2 j_2} \dots [U_{\mathbf{y}}]_{i_N j_N}}_{= \varepsilon_{j_1 j_2 \dots j_N} \det(U_{\mathbf{y}})} [t^a]_{j_1}^j \\ &= \delta_{\mathbf{x}\mathbf{y}}^{(2)} \det(U_{\mathbf{y}}) \underbrace{\frac{N}{N!} \varepsilon^{j_1 j_2 \dots j_N} \varepsilon_{j_1 j_2 \dots j_N}}_{= \delta_{j_1}^{j_1} \text{ (from [33])}} [t^a]_{j_1}^j \\ &= \delta_{\mathbf{x}\mathbf{y}}^{(2)} \det(U_{\mathbf{y}}) \delta_{j_1}^{j_1} [t^a]_{j_1}^j = -\delta_{\mathbf{x}\mathbf{y}}^{(2)} \det(U_{\mathbf{y}}) \text{Tr}(t^a) = 0 = i \nabla_{\mathbf{x}}^a \mathbb{1}. \end{aligned} \quad (5.48)$$

I shall now show how to write Eq. 5.43 as Eq. 5.44. As an intermediary step, we try to write

$$\int_{\mathbf{xy}} \frac{\delta}{\delta[U_x^\alpha]_{ij}} [\bar{\chi}_{x,y}^{\alpha\beta}[\vec{U}]]_{ij\,kl} \frac{\delta}{\delta[U_y^\beta]_{kl}} = \int_{\mathbf{xy}} [i\nabla_x^a]^\alpha [\hat{\chi}_{x,y}^{ab}[\vec{U}]]^{\alpha\beta} [i\nabla_y^b]^\beta; \quad (5.49)$$

i.e. we try to determine $[\hat{\chi}_{x,y}^{ab}[\vec{U}]]^{\alpha\beta}$. In order to determine this transformed kernel, one needs to analyze each contribution to the sum over α, β in Eq. 5.49 separately. Let us examine the contribution to the sum from $\alpha = 1 = \beta$

$$\begin{aligned} \int_{\mathbf{xy}} \frac{\delta}{\delta[U_x]_{ij}} [\bar{\chi}_{x,y}^{qq}[\vec{U}]]_{ij\,kl} \frac{\delta}{\delta[U_y]_{kl}} &= \int_{\mathbf{xy}} [i\nabla_x^a]^1 [\hat{\chi}_{x,y}^{ab}[\vec{U}]]^{qq} [i\nabla_y^b]^1 \\ &= \int_{\mathbf{xy}} [U_x t^a]_{ij} \frac{\delta}{\delta[U_x]_{ij}} [\hat{\chi}_{x,y}^{ab}[\vec{U}]]^{qq} [U_y t^b]_{kl} \frac{\delta}{\delta[U_y]_{kl}} \\ &= \int_{\mathbf{xy}} \frac{\delta}{\delta[U_x]_{ij}} [U_x t^a]_{ij} [\hat{\chi}_{x,y}^{ab}[\vec{U}]]^{qq} [U_y t^b]_{ij} \frac{\delta}{\delta[U_y]_{ij}} - \sqrt{\frac{N_c}{2}} \int_{\mathbf{xy}} \delta_{x,x}^{(2)} [\hat{\chi}_{x,y}^{0b}[\vec{U}]]^{qq} [U_y t^b]_{ij} \frac{\delta}{\delta[U_y]_{ij}}, \end{aligned} \quad (5.50)$$

where, in the last line, we produced a product rule term with $\frac{\delta}{\delta[U_x]_{ij}} [U_x t^a]_{ij} = \delta_{x,x}^{(2)} \delta^{a0} \sqrt{N_c/2}$. If we were allowed to ignore this product rule term, then immediately we would have that

$$[\hat{\chi}_{x,y}^{ab}[\vec{U}]]^{qq} = [2t^a(U_x)^{-1}]_{ji} [\bar{\chi}_{x,y}^{qq}[\vec{U}]]_{ij\,kl} [2t^b(U_y)^{-1}]_{lk}. \quad (5.51)$$

Repeating the calculations of Eq. 5.50 and Eq. 5.51 for each pair of values of α, β , one obtains

$$\begin{aligned} [\hat{\chi}_{x,y}^{ab}[\vec{U}]]^{q\bar{q}} &= [2t^a(U_x)^{-1}]_{ji} [\bar{\chi}_{x,y}^{q\bar{q}}]_{ij\,kl} [-2(U_y^\dagger)^{-1} t^b]_{lk} \\ &= -2 \frac{\alpha_s}{\pi^2} \int_z \mathcal{K}_{xyz} \left(\text{Tr} \left(t^a (U_x)^{-1} U_z t^b U_z^\dagger U_x \right) + \text{Tr} \left(t^a U_z^\dagger (U_y^\dagger)^{-1} t^b U_y^\dagger U_z \right) \right. \\ &\quad \left. - \text{Tr} \left(t^a t^b \right) - \text{Tr} \left(t^a (U_x)^{-1} (U_y^\dagger)^{-1} t^b U_y^\dagger U_x \right) \right), \end{aligned} \quad (5.52a)$$

$$\begin{aligned} [\hat{\chi}_{x,y}^{ab}[\vec{U}]]^{\bar{q}q} &= [-2(U_x^\dagger)^{-1} t^a]_{ji} [\bar{\chi}_{x,y}^{\bar{q}q}]_{ij\,kl} [2t^b(U_y)^{-1}]_{lk} \\ &= -2 \frac{\alpha_s}{\pi^2} \int_z \mathcal{K}_{xyz} \left(\text{Tr} \left(t^a U_z^\dagger U_y t^b (U_y)^{-1} U_z \right) + \text{Tr} \left((U_x^\dagger)^{-1} t^a U_x^\dagger U_z t^b U_z^\dagger \right) \right. \\ &\quad \left. - \text{Tr} \left(t^a t^b \right) - \text{Tr} \left((U_x^\dagger)^{-1} t^a U_x^\dagger U_y t^b (U_y)^{-1} \right) \right), \end{aligned} \quad (5.52b)$$

$$\begin{aligned} [\hat{\chi}_{x,y}^{ab}[\vec{U}]]^{qq} &= [2t^a(U_x)^{-1}]_{ji} [\bar{\chi}_{x,y}^{qq}]_{ij\,kl} [2t^b(U_y)^{-1}]_{lk} \\ &= -2 \frac{\alpha_s}{\pi^2} \int_z \mathcal{K}_{xyz} \left(\text{Tr} \left(t^a (U_x)^{-1} U_z t^b U_z^\dagger U_x \right) + \text{Tr} \left(t^a U_z^\dagger U_y t^b (U_y)^{-1} U_z \right) \right. \\ &\quad \left. - \text{Tr} \left(t^a t^b \right) - \text{Tr} \left(t^a (U_x)^{-1} U_y t^b (U_y)^{-1} U_x \right) \right), \end{aligned} \quad (5.52c)$$

$$\begin{aligned} [\hat{\chi}_{x,y}^{ab}[\vec{U}]]^{\bar{q}\bar{q}} &= [2(U_x^\dagger)^{-1} t^a]_{ji} [\bar{\chi}_{x,y}^{\bar{q}\bar{q}}]_{ij\,kl} [2(U_y^\dagger)^{-1} t^b]_{lk} \\ &= -2 \frac{\alpha_s}{\pi^2} \int_z \mathcal{K}_{xyz} \left(\text{Tr} \left(t^a U_z^\dagger (U_y^\dagger)^{-1} t^b U_y^\dagger U_z \right) + \text{Tr} \left((U_x^\dagger)^{-1} t^a U_x^\dagger U_z t^b U_z^\dagger \right) \right. \\ &\quad \left. - \text{Tr} \left(t^a t^b \right) - \text{Tr} \left((U_x^\dagger)^{-1} t^a U_x^\dagger (U_y^\dagger)^{-1} t^b U_y^\dagger \right) \right). \end{aligned} \quad (5.52d)$$

For $\vec{U} \in \text{SU}(N_c)$, the transformed kernels in Eq. 5.52 vanish for $\mathbf{a} = 0$ or $\mathbf{b} = 0$ which justifies

our ignoring of the product rule terms like the one in Eq. 5.50. In addition, the above four transformed kernels are identical. Consequently, the right-hand-side of Eq. 5.49 becomes

$$\begin{aligned} \int_{xy} [i\nabla_x^a]^\alpha [\hat{\chi}_{x,y}^{ab}[\vec{U}]]^{\alpha\beta} [i\nabla_y^b]^\beta &= \int_{xy} \left[[i\nabla_x^a]^1 \hat{\chi}_{x,y}^{ab}[U] [i\nabla_y^b]^1 + [i\nabla_x^a]^1 \hat{\chi}_{x,y}^{ab}[U] [i\nabla_y^b]^2 \right. \\ &\quad \left. + [i\nabla_x^a]^2 \hat{\chi}_{x,y}^{ab}[U] [i\nabla_y^b]^1 + [i\nabla_x^a]^2 \hat{\chi}_{x,y}^{ab}[U] [i\nabla_y^b]^2 \right] \\ &= \int_{xy} \left([i\nabla_x^a]^1 + [i\nabla_x^a]^2 \right) \hat{\chi}_{x,y}^{ab}[U] \left([i\nabla_y^b]^1 + [i\nabla_y^b]^2 \right) = \int_{xy} i\nabla_x^a \hat{\chi}_{x,y}^{ab}[U] i\nabla_y^b, \end{aligned} \quad (5.53)$$

which is precisely Eq. 5.44 (as promised) with $i\nabla_x^a$ defined in Eq. 5.45 and $\hat{\chi}_{x,y}^{ab}[U]$ computed from Eq. 5.52 as

$$\begin{aligned} \hat{\chi}_{x,y}^{ab}[U] &= \frac{\alpha_s}{\pi^2} \int_z \mathcal{K}_{xzy} \left[\delta^{ab} + 2\text{Tr} \left(t^a U_x^\dagger U_y t^b U_y^\dagger U_x \right) \right. \\ &\quad \left. - 2\text{Tr} \left(t^a U_z^\dagger U_y t^b U_y^\dagger U_z \right) - 2\text{Tr} \left(t^a U_x^\dagger U_z t^b U_z^\dagger U_x \right) \right] \\ &= \frac{\alpha_s}{\pi^2} \int_z \mathcal{K}_{xzy} \left[\delta^{ab} + [\tilde{U}_x^\dagger \tilde{U}_y]^{ab} - [\tilde{U}_z^\dagger \tilde{U}_y]^{ab} - [\tilde{U}_x^\dagger \tilde{U}_z]^{ab} \right] \\ &= \frac{\alpha_s}{\pi^2} \int_z \mathcal{K}_{xzy} \left[(\tilde{\mathbb{1}} - \tilde{U}_x^\dagger \tilde{U}_z)(\tilde{\mathbb{1}} - \tilde{U}_z^\dagger \tilde{U}_y) \right]^{ab}. \end{aligned} \quad (5.54)$$

Finally, we arrive at *the JIMWLK equation* in its canonical form:

$$\frac{d}{dY} \hat{Z}_Y[U] = -H_{\text{JIMWLK}}^{(\text{LL})} \hat{Z}_Y[U], \quad (5.55)$$

where the JIMWLK Hamiltonian at leading logarithmic accuracy is given by

$$H_{\text{JIMWLK}}^{(\text{LL})} = -\frac{1}{2} \int_{xy} i\nabla_x^a \hat{\chi}_{x,y}^{ab}[U] i\nabla_y^b. \quad (5.56)$$

The functional derivatives appearing in Eq. 5.56, defined in Eq. 5.45, are in fact the left-invariant vector fields on $\text{SU}(N_c)$ [42] which satisfy the (localized) $\text{SU}(N_c)$ commutation relations

$$\begin{aligned} [i\nabla_x^a, i\nabla_y^b] &= + \left(i\nabla_x^a [U_y t^b]_{ij} \right) \frac{\delta}{\delta [U_y]_{ij}} - \left(i\nabla_x^a [t^b U_y^\dagger]_{ij} \right) \frac{\delta}{\delta [U_y^\dagger]_{ij}} \\ &\quad - \left(i\nabla_y^b [U_x t^a]_{ij} \right) \frac{\delta}{\delta [U_x]_{ij}} + \left(i\nabla_y^b [t^a U_x^\dagger]_{ij} \right) \frac{\delta}{\delta [U_x^\dagger]_{ij}} \\ &= \delta_{xy}^{(2)} \left[\left(U_x [t^a, t^b] \right)_{ij} \frac{\delta}{\delta [U_x]_{ij}} + \left([t^b, t^a] U_x^\dagger \right)_{ij} \frac{\delta}{\delta [U_x^\dagger]_{ij}} \right] \\ &= \delta_{xy}^{(2)} i f^{abc} \left[[U_x t^c]_{ij} \frac{\delta}{\delta [U_x]_{ij}} - [t^c U_x^\dagger]_{ij} \frac{\delta}{\delta [U_x^\dagger]_{ij}} \right] = \delta_{xy}^{(2)} i f^{abc} i\nabla_x^c, \end{aligned} \quad (5.57)$$

where terms that cancel were already dropped in the first line. The right-invariant vector fields on $SU(N_c)$ are similarly defined through [42]

$$i\bar{\nabla}_x^a := -[t^a U_x]_{ij} \frac{\delta}{\delta[U_x]_{ij}} + [U_x^\dagger t^a]_{ij} \frac{\delta}{\delta[U_x^\dagger]_{ij}}, \quad (5.58)$$

which also satisfy the (localized) $SU(N_c)$ commutation relations as demonstrated by

$$\begin{aligned} [i\bar{\nabla}_x^a, i\bar{\nabla}_y^b] &= -\left(i\bar{\nabla}_x^a[t^b U_y]_{ij}\right) \frac{\delta}{\delta[U_y]_{ij}} + \left(i\bar{\nabla}_x^a[U_y^\dagger t^b]_{ij}\right) \frac{\delta}{\delta[U_y^\dagger]_{ij}} \\ &\quad + \left(i\bar{\nabla}_y^b[t^a U_x]_{ij}\right) \frac{\delta}{\delta[U_x]_{ij}} - \left(i\bar{\nabla}_y^b[U_x^\dagger t^a]_{ij}\right) \frac{\delta}{\delta[U_x^\dagger]_{ij}} \\ &= \delta_{xy}^{(2)} \left[\left([t^b, t^a] U_x\right)_{ij} \frac{\delta}{\delta[U_x]_{ij}} + \left(U_x^\dagger [t^a, t^b]\right)_{ij} \frac{\delta}{\delta[U_x^\dagger]_{ij}} \right] \\ &= \delta_{xy}^{(2)} i f^{abc} \left[-[t^c U_x]_{ij} \frac{\delta}{\delta[U_x]_{ij}} + [U_x^\dagger t^c]_{ij} \frac{\delta}{\delta[U_x^\dagger]_{ij}} \right] = \delta_{xy}^{(2)} i f^{abc} i\bar{\nabla}_x^c. \end{aligned} \quad (5.59)$$

The left- and right-invariant vector fields commute amongst each other since

$$\begin{aligned} [i\nabla_x^a, i\bar{\nabla}_y^b] &= -\left(i\nabla_x^a[t^b U_y]_{ij}\right) \frac{\delta}{\delta[U_y]_{ij}} + \left(i\nabla_x^a[U_y^\dagger t^b]_{ij}\right) \frac{\delta}{\delta[U_y^\dagger]_{ij}} \\ &\quad - \left(i\bar{\nabla}_y^b[U_x t^a]_{ij}\right) \frac{\delta}{\delta[U_x]_{ij}} + \left(i\bar{\nabla}_y^b[t^a U_x^\dagger]_{ij}\right) \frac{\delta}{\delta[U_x^\dagger]_{ij}} \\ &= \delta_{xy}^{(2)} \left[-[t^b U_x t^a]_{ij} \frac{\delta}{\delta[U_x]_{ij}} - [t^a U_x^\dagger t^b]_{ij} \frac{\delta}{\delta[U_x^\dagger]_{ij}} + [t^b U_x t^a]_{ij} \frac{\delta}{\delta[U_x]_{ij}} + [t^a U_x^\dagger t^b]_{ij} \frac{\delta}{\delta[U_x^\dagger]_{ij}} \right] \\ &= 0. \end{aligned} \quad (5.60)$$

Furthermore, using the Fierz identity we have that

$$\begin{aligned} [\tilde{U}_x]^{ab}[U_x t^b]_{ij} &= 2\text{Tr} \left(t^a U_x t^b U_x^\dagger \right) [U_x t^b]_{ij} = 2[U_x^\dagger t^a U_x]_{kl} [U_x]_{im} [t^b]^{kl} [t^b]^m_j \\ &= [U_x^\dagger t^a U_x]_{kl} [U_x]_{im} \left(\delta^{km} \delta^l_j - \frac{1}{N_c} \delta^{kl} \delta^m_j \right) = [t^a U_x]_{ij}, \end{aligned} \quad (5.61a)$$

$$\begin{aligned} [\tilde{U}_x]^{ab}[t^b U_x^\dagger]_{ij} &= 2\text{Tr} \left(t^a U_x t^b U_x^\dagger \right) [t^b U_x^\dagger]_{ij} = 2[U_x^\dagger t^a U_x]_{kl} [U_x^\dagger]_{mj} [t^b]^{kl} [t^b]^i_m \\ &= [U_x^\dagger t^a U_x]_{kl} [U_x^\dagger]_{mj} \left(\delta^{ki} \delta^l_m - \frac{1}{N_c} \delta^{kl} \delta^i_m \right) = [U_x^\dagger t^a]_{ij}, \end{aligned} \quad (5.61b)$$

as well as the complex conjugate relations from which we see that the left- and right-invariant vector fields of $SU(N_c)$ are inter-related through [42]

$$i\nabla_x^a = -[\tilde{U}_x^\dagger]^{ab} i\bar{\nabla}_x^b, \quad i\bar{\nabla}_x^a = -[\tilde{U}_x]^{ab} i\nabla_x^b. \quad (5.62)$$

Eq. 5.62 enables us to rewrite the JIMWLK Hamiltonian as

$$H_{\text{JIMWLK}}^{(\text{LL})} = -\frac{\alpha_s}{2\pi^2} \int_{uvz} \mathcal{K}_{uzv} \left[i\nabla_u^a i\nabla_v^a + i\bar{\nabla}_u^a i\bar{\nabla}_v^a + 2\tilde{U}_z^{ab} i\bar{\nabla}_u^a i\nabla_v^b \right] \quad (5.63)$$

which is the form that we shall use throughout the remainder of this thesis.

5.2 The JIMWLK equation and the Balitsky hierarchy

In this section, I examine the Balitsky hierarchy for the $q\bar{q}$ correlator. I show that its first two equations are contained in the first equation in the Balitsky hierarchy for the $q^2\bar{q}^2$ correlator matrix. This is not a surprising result, but rather, it is a natural consequence of the embedding of Wilson-line correlator matrices into higher-dimensional ones discussed in Sec. 4.4. This then motivates us to consider the JIMWLK evolution of a general correlator matrix from which we observed a previously overlooked property of the JIMWLK equation: it evolves symmetric and anti-symmetric components of correlator matrices separately. Knowing this property informs the parameterization ansatz we write down in the next chapter.

5.2.1 The JIMWLK evolution of the dipole operator and its associated Balitsky hierarchy

The JIMWLK evolution for the $q\bar{q}$ correlator is given by

$$\frac{d}{dY} \left\langle \frac{1}{d_f} \text{birdtracks} \right\rangle (Y) = \left\langle \frac{\alpha_s}{2\pi^2} \int_{uvz} \mathcal{K}_{uzv} \left[i\nabla_u^a i\nabla_v^a + i\bar{\nabla}_u^a i\bar{\nabla}_v^a + 2\tilde{U}_z^{ab} i\bar{\nabla}_u^a i\nabla_v^b \right] \frac{1}{d_f} \text{birdtracks} \right\rangle (Y), \quad (5.64)$$

where

$$\frac{1}{d_f} \text{birdtracks} = \frac{1}{d_f} \text{Tr} \left(U_x U_y^\dagger \right), \quad (5.65)$$

is the birdtracks representation of the $q\bar{q}$ correlator. Let us explicitly compute the result of the right-hand-side of Eq. 5.64 coming from each of the three terms in the JIMWLK Hamiltonian separately. The first term produces

$$\begin{aligned} \int_{uvz} \mathcal{K}_{uzv} i\nabla_u^a i\nabla_v^a \text{birdtracks} &= \frac{1}{2} \int_z \left[\mathcal{K}_{xxz} \text{birdtracks}_1 - \mathcal{K}_{xzy} \text{birdtracks}_2 - \mathcal{K}_{yzx} \text{birdtracks}_3 + \mathcal{K}_{zyy} \text{birdtracks}_4 \right] \\ &= -C_f \int_z \tilde{\mathcal{K}}_{xzy} \text{birdtracks}, \end{aligned} \quad (5.66)$$

which consists of is the original correlator convolved with the *Balitsky-Kovchegov (BK) kernel* which is given in terms of the JIMWLK kernel by

$$\tilde{\mathcal{K}}_{xzy} := \mathcal{K}_{xzy} + \mathcal{K}_{yzx} - \mathcal{K}_{xzx} - \mathcal{K}_{yzy} = \frac{(\mathbf{x} - \mathbf{y})^2}{(\mathbf{x} - \mathbf{z})^2(\mathbf{z} - \mathbf{y})^2}. \quad (5.67)$$

The net effect of the generator insertions in Eq. 5.66 by the Lie derivatives $i\nabla_u^a i\nabla_v^a$ was to produce a factor of the quadratic Casimir in the fundamental representation $t^a t^a = C_f \mathbb{1}$ where $C_f = \frac{N_c^2 - 1}{2N_c}$. The result of the second term in Eq. 5.64 is identical to that of the first term where

$$\begin{aligned} \int_{uvz} \mathcal{K}_{uzv} i\bar{\nabla}_u^a i\bar{\nabla}_v^a \text{diagram} &= \frac{1}{2} \int_z \left[\mathcal{K}_{xzx} \text{diagram} - \mathcal{K}_{xzy} \text{diagram} - \mathcal{K}_{yzx} \text{diagram} + \mathcal{K}_{yzy} \text{diagram} \right] \\ &= -C_f \int_z \tilde{\mathcal{K}}_{xzy} \text{diagram}. \end{aligned} \quad (5.68)$$

The third term in Eq. 5.64 inserts an additional adjoint Wilson-line or gluon into the $q\bar{q}$ correlator, producing the $q\bar{q}g$ correlator convolved with the BK kernel

$$\begin{aligned} \int_{uvz} \mathcal{K}_{uzv} 2\tilde{U}_z^{ab} i\bar{\nabla}_u^a i\bar{\nabla}_v^b \text{diagram} &= \int_z \left[-\mathcal{K}_{xzx} \text{diagram} + \mathcal{K}_{yzx} \text{diagram} + \mathcal{K}_{xzy} \text{diagram} - \mathcal{K}_{yzy} \text{diagram} \right] = \int_z \tilde{\mathcal{K}}_{xzy} \text{diagram}. \end{aligned} \quad (5.69)$$

Finally, Eq. 5.64 evaluates to

$$\frac{d}{dY} \left\langle \frac{1}{d_f} \text{diagram} \right\rangle (Y) = \frac{\alpha_s C_f}{\pi^2} \int_z \tilde{\mathcal{K}}_{xzy} \left\langle \frac{1}{d_A} \text{diagram} - \frac{1}{d_f} \text{diagram} \right\rangle (Y). \quad (5.70)$$

This equation says that the energy evolution of the $q\bar{q}$ correlator, a 2-point correlator, depends both on itself as well as the $q\bar{q}g$ correlator, a 3-point correlator. To know the latter for all Y one *must* determine its energy evolution via JIMWLK in turn. The JIMWLK evolution of the normalized $q\bar{q}g$ correlator can be similarly calculated and the result is given by

$$\begin{aligned} \frac{d}{dY} \left\langle \frac{1}{d_A} \text{diagram} \right\rangle (Y) &= \frac{\alpha_s}{2\pi^2} \int_{z_2} \left\langle \frac{1}{N_c^2 d_A} \text{diagram} \tilde{\mathcal{K}}_{xz_2y} + \frac{1}{\sqrt{2} N_c d_A} \left(\text{diagram} + \text{diagram} \right) (\tilde{\mathcal{K}}_{z_1 z_2 y} - \tilde{\mathcal{K}}_{xz_2 z_1}) \right. \\ &\quad + \frac{1}{\sqrt{2} N_c d_A} \left(\text{diagram} + \text{diagram} \right) \tilde{\mathcal{K}}_{xz_2 y} + \frac{1}{d_A} \text{diagram} \left(-\frac{1}{2} \tilde{\mathcal{K}}_{xz_2 y} + \tilde{\mathcal{K}}_{z_1 z_2 y} + \tilde{\mathcal{K}}_{xz_2 z_1} \right) \\ &\quad \left. + \frac{1}{2d_A} \left(\text{diagram} + \text{diagram} \right) (\tilde{\mathcal{K}}_{z_1 z_2 y} - \tilde{\mathcal{K}}_{xz_2 z_1}) + \frac{1}{2d_A} \text{diagram} \tilde{\mathcal{K}}_{xz_2 y} \right. \end{aligned}$$

$$+ \frac{1}{d_A} \left(\text{diagram} \right) \left(\frac{\tilde{\mathcal{K}}_{xz_2y}}{N_c} - N_c \tilde{\mathcal{K}}_{z_1 z_2 y} - N_c \tilde{\mathcal{K}}_{xz_2 z_1} \right) \rangle (Y), \quad (5.71)$$

and we see that its energy evolution depends both on itself as well as a number of 4-point correlators. This pattern continues ad infinitum: the energy evolution of an m -point correlator is driven by $(m + 1)$ -correlators. Consequently, the JIMWLK equation generates an infinite tower of coupled integro-differential equations known as the Balitsky hierarchy. Later we shall discuss in quite some detail a truncation for solving any Balitsky hierarchy which preserves both gauge invariance as well as symmetries of the underlying correlator structure. However, let us pause here for a moment and notice that we have already encountered the correlators used in Eq. 5.70 and Eq. 5.71 earlier in this thesis. For instance, the 4-point correlators appearing in Eq. 5.71 are precisely those coming from the lower-right 3-by-3 sub-block of the correlator matrix $\langle \mathcal{A}_{xz_1 z_2; yz_1 z_2}^{(3)} \rangle (Y)$ whose associated amplitude matrix was given in Eq. 4.151. In fact, if we adopt the shorthand

$$\mathcal{A}_{ij}^{(3)} = \left[\mathcal{A}_{xz_1 z_2; yz_1 z_2}^{(3)} \right]_{ij}, \quad (5.72)$$

then Eq. 5.71 can be written solely in terms of the entries in $\mathcal{A}_{xz_1 z_2; yz_1 z_2}^{(3)}$ as follows:

$$\begin{aligned} \frac{d}{dY} \langle \mathcal{A}_{22}^{(3)} \rangle (Y) &= \frac{\alpha_s}{2\pi^2} \int_{z_2} \left\langle \frac{1}{N_c} \mathcal{A}_{44}^{(3)} \tilde{\mathcal{K}}_{xz_2 y} + \frac{1}{\sqrt{2}} \left(\mathcal{A}_{45}^{(3)} + \mathcal{A}_{54}^{(3)} \right) \left(\tilde{\mathcal{K}}_{z_1 z_2 y} - \tilde{\mathcal{K}}_{xz_2 z_1} \right) \right. \\ &\quad + \frac{\sqrt{N_c^2 - 4}}{\sqrt{2} N_c} \left(\mathcal{A}_{46}^{(3)} + \mathcal{A}_{64}^{(3)} \right) \tilde{\mathcal{K}}_{xz_2 y} + N_c \mathcal{A}_{55}^{(3)} \left(-\frac{1}{2} \tilde{\mathcal{K}}_{xz_2 y} + \tilde{\mathcal{K}}_{z_1 z_2 y} + \tilde{\mathcal{K}}_{xz_2 z_1} \right) \\ &\quad + \frac{1}{2} \sqrt{N_c^2 - 4} \left(\mathcal{A}_{56}^{(3)} + \mathcal{A}_{65}^{(3)} \right) \left(\tilde{\mathcal{K}}_{z_1 z_2 y} - \tilde{\mathcal{K}}_{xz_2 z_1} \right) + \frac{(N_c^2 - 4)}{2 N_c} \mathcal{A}_{66}^{(3)} \tilde{\mathcal{K}}_{xz_2 y} \\ &\quad \left. + \mathcal{A}_{22}^{(3)} \left(\frac{\tilde{\mathcal{K}}_{xz_2 y}}{N_c} - N_c \tilde{\mathcal{K}}_{xz_2 z_1} - N_c \tilde{\mathcal{K}}_{z_1 z_2 y} \right) \right\rangle (Y). \end{aligned} \quad (5.73)$$

Using the same shorthand we can also write Eq. 5.70 solely in terms of the entries in $\mathcal{A}_{xz_1 z_2; yz_1 z_2}^{(3)}$ by

$$\frac{d}{dY} \langle \mathcal{A}_{11}^{(3)} \rangle (Y) = \frac{\alpha_s C_f}{\pi^2} \int_z \tilde{\mathcal{K}}_{xyz} \langle \mathcal{A}_{33}^{(3)} - \mathcal{A}_{11}^{(3)} \rangle (Y). \quad (5.74)$$

But remember: the $q\bar{q}$ and $q\bar{q}g$ correlators are contained on the diagonal of the $q^2\bar{q}^2$ correlator matrix (constructed in the Fierz basis) with a single quark–anti-quark coincidence limit having been taken. This diagonal 2-by-2 matrix is precisely the diagonal top-left block of the correlator matrix whose associated amplitude matrix was given in Eq. 4.152, the $q^3\bar{q}^3$ amplitude matrix (also constructed in the Fierz basis) with two quark–anti-quark coincidence limit having been taken. This means that both Eq. 5.70 and Eq. 5.71 are contained in the JIMWLK equation for the $q^2\bar{q}^2$ correlator matrix; **two iterations** of the JIMWLK Hamiltonian on the $q\bar{q}$ correlator are contained in **a single iteration** of the JIMWLK Hamiltonian on the $q^2\bar{q}^2$ correlator matrix.

Therefore, considering “**deeper**” JIMWLK evolution of a correlator matrix, that is, multiple iterations of the JIMWLK Hamiltonian on a correlator matrix, **is equivalent to** considering the JIMWLK evolution of a “**wider**” or higher-dimensional correlator matrix. In fact, it is natural to think about the JIMWLK evolution of correlator matrices as opposed to individual correlators because elements of a correlator matrix mix under JIMWLK evolution. This is somewhat analogous to how PDFs mix under DGLAP. But before we prove this to be the case, we want to highlight for future use that Eq. 5.71 contains the JIMWLK evolution of the two gluon correlator following the coincidence limit $\mathbf{y} \mapsto \mathbf{x}$; namely,

$$\frac{d}{dY} \left\langle \frac{1}{d_A} \text{ (loop diagram) } \right\rangle (Y) = \frac{\alpha_s}{2\pi^2} \int_{z_2} \tilde{\mathcal{K}}_{\mathbf{x}z_2z_1} \left\langle \frac{2}{d_A} \text{ (loop diagram with dots) } - \frac{2N_c}{d_A} \text{ (loop diagram) } \right\rangle (Y). \quad (5.75)$$

Eq. 5.75 can be written in terms of entries in $\mathcal{A}_{\mathbf{x}z_1z_2;\mathbf{x}z_1z_2}^{(3)}$ (see Eq. 4.153) as

$$\frac{d}{dY} \langle \mathcal{A}_{22}^{(3)} \rangle (Y) = \frac{\alpha_s C_A}{\pi^2} \int_{z_2} \tilde{\mathcal{K}}_{\mathbf{x}z_2z_1} \langle \mathcal{A}_{55}^{(3)} - \mathcal{A}_{22}^{(3)} \rangle (Y). \quad (5.76)$$

5.2.2 The JIMWLK equation for correlator matrices: coupling blocks in higher dimensional correlator matrices

Thus far in this thesis, we have only considered the JIMWLK evolution of individual correlators (c.f. Eq. 5.70, Eq. 5.71 and Eq. 5.75) or diagonal correlator matrices, but we have not yet considered the JIMWLK evolution of non-trivial (i.e. non-diagonal) correlator matrices. In fact, to my knowledge, and the knowledge of my supervisor, the JIMWLK evolution of non-trivial correlator matrices has not yet been considered in the literature to date. In this section, we seek to understand the structure of the JIMWLK equation for non-trivial correlator matrices: for correlator matrices larger than the $q\bar{q}$ correlator matrix which is simply a complex number.

Consider the JIMWLK equation for the $q^m \bar{q}^m$ amplitude matrix given below

$$\begin{aligned} \frac{d}{dY} \left\langle \text{ (diagram with } i, j \text{ and dots) } \right\rangle (Y) \\ = \frac{\alpha_s}{2\pi^2} \int_{uvz} \mathcal{K}_{uzv} \left\langle \left[i \nabla_u^a i \nabla_v^a + i \bar{\nabla}_u^a i \bar{\nabla}_v^a + 2 \tilde{U}_z^{ab} i \bar{\nabla}_u^a i \nabla_v^b \right] \text{ (diagram with } i, j \text{ and dots) } \right\rangle (Y). \end{aligned} \quad (5.77)$$

In order to begin understanding the structure of this equation, recall that the action of the right- and left-invariant vector fields on $\text{SU}(N_c)$ on a tensor-product of Wilson-lines of the form

given in Eq. 4.14, is given by

$$\sqrt{2} i \nabla_u^a = \begin{array}{c} \text{---} \\ \text{---} \\ \vdots \\ \text{---} \end{array} \begin{array}{c} \text{---} \\ \text{---} \\ \vdots \\ \text{---} \end{array} = \begin{array}{c} \text{---} \\ \text{---} \\ \vdots \\ \text{---} \end{array} \left[\delta_{ux_1}^{(2)} + \dots + \delta_{ux_m}^{(2)} - \delta_{uy_1}^{(2)} - \dots - \delta_{uy_m}^{(2)} \right] =: \begin{array}{c} \text{---} \\ \text{---} \\ \vdots \\ \text{---} \end{array} \begin{array}{c} \text{---} \\ \text{---} \\ \vdots \\ \text{---} \end{array}, \quad (5.78a)$$

$$\sqrt{2} i \bar{\nabla}_u^a = - \left[\delta_{ux_1}^{(2)} + \dots + \delta_{ux_m}^{(2)} - \delta_{uy_1}^{(2)} - \dots - \delta_{uy_m}^{(2)} \right] \begin{array}{c} \text{---} \\ \text{---} \\ \vdots \\ \text{---} \end{array} =: - \begin{array}{c} \text{---} \\ \text{---} \\ \vdots \\ \text{---} \end{array} \begin{array}{c} \text{---} \\ \text{---} \\ \vdots \\ \text{---} \end{array}, \quad (5.78b)$$

where $\text{---}_a = \sqrt{2} t^a$ (see Eq. 4.24) and the gray shadow behind the dotted black line in the last equality of each line represents the sum over all generator insertions. As we did when we examined the action of the JIMWLK Hamiltonian on the dipole operator in the previous subsection, let us analyze each term on the left-hand-side of Eq. 5.77 separately. The first term is calculated as

$$\begin{aligned} \int_{uvz} \mathcal{K}_{uzv} i \nabla_u^a i \nabla_v^a & \begin{array}{c} \text{---} \\ \text{---} \\ \vdots \\ \text{---} \end{array} \begin{array}{c} \text{---} \\ \text{---} \\ \vdots \\ \text{---} \end{array} = \frac{1}{2} \int_{uvz} \mathcal{K}_{uzv} \begin{array}{c} \text{---} \\ \text{---} \\ \vdots \\ \text{---} \end{array} \begin{array}{c} \text{---} \\ \text{---} \\ \vdots \\ \text{---} \end{array} \\ & = \sum_k \frac{1}{2} \int_{uvz} \mathcal{K}_{uzv} \begin{array}{c} \text{---} \\ \text{---} \\ \vdots \\ \text{---} \end{array} \begin{array}{c} \text{---} \\ \text{---} \\ \vdots \\ \text{---} \end{array} \begin{array}{c} \text{---} \\ \text{---} \\ \vdots \\ \text{---} \end{array} \begin{array}{c} \text{---} \\ \text{---} \\ \vdots \\ \text{---} \end{array} = \sum_k \frac{1}{2} \int_z \begin{array}{c} \text{---} \\ \text{---} \\ \vdots \\ \text{---} \end{array} \begin{array}{c} \text{---} \\ \text{---} \\ \vdots \\ \text{---} \end{array} \left[\int_{uv} \mathcal{K}_{uzv} \begin{array}{c} \text{---} \\ \text{---} \\ \vdots \\ \text{---} \end{array} \begin{array}{c} \text{---} \\ \text{---} \\ \vdots \\ \text{---} \end{array} \right] \\ & = \sum_k \frac{1}{2} \int_z \begin{array}{c} \text{---} \\ \text{---} \\ \vdots \\ \text{---} \end{array} \begin{array}{c} \text{---} \\ \text{---} \\ \vdots \\ \text{---} \end{array} [\mathcal{K}_{\vec{x}; \vec{y}; z}]_{kj}, \end{aligned} \quad (5.79)$$

where in the second line we inserted a complete sum over colour singlet projection operators⁴ $\sum_k |m; k\rangle \langle m; k|$, and in the last line we defined the matrix the *kernel matrix* $\mathcal{K}_{\vec{x}; \vec{y}; z}$ whose k^{th} row and j^{th} column is given by

$$\begin{array}{c} \text{---} \\ \text{---} \\ \vdots \\ \text{---} \end{array} \begin{array}{c} \text{---} \\ \text{---} \\ \vdots \\ \text{---} \end{array}, \quad (5.80)$$

is a colour singlet state. We shall postpone the proof of this until the next chapter.

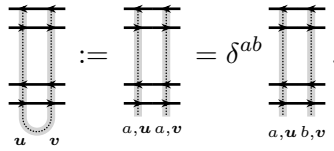
⁴The reason why it is sufficient for us to insert a complete sum over colour singlet projection operators (which do not sum to $id_{W \otimes m}$) is that

$$[\mathcal{K}_{\vec{x};\vec{y};z}]_{kj} := \int_{uv} \mathcal{K}_{uzv} \text{ (diagram) }, \quad (5.81)$$


with

$$\vec{x} = \begin{pmatrix} x_1 \\ \vdots \\ x_m \end{pmatrix}, \quad \vec{y} = \begin{pmatrix} y_1 \\ \vdots \\ y_m \end{pmatrix}. \quad (5.82)$$

and

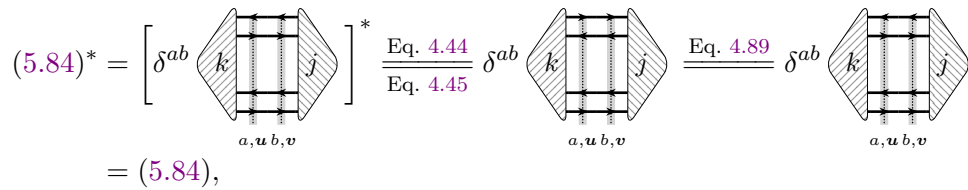
$$\text{(diagram)} := \text{(diagram)} = \delta^{ab} \text{(diagram)}. \quad (5.83)$$


Before proceeding to analyze the contributions from the second and third terms in Eq. 5.77, let us pause to comment on two properties of the kernel matrix given in Eq. 5.81:

- **The kernel matrix is real:** Since the JIMWLK kernel is real, all that needs to be shown is that

$$\text{(diagram)} = \delta^{ab} \text{(diagram)}, \quad (5.84)$$


is real. Eq. 5.84 is real since

$$\begin{aligned} (5.84)^* &= \left[\delta^{ab} \text{(diagram)} \right]^* \xrightarrow[\text{Eq. 4.45}]{\text{Eq. 4.44}} \delta^{ab} \text{(diagram)} \xrightarrow{\text{Eq. 4.89}} \delta^{ab} \text{(diagram)} \\ &= (5.84), \end{aligned} \quad (5.85)$$


where the second equality follows from the diagrammatic rules for complex conjugation given in Sec. 4.1 (specifically Eq. 4.44 and Eq. 4.45), the third equality follows from Lemma 4.1 (actually just the reality of the projection operator $P_A = \text{diagram}$ as recorded in Eq. 4.89) and the forth equality follows from $(\delta^{ab})^* = \delta^{ab}$.

- **The kernel matrix is symmetric:** In order to prove that the kernel matrix is symmetric, examine

$$\begin{aligned}
& [\mathcal{K}_{\vec{x};\vec{y};z}]_{kj}^t = [\mathcal{K}_{\vec{x};\vec{y};z}]_{jk} \\
&= \int_{uv} \mathcal{K}_{uzv} \text{ (diagram with } j \text{ on left, } k \text{ on right, } a, u, b, v \text{ at bottom)} \delta^{ab} \\
&= \int_{uv} \mathcal{K}_{uzv} \text{ (diagram with } k \text{ on left, } j \text{ on right, } b, v, a, u \text{ at bottom)} \delta^{ab} \quad (\text{flipping the diagram}) \\
&= \int_{uv} \mathcal{K}_{uzv} \text{ (diagram with } k \text{ on left, } j \text{ on right, } b, v, a, u \text{ at bottom)} \delta^{ab} \quad (\text{using Lemma 4.1 and } (\delta^{ab})^* = \delta^{ab}) \\
&= \int_{vu} \mathcal{K}_{vzu} \text{ (diagram with } k \text{ on left, } j \text{ on right, } a, u, b, v \text{ at bottom)} \delta^{ba} \quad (\text{relabelling dummy indices } a, b \text{ and variables } \mathbf{u}, \mathbf{v}) \\
&= \int_{uv} \mathcal{K}_{uzv} \text{ (diagram with } k \text{ on left, } j \text{ on right, } a, u, b, v \text{ at bottom)} \delta^{ab} \quad (\mathcal{K}_{vzu} = \mathcal{K}_{uzv} \text{ and } \delta^{ba} = \delta^{ab}) \\
&= [\mathcal{K}_{\vec{x};\vec{y};z}]_{kj}, \tag{5.86}
\end{aligned}$$

which proves $[\mathcal{K}_{\vec{x};\vec{y};z}]_{kj}^t = [\mathcal{K}_{\vec{x};\vec{y};z}]_{kj}$.

The second term coming from the left-hand-side of Eq. 5.77 is similar to that of the first except with the kernel matrix acting to the left of the amplitude matrix as opposed to the right

$$\begin{aligned}
& \int_{uvz} \mathcal{K}_{uzv} i\bar{\nabla}_u^a i\bar{\nabla}_v^a \text{ (diagram with } i \text{ on left, } j \text{ on right, } v \text{ on left, } u \text{ on right)} = \frac{1}{2} \int_{uvz} \mathcal{K}_{uzv} \text{ (diagram with } i \text{ on left, } j \text{ on right, } v \text{ on left, } u \text{ on right)} \\
&= \sum_k \frac{1}{2} \int_{vuz} \mathcal{K}_{vzu} \text{ (diagram with } i \text{ on left, } k \text{ on right, } u \text{ on left, } v \text{ on right)} \text{ (diagram with } k \text{ on left, } j \text{ on right)} = \sum_k \frac{1}{2} \int_z \left[\int_{uv} \mathcal{K}_{uzv} \text{ (diagram with } i \text{ on left, } k \text{ on right, } u \text{ on left, } v \text{ on right)} \right] \text{ (diagram with } k \text{ on left, } j \text{ on right)} \\
&= \sum_k \int_z [\mathcal{K}_{\vec{x};\vec{y};z}]_{ik} \text{ (diagram with } k \text{ on left, } j \text{ on right)} \tag{5.87}
\end{aligned}$$

where we used the symmetry of the JIMWLK kernel under simultaneous exchange of \mathbf{u} and \mathbf{v} to relabel dummy variables \mathbf{u}, \mathbf{v} in order to identify the term inside the square parentheses as the i^{th} row and k^{th} column of the kernel matrix. The third term in Eq. 5.77 is calculated as

$$\begin{aligned}
& \int_{uvz} \mathcal{K}_{uzv} 2\tilde{U}_z^{ab} i \bar{\nabla}_u^a i \nabla_v^b \text{ (diagram with two blue arrows) } = - \int_{uvz} \mathcal{K}_{uzv} \text{ (diagram with two grey arrows) } \\
& = - \int_{uvz} \mathcal{K}_{uzv} \text{ (diagram with two grey arrows and a loop) } \\
& = - \sum_{k,l} \int_{uvz} \mathcal{K}_{uzv} \text{ (diagram with three grey arrows and loops) } \\
& = - \sum_{k,l} \int_{uvz} \mathcal{K}_{uzv} \text{ (diagram with three grey arrows and loops, different orientation) } \\
& = - \sum_{k,l} \int_{uvz} \mathcal{K}_{uzv} \text{ (diagram with three grey arrows and loops, different orientation) }, \tag{5.88}
\end{aligned}$$

where in the third line we inserted two complete sums over colour singlet projection operators on $W^{\otimes(m+1)}$. (Refer to Sec. 4.4.1 for more information about the birdtrack notation used here.) Using the fact that the LO JIMWLK kernel factorizes

$$\mathcal{K}_{uvz} = \sum_{h=1}^2 \mathcal{K}_{uz}^h \mathcal{K}_{zv}^h = - \sum_{h=1}^2 \mathcal{K}_{uz}^h \mathcal{K}_{vz}^h, \quad \mathcal{K}_{uz}^h = \frac{(\mathbf{u} - \mathbf{z})^h}{(\mathbf{u} - \mathbf{z})^2}, \tag{5.89}$$

Eq. 5.88 can be written as

$$\begin{aligned}
(5.88) &= \sum_{k,l} \sum_{h=1}^2 \int_z \left[\int_u \mathcal{K}_{uz}^h \right] \left[\text{diagram with vertices } i, k \text{ and } u \right] \left[\text{diagram with vertices } k, \dots, l \text{ and } v \right] \left[\int_v \mathcal{K}_{vz}^h \right] \left[\text{diagram with vertices } l, j \text{ and } v \right] \\
&= \sum_{k,l} \sum_{h=1}^2 \int_z \left[\mathcal{K}_{\vec{x};\vec{y};z}^{(L)h} \right]_{ik} \left[\text{diagram with vertices } k, \dots, l \text{ and } v \right] \left[\mathcal{K}_{\vec{x};\vec{y};z}^{(R)h} \right]_{lj}, \tag{5.90}
\end{aligned}$$

where in the last line we defined the non-square matrices

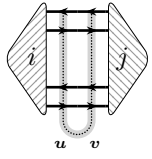
$$\left[\mathcal{K}_{\vec{x};\vec{y};z}^{(L)h} \right]_{ik} := \int_u \mathcal{K}_{uz}^h \left[\text{diagram with vertices } i, k \text{ and } u \right], \quad \left[\mathcal{K}_{\vec{x};\vec{y};z}^{(R)h} \right]_{lj} := \int_v \mathcal{K}_{vz}^h \left[\text{diagram with vertices } l, j \text{ and } v \right], \tag{5.91}$$

which are $m! \times m \cdot m!$ and $m \cdot m! \times m!$, respectively. We shall refer to these non-square matrices as *the left and right factors of the kernel matrix*. They are hermitian pairs, related through

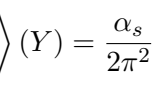
$$\left[\mathcal{K}_{\vec{x};\vec{y};z}^{(L)h} \right]_{ij}^\dagger = \left[\int_u \mathcal{K}_{uz}^h \right] \left[\text{diagram with vertices } i, j \text{ and } u \right]^\dagger = \int_u \mathcal{K}_{uz}^h \left[\text{diagram with vertices } j, i \text{ and } u \right] = \left[\mathcal{K}_{\vec{x};\vec{y};z}^{(R)h} \right]_{ji}. \tag{5.92}$$

However, since these matrices are real, they are simply related by transposition. They are called the left and right factors of the kernel matrix and suggestively labelled similarly to the kernel matrix because their matrix product summed over h is equal to minus the kernel matrix:

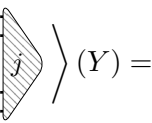

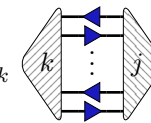

$$\begin{aligned}
&\sum_k \sum_{h=1}^2 \left[\mathcal{K}_{\vec{x};\vec{y};z}^{(L)h} \right]_{ik} \left[\mathcal{K}_{\vec{x};\vec{y};z}^{(R)h} \right]_{kj} = \sum_k \sum_{h=1}^2 \left[\int_u \mathcal{K}_{uz}^h \right] \left[\text{diagram with vertices } i, k \text{ and } u \right] \left[\int_v \mathcal{K}_{vz}^h \right] \left[\text{diagram with vertices } k, j \text{ and } v \right] \\
&= \sum_k \int_{uv} \left[- \sum_{h=1}^2 \mathcal{K}_{uz}^h \mathcal{K}_{zv}^h \right] \left[\text{diagram with vertices } i, k \text{ and } u \right] \left[\text{diagram with vertices } k, j \text{ and } v \right] \\
&= - \sum_k \int_{uv} \mathcal{K}_{uzv} \left[\text{diagram with vertices } i, k \text{ and } u \right] \left[\text{diagram with vertices } k, j \text{ and } v \right]
\end{aligned}$$

$$= - \int_{uv} \mathcal{K}_{uzv} \left(\text{diagram} \right) = - [\mathcal{K}_{\vec{x};\vec{y};z}]_{ij}. \quad (5.93)$$


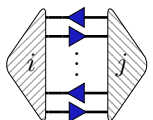
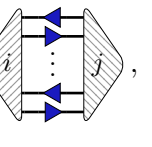
Putting all the pieces together, Eq. 5.77, which I quote again here for convenience

$$\frac{d}{dY} \left\langle \left(\text{diagram} \right) \right\rangle (Y) = \frac{\alpha_s}{2\pi^2} \int_{uvz} \mathcal{K}_{uzv} \left\langle \left[i \nabla_u^a i \nabla_v^a + i \bar{\nabla}_u^a i \bar{\nabla}_v^a + 2 \tilde{U}_z^{ab} i \bar{\nabla}_u^a i \nabla_v^b \right] \left(\text{diagram} \right) \right\rangle (Y),$$


becomes

$$\begin{aligned} \frac{d}{dY} \left\langle \left(\text{diagram} \right) \right\rangle (Y) &= \frac{\alpha_s}{2\pi^2} \int_z \left\langle \underbrace{\frac{1}{2} \left(\text{diagram} \right) [\mathcal{K}_{\vec{x};\vec{y};z}]_{kj}}_{= \int_{uv} \mathcal{K}_{uzv} i \nabla_u^a i \nabla_v^a \left(\text{diagram} \right)} + \underbrace{\frac{1}{2} [\mathcal{K}_{\vec{x};\vec{y};z}]_{ik} \left(\text{diagram} \right)}_{= \int_{uv} \mathcal{K}_{uzv} i \bar{\nabla}_u^a i \bar{\nabla}_v^a \left(\text{diagram} \right)} \right. \\ &\quad \left. + \sum_{h=1}^2 [\mathcal{K}_{\vec{x};\vec{y};z}^{(L)h}]_{ik} \underbrace{\left(\text{diagram} \right) [\mathcal{K}_{\vec{x};\vec{y};z}^{(R)h}]_{lj}}_{= \int_{uv} \mathcal{K}_{uzv} 2 \tilde{U}_z^{ab} i \bar{\nabla}_u^a i \nabla_v^b \left(\text{diagram} \right)} \right\rangle (Y), \end{aligned} \quad (5.94)$$





where the sums over indices k and l associated with matrix multiplication are now made implicit. Recalling the notation

$$[\mathcal{A}_{\vec{x};\vec{y}}^{(m)}]_{ij} := \left(\text{diagram} \right), \quad [\mathcal{A}_{\vec{x};\vec{y};z}^{(m;g)}]_{ij} := \left(\text{diagram} \right), \quad (5.95)$$



Eq. 5.94 can be written

$$\begin{aligned} \frac{d}{dY} \left\langle \mathcal{A}_{\vec{x};\vec{y}}^{(m)} \right\rangle (Y) &= \frac{\alpha_s}{2\pi^2} \int_z \left[\frac{1}{2} \left\{ \mathcal{K}_{\vec{x};\vec{y};z}, \left\langle \mathcal{A}_{\vec{x};\vec{y}}^{(m)} \right\rangle (Y) \right\} + \sum_{h=1}^2 \mathcal{K}_{\vec{x};\vec{y};z}^{(L)h} \cdot \left\langle \mathcal{A}_{\vec{x};\vec{y};z}^{(m;g)} \right\rangle (Y) \cdot \mathcal{K}_{\vec{x};\vec{y};z}^{(R)h} \right] \\ &= \frac{\alpha_s}{4\pi^2} \sum_{h=1}^2 \int_z \left[- \left\{ \mathcal{K}_{\vec{x};\vec{y};z}^{(L)h} \cdot \mathcal{K}_{\vec{x};\vec{y};z}^{(R)h}, \left\langle \mathcal{A}_{\vec{x};\vec{y}}^{(m)} \right\rangle (Y) \right\} + 2 \mathcal{K}_{\vec{x};\vec{y};z}^{(L)h} \cdot \left\langle \mathcal{A}_{\vec{x};\vec{y};z}^{(m;g)} \right\rangle (Y) \cdot \mathcal{K}_{\vec{x};\vec{y};z}^{(R)h} \right], \\ &= \frac{\alpha_s}{4\pi^2} \sum_{h=1}^2 \int_z \left[- \left\{ \mathcal{K}_{\vec{x};\vec{y};z}^{(L)h} \cdot \left(\mathcal{K}_{\vec{x};\vec{y};z}^{(L)h} \right)^t, \left\langle \mathcal{A}_{\vec{x};\vec{y}}^{(m)} \right\rangle (Y) \right\} + 2 \mathcal{K}_{\vec{x};\vec{y};z}^{(L)h} \cdot \left\langle \mathcal{A}_{\vec{x};\vec{y};z}^{(m;g)} \right\rangle (Y) \cdot \left(\mathcal{K}_{\vec{x};\vec{y};z}^{(L)h} \right)^t \right], \end{aligned} \quad (5.96)$$

If we define the following non-square $m! \times (m+1)!$ matrices

$$\mathcal{P}_{\vec{x};\vec{y};z}^{(1)h} := \left[-\mathcal{K}_{\vec{x};\vec{y};z}^{(L)h} \cdot \left(\mathcal{K}_{\vec{x};\vec{y};z}^{(L)h} \right)^t \quad \mathcal{K}_{\vec{x};\vec{y};z}^{(L)h} \right], \quad \mathcal{P}_{\vec{x};\vec{y};z}^{(2)h} := \left[\mathbb{1}_{m! \times m!} \quad \mathcal{K}_{\vec{x};\vec{y};z}^{(L)h} \right], \quad (5.97)$$

then Eq. 5.96 can be written in the compact form

$$\begin{aligned} \frac{d}{dY} \langle \mathcal{A}_{\vec{x};\vec{y}}^{(m)} \rangle (Y) &= \frac{\alpha_s}{4\pi^2} \sum_{h=1}^2 \int_z \left(\mathcal{P}_{\vec{x};\vec{y};z}^{(1)h} \cdot \left\langle \begin{bmatrix} \mathcal{A}_{\vec{x};\vec{y}}^{(m)} & 0 \\ 0 & \mathcal{A}_{\vec{x};\vec{y};z}^{(m;g)} \end{bmatrix} \right\rangle (Y) \cdot \left(\mathcal{P}_{\vec{x};\vec{y};z}^{(2)h} \right)^t \right. \\ &\quad \left. + \mathcal{P}_{\vec{x};\vec{y};z}^{(2)h} \cdot \left\langle \begin{bmatrix} \mathcal{A}_{\vec{x};\vec{y}}^{(m)} & 0 \\ 0 & \mathcal{A}_{\vec{x};\vec{y};z}^{(m;g)} \end{bmatrix} \right\rangle (Y) \cdot \left(\mathcal{P}_{\vec{x};\vec{y};z}^{(1)h} \right)^t \right). \end{aligned} \quad (5.98)$$

Eq. 5.98, being an original result, contains important information which I discuss below:

- From Eq. 5.98, we see that the evolution of the $q^m \bar{q}^m$ correlator matrix is driven by itself as well as by the $q^m \bar{q}^m g$ correlator matrix: **the JIMWLK equation couples the disjoint blocks of $q^{m+1} \bar{q}^{m+1}$ correlator matrix, given in Eq. 4.146, through evolution.**
- Another important observation from Eq. 5.98 is that the JIMWLK equation automatically preserves the symmetry of the underlying amplitude matrix in the sense that **the JIMWLK evolution of the symmetric part of a correlator matrix remains symmetric while the JIMWLK evolution of the anti-symmetric part remains anti-symmetric.** To see this, note that the integrand in Eq. 5.98 is symmetric for a symmetric $q^{m+1} \bar{q}^{m+1}$ correlator matrix and anti-symmetric if the $q^{m+1} \bar{q}^{m+1}$ correlator matrix anti-symmetric. But even more generally, we can decompose the $q^{m+1} \bar{q}^{m+1}$ correlator matrix into a sum of its symmetric and anti-symmetric parts and show that only the symmetric parts feed the evolution of the symmetric part of the $q^m \bar{q}^m$ correlator matrix while, conversely, only the anti-symmetric parts of the $q^{m+1} \bar{q}^{m+1}$ correlator matrix feed the evolution of the anti-symmetric part of the $q^m \bar{q}^m$ correlator matrix.
- Lastly, from the above analysis one sees that **in order to write down the JIMWLK equation for a general correlator matrix, one only needs to compute the left factor of the kernel matrix.**

In the hopes of clarifying some of the above discussion, we conclude this chapter by computing the left factors of the kernel matrices for evolving the $q\bar{q}$ and $q\bar{q}g$ correlators and use them to reconstruct the kernel matrices. The left factor of the kernel matrix associated with the $q\bar{q}$

correlator is calculated as

$$\begin{aligned}\mathcal{K}_{x;y;z}^{(L)h} &= \int_u \mathcal{K}_{uz}^h \frac{1}{\sqrt{d_f d_A}} \text{Diagram}_u = \int_u \mathcal{K}_{uz}^h \frac{1}{\sqrt{d_f d_A}} \left(\delta_{ux}^{(2)} \text{Diagram}_u - \delta_{uy}^{(2)} \text{Diagram}_u \right) \\ &= \frac{2d_f C_f}{\sqrt{d_f d_A}} (\mathcal{K}_{xz}^h - \mathcal{K}_{yz}^h) = \sqrt{2C_f} (\mathcal{K}_{xz}^h - \mathcal{K}_{yz}^h),\end{aligned}\quad (5.99)$$

from which we can calculate the kernel matrix using Eq. 5.93 as

$$\begin{aligned}-\sum_{h=1}^2 \mathcal{K}_{x;y;z}^{(L)h} \left(\mathcal{K}_{x;y;z}^{(L)h} \right)^t &= -\sum_{h=1}^2 \left(\sqrt{2C_f} (\mathcal{K}_{xz}^h - \mathcal{K}_{yz}^h) \right)^2 \\ &= -2C_f \sum_{h=1}^2 \left((\mathcal{K}_{xz}^h)^2 - \mathcal{K}_{xz}^h \mathcal{K}_{yz}^h - \mathcal{K}_{yz}^h \mathcal{K}_{xz}^h + (\mathcal{K}_{yz}^h)^2 \right) \\ &= -2C_f (\mathcal{K}_{xzy} + \mathcal{K}_{yzx} - \mathcal{K}_{xxz} - \mathcal{K}_{yyz}) = -2C_f \tilde{\mathcal{K}}_{xzy}.\end{aligned}\quad (5.100)$$

Eq. 5.100 is precisely as expected (see Eq. 5.70). Similarly one can show that the left factor of the kernel matrix associated with the $q\bar{q}$ correlator is given by

$$\begin{aligned}\mathcal{K}_{xz_1;y z_1;z_2}^{(L)h} &= \\ \begin{bmatrix} \sqrt{2C_f} (\mathcal{K}_{xz_2}^h - \mathcal{K}_{yz_2}^h) & 0 & 0 & 0 \\ 0 & \frac{1}{\sqrt{N_c}} (\mathcal{K}_{xz_2}^h - \mathcal{K}_{yz_2}^h) & \sqrt{\frac{C_A}{2}} (2\mathcal{K}_{z_1 z_2}^h - \mathcal{K}_{xz_2}^h - \mathcal{K}_{yz_2}^h) & \sqrt{\frac{C_d}{2}} (\mathcal{K}_{xz_2}^h - \mathcal{K}_{yz_2}^h) \end{bmatrix},\end{aligned}\quad (5.101)$$

from which one can compute the kernel matrix to be

$$-\sum_{h=1}^2 \mathcal{K}_{xz_1;y z_1;z_2}^{(L)h} \left(\mathcal{K}_{xz_1;y z_1;z_2}^{(L)h} \right)^t = \begin{bmatrix} -2C_f \tilde{\mathcal{K}}_{xzy} & 0 \\ 0 & \frac{\tilde{\mathcal{K}}_{xzy}}{N_c} - N_c \tilde{\mathcal{K}}_{xz_2 z_1} - N_c \tilde{\mathcal{K}}_{z_1 z_2 y} \end{bmatrix}. \quad (5.102)$$

The top-left entry in Eq. 5.102 is simply the kernel matrix given in Eq. 5.100 except with z replaced by z_2 . The bottom-right entry is precisely the term in parentheses multiplying the $q\bar{q}g$ correlator in Eq. 5.73. In fact, it is easy to show that using Eq. 5.101 in Eq. 5.96 one can reproduce Eq. 5.73.

Chapter 6

The exponential parameterization

6.1 A systematic derivation of the exponential parameterization

Let $\langle \mathcal{A} \rangle(Y)$ be a general Wilson-line correlator matrix (with coordinate dependence suppressed in order to simplify notation). In this section, we present a novel parameterization for the Y -dependence of $\langle \mathcal{A} \rangle(Y)$ which naturally admits a gauge-invariant and symmetry-preserving truncation of the Balitsky hierarchy associated with $\langle \mathcal{A} \rangle(Y)$.

Recall that the JIMWLK equation for $\langle \mathcal{A} \rangle(Y)$ is given by

$$\frac{d}{dY} \langle \mathcal{A} \rangle(Y) = -\langle H_{\text{JIMWLK}}^{(\text{LL})} \mathcal{A} \rangle(Y), \quad (6.1)$$

where

$$H_{\text{JIMWLK}}^{(\text{LL})} = -\frac{\alpha_s}{2\pi^2} \int_{uvz} \mathcal{K}_{uzv} \left[i\bar{\nabla}_u^a i\bar{\nabla}_v^a + i\nabla_u^a i\nabla_v^a + 2\tilde{U}_z^{ab} i\bar{\nabla}_u^a i\nabla_v^b \right], \quad (6.2)$$

is the JIMWLK Hamiltonian derived in Sec. 5.1 to leading logarithmic (LL) accuracy, and the integration kernel (which was also derived in Sec. 5.1) is given by

$$\mathcal{K}_{uzv} = \frac{(\mathbf{u} - \mathbf{z}) \cdot (\mathbf{z} - \mathbf{v})}{(\mathbf{u} - \mathbf{z})^2 (\mathbf{z} - \mathbf{v})^2}. \quad (6.3)$$

From the discussion of the previous chapter, we know that Eq. 6.1 is not closed, but rather it is the first equation in an infinite tower of coupled equations; this infinite tower is known as the Balitsky hierarchy associated with $\langle \mathcal{A} \rangle(Y)$. It is the third term in the JIMWLK Hamiltonian, the operator $2\tilde{U}_z^{ab} i\bar{\nabla}_u^a i\nabla_v^b$, which is responsible for generating the Balitsky hierarchy. If this third term was not present (and the JIMWLK kernel remained finite as the integration variable

\mathbf{z} became coincident with either of the transverse coordinates \mathbf{u} or \mathbf{v}), then Eq. 6.1 would be closed and the following formal solution would be exact

$$\langle \mathcal{A} \rangle(Y) = \langle \exp \left[-(Y - Y_0) H_{\text{JIMWLK}}^{(\text{LL})} \right] \mathcal{A} \rangle(Y_0), \quad (6.4)$$

in terms of an initial condition specified at some Y_0 . Note that Eq. 6.4 is different from the formal solution for the distribution $\hat{Z}_Y[U]$, given by

$$\hat{Z}_Y[U] = \exp \left[-(Y - Y_0) H_{\text{JIMWLK}}^{(\text{LL})} \right] \hat{Z}_{Y_0}[U], \quad (6.5)$$

since the former is contained in the latter; Eq. 6.5 summarizes information about every Balitsky hierarchy, not just the Balitsky hierarchy associated with our $\langle \mathcal{A} \rangle(Y)$.

At leading logarithm, one can sidestep the problem of the Balitsky hierarchy altogether since the LL JIMWLK Hamiltonian is a Fokker-Planck Hamiltonian which means that Eq. 6.1 can be recast as a Langevin equation for an ensemble of Wilson-lines [9]. The Langevin equation can be solved numerically in order to determine the Y -evolution of the ensemble and this ensemble can be used to compute any Wilson-line correlator numerically. But at next-to-leading logarithmic (NLL) accuracy this is no longer the case [43–45]; the NLL JIMWLK Hamiltonian is no longer just quadratic in Lie derivatives, but also contains cubic products of Lie derivatives and, hence, cannot be formulated as a Langevin equation. In this case there are no other known ways of sidestepping the Balitsky hierarchy and one really needs a truncation in order to obtain a solution, even if only an approximate one. It makes sense, however, to first develop the machinery for truncating the Balitsky hierarchy in the context of the LL JIMWLK equation because it is a manifestly simpler setting than that of NLL order. Also one can check the validity and quality of the approximation by comparing it with the Langevin implementation of JIMWLK which is only available at LL order.

It is important to briefly mention the BK (Balitsky+Kovchegov) mean-field approximation, a well-known truncation, which produces the BK equation from the JIMWLK equation for the $q\bar{q}$ correlator. To this end, the JIMWLK equation for the $q\bar{q}$ correlator, given in Eq. 5.70, reads

$$\frac{d}{dY} \langle \frac{1}{d_f} \text{Tr} (U_x U_y^\dagger) \rangle(Y) = \frac{\alpha_s C_f}{\pi^2} \int_z \tilde{\mathcal{K}}_{xzy} \langle \frac{2}{d_A} \tilde{U}_z^{ab} \text{Tr} (t^a U_x t^b U_y^\dagger) - \frac{1}{d_f} \text{Tr} (U_x U_y^\dagger) \rangle(Y). \quad (6.6)$$

Using the Fierz identity, the term in Eq. 6.6 containing the adjoint Wilson-line can be rewritten as

$$2\tilde{U}_z^{ab} \text{Tr} (t^a U_x t^b U_y^\dagger) = \text{Tr} (U_x U_z^\dagger) \text{Tr} (U_z U_y^\dagger) - \frac{1}{d_f} \text{Tr} (U_x U_y^\dagger). \quad (6.7)$$

Consequently, Eq. 6.6 can be re-expressed as

$$\frac{d}{dY} \langle \mathcal{A}_{x;y}^{(1)} \rangle(Y) = \frac{\alpha_s}{2\pi^2} \int_z \tilde{\mathcal{K}}_{xzy} \langle \mathcal{A}_{x;z}^{(1)} \mathcal{A}_{z;y}^{(1)} - \mathcal{A}_{x;y}^{(1)} \rangle(Y), \quad (6.8)$$

where $\mathcal{A}_{x;y}^{(1)}$ is defined in Eq. 4.6 as

$$\mathcal{A}_{x;y}^{(1)} := \frac{1}{d_f} \text{Tr} \left(U_x U_y^\dagger \right). \quad (6.9)$$

The BK mean-field approximation assumes that the non-linearity on the right-hand-side of Eq. 6.8 factorizes [9] such that one may replace

$$\langle \mathcal{A}_{x;z}^{(1)} \mathcal{A}_{z;y}^{(1)} \rangle(Y) \rightarrow \langle \mathcal{A}_{x;z}^{(1)} \rangle(Y) \langle \mathcal{A}_{z;y}^{(1)} \rangle(Y). \quad (6.10)$$

Employing Eq. 6.10 in Eq. 6.8, one obtains a closed equation for the $q\bar{q}$ correlator

$$\frac{d}{dY} \langle \mathcal{A}_{x;y}^{(1)} \rangle(Y) = \frac{\alpha_s}{2\pi^2} \int_z \tilde{\mathcal{K}}_{xzy} \left[\langle \mathcal{A}_{x;z}^{(1)} \rangle(Y) \langle \mathcal{A}_{z;y}^{(1)} \rangle(Y) - \langle \mathcal{A}_{x;y}^{(1)} \rangle(Y) \right], \quad (6.11)$$

known as the BK equation. The BK equation is used extensively in high-energy QCD phenomenology. However, the BK mean-field approximation certainly has its limitations. For example, there exist a set of diffractive observables in DIS which depend on the difference [19]

$$\langle \mathcal{A}_{y'x'}^{(1)} \mathcal{A}_{xy}^{(1)} \rangle(Y) - \langle \mathcal{A}_{y'x'}^{(1)} \rangle(Y) \langle \mathcal{A}_{xy}^{(1)} \rangle(Y). \quad (6.12)$$

Applying Eq. 6.10 to Eq. 6.12 immediately sets the difference in Eq. 6.12 to zero. Since the BK mean-field approximation is insensitive to the differences of the form given in Eq. 6.12, there is clearly a need for a more sophisticated truncation.

The focus for the remainder of this chapter will be to systematically derive a particular truncation of the Balitsky hierarchy, which is more sophisticated than the BK mean-field approximation. We shall require that this truncation maintain as many of the known features of the exact solution as possible. One such feature is gauge-invariance. Gauge-invariance is a strong group-theoretic constraint on $\langle \mathcal{A} \rangle(Y)$ enforced as a consequence of constructing the underlying Wilson-line amplitude matrix \mathcal{A} in terms of overlaps between colour singlet states (invariants of $\text{SU}(N_c)$). A particular manifestation of gauge-invariance is coincidence-limits: as certain transverse coordinates on the Wilson-lines in \mathcal{A} become coincident, so certain entries in \mathcal{A} vanish which means that certain entries in $\langle \mathcal{A} \rangle(Y)$ vanish too. In the limit that all transverse coordinates become coincident, \mathcal{A} reduces to the overlap of basis colour singlet states. If these basis colour singlet states are orthonormal, then \mathcal{A} reduces to the identity matrix $\mathbb{1}$, and so does $\langle \mathcal{A} \rangle(Y)$ since the target average is normalized such that $\langle 1 \rangle(Y) = 1$. Thus, we require that our truncation at least preserve the coincidence limit properties of the underlying amplitude

matrix, and in this sense maintain gauge-invariance. This requirement is summarized in the commutative diagram in Fig. 6.1.

$$\begin{array}{ccc}
 \langle \mathcal{A} \rangle(Y) & \xrightarrow[\text{limit}]{\text{coincidence}} & \langle \mathcal{A}' \rangle(Y) \\
 \text{truncate} \downarrow & & \downarrow \text{truncate} \\
 \langle \mathcal{A} \rangle(Y)_{\text{trunc.}} & \xrightarrow[\text{limit}]{\text{coincidence}} & \langle \mathcal{A}' \rangle(Y)_{\text{trunc.}}
 \end{array}$$

FIGURE 6.1: The gauge-invariance property of a truncation.

Another feature of the exact solution that we wish to capture is the “symmetry” of $\langle \mathcal{A} \rangle(Y)$. In order to clarify what we mean by “symmetry”, let us decompose \mathcal{A} into a sum of its symmetric and anti-symmetric components

$$\mathcal{A} = \sum_{\alpha=\pm} \mathcal{A}_{(\alpha)}, \quad \mathcal{A}_{(\pm)} = \frac{1}{2}(\mathcal{A} \pm \mathcal{A}^t), \quad (6.13)$$

where $\mathcal{A}_{(+)}$ is the symmetric component of \mathcal{A} and $\mathcal{A}_{(-)}$ is the anti-symmetric component of \mathcal{A} . Since the target average is linear in its arguments and acts component-wise, the symmetric and anti-symmetric components of $\langle \mathcal{A} \rangle(Y)$ are given precisely by $\langle \mathcal{A}_{(+)} \rangle(Y)$ and $\langle \mathcal{A}_{(-)} \rangle(Y)$, respectively. Note that this is true for all Y . This decoupling of the (anti-)symmetric components of $\langle \mathcal{A} \rangle(Y)$ for all Y means that the JIMWLK equation must evolve (anti-)symmetric components of $\langle \mathcal{A} \rangle(Y)$ separately. Indeed this is the case. In the previous chapter we showed that Eq. 6.1 can be schematically rewritten as

$$\begin{aligned}
 \frac{d}{dY} \langle \mathcal{A} \rangle(Y) = & \frac{\alpha_s}{4\pi^2} \sum_{h=1}^2 \int_{\mathbf{z}} \left[\mathcal{P}_{\mathbf{z}}^{(1)h} \cdot \left\langle \begin{bmatrix} \mathcal{A} & 0 \\ 0 & \mathcal{A}_z^{(+g)} \end{bmatrix} \right\rangle(Y) \cdot (\mathcal{P}_{\mathbf{z}}^{(2)h})^t \right. \\
 & \left. + \mathcal{P}_{\mathbf{z}}^{(2)h} \cdot \left\langle \begin{bmatrix} \mathcal{A} & 0 \\ 0 & \mathcal{A}_z^{(+g)} \end{bmatrix} \right\rangle(Y) \cdot (\mathcal{P}_{\mathbf{z}}^{(1)h})^t \right], \quad (6.14)
 \end{aligned}$$

where $\langle \mathcal{A}_z^{(+g)} \rangle(Y)$ denotes the correlator matrix obtained by inserting an adjoint Wilson-line with transverse coordinate \mathbf{z} into $\langle \mathcal{A} \rangle(Y)$ in all possible ways, and $\mathcal{P}_{\mathbf{z}}^{(1)h}$ and $\mathcal{P}_{\mathbf{z}}^{(2)h}$ are real $m! \times (m+1)!$ matrices. Note that we have omitted all dependence on the transverse coordinates of $\langle \mathcal{A} \rangle(Y)$ in $\langle \mathcal{A}_z^{(+g)} \rangle(Y)$, $\mathcal{P}_{\mathbf{z}}^{(1)h}$ and $\mathcal{P}_{\mathbf{z}}^{(2)h}$ for the sake of brevity. Eq. 6.14 says that only the symmetric part of the larger correlator matrix contributes to the Y -evolution of the symmetric part of the original correlator matrix, and the same is true for the anti-symmetric parts. In this sense, the JIMWLK equation is said to preserve the “symmetry” of $\langle \mathcal{A} \rangle(Y)$ because its symmetric and anti-symmetric parts evolve independently under JIMWLK evolution.

Knowing the desired properties of our truncation, let us now systematically derive it. Suppose, in addition to being differentiable with respect to Y (which is already assumed in writing down

Eq. 6.1), that $\langle \mathcal{A} \rangle(Y)$ is invertible. The latter condition is automatically satisfied if the initial condition $\langle \mathcal{A} \rangle(Y_0)$ is invertible, because for colour singlet channels the JIMWLK Hamiltonian is infrared finite [17] which implies that the Y -evolution operator $\exp \left[-(Y - Y_0) H_{\text{JIMWLK}}^{(LL)} \right]$ in Eq. 6.4 is never vanishing. In this case, we may write

$$\begin{aligned}
\frac{d}{dY} \langle \mathcal{A} \rangle(Y) &= \sum_{\alpha=\pm} \frac{d}{dY} \langle \mathcal{A}_{(\alpha)} \rangle(Y) \\
&= \frac{1}{2} \sum_{\alpha=\pm} \left(\left[\left(\frac{d}{dY} \langle \mathcal{A}_{(\alpha)} \rangle(Y) \right) \langle \mathcal{A}_{(\alpha)} \rangle^{-1}(Y) \right] \langle \mathcal{A}_{(\alpha)} \rangle(Y) \right. \\
&\quad \left. + \langle \mathcal{A}_{(\alpha)} \rangle(Y) \left[\langle \mathcal{A}_{(\alpha)} \rangle^{-1}(Y) \left(\frac{d}{dY} \langle \mathcal{A}_{(\alpha)} \rangle(Y) \right) \right] \right) \\
&= -\frac{1}{2} \sum_{\alpha=\pm} \left[\mathcal{M}_{(\alpha)}(Y) \langle \mathcal{A}_{(\alpha)} \rangle(Y) + \langle \mathcal{A}_{(\alpha)} \rangle(Y) \mathcal{M}_{(\alpha)}^t(Y) \right], \tag{6.15}
\end{aligned}$$

where in the first equality we explicitly distinguished symmetric from anti-symmetric contributions to the derivative of $\langle \mathcal{A} \rangle(Y)$, in the second equality we split each of the derivative terms into a sum of two half contributions each multiplied by a clever “one”, and in the last line we defined the matrices

$$\mathcal{M}_{(\alpha)}(Y) := - \left(\frac{d}{dY} \langle \mathcal{A}_{(\alpha)} \rangle(Y) \right) \langle \mathcal{A}_{(\alpha)} \rangle^{-1}(Y), \tag{6.16}$$

for $\alpha = \pm$. In the last line of Eq. 6.15, we also anticipated that $\langle \mathcal{A}_{(\alpha)} \rangle^{-1}(Y) \left(\frac{d}{dY} \langle \mathcal{A}_{(\alpha)} \rangle(Y) \right)$ is indeed the transpose of $\mathcal{M}_{(\alpha)}(Y)$ as can be easily seen from

$$\begin{aligned}
\mathcal{M}_{(\alpha)}^t(Y) &= \left[- \left(\frac{d}{dY} \langle \mathcal{A}_{(\alpha)} \rangle(Y) \right) \langle \mathcal{A}_{(\alpha)} \rangle^{-1}(Y) \right]^t \\
&= - \left[\langle \mathcal{A}_{(\alpha)} \rangle^{-1}(Y) \right]^t \left(\frac{d}{dY} \langle \mathcal{A}_{(\alpha)} \rangle(Y) \right) \\
&= - \left[\alpha \langle \mathcal{A}_{(\alpha)} \rangle^{-1}(Y) \right] \left(\alpha \frac{d}{dY} \langle \mathcal{A}_{(\alpha)} \rangle(Y) \right) \\
&= - \langle \mathcal{A}_{(\alpha)} \rangle^{-1}(Y) \left(\frac{d}{dY} \langle \mathcal{A}_{(\alpha)} \rangle(Y) \right), \tag{6.17}
\end{aligned}$$

where we used Eq. 6.13 in order to conclude that

$$\frac{d}{dY} \langle \mathcal{A}_{(\alpha)}^t \rangle(Y) = \alpha \frac{d}{dY} \langle \mathcal{A}_{(\alpha)} \rangle(Y), \tag{6.18}$$

and

$$\left[\langle \mathcal{A}_{(\alpha)} \rangle^{-1}(Y) \right]^t = \left[\langle \mathcal{A}_{(\alpha)}^t \rangle(Y) \right]^{-1} = \left[\alpha \langle \mathcal{A}_{(\alpha)} \rangle(Y) \right]^{-1} = \alpha \langle \mathcal{A}_{(\alpha)} \rangle^{-1}(Y). \tag{6.19}$$

In what follows we shall refer to the matrix $\mathcal{M}_{(\alpha)}(Y)$ defined in Eq. 6.16 as *the exponentiating matrix associated with $\langle \mathcal{A}_{(\alpha)} \rangle(Y)$* . Given some initial condition $\langle \mathcal{A} \rangle(Y_0)$, Eq. 6.15 admits the

following formal solution

$$\langle \mathcal{A} \rangle(Y) = \sum_{\alpha=\pm} \langle \mathcal{A}_{(\alpha)} \rangle(Y) = \sum_{\alpha=\pm} \mathcal{E}_{(\alpha)}(Y, Y_0) \langle \mathcal{A}_{(\alpha)} \rangle(Y_0) \mathcal{E}_{(\alpha)}^t(Y, Y_0), \quad (6.20)$$

where the evolution operators $\mathcal{E}_{(\alpha)}(Y, Y_0)$ for $\alpha = \pm$ are given by

$$\mathcal{E}_{(\alpha)}(Y, Y_0) = P \exp \left[-\frac{1}{2} \int_{Y_0}^Y dY' \mathcal{M}_{(\alpha)}(Y') \right], \quad (6.21a)$$

$$\mathcal{E}_{(\alpha)}^t(Y, Y_0) = \bar{P} \exp \left[-\frac{1}{2} \int_{Y_0}^Y dY' \mathcal{M}_{(\alpha)}^t(Y') \right], \quad (6.21b)$$

with P being the path-ordering symbol in Y and \bar{P} the anti-path-ordering symbol. It is easy to see that Eq. 6.21b is the transpose of 6.21a by examining each term in the Dyson series expansions of both.

The first term in Eq. 6.20 is automatically symmetric, for all Y and regardless of the precise properties of $\mathcal{E}_{(+)}(Y, Y_0)$, and, similarly, the second term in Eq. 6.20 is automatically anti-symmetric. Therefore our parameterizing of the symmetric and anti-symmetric contributions of $\langle \mathcal{A} \rangle(Y)$ separately in Eq. 6.20 means that the formal solution manifestly shares the “symmetry” of the exact solution. Notice that among other differences between Eq. 6.4 and Eq. 6.20, the former writes $\langle \mathcal{A} \rangle(Y)$ as the evolution of $\langle \mathcal{A} \rangle(Y_0)$ with the evolution operator inside the target average while the latter has the evolution operators operating from outside the target average.

Certainly, if one knew the Y -dependence of the exponentiating matrices, then one would know the Y -dependence of $\langle \mathcal{A} \rangle(Y)$ through Eq. 6.20, but knowing the full Y -dependence of the exponentiating matrices is equivalent to solving the entire Balitsky hierarchy generated by Eq. 6.1. Instead, our aim will be to parameterize the Y -dependence of the exponentiating matrices in a manner that naturally permits a gauge-invariant truncation of the Balitsky hierarchy, a truncation which preserves the coincidence limits of the underlying amplitude matrix as imposed by the group theory of $SU(N_c)$.

In order for $\mathcal{M}_{(\alpha)}(Y)$ for $\alpha = \pm$ to correctly capture coincidence limit properties of $\langle \mathcal{A} \rangle(Y)$, $\mathcal{M}_{(\alpha)}(Y)$ needs to be a function of the transverse coordinates on the Wilson-lines present in $\langle \mathcal{A} \rangle(Y)$ in a manner that is “conscious” of these coincidence limits. Thus, it is natural to consider $\mathcal{M}_{(\alpha)}(Y)$ as being extracted from $\langle \mathcal{A} \rangle(Y)$ via some operator. Let us define the operators $\hat{L}_{(\alpha)}(Y)$ and $\hat{R}_{(\alpha)}(Y)$ through their actions on $\langle \mathcal{A} \rangle(Y)$ which are given by

$$\langle \hat{L}_{(\alpha)}(Y) \mathcal{A} \rangle(Y) := \mathcal{M}_{(\alpha)}(Y) \langle \mathcal{A} \rangle(Y), \quad (6.22a)$$

$$\langle \hat{R}_{(\alpha)}(Y) \mathcal{A} \rangle(Y) := \langle \mathcal{A} \rangle(Y) \mathcal{M}_{(\alpha)}^t(Y). \quad (6.22b)$$

The actions of these operators on $\langle \mathcal{A}^t \rangle(Y)$ are easily calculated from 6.22 (or the component version thereof) and are given by

$$\langle \hat{L}_{(\alpha)}(Y) \mathcal{A}^t \rangle(Y) := \langle \mathcal{A}^t \rangle(Y) \mathcal{M}_{(\alpha)}^t(Y), \quad (6.23a)$$

$$\langle \hat{R}_{(\alpha)}(Y) \mathcal{A}^t \rangle(Y) := \mathcal{M}_{(\alpha)}(Y) \langle \mathcal{A}^t \rangle(Y). \quad (6.23b)$$

From Eq. 6.22 and Eq. 6.23 we have that

$$\begin{aligned} \sum_{\alpha=\pm} \langle [\hat{L}_{(\alpha)}(Y) + \hat{R}_{(\alpha)}(Y)] \mathcal{A}_{(\alpha)} \rangle(Y) &= \frac{1}{2} \sum_{\alpha=\pm} \langle [\hat{L}_{(\alpha)}(Y) + \hat{R}_{(\alpha)}(Y)] [\mathcal{A} + \alpha \mathcal{A}^t] \rangle(Y) \\ &= \frac{1}{2} \sum_{\alpha=\pm} [\langle \hat{L}_{(\alpha)}(Y) \mathcal{A} \rangle(Y) + \alpha \langle \hat{L}_{(\alpha)}(Y) \mathcal{A}^t \rangle(Y) + \langle \hat{R}_{(\alpha)}(Y) \mathcal{A} \rangle(Y) + \alpha \langle \hat{R}_{(\alpha)}(Y) \mathcal{A}^t \rangle(Y)] \\ &= \frac{1}{2} \sum_{\alpha=\pm} [\mathcal{M}_{(\alpha)}(Y) \langle \mathcal{A} \rangle(Y) + \alpha \langle \mathcal{A}^t \rangle(Y) \mathcal{M}_{(\alpha)}^t(Y) \\ &\quad + \langle \mathcal{A} \rangle(Y) \mathcal{M}_{(\alpha)}^t(Y) + \alpha \mathcal{M}_{(\alpha)}(Y) \langle \mathcal{A}^t \rangle(Y)] \\ &= \sum_{\alpha=\pm} [\mathcal{M}_{(\alpha)}(Y) \frac{1}{2} \langle \mathcal{A} + \alpha \mathcal{A}^t \rangle(Y) + \frac{1}{2} \langle \mathcal{A} + \alpha \mathcal{A}^t \rangle(Y) \mathcal{M}_{(\alpha)}^t(Y)] \\ &= \sum_{\alpha=\pm} [\mathcal{M}_{(\alpha)}(Y) \langle \mathcal{A}_{(\alpha)} \rangle(Y) + \langle \mathcal{A}_{(\alpha)} \rangle(Y) \mathcal{M}_{(\alpha)}^t(Y)]. \end{aligned} \quad (6.24)$$

Comparing Eq. 6.24 with Eq. 6.15, we see that we can rewrite Eq. 6.15 in terms of the above operators through

$$\frac{d}{dY} \langle \mathcal{A} \rangle(Y) = -\frac{1}{2} \sum_{\alpha=\pm} \langle [\hat{L}_{(\alpha)}(Y) + \hat{R}_{(\alpha)}(Y)] \mathcal{A}_{(\alpha)} \rangle(Y). \quad (6.25)$$

It is worthwhile noting that although $\mathcal{M}_{(\alpha)}(Y)$ is the exponentiating matrix associated with $\langle \mathcal{A}_{(\alpha)} \rangle(Y)$, it is extracted from the full correlator matrix $\langle \mathcal{A} \rangle(Y)$ through Eq. 6.22a.

We now seek to write down the most general ansatz for $\hat{L}_{(\alpha)}(Y)$ and $\hat{R}_{(\alpha)}(Y)$. We shall focus on $\hat{L}_{(\alpha)}(Y)$, and then return briefly to $\hat{R}_{(\alpha)}(Y)$ at the end. The following parameterization of $\hat{L}_{(\alpha)}(Y)$ was originally conceived by [17], but the details have been explicitly work through here for the first time ever. The only operators available for extracting information about the transverse coordinates of Wilson-lines present in \mathcal{A} are the right- and left-invariant vector fields $i\bar{\nabla}_u^a$ and $i\nabla_u^a$, respectively. Recall that the action of $i\bar{\nabla}_u^a$ and $i\nabla_u^a$ on a tensor product of (anti-)fundamental Wilson-lines of the form given by Eq. 4.14 is represented in birdtrack notation by

$$i\bar{\nabla}_u^a \begin{array}{c} \text{---} \text{---} \text{---} \\ \text{---} \text{---} \text{---} \\ \vdots \\ \text{---} \text{---} \text{---} \end{array} = -\frac{1}{\sqrt{2}} \left[\delta_{ux_1}^{(2)} \begin{array}{c} \text{---} \text{---} \text{---} \\ \text{---} \text{---} \text{---} \\ \vdots \\ \text{---} \text{---} \text{---} \\ \text{---} \text{---} \end{array} + \dots + \delta_{ux_m}^{(2)} \begin{array}{c} \text{---} \text{---} \text{---} \\ \text{---} \text{---} \text{---} \\ \vdots \\ \text{---} \text{---} \text{---} \\ \text{---} \text{---} \end{array} - \delta_{uy_1}^{(2)} \begin{array}{c} \text{---} \text{---} \text{---} \\ \text{---} \text{---} \text{---} \\ \vdots \\ \text{---} \text{---} \text{---} \\ \text{---} \text{---} \end{array} - \dots - \delta_{uy_m}^{(2)} \begin{array}{c} \text{---} \text{---} \text{---} \\ \text{---} \text{---} \text{---} \\ \vdots \\ \text{---} \text{---} \text{---} \\ \text{---} \text{---} \end{array} \right] \begin{array}{c} \text{---} \text{---} \text{---} \\ \text{---} \text{---} \text{---} \\ \vdots \\ \text{---} \text{---} \text{---} \end{array} =: -\frac{1}{\sqrt{2}} \begin{array}{c} \text{---} \text{---} \text{---} \\ \text{---} \text{---} \text{---} \\ \vdots \\ \text{---} \text{---} \text{---} \\ \text{---} \text{---} \end{array}, \quad (6.26a)$$

$$i\nabla_u^a = \frac{1}{\sqrt{2}} \left[\delta_{ux_1}^{(2)} + \dots + \delta_{ux_m}^{(2)} - \delta_{uy_1}^{(2)} - \dots - \delta_{uy_m}^{(2)} \right] =: \frac{1}{\sqrt{2}} \quad (6.26b)$$

Notice, in particular, that in Eq. 6.26a the generators are inserted to the left of the diagram representing the tensor product of (anti-)fundamental Wilson-lines, while in Eq. 6.26b they are inserted to the right. As we shall show, in order to parameterize $\hat{L}_{(\alpha)}(Y)$ such that its action on \mathcal{A} produces a matrix multiplying \mathcal{A} from the left, the most general ansatz is an expansion in “powers” of the right-invariant vector fields. But before we show this, we need to introduce a few more ingredients.

Take¹ $n \in \mathbb{N}^+ \geq 2$. Let $\mathcal{C}^{(n;s)a_1 \dots a_n} \in \mathfrak{C}(A^{\otimes n})$ be some colour structure and $G_{(\alpha)u_1 \dots u_n}^{(n;s)}(Y)$ be some yet-to-be determined function of n transverse coordinates as well as a function of Y which we shall refer to as the colour structure function associated with the colour structure $\mathcal{C}^{(n;s)a_1 \dots a_n}$. This colour structure function is a Y -dependent n -point function. Using these objects, consider the following operator²

$$\hat{L}_{(\alpha)}^{(n;s)}(Y) := \int_{u_1 \dots u_n} G_{(\alpha)u_1 \dots u_n}^{(n;s)}(Y) \mathcal{C}^{(n;s)a_1 \dots a_n} (-1)^n i\bar{\nabla}_{u_1}^{a_1} \dots i\bar{\nabla}_{u_n}^{a_n}, \quad (6.27)$$

which is only a function of Y . Let us examine the action of Eq. 6.27 on the $q^m \bar{q}^m$ amplitude matrix $\mathcal{A}_{\vec{x};\vec{y}}^{(m)}$ (where $m \in \mathbb{N}^+$) whose i^{th} row and j^{th} column (in some orthonormal basis of colour singlet states) is given by

$$[\mathcal{A}_{\vec{x};\vec{y}}^{(m)}]_{ij} = \text{Diagram} \quad (6.28)$$

The action of n right-invariant vector fields (as in Eq. 6.27) on $[\mathcal{A}_{\vec{x};\vec{y}}^{(m)}]_{ij}$ is easily calculated using Eq. 6.26a to be

$$(-1)^n i\bar{\nabla}_{u_1}^{a_1} \dots i\bar{\nabla}_{u_n}^{a_n} \text{Diagram} = \frac{1}{\sqrt{2}^n} \text{Diagram} \quad (6.29)$$

In order to further simplify Eq. 6.29, note that

$$\tilde{U}^{ab}[U]_{i_2}^{i_1} [t^b]_{j_2}^{i_2} [U^\dagger]_{j_1}^{j_2} = [t^a]_{j_1}^{i_1}, \quad (6.30)$$

¹We exclude the case where $n = 1$ since $\mathfrak{C}(A^{\otimes(n=1)}) = \mathfrak{C}(A) = \{0\}$ is trivial.

²The factor of $(-1)^n$ is included explicitly so as to cancel the factor of $(-1)^n$ produced by the n -fold product of right-invariant vector fields acting on $[\mathcal{A}_{\vec{x};\vec{y}}^{(m)}]_{ij}$ in Eq. 6.29.

which follows from the Fierz identity and which is equivalent to

$$\tilde{U}^{ab}[U]_{i_2}^{i_1}[t^b]_{j_1}^{i_2} = [t^a]_{j_2}^{i_1}[U]_{j_1}^{j_2}, \quad \tilde{U}^{ab} \begin{array}{c} \leftarrow \\ \leftarrow \\ \vdots \\ \leftarrow \end{array} \begin{array}{c} \leftarrow \\ \leftarrow \\ \vdots \\ \leftarrow \end{array} = \begin{array}{c} \leftarrow \\ \leftarrow \\ \vdots \\ \leftarrow \end{array} \begin{array}{c} \leftarrow \\ \leftarrow \\ \vdots \\ \leftarrow \end{array}, \quad (6.31a)$$

$$\tilde{U}^{ab}[t^b]_{j_2}^{i_1}[U^\dagger]_{j_1}^{i_2} = [U^\dagger]_{i_2}^{i_1}[t^a]_{j_1}^{i_2}, \quad \tilde{U}^{ab} \begin{array}{c} \rightarrow \\ \rightarrow \\ \vdots \\ \rightarrow \end{array} \begin{array}{c} \rightarrow \\ \rightarrow \\ \vdots \\ \rightarrow \end{array} = \begin{array}{c} \rightarrow \\ \rightarrow \\ \vdots \\ \rightarrow \end{array} \begin{array}{c} \rightarrow \\ \rightarrow \\ \vdots \\ \rightarrow \end{array}. \quad (6.31b)$$

From Eq. 6.31 one has that

$$\begin{array}{c} \text{Diagram with } i \text{ and } a_n, u_n \text{ lines} \end{array} \dots \begin{array}{c} \text{Diagram with } a_1, u_1 \text{ lines} \end{array} = \tilde{U}^{a_1 b_1} \dots \tilde{U}^{a_n b_n} \begin{array}{c} \text{Diagram with } i \text{ and } b_n, u_n \text{ lines} \end{array} \dots \begin{array}{c} \text{Diagram with } b_1, u_1 \text{ lines} \end{array} = \tilde{U}^{a_1 b_1} \dots \tilde{U}^{a_n b_n} \begin{array}{c} \text{Diagram with } i \text{ and } b_n, u_n \text{ lines} \end{array} \dots \begin{array}{c} \text{Diagram with } b_1, u_1 \text{ lines} \end{array}, \quad (6.32)$$

where in the last equality we used Eq. 4.17. Eq. 6.32 proves that

$$\begin{array}{c} \text{Diagram with } i \text{ and } a_n, u_n \text{ lines} \end{array} \dots \begin{array}{c} \text{Diagram with } a_1, u_1 \text{ lines} \end{array}, \quad (6.33)$$

is not a colour singlet state. However, if one contracted the adjoint indices of the generators in Eq. 6.33 into a colour structure $\mathcal{C}^{(n;s)a_1 \dots a_n} \in \mathfrak{C}(A^{\otimes n})$ (which is a colour singlet state of $A^{\otimes n}$), then

$$\mathcal{C}^{(n;s)a_1 \dots a_n} \begin{array}{c} \text{Diagram with } i \text{ and } a_n, u_n \text{ lines} \end{array} \dots \begin{array}{c} \text{Diagram with } a_1, u_1 \text{ lines} \end{array}, \quad (6.34)$$

is a colour singlet state since

$$\mathcal{C}^{(n;s)a_1 \dots a_n} \begin{array}{c} \text{Diagram with } i \text{ and } a_n, u_n \text{ lines} \end{array} \dots \begin{array}{c} \text{Diagram with } a_1, u_1 \text{ lines} \end{array} = \mathcal{C}^{(n;s)a_1 \dots a_n} \tilde{U}^{a_1 b_1} \dots \tilde{U}^{a_n b_n} \begin{array}{c} \text{Diagram with } i \text{ and } b_n, u_n \text{ lines} \end{array} \dots \begin{array}{c} \text{Diagram with } b_1, u_1 \text{ lines} \end{array} = \mathcal{C}^{(n;s)a_1 \dots a_n} \begin{array}{c} \text{Diagram with } i \text{ and } a_n, u_n \text{ lines} \end{array} \dots \begin{array}{c} \text{Diagram with } a_1, u_1 \text{ lines} \end{array}, \quad (6.35)$$

where in going to the last line we used

$$\mathcal{C}^{(n;s)a_1 \dots a_n} \tilde{U}^{a_1 b_1} \dots \tilde{U}^{a_n b_n} = \mathcal{C}^{(n;s)b_1 \dots b_n}. \quad (6.36)$$

Since Eq. 6.34 is a colour singlet state, we can write it in terms of the same basis of colour singlet states used to construct the amplitude matrix as follows

$$\mathcal{C}^{(n;s)a_1 \dots a_n} \begin{array}{c} \text{Diagram with } i \text{ and } a_n, u_n \text{ lines} \end{array} \dots \begin{array}{c} \text{Diagram with } a_1, u_1 \text{ lines} \end{array} = \sum_l \mathcal{C}^{(n;s)a_1 \dots a_n} \begin{array}{c} \text{Diagram with } i \text{ and } a_n, u_n \text{ lines} \end{array} \dots \begin{array}{c} \text{Diagram with } l \text{ and } a_1, u_1 \text{ lines} \end{array} \begin{array}{c} \text{Diagram with } l \text{ and } a_1, u_1 \text{ lines} \end{array}. \quad (6.37)$$

Finally, we can write the action of Eq. 6.27 on \mathcal{A}_{ij} as

$$\begin{aligned}
\hat{L}_{(\alpha)}^{(n;s)}(Y)[\mathcal{A}_{\vec{x};\vec{y}}^{(m)}]_{ij} &= \int_{\mathbf{u}_1 \dots \mathbf{u}_n} G_{(\alpha)\mathbf{u}_1 \dots \mathbf{u}_n}^{(n;s)}(Y) \mathcal{C}^{(n;s)a_1 \dots a_n} (-1)^n i \bar{\nabla}_{\mathbf{u}_1}^{a_1} \dots i \bar{\nabla}_{\mathbf{u}_n}^{a_n} \text{Diagram} \\
&= \sum_l \frac{1}{\sqrt{2^n}} \int_{\mathbf{u}_1 \dots \mathbf{u}_n} G_{(\alpha)\mathbf{u}_1 \dots \mathbf{u}_n}^{(n;s)}(Y) \mathcal{C}^{(n;s)a_1 \dots a_n} \text{Diagram} \\
&= \sum_l [\mathcal{M}_{(\alpha)}^{(n;s)}(Y)]_{il} [\mathcal{A}_{\vec{x};\vec{y}}^{(m)}]_{lj},
\end{aligned} \tag{6.38}$$

where in the second line we used Eq. 6.29 and Eq. 6.37 and in the last line we defined the matrix $\mathcal{M}_{(\alpha)}^{(n;s)}(Y)$ which has components

$$[\mathcal{M}_{(\alpha)}^{(n;s)}(Y)]_{ij} := \frac{1}{\sqrt{2^n}} \int_{\mathbf{u}_1 \dots \mathbf{u}_n} G_{(\alpha)\mathbf{u}_1 \dots \mathbf{u}_n}^{(n;s)}(Y) \mathcal{C}^{(n;s)a_1 \dots a_n} \text{Diagram} . \tag{6.39}$$

As a matrix equation, Eq. 6.38 reads

$$\langle \hat{L}_{(\alpha)}^{(n;s)}(Y) \mathcal{A}_{\vec{x};\vec{y}}^{(m)} \rangle(Y) = \mathcal{M}_{(\alpha)}^{(n;s)}(Y) \langle \mathcal{A}_{\vec{x};\vec{y}}^{(m)} \rangle(Y), \tag{6.40}$$

which is precisely of the form given in Eq. 6.22a. Since Eq. 6.40 is true for any $n \in \mathbb{N}^+ \geq 2$ and any colour structure $\mathcal{C}^{(n;s)a_1 \dots a_n} \in \mathfrak{C}(A^{\otimes n})$, the most general ansatz for $\hat{L}_i(Y)$ is the linear combination

$$\hat{L}_{(\alpha)}(Y) = \sum_{n=2}^{\infty} \hat{L}_{(\alpha)}^{(n)}(Y) = \sum_{n=2}^{\infty} \sum_k \hat{L}_{(\alpha)}^{(n;k)}(Y), \tag{6.41}$$

where $\hat{L}_{(\alpha)}^{(n;k)}(Y)$ is given by Eq. 6.27, the sum over k is over all colour structures in some orthonormal basis $\mathfrak{B}_{\text{ON}}(A^{\otimes n}) = \{\mathcal{C}^{(n;k)}\}_k$ for the colour space of $A^{\otimes n}$ where $\mathcal{C}^{(n;k)a_1 \dots a_n}$ is the k^{th} basis colour structure, and the sum over n starts at 2 because for $n = 0, 1$ the colour space of $A^{\otimes n}$ is trivial (contains only the zero vector). Correspondingly, the most general parameterization for $\mathcal{M}_i(Y)$ (which is strictly defined through Eq. 6.16) is given by

$$\mathcal{M}_{(\alpha)}(Y) = \sum_{n=2}^{\infty} \mathcal{M}_{(\alpha)}^{(n)}(Y) = \sum_{n=2}^{\infty} \sum_k \mathcal{M}_{(\alpha)}^{(n;k)}(Y), \tag{6.42}$$

where $\mathcal{M}_{(\alpha)}^{(n;k)}(Y)$ is given by Eq. 6.38. We call $\mathcal{M}_{(\alpha)}^{(n;k)}(Y)$ the n^{th} order contribution to the exponentiating matrix associated with $\langle \mathcal{A}_{(\alpha)} \rangle(Y)$ from the k^{th} colour structure $\mathcal{C}^{(n;k)a_1 \dots a_n} \in \mathfrak{B}_{\text{ON}}(A^{\otimes n})$. Although the sum only starts at $n = 2$, we shall refer to this as the second order (even though, strictly speaking, it is the lowest order).

Eq. 6.41 contains, amongst other things, a sum over colour structure functions. These colour structure functions are analogous to the structure functions introduced in Sec. 2.1 in the sense that in that context, the less inclusive an observable was, the greater the number of structure functions was needed in order to parameterize the dependence of the hadronic tensor on the Lorentz invariants x_{bj} and Q^2 . Likewise here, the understanding is that the greater the number of fundamental and anti-fundamental Wilson-lines entering a correlator matrix, the greater the number of colour structures required to parameterize its Y -dependence. This analogy certainly holds for the dipole operator [32] as we shall elaborate on shortly.

Truncating the sum over n in Eq. 6.41 and in Eq. 6.42 after $p \in \mathbb{N}^+ \geq 2$ terms produces the so-called p -point truncation. To date, only the properties of the 2-point truncation (also known as the Gaussian truncation) as well as a particular anti-symmetric coincidence limit contribution (the so-called parity-odd Odderon contribution) from the 3-point truncation have been explored in the literature [19, 32]. However, to our knowledge there has been no progress made in understanding any of the all-orders structure of this exponential parameterization. One of the major results of this thesis is an understanding of some of this all-orders structure.

Returning to our earlier discussion of the $q\bar{q}$ correlator, note that it can be viewed as a complex function of the form $\mathcal{A}_{\cdot,\cdot}^{(1)} : \mathbb{R}^2 \times \mathbb{R}^2 \rightarrow \mathbb{C}; (\mathbf{x}, \mathbf{y}) \mapsto \mathcal{A}_{\mathbf{x};\mathbf{y}}^{(1)}$. It was found that both the real and the imaginary parts of the $q\bar{q}$ correlator could be parameterized at third order in the truncation [32]. However, to parameterize the real part of the dipole operator it is sufficient to consider only the Gaussian truncation. This is the motivation behind the analogy between structure functions and colour structure functions mentioned earlier: for a cross-section such as that of deep inelastic scattering which depends only on the real part of the dipole operator, one can make do with the (lowest-order) Gaussian truncation, but for observables such as Single Transverse Spin Asymmetry which triggers both real and imaginary parts of the dipole operator, one needs to go beyond the Gaussian to the (next-lowest) 3-point truncation in order to faithfully parameterize evolution.

Having systematically constructed $\hat{L}_{(\alpha)}(Y)$, we now give $\hat{R}_{(\alpha)}(Y)$ and show that it satisfies Eq. 6.22b. The most general ansatz for $\hat{R}_{(\alpha)}$ is given by

$$\hat{R}_{(\alpha)}(Y) = \sum_{n=2}^{\infty} \hat{R}_{(\alpha)}^{(n)}(Y) = \sum_{n=2}^{\infty} \sum_k \hat{R}_{(\alpha)}^{(n;k)}(Y), \quad (6.43)$$

where

$$\hat{R}_{(\alpha)}^{(n;k)}(Y) = \int_{\mathbf{u}_1 \dots \mathbf{u}_n} G_{(\alpha)\mathbf{u}_1 \dots \mathbf{u}_n}^{(n;k)}(Y) \left(\mathcal{C}^{(n;k)a_1 \dots a_n} \right)^* i \nabla_{\mathbf{u}_1}^{a_1} \dots i \nabla_{\mathbf{u}_n}^{a_n}. \quad (6.44)$$

The action of $\hat{R}_{(\alpha)}(Y)$ of $[\mathcal{A}_{\vec{x};\vec{y}}^{(m)}]_{ij}$ is calculated as

$$\begin{aligned}
& \hat{R}_{(\alpha)}(Y)[\mathcal{A}_{\vec{x};\vec{y}}^{(m)}]_{ij} \\
&= \sum_{n=2}^{\infty} \sum_k \int_{\mathbf{u}_1 \dots \mathbf{u}_n} G_{(\alpha)\mathbf{u}_1 \dots \mathbf{u}_n}^{(n;k)}(Y) \left(\mathcal{C}^{(n;k)}_{a_1 \dots a_n} \right)^* i \nabla_{\mathbf{u}_1}^{a_1} \dots i \nabla_{\mathbf{u}_n}^{a_n} \text{Diagram} \\
&= \sum_{n=2}^{\infty} \sum_k \frac{1}{\sqrt{2^n}} \int_{\mathbf{u}_1 \dots \mathbf{u}_n} G_{(\alpha)\mathbf{u}_1 \dots \mathbf{u}_n}^{(n;k)} Y \left(\mathcal{C}^{(n;k)}_{a_1 \dots a_n} \right)^* \text{Diagram} \\
&= \sum_l \text{Diagram} \sum_{n=2}^{\infty} \sum_k \frac{1}{\sqrt{2^n}} \int_{\mathbf{u}_1 \dots \mathbf{u}_n} G_{(\alpha)\mathbf{u}_1 \dots \mathbf{u}_n}^{(n;k)}(Y) \left(\mathcal{C}^{(n;k)}_{a_1 \dots a_n} \right)^* \text{Diagram} \\
&= \sum_l [\mathcal{A}_{\vec{x};\vec{y}}^{(m)}]_{il} [(\mathcal{M}_{(\alpha)}(Y))^t]_{lj}, \tag{6.45}
\end{aligned}$$

where

$$(\mathcal{M}_{(\alpha)}(Y))^t = \sum_{n=2}^{\infty} (\mathcal{M}_{(\alpha)}^{(n)}(Y))^t = \sum_{n=2}^{\infty} \sum_k (\mathcal{M}_{(\alpha)}^{(n;k)}(Y))^t, \tag{6.46}$$

and

$$[(\mathcal{M}_{(\alpha)}^{(n;k)}(Y))^t]_{ij} = \frac{1}{\sqrt{2^n}} \int_{\mathbf{u}_1 \dots \mathbf{u}_n} G_{(\alpha)\mathbf{u}_1 \dots \mathbf{u}_n}^{(n;k)}(Y) \left(\mathcal{C}^{(n;k)}_{a_1 \dots a_n} \right)^* \text{Diagram}. \tag{6.47}$$

To see that $(\mathcal{M}_{(\alpha)}^{(n;k)}(Y))^t$ as defined in Eq. 6.47 really is the transpose of $\mathcal{M}_{(\alpha)}^{(n;k)}(Y)$ examine

$$\begin{aligned}
& [(\mathcal{M}_{(\alpha)}^{(n;k)}(Y))^t]_{ij} = \frac{1}{\sqrt{2^n}} \int_{\mathbf{u}_1 \dots \mathbf{u}_n} G_{(\alpha)\mathbf{u}_1 \dots \mathbf{u}_n}^{(n;k)}(Y) \left(\mathcal{C}^{(n;k)}_{a_1 \dots a_n} \right)^* \text{Diagram} \\
&= \frac{1}{\sqrt{2^n}} \int_{\mathbf{u}_1 \dots \mathbf{u}_n} G_{(\alpha)\mathbf{u}_1 \dots \mathbf{u}_n}^{(n;k)}(Y) \left(\mathcal{C}^{(n;k)}_{a_1 \dots a_n} \right)^* \text{Diagram} \\
&= \frac{1}{\sqrt{2^n}} \int_{\mathbf{u}_1 \dots \mathbf{u}_n} G_{(\alpha)\mathbf{u}_1 \dots \mathbf{u}_n}^{(n;k)}(Y) \mathcal{C}^{(n;k)}_{a_1 \dots a_n} \text{Diagram} = [\mathcal{M}_{(\alpha)}^{(n;k)}(Y)]_{ji}, \tag{6.48}
\end{aligned}$$

where in the second line we flipped the entire birdtracks diagram (which does not change anything), in the third line we used Lemma 4.1 to reverse the arrows on each sum-over-generators

insertion at the cost of complex conjugating the already complex conjugated colour structure, and in the last line we identified the expression with Eq. 6.42. Thus, we have confirmed that the operator $\hat{R}_i(Y)$ given in Eq. 6.43 satisfies Eq. 6.22b.

Let us conclude this section by introducing the following notation for the p -point truncation of $\langle \mathcal{A} \rangle(Y)$ given some initial condition $\langle \mathcal{A} \rangle(Y_0)$. We write the p -truncation as

$$\langle \mathcal{A} \rangle_p(Y) := \sum_{\alpha=\pm} \langle \mathcal{A}_{(\alpha)} \rangle_p(Y) = \sum_{\alpha=\pm} \mathcal{E}_{(\alpha)}^{[p]}(Y, Y_0) \langle \mathcal{A}_{(\alpha)} \rangle(Y_0) \mathcal{E}_{(\alpha)}^{[p]^\dagger}(Y, Y_0) \quad (6.49)$$

where

$$\mathcal{E}_{(\alpha)}^{[p]}(Y, Y_0) := P \exp \left[-\frac{1}{2} \int_{Y_0}^Y dY' \mathcal{M}_{(\alpha)}^{[p]}(Y') \right], \quad (6.50)$$

and

$$\mathcal{M}_{(\alpha)}^{[p]}(Y) := \sum_{n=2}^p \mathcal{M}_{(\alpha)}^{(n)}(Y). \quad (6.51)$$

6.2 Imprinting symmetries of Young colour structures onto Young colour structure functions

The appeal of the Young colour structures introduced in Sec. 4.2.3 is that they possess definite symmetry properties; they are simultaneous eigenstates of Hermitian Young projection operators. In this section I discuss how the symmetry properties of the Young colour structures imprint themselves onto the associated Young colour structure functions; that is I discuss how, for a given Young colour structure $\mathcal{C}^{(n;I;i,m_i)_{a_1 \dots a_n}} \in \mathfrak{B}_{\text{Young}}(A^{\otimes n})$, the symmetry features of $\mathcal{C}^{(n;I;i,m_i)_{a_1 \dots a_n}}$ imprint themselves onto the associated Young colour structure function $G_{(\alpha)u_1 \dots u_n}^{(n;I;i;m_i)}(Y)$ in

$$\hat{L}_{(\alpha)}^{(n;I;i;m_i)}(Y) := \int_{u_1 \dots u_n} G_{(\alpha)u_1 \dots u_n}^{(n;I;i;m_i)}(Y) \alpha_{n;I;i;m_i} \mathcal{C}^{(n;I;i;m_i)_{a_1 \dots a_n}} (-1)^n i \bar{\nabla}_{u_1}^{a_1} \dots i \bar{\nabla}_{u_n}^{a_n}. \quad (6.52)$$

The constant $\alpha_{n;I;i;m_i} \in \mathbb{R} \neq 0$ in Eq. 6.52 is introduced for convenience. The idea for this discussion was originally conceived by [17], but the details have been explicitly work through here for the first time ever.

Throughout this section we shall adopt the notation of Sec. 4.2.3.

Let us warm up by considering the simplest possible example, the case when $n = 2$. The only normalized colour structure in $A^{\otimes 2}$ is

$$\mathcal{C}^{(2;1;1;1)a_1a_2} = \frac{1}{\sqrt{d_A}} \delta^{a_1a_2}, \quad (6.53)$$

which is a simultaneous eigenstate of the total symmetrizer in $\mathbb{R}[S_2]$

$$[\mathfrak{M}_1^{(2)}]_{11} = \text{---} \text{---} = \frac{1}{2} \sum_{\sigma \in S_2} \sigma = \frac{1}{2} [\text{---} + \times], \quad (6.54a)$$

and the total anti-symmetrizer in $\mathbb{R}[S_2]$

$$[\mathfrak{M}_2^{(2)}]_{11} = \text{---} \text{---} = \frac{1}{2} \sum_{\sigma \in S_2} \text{sign}(\sigma) \sigma = \frac{1}{2} [\text{---} - \times], \quad (6.54b)$$

with eigenvalues 1 and 0, respectively; i.e.

$$[\mathfrak{M}_1^{(2)}]_{11} \circ \mathcal{C}^{(2;1;1;1)a_1a_2} = \mathcal{C}^{(2;1;1;1)a_1a_2}, \quad [\mathfrak{M}_2^{(2)}]_{11} \circ \mathcal{C}^{(2;1;1;1)a_1a_2} = 0. \quad (6.55)$$

Taking $\alpha_{2;1;1;1} = \sqrt{d_A}$ for convenience, our task is to examine in detail how the total symmetry of $\delta^{a_1a_2}$ in its adjoint indices imprints itself onto $G_{(\alpha)u_1u_2}^{(2;1;1;1)}(Y)$ in

$$\hat{L}_{(\alpha)}^{(2;1;1;1)}(Y) = \int_{u_1u_2} G_{(\alpha)u_1u_2}^{(2;1;1;1)}(Y) \delta^{a_1a_2} (-1)^2 i \bar{\nabla}_{u_1}^{a_1} i \bar{\nabla}_{u_2}^{a_2}. \quad (6.56)$$

We shall perform our analysis in four steps. Although these steps (or certain aspects thereof) may seem unnecessarily complicated for the simple example being considered, we shall later see that for the general case these steps help to clarify what is being done.

- **Step 1:** *Symmetrize over all integration variables/transverse coordinates.*

Since the integration measure $d^2u_1 d^2u_2$ in Eq. 6.56 is totally symmetric (i.e. the order of integration is irrelevant) we may symmetrize over all integration variables/transverse coordinates without affecting the result of the integral. Performing this symmetrization yields

$$(6.56) = \int_{u_1u_2} \frac{1}{2!} \sum_{\sigma \in S_2} G_{(\alpha)u_{\sigma(1)}u_{\sigma(2)}}^{(2;1;1;1)}(Y) \delta^{a_1a_2} (-1)^2 i \bar{\nabla}_{u_{\sigma(1)}}^{a_1} i \bar{\nabla}_{u_{\sigma(2)}}^{a_2}. \quad (6.57)$$

Notice that the integration measure is left invariant by the symmetrization.

- **Step 2:** *Re-arrange the derivatives such that the transverse coordinates on the derivatives appear in the original ascending order.*

Using the commutation relation

$$[i\bar{\nabla}_{u_1}^{a_1}, i\bar{\nabla}_{u_2}^{a_2}] = \delta_{u_1 u_2}^{(2)} i f^{a_1 a_2 b} i\bar{\nabla}_{u_1}^b, \quad (6.58)$$

we may write

$$\bar{\nabla}_{u_{\sigma(1)}}^{a_1} i\bar{\nabla}_{u_{\sigma(2)}}^{a_2} = \begin{cases} \bar{\nabla}_{u_1}^{a_1} i\bar{\nabla}_{u_2}^{a_2}, & \text{if } \sigma = \text{---}, \\ \bar{\nabla}_{u_1}^{a_2} i\bar{\nabla}_{u_2}^{a_1} + \delta_{u_1 u_2}^{(2)} i f^{a_1 a_2 b} i\bar{\nabla}_{u_1}^b, & \text{if } \sigma = \times, \end{cases} \quad (6.59)$$

Having foreknowledge of the general case which we shall analyze next, we shall choose to write Eq. 6.59 as

$$\bar{\nabla}_{u_{\sigma(1)}}^{a_1} i\bar{\nabla}_{u_{\sigma(2)}}^{a_2} = \bar{\nabla}_{u_1}^{a_{\sigma^{-1}(1)}} i\bar{\nabla}_{u_2}^{a_{\sigma^{-1}(2)}} + \Theta_{-}(\text{ord}(\sigma) - 1) \delta_{u_1 u_2}^{(2)} i f^{a_1 a_2 b} i\bar{\nabla}_{u_1}^b, \quad (6.60)$$

where $\text{ord}(\sigma)$ is the order³ of the permutation σ ($\text{ord}(\text{---}) = 1$ and $\text{ord}(\times) = 2$) and $\Theta_{-}(x)$ denotes the right-continuous definition for the Heaviside function

$$\Theta_{-}(x) := \begin{cases} 0 & \text{if } x \leq 1, \\ 1 & \text{if } 0 < x, \end{cases} \quad (6.61)$$

Substituting Eq. 6.60 into Eq. 6.57 one obtains

$$\begin{aligned} (6.57) &= \int_{u_1 u_2} \frac{1}{2!} \sum_{\sigma \in S_2} G_{(\alpha)u_{\sigma(1)}u_{\sigma(2)}}^{(2;1;1;1)}(Y) \delta^{a_1 a_2}(-1)^2 i\bar{\nabla}_{u_1}^{a_{\sigma^{-1}(1)}} i\bar{\nabla}_{u_2}^{a_{\sigma^{-1}(2)}} \\ &\quad + \text{commutator terms}, \end{aligned} \quad (6.62)$$

where

$$\text{commutator terms} = \int_{u_1 u_2} \frac{1}{2!} G_{(\alpha)u_2 u_1}^{(2;1;1;1)}(Y) \delta_{u_1 u_2}^{(2)} \underbrace{\delta^{a_1 a_2} i f^{a_1 a_2 b}}_{=0} i\bar{\nabla}_{u_1}^b = 0. \quad (6.63)$$

Lastly, by relabeling dummy adjoint indices in Eq. 6.62, we can write

$$(6.57) = \int_{u_1 u_2} \frac{1}{2!} \sum_{\sigma \in S_2} G_{(\alpha)u_{\sigma(1)}u_{\sigma(2)}}^{(2;1;1;1)}(Y) \delta^{a_{\sigma(1)} a_{\sigma(2)}}(-1)^2 i\bar{\nabla}_{u_1}^{a_1} i\bar{\nabla}_{u_2}^{a_2}, \quad (6.64)$$

having already observed that the commutator terms in Eq. 6.62 vanish.

- **Step 3:** Ignore commutator terms and re-express the Young colour structure whose adjoint indices are not (necessarily) in the original ascending order in terms of all available Young colour structures whose adjoint indices are in the original ascending order.

³The smallest $n \in \mathbb{N}^+$ such that $\sigma^n = id$.

Note that the Young colour structure $\delta^{a_1 a_2}$ is totally symmetric with respect to the order of its adjoint indices. Consequently $\delta^{a_{\sigma(1)} a_{\sigma(2)}} = \delta^{a_1 a_2}$ for any $\sigma \in S_2$ and Eq. 6.64 becomes

$$\begin{aligned} (6.64) &= \int_{\mathbf{u}_1 \mathbf{u}_2} \frac{1}{2!} \sum_{\sigma \in S_2} G_{(\alpha) \mathbf{u}_{\sigma(1)} \mathbf{u}_{\sigma(2)}}^{(2;1;1;1)}(Y) \delta^{a_1 a_2} (-1)^2 i \bar{\nabla}_{\mathbf{u}_1}^{a_1} i \bar{\nabla}_{\mathbf{u}_2}^{a_2} \\ &= \int_{\mathbf{u}_1 \mathbf{u}_2} \left([\mathfrak{M}_1^{(2)}]_{11} \circ G_{(\alpha) \mathbf{u}_1 \mathbf{u}_2}^{(2;1;1;1)}(Y) \right) \delta^{a_1 a_2} (-1)^2 i \bar{\nabla}_{\mathbf{u}_1}^{a_1} i \bar{\nabla}_{\mathbf{u}_2}^{a_2}, \end{aligned} \quad (6.65)$$

where the composition \circ used in Eq. 6.65 is defined in Eq. 6.67.

- **Step 4:** *With the Young colour structure(s) and the derivatives as they were originally, compare the result of the above procedure with the original expression and read off the symmetry features of the associated Young colour structure function(s).*

Notice that only the totally symmetric part of $G_{(\alpha) \mathbf{u}_1 \mathbf{u}_2}^{(2;1;1;1)}(Y)$ is probed in Eq. 6.65 which means that we can just as well take $G_{(\alpha) \mathbf{u}_1 \mathbf{u}_2}^{(2;1;1;1)}(Y)$ to be *totally symmetric in its transverse coordinates*.

Having illustrated the above procedure with through a concrete example, we can now turn our attention to the general case.

- **Step 1:** *Symmetrize over all integration variables/transverse coordinates.*

Since the integration measure in Eq. 6.52 is totally symmetric, we may symmetrize the transverse coordinate dependence of the integrand without changing the value of the integral, producing

$$\begin{aligned} (6.52) &= \int_{\mathbf{u}_1 \dots \mathbf{u}_n} \frac{1}{n!} \sum_{\sigma \in S_n} \left(\sigma \circ G_{(\alpha) \mathbf{u}_1 \dots \mathbf{u}_n}^{(n;I;i;m_i)}(Y) \right) \alpha_{n;I;i;m_i} \mathcal{C}^{(n;I;i;m_i) a_1 \dots a_n} (-1)^n \\ &\quad \times i \bar{\nabla}_{\mathbf{u}_{\sigma(1)}}^{a_1} \dots i \bar{\nabla}_{\mathbf{u}_{\sigma(n)}}^{a_n}, \end{aligned} \quad (6.66)$$

where

$$\sigma \circ G_{(\alpha) \mathbf{u}_1 \dots \mathbf{u}_n}^{(n;I;i;m_i)}(Y) = G_{(\alpha) \mathbf{u}_{\sigma(1)} \dots \mathbf{u}_{\sigma(n)}}^{(n;I;i;m_i)}(Y). \quad (6.67)$$

- **Step 2:** *Re-arrange the derivatives such that the transverse coordinates on the derivatives appear in the original ascending order.*

Re-arranging the derivative in Eq. 6.66 such that the transverse coordinates on the derivatives appear in original ascending order comes at the cost of introducing commutator terms

and it leads to a permutation of the order of the adjoint indices on the Young colour structure:

$$\begin{aligned}
(6.66) &= \int_{\mathbf{u}_1 \dots \mathbf{u}_n} \frac{1}{n!} \sum_{\sigma \in S_n} \left(\sigma \circ G_{(\alpha)\mathbf{u}_1 \dots \mathbf{u}_n}^{(n;I;i;m_i)}(Y) \right) \alpha_{n;I;i;m_i} \mathcal{C}^{(n;I;i;m_i)a_1 \dots a_n} (-1)^n \\
&\quad \times i \bar{\nabla}_{\mathbf{u}_1}^{a_{\sigma^{-1}(1)}} \dots i \bar{\nabla}_{\mathbf{u}_n}^{a_{\sigma^{-1}(n)}} + \text{commutator terms} \\
&= \int_{\mathbf{u}_1 \dots \mathbf{u}_n} \frac{1}{n!} \sum_{\sigma \in S_n} \left(\sigma \circ G_{(\alpha)\mathbf{u}_1 \dots \mathbf{u}_n}^{(n;I;i;m_i)}(Y) \right) \alpha_{n;I;i;m_i} \left(\sigma \circ \mathcal{C}^{(n;I;i;m_i)a_1 \dots a_n} \right) (-1)^n \\
&\quad \times i \bar{\nabla}_{\mathbf{u}_1}^{a_1} \dots i \bar{\nabla}_{\mathbf{u}_n}^{a_n} + \text{commutator terms}, \tag{6.68}
\end{aligned}$$

where

$$\sigma \circ \mathcal{C}^{(n;I;i;m_i)a_1 \dots a_n} = \mathcal{C}^{(n;I;i;m_i)a_{\sigma(1)} \dots a_{\sigma(n)}}. \tag{6.69}$$

- **Step 3:** Ignore commutator terms and re-express the Young colour structure whose adjoint indices are not (necessarily) in the original ascending order in terms of all available Young colour structures whose adjoint indices are in the original ascending order.

Let us ignore the commutator terms in Eq. 6.68 for now. We know that the Hermitian Young projectors and transition operators in $\mathbb{R}[S_n]$, given by (see Sec. 4.2.3 for a recap of the notation used)

$$\bigcup_J^{\text{blocks}} \bigcup_{j_1 \in J}^{\text{rows}} \bigcup_{j_2 \in J}^{\text{cols}} \left\{ [\mathfrak{M}_J^{(n)}]_{j_1 j_2} \right\}, \tag{6.70}$$

form a basis for the permutation algebra [40]. Consequently, we may express each $\sigma \in S_n$ as

$$\sigma = \sum_J^{\text{blocks}} \sum_{j_1 \in J}^{\text{rows}} \sum_{j_2 \in J}^{\text{cols}} [\beta_J^{(\sigma)}]_{j_1 j_2} [\mathfrak{M}_J^{(n)}]_{j_1 j_2} \tag{6.71}$$

where $[\beta_J^{(\sigma)}]_{j_1 j_2}$ is the real coefficient tensor of σ in the basis of the Hermitian Young projectors and transition operators.

One should read \sum_J^{blocks} as the sum over all blocks in $\mathfrak{M}^{(n)}$ where $J = 1, \dots, |\mathbf{Y}_n|$, and $\sum_{j_1 \in J}^{\text{rows}}$ and $\sum_{j_2 \in J}^{\text{cols}}$ as the sum over all rows and columns, respectively, in the J^{th} block of $\mathfrak{M}^{(n)}$ where $j_1, j_2 = 1, \dots, |\mathcal{Y}_J^{(n)}|$.

Using Eq. 6.71, Eq. 6.69 becomes

$$\begin{aligned}\sigma \circ \mathcal{C}^{(n;I;i;m_i)a_1 \cdots a_n} &= \sum_J \sum_{j_1 \in J}^{\text{rows}} \sum_{j_2 \in J}^{\text{cols}} [\beta_J^{(\sigma)}]_{j_1 j_2} [\mathfrak{M}_J^{(n)}]_{j_1 j_2} \circ \mathcal{C}^{(n;I;i;m_i)a_1 \cdots a_n} \\ &= \sum_{j_1 \in I}^{\text{rows}} \sum_{j_2 \in I}^{\text{cols}} [\beta_I^{(\sigma)}]_{j_1 j_2} [\mathfrak{M}_I^{(n)}]_{j_1 j_2} \circ \mathcal{C}^{(n;I;i;m_i)a_1 \cdots a_n}\end{aligned}\quad (6.72)$$

where in the last equality we used the fact that the sub-blocks of $\mathfrak{M}^{(n)}$ are orthogonal in order to eliminate the sum over blocks J ; i.e.

$$[\mathfrak{M}_J^{(n)}]_{j_1 j_2} \circ \mathcal{C}^{(n;I;i;m_i)a_1 \cdots a_n} = \delta_{IJ} [\mathfrak{M}_I^{(n)}]_{j_1 j_2} \circ \mathcal{C}^{(n;I;i;m_i)a_1 \cdots a_n}. \quad (6.73)$$

The reason why we did not use a compound label to iterate over all Hermitian Young projection operators and transition operators and instead iterated over blocks and then rows and columns in each block was so that the orthogonality of blocks may be exploited as was done in Eq. 6.72.

Re-expanding Eq. 6.72 in terms of all available Young colour structures in $A^{\otimes n}$ with adjoint indices in ascending order yields

$$\begin{aligned}\sigma \circ \mathcal{C}^{(n;I;i;m_i)a_1 \cdots a_n} &= \sum_K^{\text{blocks}} \sum_{k \in K}^{\text{diag.}} \sum_{m_k=1}^{d(K;k)} \mathcal{C}^{(n;K;k;m_k)a_1 \cdots a_n} \underbrace{\left[\mathcal{C}^{(n;K;k;m_k)b_1 \cdots b_n} \left(\sigma \circ \mathcal{C}^{(n;I;i;m_i)b_1 \cdots b_n} \right) \right]}_{\text{coefficient}} \\ &= \sum_K^{\text{blocks}} \sum_{k \in K}^{\text{diag.}} \sum_{m_k=1}^{d(K;k)} \mathcal{C}^{(n;K;k;m_k)a_1 \cdots a_n} \\ &\quad \times \left[\mathcal{C}^{(n;K;k;m_k)b_1 \cdots b_n} \left(\sum_{j_1 \in I}^{\text{rows}} \sum_{j_2 \in I}^{\text{cols}} [\beta_I^{(\sigma)}]_{j_1 j_2} [\mathfrak{M}_I^{(n)}]_{j_1 j_2} \circ \mathcal{C}^{(n;I;i;m_i)b_1 \cdots b_n} \right) \right] \\ &= \sum_K^{\text{blocks}} \sum_{k \in K}^{\text{diag.}} \sum_{m_k=1}^{d(K;k)} \mathcal{C}^{(n;K;k;m_k)a_1 \cdots a_n} \sum_{j_1 \in I}^{\text{rows}} \sum_{j_2 \in I}^{\text{cols}} [\beta_I^{(\sigma)}]_{j_1 j_2} \\ &\quad \times \left[\mathcal{C}^{(n;K;k;m_k)b_1 \cdots b_n} \left([\mathfrak{M}_I^{(n)}]_{j_1 j_2} \circ \mathcal{C}^{(n;I;i;m_i)b_1 \cdots b_n} \right) \right] \\ &= \sum_{k \in I}^{\text{diag.}} \sum_{m_k=1}^{d(I;k)} \mathcal{C}^{(n;I;k;m_k)a_1 \cdots a_n} \sum_{j_1 \in I}^{\text{rows}} \sum_{j_2 \in I}^{\text{cols}} [\beta_I^{(\sigma)}]_{j_1 j_2} \\ &\quad \times \left[\mathcal{C}^{(n;I;k;m_k)b_1 \cdots b_n} \left([\mathfrak{M}_I^{(n)}]_{j_1 j_2} \circ \mathcal{C}^{(n;I;i;m_i)b_1 \cdots b_n} \right) \right].\end{aligned}\quad (6.74)$$

One should read $\sum_{k \in K}^{\text{diag.}}$ as the sum over all diagonal entries in the K^{th} block of $\mathfrak{M}^{(n)}$ where $k = 1, \dots, |\mathcal{Y}_K^{(n)}|$.

It is easy to check that Eq. 6.74 reduces to $\delta^{a_{\sigma(1)}a_{\sigma(2)}} = \delta^{a_1a_2}$.

- **Step 4:** With the Young colour structure(s) and the derivatives as they were originally, compare the result of the above procedure with the original expression and read off the symmetry features of the associated Young colour structure function(s).

Similarly, we can use Eq. 6.71 to re-express Eq. 6.67 as

$$\sigma \circ G_{(\alpha)\mathbf{u}_1 \dots \mathbf{u}_n}^{(n;I;i;m_i)}(Y) = \sum_L^{\text{blocks}} \sum_{l_1 \in L}^{\text{rows}} \sum_{l_2 \in L}^{\text{cols}} [\beta_L^{(\sigma)}]_{l_1 l_2} [\mathfrak{M}_L^{(n)}]_{l_1 l_2} \circ G_{(\alpha)\mathbf{u}_1 \dots \mathbf{u}_n}^{(n;I;i;m_i)}(Y). \quad (6.75)$$

Reinserting Eq. 6.75 and Eq. 6.74 into Eq. 6.68, we finally obtain

$$\begin{aligned} (6.68) &= \int_{\mathbf{u}_1 \dots \mathbf{u}_n} \frac{1}{n!} \sum_{\sigma \in S_n} \left[\sum_L^{\text{blocks}} \sum_{l_1 \in L}^{\text{rows}} \sum_{l_2 \in L}^{\text{cols}} [\beta_L^{(\sigma)}]_{l_1 l_2} [\mathfrak{M}_L^{(n)}]_{l_1 l_2} \circ G_{(\alpha)\mathbf{u}_1 \dots \mathbf{u}_n}^{(n;I;i;m_i)}(Y) \right] \alpha_{n;I;i;m_i} \\ &\times \left\{ \sum_{k \in I}^{\text{diag.}} \sum_{m_k=1}^{d(I;k)} \mathcal{C}^{(n;I;k;m_k)a_1 \dots a_n} \sum_{j_1 \in I}^{\text{rows}} \sum_{j_2 \in I}^{\text{cols}} [\beta_I^{(\sigma)}]_{j_1 j_2} \right. \\ &\times \left. \left[\mathcal{C}^{(n;I;k;m_k)b_1 \dots b_n} \left([\mathfrak{M}_I^{(n)}]_{j_1 j_2} \circ \mathcal{C}^{(n;I;i;m_i)b_1 \dots b_n} \right) \right] \right\} (-1)^n i \bar{\nabla}_{\mathbf{u}_1}^{a_1} \dots i \bar{\nabla}_{\mathbf{u}_n}^{a_n} \\ &= \sum_L^{\text{blocks}} \sum_{l_1 \in L}^{\text{rows}} \sum_{l_2 \in L}^{\text{cols}} \sum_{k \in I}^{\text{diag.}} \sum_{m_k=1}^{d(K;k)} \int_{\mathbf{u}_1 \dots \mathbf{u}_n} \left([\mathfrak{M}_L^{(n)}]_{l_1 l_2} \circ G_{(\alpha)\mathbf{u}_1 \dots \mathbf{u}_n}^{(n;I;i;m_i)}(Y) \right) \alpha_{n;I;i;m_i} \\ &\times \left\{ \frac{1}{n!} \sum_{\sigma \in S_n} [\beta_L^{(\sigma)}]_{l_1 l_2} \sum_{j_1 \in I}^{\text{rows}} \sum_{j_2 \in I}^{\text{cols}} [\beta_I^{(\sigma)}]_{j_1 j_2} \left[\mathcal{C}^{(n;I;k;m_k)b_1 \dots b_n} \left([\mathfrak{M}_I^{(n)}]_{j_1 j_2} \circ \mathcal{C}^{(n;I;i;m_i)b_1 \dots b_n} \right) \right] \right\} \\ &\times \mathcal{C}^{(n;I;k;m_k)a_1 \dots a_n} (-1)^n i \bar{\nabla}_{\mathbf{u}_1}^{a_1} \dots i \bar{\nabla}_{\mathbf{u}_n}^{a_n} \\ &= \sum_L^{\text{blocks}} \sum_{l_1 \in L}^{\text{rows}} \sum_{l_2 \in L}^{\text{cols}} \sum_{k \in I}^{\text{diag.}} \sum_{m_k=1}^{d(K;k)} \int_{\mathbf{u}_1 \dots \mathbf{u}_n} \left([\mathfrak{M}_L^{(n)}]_{l_1 l_2} \circ G_{(\alpha)\mathbf{u}_1 \dots \mathbf{u}_n}^{(n;I;i;m_i)}(Y) \right) \alpha_{n;I;i;m_i} \\ &\times \Omega_{\{L;l_1,l_2\};\{I;(k,m_k),(i,m_i)\}}^{(n)} \mathcal{C}^{(n;I;k;m_k)a_1 \dots a_n} (-1)^n i \bar{\nabla}_{\mathbf{u}_1}^{a_1} \dots i \bar{\nabla}_{\mathbf{u}_n}^{a_n}, \quad (6.76) \end{aligned}$$

where

$$\begin{aligned} \Omega_{\{L;l_1,l_2\};\{I;(k,m_k),(i,m_i)\}}^{(n)} &:= \\ \frac{1}{n!} \sum_{\sigma \in S_n} [\beta_L^{(\sigma)}]_{l_1 l_2} \sum_{j_1 \in I}^{\text{rows}} \sum_{j_2 \in I}^{\text{cols}} [\beta_I^{(\sigma)}]_{j_1 j_2} &\left[\mathcal{C}^{(n;I;k;m_k)b_1 \dots b_n} \left([\mathfrak{M}_I^{(n)}]_{j_1 j_2} \circ \mathcal{C}^{(n;I;i;m_i)b_1 \dots b_n} \right) \right]. \quad (6.77) \end{aligned}$$

- **Commutator terms:** What happens to the commutator terms?

Recall that the commutator of two right-invariant vector fields is given by

$$[i \bar{\nabla}_{\mathbf{u}_1}^{a_1}, i \bar{\nabla}_{\mathbf{u}_2}^{a_2}] = \delta_{\mathbf{u}_1 \mathbf{u}_2}^{(2)} i f^{a_1 a_2 b} i \bar{\nabla}_{\mathbf{u}_2}^b. \quad (6.78)$$

For the case when $n = 2$ (as we have already seen) there is only one commutator term and it is proportional to

$$\delta^{a_1 a_2} i f^{a_1 a_2 b} = 0, \quad (6.79)$$

where the above vanishes due to the antisymmetry of $i f^{a_1 a_2 b}$. For $n \geq 3$, consider a general commutator term which involves some number, say⁴ $n' \in \mathbb{N}^+ \leq \lfloor \frac{n}{2} \rfloor$, of factors of the form given in Eq. 6.78. The resulting expression will contain $n - n' \leq n - 1$ right invariant vector fields contracted into a colour structure with the same number of adjoint indices. In addition, the commutator term will involve a convolution with an n -point colour structure function multiplying n' Dirac delta functions which reduces the n -point function to an $(n - n')$ -point function. Since the resulting colour structure in the commutator terms is an element of $\mathfrak{C}(A^{\otimes(n-n')})$ it can be expressed as a linear combination of elements of $\mathfrak{B}_{\text{Young}}(A^{\otimes(n-n')})$ in which case the above procedure can be recycled. Consequently, we can ignore the commutator terms since they either *trickle down* — can be subsumed into lower order contributions — or they are zero.

Returning to the example given at the beginning of this section, let us check that for $n = 2$ Eq. 6.76 reproduces Eq. 6.65. It is easy but tedious to show that for $n = 2$ Eq. 6.77 becomes

$$\Omega_{\{L;l_1;l_2\};\{I;(k,m_k);(i,m_i)\}}^{(2)} = \delta_{L1} \delta_{l_1 1} \delta_{l_2 1} \delta_{I1} \delta_{k1} \delta_{m_k 1} \delta_{i1} \delta_{m_i 1}, \quad (6.80)$$

which means that

$$\hat{L}_{(\alpha)}^{(2;I;i;m_i)}(Y) = \delta_{I1} \delta_{i1} \delta_{m_i 1} \frac{\alpha_{2;1;1;1}}{\sqrt{N_c^2 - 1}} \int_{\mathbf{u}_1 \mathbf{u}_2} \left([\mathfrak{M}_1^{(2)}]_{11} \circ G_{(\alpha)\mathbf{u}_1 \mathbf{u}_2}^{(2;1;1;1)}(Y) \right) \delta^{a_1 a_2} (-1)^2 i \bar{\nabla}_{\mathbf{u}_1}^{a_1} i \bar{\nabla}_{\mathbf{u}_2}^{a_2},$$

where the factor multiplying the Kronecker deltas and constant factors corresponds to Eq. 6.65. Since only the totally symmetric part of $G_{(\alpha)\mathbf{u}_1 \mathbf{u}_2}^{(2;1;1;1)}(Y)$ is ever accessed, let us define

$$G_{(\alpha)\mathbf{u}_1 \mathbf{u}_2}^{(2;\delta)}(Y) := [\mathfrak{M}_1^{(2)}]_{11} \circ G_{(\alpha)\mathbf{u}_1 \mathbf{u}_2}^{(2;1;1;1)}(Y), \quad (6.81)$$

and let us redefine Eq. 6.65 to be

$$\hat{L}_{(\alpha)}^{(2;\delta)}(Y) := \int_{\mathbf{u}_1 \mathbf{u}_2} G_{(\alpha)\mathbf{u}_1 \mathbf{u}_2}^{(2;\delta)}(Y) \delta^{a_1 a_2} (-1)^2 i \bar{\nabla}_{\mathbf{u}_1}^{a_1} i \bar{\nabla}_{\mathbf{u}_2}^{a_2}. \quad (6.82)$$

Taking $\alpha_{2;1;1;1} = \sqrt{N_c^2 - 1}$ as before, we obtain

$$\hat{L}_{(\alpha)}^{(2)}(Y) = \sum_I \sum_{i \in I}^{\text{blocks}} \sum_{m_i=1}^{\text{diag.}} \hat{L}_{(\alpha)}^{(2;I;i;m_i)}(Y) = \hat{L}_{(\alpha)}^{(2;\delta)}(Y). \quad (6.83)$$

⁴ $\lfloor \frac{n}{2} \rfloor$ denotes the floor of $\frac{n}{2}$.

Similarly, for $n = 3$ one finds that

$$\Omega_{\{L;l_1;l_2\};\{I;(k,m_k);(i,m_i)\}}^{(3)} = (\delta_{L1}\delta_{I1} + \delta_{L3}\delta_{I3})\delta_{l_11}\delta_{l_21}\delta_{k1}\delta_{m_k1}\delta_{i1}\delta_{m_i1}, \quad (6.84)$$

which means that

$$\begin{aligned} \hat{L}_{(\alpha)}^{(3;I;i;m_i)}(Y) &= \delta_{i1}\delta_{m_i1} \int_{\mathbf{u}_1\mathbf{u}_2\mathbf{u}_3} \\ &\times \left\{ \delta_{I1} \left([\mathfrak{M}_1^{(3)}]_{11} \circ G_{(\alpha)\mathbf{u}_1\mathbf{u}_2\mathbf{u}_3}^{(3;1;1;1)}(Y) \right) \alpha_{3;1;1;1} C^{(3;1;1;1)a_1a_2a_3} \right. \\ &\quad \left. + \delta_{I3} \left([\mathfrak{M}_3^{(3)}]_{11} \circ G_{(\alpha)\mathbf{u}_1\mathbf{u}_2\mathbf{u}_3}^{(3;3;1;1)}(Y) \right) \alpha_{3;3;1;1} C^{(3;3;1;1)a_1a_2a_3} \right\} (-1)^3 i \bar{\nabla}_{\mathbf{u}_1}^{a_1} i \bar{\nabla}_{\mathbf{u}_2}^{a_2} i \bar{\nabla}_{\mathbf{u}_3}^{a_3} \\ &= \delta_{i1}\delta_{m_i1} \left[\delta_{I1} \frac{\alpha_{3;1;1;1}}{\sqrt{(N_c^2 - 1)(N_c^2 - 4)/N_c}} \right. \\ &\quad \times \int_{\mathbf{u}_1\mathbf{u}_2\mathbf{u}_3} \left([\mathfrak{M}_1^{(3)}]_{11} \circ G_{(\alpha)\mathbf{u}_1\mathbf{u}_2\mathbf{u}_3}^{(3;1;1;1)}(Y) \right) d^{a_1a_2a_3} (-1)^3 i \bar{\nabla}_{\mathbf{u}_1}^{a_1} i \bar{\nabla}_{\mathbf{u}_2}^{a_2} i \bar{\nabla}_{\mathbf{u}_3}^{a_3} \\ &\quad \left. + \delta_{I3} \frac{\alpha_{3;3;1;1}}{\sqrt{N_c(N_c^2 - 1)}} \int_{\mathbf{u}_1\mathbf{u}_2\mathbf{u}_3} \left([\mathfrak{M}_3^{(3)}]_{11} \circ G_{(\alpha)\mathbf{u}_1\mathbf{u}_2\mathbf{u}_3}^{(3;3;1;1)}(Y) \right) i f^{a_1a_2a_3} (-1)^3 i \bar{\nabla}_{\mathbf{u}_1}^{a_1} i \bar{\nabla}_{\mathbf{u}_2}^{a_2} i \bar{\nabla}_{\mathbf{u}_3}^{a_3} \right]. \end{aligned}$$

Defining

$$G_{(\alpha)\mathbf{u}_1\mathbf{u}_2\mathbf{u}_3}^{(3;d)}(Y) := [\mathfrak{M}_1^{(3)}]_{11} \circ G_{(\alpha)\mathbf{u}_1\mathbf{u}_2\mathbf{u}_3}^{(3;1;1;1)}(Y), \quad (6.85a)$$

$$G_{(\alpha)\mathbf{u}_1\mathbf{u}_2\mathbf{u}_3}^{(3;f)}(Y) := [\mathfrak{M}_3^{(3)}]_{11} \circ G_{(\alpha)\mathbf{u}_1\mathbf{u}_2\mathbf{u}_3}^{(3;3;1;1)}(Y), \quad (6.85b)$$

and

$$\hat{L}_{(\alpha)}^{(3;d)}(Y) := \int_{\mathbf{u}_1\mathbf{u}_2\mathbf{u}_3} G_{(\alpha)\mathbf{u}_1\mathbf{u}_2\mathbf{u}_3}^{(3;d)}(Y) d^{a_1a_2a_3} (-1)^3 i \bar{\nabla}_{\mathbf{u}_1}^{a_1} i \bar{\nabla}_{\mathbf{u}_2}^{a_2} i \bar{\nabla}_{\mathbf{u}_3}^{a_3}, \quad (6.86a)$$

$$\hat{L}_{(\alpha)}^{(3;f)}(Y) := \int_{\mathbf{u}_1\mathbf{u}_2\mathbf{u}_3} G_{(\alpha)\mathbf{u}_1\mathbf{u}_2\mathbf{u}_3}^{(3;f)}(Y) i f^{a_1a_2a_3} (-1)^3 i \bar{\nabla}_{\mathbf{u}_1}^{a_1} i \bar{\nabla}_{\mathbf{u}_2}^{a_2} i \bar{\nabla}_{\mathbf{u}_3}^{a_3}, \quad (6.86b)$$

and taking $\alpha_{3;1;1;1} = \sqrt{d_A C_d}$, $\alpha_{3;3;1;1} = \sqrt{d_A d_f}$, Eq. 6.85a becomes

$$\hat{L}_{(\alpha)}^{(3;I;i;m_i)}(Y) = \delta_{i1}\delta_{m_i1} \left[\delta_{I1} \hat{L}_{(\alpha)}^{(3;d)}(Y) + \delta_{I3} \hat{L}_{(\alpha)}^{(3;f)}(Y) \right]. \quad (6.87)$$

Consequently

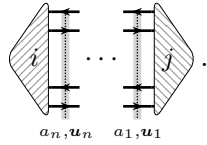
$$\hat{L}_{(\alpha)}^{(3)}(Y) = \sum_I \sum_{i \in I} \sum_{m_i=1}^{\text{diag } d(I;i)} \hat{L}_{(\alpha)}^{(3;I;i;m_i)}(Y) = \hat{L}_{(\alpha)}^{(3;d)}(Y) + \hat{L}_{(\alpha)}^{(3;f)}(Y). \quad (6.88)$$

6.3 Properties of the exponentiating matrix

Let us return to the notation of Sec. 6.1 where in Eq. 6.42 we wrote

$$\mathcal{M}_{(\alpha)}(Y) = \sum_{n=2}^{\infty} \mathcal{M}_{(\alpha)}^{(n)}(Y) = \sum_{n=2}^{\infty} \sum_k \mathcal{M}_{(\alpha)}^{(n;k)}(Y), \quad (6.89)$$

where the components of $\mathcal{M}_{(\alpha)}^{(n;k)}(Y)$ are defined with respect to some orthonormal basis of colour singlet states through

$$\left[\mathcal{M}_{(\alpha)}^{(n;k)}(Y) \right]_{ij} = \frac{1}{\sqrt{2^n}} \int_{\mathbf{u}_1 \dots \mathbf{u}_n} G_{(\alpha)\mathbf{u}_1 \dots \mathbf{u}_n}^{(n;k)}(Y) \mathcal{C}^{(n;k)a_1 \dots a_n} \begin{array}{c} \text{diagram} \end{array}. \quad (6.90)$$


Remember that $\mathcal{M}_{(\alpha)}^{(n;k)}(Y)$ is referred to as the n^{th} order contribution to the exponentiating matrix associated with $\langle \mathcal{A}_{(\alpha)} \rangle(Y)$ from the k^{th} colour structure $\mathcal{C}^{(n;k)a_1 \dots a_n} \in \mathfrak{B}_{\text{ON}}(A^{\otimes n})$.

In section, we consider the following two questions:

- When is $\mathcal{M}_{(\alpha)}^{(n;k)}(Y)$ a purely symmetric or a purely anti-symmetric matrix?
- When is $\mathcal{M}_{(\alpha)}^{(n;k)}(Y)$ purely even or purely odd under \tilde{S} ?

In answering these two questions, I derive two original results; these are recorded in Thm 6.1 and Thm 6.2.

Theorem 6.1. The n^{th} order contribution to the exponentiating matrix associated with $\langle \mathcal{A}_{(\alpha)} \rangle(Y)$ from the k^{th} colour structure $\mathcal{C}^{(n;k)} \in \mathfrak{B}_{\text{ON}}(A^{\otimes n})$, denoted $\mathcal{M}_{(\alpha)}^{(n;k)}(Y)$, is purely symmetric if

$$G_{(\alpha)\mathbf{u}_1 \dots \mathbf{u}_n}^{(n;k)}(Y) \mathcal{C}^{(n;k)a_1 \dots a_n} - \left[\sigma \circ G_{(\alpha)\mathbf{u}_1 \dots \mathbf{u}_n}^{(n;k)}(Y) \right] \left[\sigma \circ \mathcal{C}^{(n;k)a_1 \dots a_n} \right]^* = 0, \quad (6.91a)$$

or purely anti-symmetric if

$$G_{(\alpha)\mathbf{u}_1 \dots \mathbf{u}_n}^{(n;k)}(Y) \mathcal{C}^{(n;k)a_1 \dots a_n} + \left[\sigma \circ G_{(\alpha)\mathbf{u}_1 \dots \mathbf{u}_n}^{(n;k)}(Y) \right] \left[\sigma \circ \mathcal{C}^{(n;k)a_1 \dots a_n} \right]^* = 0, \quad (6.91b)$$

where $\sigma \in S_n$ is the permutation on n symbols which reverses the order of the n symbols

$$\sigma(i) = n + 1 - i, \quad (6.92)$$

and

$$\sigma \circ G_{(\alpha)u_1 \dots u_n}^{(n;k)}(Y) = G_{(\alpha)u_{\sigma(1)} \dots u_{\sigma(n)}}^{(n;k)}(Y), \quad \sigma \circ \mathcal{C}^{(n;k)a_1 \dots a_n} = \mathcal{C}^{(n;k)a_{\sigma(1)} \dots a_{\sigma(n)}}. \quad (6.93)$$

Proof. In order to prove Thm 6.1, simply consider the matrix components of the transpose of $\mathcal{M}_{(\alpha)}^{(n;k)}$

$$\begin{aligned} [(\mathcal{M}_{(\alpha)}^{(n;k)} \vec{x}; \vec{y})^t]_{ij} &= [\mathcal{M}_{(\alpha)}^{(n;k)} \vec{x}; \vec{y}]_{ji} = \frac{1}{\sqrt{2^n}} \int_{u_1 \dots u_n} G_{(\alpha)u_1 \dots u_n}^{(n;k)}(Y) \mathcal{C}^{(n;k)a_1 \dots a_n} \begin{array}{c} \text{diagram with } j \text{ lines} \\ a_n, u_n \quad a_1, u_1 \end{array} \\ &= \frac{1}{\sqrt{2^n}} \int_{u_1 \dots u_n} G_{(\alpha)u_1 \dots u_n}^{(n;k)}(Y) \mathcal{C}^{(n;k)a_1 \dots a_n} \begin{array}{c} \text{diagram with } i \text{ lines} \\ a_1, u_1 \quad a_n, u_n \end{array} \\ &= \frac{1}{\sqrt{2^n}} \int_{u_1 \dots u_n} G_{(\alpha)u_1 \dots u_n}^{(n;k)}(Y) [\mathcal{C}^{(n;k)a_1 \dots a_n}]^* \begin{array}{c} \text{diagram with } i \text{ lines} \\ a_1, u_1 \quad a_n, u_n \end{array} \\ &= \frac{1}{\sqrt{2^n}} \int_{u_1 \dots u_n} [\sigma \circ G_{(\alpha)u_1 \dots u_n}^{(n;k)}(Y)] [\sigma \circ \mathcal{C}^{(n;k)a_1 \dots a_n}]^* \begin{array}{c} \text{diagram with } i \text{ lines} \\ a_n, u_n \quad a_1, u_1 \end{array}, \end{aligned} \quad (6.94)$$

where in the first line I used Eq. 6.90, in the second line I flipped the diagram, in the third line I used Lemma 4.1 to reverse the directions of the lines in the diagrams representing sum-over-generators insertions, and in the last line I relabeled dummy integration variables and dummy adjoint indices. Comparing Eq. 6.94 with Eq. 6.90, one obtains the sufficient conditions specified in Thm 6.1. This concludes the proof of Thm 6.1. \blacksquare

For the Young colour structures and the Young colour structure functions explored in the previous section, Thm 6.1 implies the following:

- $\mathcal{M}_{(\alpha)}^{(2;\delta)}(Y)$ is a symmetric matrix,
- $\mathcal{M}_{(\alpha)}^{(3;d)}(Y)$ is a symmetric matrix, and
- $\mathcal{M}_{(\alpha)}^{(3;f)}(Y)$ is an anti-symmetric matrix.

These results essentially follow from the fact that the colour structures $\delta^{a_1 a_2}$ and $d^{a_1 a_2 a_3}$ are purely real while $if^{a_1 a_2 a_3}$ is purely imaginary. The fact that $\mathcal{M}_{(\alpha)}^{(3;f)}(Y)$ is an anti-symmetric matrix is the reason why the $q\bar{q}$ correlator does not receive any contributions to

$$\begin{aligned}
&= \delta_{\mathbf{u}y_1}^{(2)} + \cdots + \delta_{\mathbf{u}y_m}^{(2)} - \delta_{\mathbf{u}x_1}^{(2)} - \cdots - \delta_{\mathbf{u}x_m}^{(2)} \\
&= - \left[\delta_{\mathbf{u}x_1}^{(2)} + \cdots + \delta_{\mathbf{u}x_m}^{(2)} - \delta_{\mathbf{u}y_1}^{(2)} - \cdots - \delta_{\mathbf{u}y_m}^{(2)} \right] \\
&= - \left[\text{diagram with two crossings and a vertical line } a \right] = - \bar{\mathbf{S}}^{\otimes m} \text{diagram with two crossings and a vertical line } a, \mathbf{u},
\end{aligned} \tag{6.99}$$

where $\bar{\mathbf{S}}^{\otimes m} : \bar{W}^{\otimes m} \rightarrow W^{\otimes m}; (\bar{v}_1, v_1, \dots, \bar{v}_m, v_m) \mapsto (v_1, \bar{v}_1, \dots, v_m, \bar{v}_m)$ is represented in bird-tracks by

$$\bar{\mathbf{S}}^{\otimes m} = \left. \begin{array}{c} \times \\ \vdots \\ \times \end{array} \right\} m \text{ pairs}. \tag{6.100}$$

and $\mathbf{S}^{\otimes m} \bar{\mathbf{S}}^{\otimes m} = i_{W^{\otimes m}}$ and $\bar{\mathbf{S}}^{\otimes m} \mathbf{S}^{\otimes m} = i_{\bar{W}^{\otimes m}}$. Having computed Eq. 6.99, examine

$$\begin{aligned}
\tilde{\mathbf{S}} \circ [\mathcal{M}_{(\alpha)\vec{x};\vec{y}}^{(n;k)}]_{ij} &= \frac{1}{\sqrt{2^n}} \int_{\mathbf{u}_1 \dots \mathbf{u}_n} G_{(\alpha)\mathbf{u}_1 \dots \mathbf{u}_n}^{(n;k)}(Y) \mathcal{C}^{(n;k)}_{a_1 \dots a_n} \tilde{\mathbf{S}} \circ \left[\text{diagram with two crossings and a vertical line } a_n, \mathbf{u}_n \right] \dots \left[\text{diagram with two crossings and a vertical line } a_1, \mathbf{u}_1 \right] \\
&= (-1)^n \frac{1}{\sqrt{2^n}} \int_{\mathbf{u}_1 \dots \mathbf{u}_n} G_{(\alpha)\mathbf{u}_1 \dots \mathbf{u}_n}^{(n;k)}(Y) \mathcal{C}^{(n;k)}_{a_1 \dots a_n} \left[\text{diagram with two crossings and a vertical line } a_n, \mathbf{u}_n \right] \dots \left[\text{diagram with two crossings and a vertical line } a_1, \mathbf{u}_1 \right] \\
&= (-1)^n \frac{1}{\sqrt{2^n}} \int_{\mathbf{u}_1 \dots \mathbf{u}_n} G_{(\alpha)\mathbf{u}_1 \dots \mathbf{u}_n}^{(n;k)}(Y) [\mathcal{C}^{(n;k)}_{a_1 \dots a_n}]^* \left[\text{diagram with two crossings and a vertical line } a_n, \mathbf{u}_n \right] \dots \left[\text{diagram with two crossings and a vertical line } a_1, \mathbf{u}_1 \right] \\
&= \mathbf{c}^{(n;k)} \mathbf{s}_i \mathbf{s}_j (-1)^n \frac{1}{\sqrt{2^n}} \int_{\mathbf{u}_1 \dots \mathbf{u}_n} G_{(\alpha)\mathbf{u}_1 \dots \mathbf{u}_n}^{(n;k)}(Y) [\mathcal{C}^{(n;k)}_{a_1 \dots a_n}]^* \left[\text{diagram with two crossings and a vertical line } a_n, \mathbf{u}_n \right] \dots \left[\text{diagram with two crossings and a vertical line } a_1, \mathbf{u}_1 \right] \\
&= \mathbf{c}^{(n;k)} \mathbf{s}_i \mathbf{s}_j (-1)^n [\mathcal{M}_{(\alpha)\vec{x};\vec{y}}^{(n;k)}]_{ij},
\end{aligned} \tag{6.101}$$

where in the second line I used Eq. 6.99, in the third line I used Lemma 4.1 to reverse the directions of the lines in the diagrams representing sum-over-generators insertions, and in the fourth line I used Eq. 6.95 and Eq. 6.97. This concludes the proof of Thm 6.2. \blacksquare

Chapter 7

The 3-point truncation

7.1 JIMWLK evolution of the $q\bar{q}$ correlator: needing the 3-point truncation

In this section, I argue that the 3-point truncation is necessary in order to provide a non-trivial parameterization for the JIMWLK evolution of the argument of the $q\bar{q}$ correlator.

The JIMWLK equation for the $q\bar{q}$ correlator (the first DS equation of the $q\bar{q}$ correlator) derived in Eq. 5.70 is given by

$$\frac{d}{dY} \langle \mathcal{A}_{xy}^{(1)} \rangle(Y) = \frac{\alpha_s C_f}{\pi^2} \int_z \tilde{\mathcal{K}}_{xzy} \left[\langle \mathcal{A}_{xy;z}^{(1+g)} \rangle(Y) - \langle \mathcal{A}_{xy}^{(1)} \rangle(Y) \right], \quad (7.1)$$

where $C_f = \frac{N_c^2 - 1}{2N_c}$ is the quadratic Casimir in the fundamental representation and

$$\langle \mathcal{A}_{xy}^{(1)} \rangle(Y) = \left\langle \frac{1}{d_f} \text{dipole diagram} \right\rangle(Y), \quad \langle \mathcal{A}_{xy;z}^{(1+g)} \rangle(Y) = \left\langle \frac{1}{d_A} \text{3-point diagram} \right\rangle(Y), \quad (7.2)$$

are the $q\bar{q}$ and $q\bar{q}g$ correlators, respectively. The dimensions of the fundamental and the adjoint representations of $\text{SU}(N_c)$ appearing in Eq. 7.2 are given by $d_f = N_c$ and $d_A = N_c^2 - 1$, respectively. Since these correlators are complex numbers (as opposed to complex matrices) they can be expressed in modulus-argument form through

$$\langle \mathcal{A}_{xy}^{(1)} \rangle(Y) = r_{xy}^{(1)}(Y) e^{i\theta_{xy}^{(1)}(Y)}, \quad \langle \mathcal{A}_{xy;z}^{(1+g)} \rangle(Y) = r_{xy;z}^{(1+g)}(Y) e^{i\theta_{xy;z}^{(1+g)}(Y)}. \quad (7.3)$$

Recasting Eq. 7.1 in terms of Eq. 7.3, the real and imaginary parts of the equation correspond to equations for the modulus $r_{xy}^{(1)}(Y)$ and the argument $\theta_{xy}^{(1)}(Y)$ of the $q\bar{q}$ dipole which are given

by

$$\frac{d}{dY} r_{xy}^{(1)}(Y) = \frac{\alpha_s C_f}{\pi^2} \int_z \tilde{\mathcal{K}}_{xzy} \left[r_{xy;z}^{(1+g)}(Y) \cos \left[\theta_{xy;z}^{(1+g)}(Y) - \theta_{xy}^{(1)}(Y) \right] - r_{xy}^{(1)}(Y) \right], \quad (7.4a)$$

$$\frac{d}{dY} \theta_{xy}^{(1)}(Y) = \frac{\alpha_s C_f}{\pi^2} \int_z \tilde{\mathcal{K}}_{xzy} \frac{r_{xy;z}^{(1+g)}(Y)}{r_{xy}^{(1)}(Y)} \sin \left[\theta_{xy;z}^{(1+g)}(Y) - \theta_{xy}^{(1)}(Y) \right], \quad (7.4b)$$

respectively. The 3-point truncation of the $q\bar{q}$ and $q\bar{q}g$ correlators are easily computed as

$$\langle \mathcal{A}_{xy}^{(1)} \rangle_3(Y) = \exp \left[-C_f \mathcal{G}_{xy}(Y, Y_0) \right] \langle \mathcal{A}_{xy}^{(1)} \rangle(Y_0), \quad (7.5a)$$

$$\langle \mathcal{A}_{xy;z}^{(1+g)} \rangle_3(Y) = \exp \left[-\frac{C_A}{2} (\mathcal{G}_{xz} + \mathcal{G}_{zy} - \mathcal{G}_{xy})(Y, Y_0) - C_f \mathcal{G}_{xy}(Y, Y_0) \right] \langle \mathcal{A}_{xy;z}^{(1+g)} \rangle(Y_0), \quad (7.5b)$$

where $C_A = N_c$ is the quadratic Casimir in the adjoint representation and for convenience (and following the notation of [32]) we have defined

$$\mathcal{G}_{xy}(Y, Y_0) = \mathcal{P}_{xy}(Y, Y_0) + i \mathcal{O}_{xy}(Y, Y_0), \quad (7.6)$$

with

$$\mathcal{P}_{xy}(Y, Y_0) := \int_{Y_0}^Y dY' G_{(1)xy}^{(2;\delta)}(Y'), \quad (7.7a)$$

$$\mathcal{O}_{xy}(Y, Y_0) := -i C_d \int_{Y_0}^Y dY' \frac{1}{2} \left(G_{(1)xy}^{(3;d)}(Y') - G_{(1)yx}^{(3;d)}(Y') \right) =: -i C_d \int_{Y_0}^Y dY' G_{(1)(xy)}^{(3;d)}(Y'). \quad (7.7b)$$

The constant C_d is defined such that $d^{ac_1 c_2} d^{c_1 c_2 b} = C_d \delta^{ab}$ where $C_d = \frac{N_c^2 - 4}{N_c}$. Under an interchange of transverse coordinates \mathbf{x} and \mathbf{y} , the so-called ‘‘Pomeron’’ contribution \mathcal{P}_{xy} is symmetric since $G_{(1)xy}^{(2;\delta)}$ is symmetric while the so-called ‘‘Odderon’’ contribution \mathcal{O}_{xy} is anti-symmetric by construction. Despite the suggestive notation used in Eq. 7.6, at this stage both the Pomeron and the Odderon are complex-valued functions. However, we can easily show that both are real which we do below. To this end, notice that the $q\bar{q}$ correlator has the following symmetry under complex conjugation¹

$$\langle \mathcal{A}_{xy}^{(1)} \rangle^*(Y) = \langle \mathcal{A}_{xy}^{(1)*} \rangle(Y) = \langle \mathcal{A}_{yx}^{(1)} \rangle(Y) = \tilde{S} \circ \langle \mathcal{A}_{xy}^{(1)} \rangle(Y). \quad (7.8)$$

¹Notice that we are assuming that the complex conjugate of the target average is equal to the target average of the complex conjugate. This is certainly true in the Langevin picture of JIMWLK evolution [17], but this picture is only available at leading logarithmic order in $1/x_{bj}$.

Requiring that any truncation of the $q\bar{q}$ correlator (in particular the 3-point truncation recorded in Eq. 7.5a) preserves this same symmetry, we have that for non-trivial initial conditions

$$\begin{aligned} \exp \left[-C_f(\mathcal{P}_{xy}^* - i\mathcal{O}_{xy}^*)(Y, Y_0) \right] &= \exp \left[-C_f(\mathcal{P}_{xy} - i\mathcal{O}_{xy})(Y, Y_0) \right] \\ \iff \exp [2C_f(i\text{Im} [\mathcal{P}_{xy}(Y, Y_0)] + \text{Im} [\mathcal{O}_{xy}(Y, Y_0)])] &= 1, \end{aligned} \quad (7.9)$$

which implies that

$$\text{Im} [\mathcal{P}_{xy}(Y, Y_0)] = \frac{\pi}{C_f} n_{xy}(Y, Y_0), \quad (7.10a)$$

$$\text{Im} [\mathcal{O}_{xy}(Y, Y_0)] = 0, \quad (7.10b)$$

where $n_{xy}(Y, Y_0)$ is an integer-valued function. Eq. 7.10b says that \mathcal{O}_{xy} is purely real. In order to draw a concrete conclusion from Eq. 7.10a, we note that it is reasonable to assume that JIMWLK evolution is continuous. This assumption requires $n_{xy}(Y, Y_0)$ to be continuous, but since it is an integer-valued function it must then be constant. Consequently, $n_{xy}(Y, Y_0) = n_{xy}(Y_0, Y_0) = 0$ since $\mathcal{P}_{xy}(Y_0, Y_0) = 0$. Therefore Eq. 7.10a says that \mathcal{P}_{xy} is purely real too. Furthermore, differentiating Eq. 7.10 with respect to Y yields

$$\text{Im} \left[G_{(1)xy}^{(2;\delta)}(Y) \right] = 0, \quad (7.11a)$$

$$\text{Re} \left[G_{(1)(xy)}^{(3;d)}(Y) \right] = 0. \quad (7.11b)$$

Since both the Pomeron and the Odderon are real, we that the JIMWLK evolution of the modulus and the argument of the $q\bar{q}$ correlator is parameterized as

$$r_{xy}^{(1)}(Y) = \exp \left[-C_f \mathcal{P}_{xy}(Y, Y_0) \right] r_{xy}^{(1)}(Y_0), \quad (7.12a)$$

$$\theta_{xy}^{(1)}(Y) = \theta_{xy}^{(1)}(Y_0) - C_f \mathcal{O}_{xy}(Y, Y_0), \quad (7.12b)$$

and that of the $q\bar{q}g$ correlator is parameterized as

$$r_{xy;z}^{(1+g)}(Y) = \exp \left[-\frac{C_A}{2} (\mathcal{P}_{xz} + \mathcal{P}_{zy} - \mathcal{P}_{xy})(Y, Y_0) - C_f \mathcal{P}_{xy}(Y, Y_0) \right] r_{xy;z}^{(1+g)}(Y_0), \quad (7.13a)$$

$$\theta_{xy;z}^{(1+g)}(Y) = \theta_{xy;z}^{(1+g)}(Y_0) - \frac{C_A}{2} (\mathcal{O}_{xz} + \mathcal{O}_{zy} - \mathcal{O}_{xy})(Y, Y_0) - C_f \mathcal{O}_{xy}(Y, Y_0). \quad (7.13b)$$

If we were working only in the 2-point truncation of the $q\bar{q}$ correlator then Eq. 7.12b would reduce to $\theta_{xy}^{(1)}(Y) = \theta_{xy}^{(1)}(Y_0)$ which provides only a trivial parameterization for Eq. 7.4b with $\frac{d}{dY} \theta_{xy}^{(1)}(Y) = 0$. Therefore, in order to provide a non-trivial parameterization for Eq. 7.4b one

clearly needs the 3-point truncation. Writing Eq. 7.4 in terms of Eq. 7.12 and Eq. 7.13 yields

$$\begin{aligned} \frac{d}{dY} \mathcal{P}_{xy}(Y, Y_0) &= \frac{\alpha_s}{\pi^2} \int_z \tilde{\mathcal{K}}_{xzy} \left[1 - \exp \left[-\frac{C_A}{2} (\mathcal{P}_{xz} + \mathcal{P}_{zy} - \mathcal{P}_{xy})(Y, Y_0) \right] \right] \\ &\times \cos \left[\frac{C_A}{2} (\mathcal{O}_{xz} + \mathcal{O}_{zy} - \mathcal{O}_{xy})(Y, Y_0) - \theta_{xy;z}^{(1+g)}(Y_0) + \theta_{xy}^{(1)}(Y_0) \right] \\ &\times r_{xy;z}^{(1+g)}(Y_0) \left(r_{xy}^{(1)}(Y_0) \right)^{-1}, \end{aligned} \quad (7.14a)$$

$$\begin{aligned} \frac{d}{dY} \mathcal{O}_{xy}(Y, Y_0) &= \frac{\alpha_s}{\pi^2} \int_z \tilde{\mathcal{K}}_{xzy} \exp \left[-\frac{C_A}{2} (\mathcal{P}_{xz} + \mathcal{P}_{zy} - \mathcal{P}_{xy})(Y, Y_0) \right] \\ &\times \sin \left[\frac{C_A}{2} (\mathcal{O}_{xz} + \mathcal{O}_{zy} - \mathcal{O}_{xy})(Y, Y_0) - \theta_{xy;z}^{(1+g)}(Y_0) + \theta_{xy}^{(1)}(Y_0) \right] \\ &\times r_{xy;z}^{(1+g)}(Y_0) \left(r_{xy}^{(1)}(Y_0) \right)^{-1}, \end{aligned} \quad (7.14b)$$

where I assumed that $r_{xy}^{(1)}(Y_0) \neq 0$. Eq. 7.14 differs slightly from Eq. (34) of [32] in that we have not assumed that the initial conditions for the $q\bar{q}$ and $q\bar{q}g$ correlators coincide; such an assumption is unmotivated and unnecessary.

7.2 The 3-point truncation of the full $q^2\bar{q}^2$ correlator matrix

Having motivated the need for the 3-point truncation in the context of the $q\bar{q}$ correlator, in this section we examine the 3-point truncation of the smallest correlator matrix capable of accessing all available colour structure functions in the 3-point truncation — namely $G_{(\alpha)u_1u_2}^{(2;\delta)}$, $G_{(\alpha)u_1u_2u_3}^{(3;d)}$ and $G_{(\alpha)u_1u_2u_3}^{(3;f)}$ (where we have dropped the Y -dependence of these colour structure functions for brevity). The smallest such correlator matrix is the $q^2\bar{q}^2$ correlator matrix given by

$$\langle \mathcal{A}_{x_1x_2;y_1y_2}^{(2)} \rangle(Y) = \left\langle \begin{bmatrix} A_{11}^{(2)} & A_{12}^{(2)} \\ A_{12}^{(2)} & A_{22}^{(2)} \end{bmatrix} \right\rangle(Y), \quad (7.15)$$

where the normalizations are

$$A_{11}^{(2)} = \frac{1}{d_f^2}, \quad A_{12}^{(2)} = \frac{1}{d_f \sqrt{d_A}}, \quad A_{22}^{(2)} = \frac{1}{d_A}. \quad (7.16)$$

Examples of observable within the CGC formalism that is expressed either entirely or partly in terms of the entries of Eq. 7.15 include the cross-section for dijet production in DIS [30], the cross-section for dijet production in pA collisions [30] and the cross-section for medium-induced gluon radiation in hard forward parton scattering [31].

The 3-point truncation of Eq. 7.15, denoted $\langle \mathcal{A}_{x_1 x_2; y_1 y_2}^{(2)} \rangle_3(Y)$, is given in terms of some initial condition $\langle \mathcal{A}_{x_1 x_2; y_1 y_2}^{(2)} \rangle(Y_0)$ by

$$\langle \mathcal{A}_{x_1 x_2; y_1 y_2}^{(2)} \rangle_3(Y) = \sum_{\alpha=1}^2 \mathcal{E}_{(\alpha)x_1 x_2; y_1 y_2}^{[3]}(Y, Y_0) \langle \mathcal{A}_{x_1 x_2; y_1 y_2}^{(2)} \rangle(Y_0) \mathcal{E}_{(\alpha)x_1 x_2; y_1 y_2}^{[3]t}(Y, Y_0), \quad (7.17)$$

where for $\alpha = 1, 2$

$$\mathcal{E}_{(\alpha)x_1 x_2; y_1 y_2}^{[3]}(Y, Y_0) = P \exp \left[-\frac{1}{2} \int_{Y_0}^Y dY' \mathcal{M}_{(\alpha)x_1 x_2; y_1 y_2}^{[3]}(Y') \right], \quad (7.18)$$

and

$$\mathcal{M}_{(\alpha)x_1 x_2; y_1 y_2}^{[3]}(Y) = \mathcal{M}_{(\alpha)x_1 x_2; y_1 y_2}^{(2;\delta)}(Y) + \mathcal{M}_{(\alpha)x_1 x_2; y_1 y_2}^{(3;d)}(Y) + \mathcal{M}_{(\alpha)x_1 x_2; y_1 y_2}^{(3;f)}(Y). \quad (7.19)$$

In what follows we will drop the Y -dependence of exponentiating matrices as well as their dependence on transverse coordinates for brevity. Before explicitly computing each of the three contributions to Eq. 7.19, one already knows some of their properties. Firstly, using Thm 6.1 one knows that $\mathcal{M}_{(\alpha)}^{(2;\delta)}$ and $\mathcal{M}_{(\alpha)}^{(3;d)}$ are symmetric matrices while $\mathcal{M}_{(\alpha)}^{(3;f)}$ is an anti-symmetric matrix. This result essentially follows from the fact that the colour structures $\delta^{a_1 a_2}$ and $d^{a_1 a_2 a_3}$ are purely real while $if^{a_1 a_2 a_3}$ is purely imaginary. Secondly, since Eq. 7.15 is constructed in terms of colour singlet states which are eigenstates of $\mathbf{S}^{\otimes 2}$ with eigenvalue 1 (with respect to \cong), one knows that $\mathcal{M}_{(\alpha)}^{(2;\delta)}$ and $\mathcal{M}_{(\alpha)}^{(3;f)}$ are even under $\tilde{\mathbf{S}}$ while $\mathcal{M}_{(\alpha)}^{(3;d)}$ is odd under $\tilde{\mathbf{S}}$. These properties are confirmed in the explicit calculation of each of the three contributions to Eq. 7.19 performed below.

The matrix components of $\mathcal{M}_{(\alpha)}^{(2;\delta)}$ are computed to be

$$[\mathcal{M}_{(\alpha)}^{(2;\delta)}]_{11} = C_f \left[G_{(\alpha)x_1 y_1}^{(2;\delta)} + G_{(\alpha)x_2 y_2}^{(2;\delta)} \right], \quad (7.20a)$$

$$[\mathcal{M}_{(\alpha)}^{(2;\delta)}]_{12} = -\frac{C_f}{\sqrt{d_A}} \left[G_{(\alpha)x_1 x_2}^{(2;\delta)} - G_{(\alpha)x_1 y_2}^{(2;\delta)} - G_{(\alpha)x_2 y_1}^{(2;\delta)} + G_{(\alpha)y_1 y_2}^{(2;\delta)} \right] = [\mathcal{M}_{(\alpha)}^{(2;\delta)}]_{21}, \quad (7.20b)$$

$$\begin{aligned} [\mathcal{M}_{(\alpha)}^{(2;\delta)}]_{22} &= \frac{C_A + C_d}{4} \left(G_{(\alpha)x_1 y_2}^{(2;\delta)} + G_{(\alpha)x_2 y_1}^{(2;\delta)} \right) + \frac{C_A - C_d}{4} \left(G_{(\alpha)x_1 x_2}^{(2;\delta)} + G_{(\alpha)y_1 y_2}^{(2;\delta)} \right) \\ &\quad + \left(C_f - \frac{C_A}{2} \right) \left(G_{(\alpha)x_1 y_1}^{(2;\delta)} + G_{(\alpha)x_2 y_2}^{(2;\delta)} \right). \end{aligned} \quad (7.20c)$$

Eq. 7.20 was first recorded in [19] (see Eq. (44) therein). However there are typographical errors in the numerical factors in Eq. (44b) and Eq. (44c) of [19] which we correct in Eq. 7.20c and Eq. 7.20b, respectively. Clearly, $\mathcal{M}_{(\alpha)}^{(2;\delta)}$ is a symmetric matrix and one can easily check that it is invariant under $\tilde{\mathbf{S}}$.

The matrix components of $\mathcal{M}_{(\alpha)}^{(3;d)}$ are given by

$$[\mathcal{M}_{(\alpha)}^{(3;d)}]_{11} = C_f C_d \left[G_{(\alpha)(x_1 y_1)}^{(3;d)} + G_{(\alpha)(x_2 y_2)}^{(3;d)} \right], \quad (7.21a)$$

$$[\mathcal{M}_{(\alpha)}^{(3;d)}]_{12} = \frac{C_f C_d}{\sqrt{d_A}} \left[G_{(\alpha)(x_1 y_2)}^{(3;d)} + G_{(\alpha)(x_2 y_1)}^{(3;d)} - G_{(\alpha)[x_1 x_2]}^{(3;d)} + G_{(\alpha)[y_1 y_2]}^{(3;d)} + G_{(\alpha)x_1 x_2 y_1 y_2}^{(3;d|++--)} \right] \quad (7.21b)$$

$$\begin{aligned} &= [\mathcal{M}_{(\alpha)}^{(3;d)}]_{21}, \\ [\mathcal{M}_{(\alpha)}^{(3;d)}]_{22} &= C_d \left[\frac{C_A + C_d}{4} \left(G_{(\alpha)(x_1 y_2)}^{(3;d)} + G_{(\alpha)(x_2 y_1)}^{(3;d)} \right) \right. \\ &\quad + \frac{C_A - C_d}{4} \left(G_{(\alpha)[x_1 x_2]}^{(3;d)} - G_{(\alpha)[y_1 y_2]}^{(3;d)} + G_{(\alpha)x_1 x_2 y_1 y_2}^{(3;d|++--)} \right) \\ &\quad \left. + \left(C_f - \frac{C_A}{2} \right) \left(G_{(\alpha)(x_1 y_1)}^{(3;d)} + G_{(\alpha)(x_2 y_2)}^{(3;d)} \right) \right], \end{aligned} \quad (7.21c)$$

where

$$G_{(\alpha)(u_1 u_2)}^{(3;d)} := \frac{1}{2} \left[G_{(\alpha)u_1 u_1 u_2}^{(3;d)} - G_{(\alpha)u_1 u_2 u_2}^{(3;d)} \right], \quad (7.22a)$$

$$G_{(\alpha)[u_1 u_2]}^{(3;d)} := \frac{1}{2} \left[G_{(\alpha)u_1 u_1 u_2}^{(3;d)} + G_{(\alpha)u_1 u_2 u_2}^{(3;d)} \right], \quad (7.22b)$$

are anti-symmetric and symmetric 2-point functions (as suggested by the round and square braces enclosing the transverse coordinates) and

$$G_{(\alpha)u_1 u_2 u_3 u_4}^{(3;d|++--)} := G_{(\alpha)u_1 u_2 u_3}^{(3;d)} + G_{(\alpha)u_1 u_2 u_4}^{(3;d)} - G_{(\alpha)u_1 u_3 u_4}^{(3;d)} - G_{(\alpha)u_2 u_3 u_4}^{(3;d)}, \quad (7.23)$$

is a 4-point function. Eq. 7.23 is separately symmetric in the first two and the last two transverse coordinates, and is anti-symmetric under the interchange of the first two with the last two transverse coordinates; i.e.

$$G_{(\alpha)x_2 x_1 y_1 y_2}^{(3;d|++--)} = G_{(\alpha)x_1 x_2 y_1 y_2}^{(3;d|++--)}, \quad (7.24a)$$

$$G_{(\alpha)x_1 x_2 y_2 y_1}^{(3;d|++--)} = G_{(\alpha)x_1 x_2 y_1 y_2}^{(3;d|++--)}, \quad (7.24b)$$

$$G_{(\alpha)y_1 y_2 x_1 x_2}^{(3;d|++--)} = \tilde{S} \circ G_{(\alpha)x_1 x_2 y_1 y_2}^{(3;d|++--)} = -G_{(\alpha)x_1 x_2 y_1 y_2}^{(3;d|++--)}. \quad (7.24c)$$

Clearly $\mathcal{M}_{(\alpha)}^{(3;d)}$ is an anti-symmetric matrix and it picks up a minus sign under the action of \tilde{S} .

Finally, $\mathcal{M}_{(\alpha)}^{(3;f)}$ is an anti-symmetric matrix with non-zero (off-diagonal) components

$$[\mathcal{M}_{(\alpha)}^{(3;f)}]_{12} = \frac{\sqrt{d_A}}{2} G_{(\alpha)x_1 x_2 y_1 y_2}^{(3;f|++--)} = -[\mathcal{M}_{(\alpha)}^{(3;f)}]_{21}, \quad (7.25)$$

where

$$G_{(\alpha)u_1 u_2 u_3 u_4}^{(3;f|++--)} := G_{(\alpha)u_1 u_2 u_3}^{(3;f)} - G_{(\alpha)u_1 u_2 u_4}^{(3;f)} + G_{(\alpha)u_1 u_3 u_4}^{(3;f)} - G_{(\alpha)u_2 u_3 u_4}^{(3;f)}, \quad (7.26)$$

is a totally anti-symmetric 4-point function. Since this 4-point function is totally anti-symmetric, it vanishes under any single coincidence limit which makes the full $q^2\bar{q}^2$ correlator matrix really the smallest correlator matrix capable of accessing all colour structure functions available to the 3-point truncation. Clearly, $\mathcal{M}_{(\alpha)}^{(3;f)}$ is invariant under \tilde{S} .

In the limit that $\mathbf{y}_2 \mapsto \mathbf{x}_2 := \mathbf{z}_2$, Eq. 7.15 becomes

$$\langle \mathcal{A}_{\mathbf{x}_1 \mathbf{z}_2; \mathbf{y}_1 \mathbf{z}_2}^{(2)} \rangle(Y) = \left\langle \begin{bmatrix} A_{11}^{(2)} & 0 \\ 0 & A_{22}^{(2)} \end{bmatrix} \right\rangle(Y), \quad (7.27)$$

where the top-left entry is the $q\bar{q}$ correlator $\langle \mathcal{A}_{\mathbf{x}_1 \mathbf{y}_1}^{(1)} \rangle(Y)$ and the bottom-right entry is the $q\bar{q}g$ correlator $\langle \mathcal{A}_{\mathbf{x}_1 \mathbf{y}_1; \mathbf{z}_2}^{(1+g)} \rangle(Y)$, both of whom we already encountered in Eq. 7.2. Since Eq. 7.27 is diagonal, it has no anti-symmetric part. Consequently, in order to write down Eq. 7.17 we need only consider the exponentiating matrix corresponding to its symmetric part which in the 3-point truncation has non-zero components

$$[\mathcal{M}_{(1)}^{[3]}]_{11} = C_f \mathcal{G}_{\mathbf{x}_1 \mathbf{y}_1}, \quad (7.28a)$$

$$[\mathcal{M}_{(1)}^{[3]}]_{22} = \frac{C_A}{2} (\mathcal{G}_{\mathbf{x}_1 \mathbf{z}_2} + \mathcal{G}_{\mathbf{z}_2 \mathbf{y}_1} - \mathcal{G}_{\mathbf{x}_1 \mathbf{y}_1}) + C_f \mathcal{G}_{\mathbf{x}_1 \mathbf{y}_1}, \quad (7.28b)$$

where \mathcal{G} is as defined in Eq. 7.6. The resultant 3-point truncation of Eq. 7.27 is then given by

$$\begin{aligned} \langle \mathcal{A}_{(1)\mathbf{x}_1 \mathbf{z}_2; \mathbf{y}_1 \mathbf{z}_2}^{(2)} \rangle_3(Y) = & \quad (7.29) \\ \begin{bmatrix} \exp[-C_f \mathcal{G}_{\mathbf{x}_1 \mathbf{z}_2}(Y, Y_0)] \langle \mathcal{A}_{\mathbf{x}_1 \mathbf{y}_1}^{(1)} \rangle(Y_0) & 0 \\ 0 & \exp\left[-\frac{C_A}{2} (\mathcal{G}_{\mathbf{x}_1 \mathbf{z}_2} + \mathcal{G}_{\mathbf{z}_2 \mathbf{y}_1} - \mathcal{G}_{\mathbf{x}_1 \mathbf{y}_1})(Y, Y_0) - C_f \mathcal{G}_{\mathbf{x}_1 \mathbf{y}_1}(Y, Y_0)\right] \langle \mathcal{A}_{\mathbf{x}_1 \mathbf{y}_1; \mathbf{z}_2}^{(1+g)} \rangle(Y_0) \end{bmatrix}, & \quad (7.30) \end{aligned}$$

which coincides (up to a relabeling of transverse coordinates) precisely with Eq. 7.5. Given that the full $q^2\bar{q}^2$ correlator matrix contains the $q\bar{q}$ correlator in a coincidence limit and that for the $q\bar{q}$ correlator $G_{(1)\mathbf{xy}}^{(2;\delta)}$ is purely real and $G_{(1)(\mathbf{xy})}^{(3;d)}$ is purely imaginary, it must also be that case $G_{(1)\mathbf{xy}}^{(2;\delta)}$ is purely real and $G_{(1)(\mathbf{xy})}^{(3;d)}$ is purely imaginary in the 3-point truncation of the full $q^2\bar{q}^2$ correlator matrix.

7.3 Inconsistent JIMWLK evolution of the 3-point truncation: needing still higher order truncations

The 3-point truncation of the full $q^2\bar{q}^2$ correlator matrix is not sufficient to consistently parameterize the JIMWLK evolution of the full $q^2\bar{q}^2$ correlator matrix. This inconsistency becomes

manifest when comparing the evolution equations of correlators contained inside the $q^2\bar{q}^2$ correlator matrix in certain coincidence limits. In particular, we shall compare the evolution equations of the $q\bar{q}$ correlator and the g^2 correlator both expressed in the 3-point truncation and show that the two equations cannot be simultaneously satisfied. The JIMWLK equation for the $q\bar{q}$ correlator expressed in the 3-point truncation is already given by Eq. 7.14. Consequently, the majority of the section will be devoted to expressing the JIMWLK equation for the g^2 correlator in the 3-point truncation.

In the limit that $\mathbf{y}_1 \mapsto \mathbf{x}_1 =: \mathbf{z}_1$, Eq. 7.27 further reduces to

$$\langle \mathcal{A}_{\mathbf{z}_1 \mathbf{z}_2; \mathbf{z}_1 \mathbf{z}_2}^{(2)} \rangle(Y) = \left\langle \begin{bmatrix} A_{11}^{(2)} \text{ (diagram)} & 0 \\ 0 & A_{22}^{(2)} \text{ (diagram)} \end{bmatrix} \right\rangle(Y), \quad (7.31)$$

where the top-left entry is equal to 1 and the bottom-right entry is the g^2 correlator. Recall that in Sec. 4.4.2, specifically in Eq. 4.153, we saw that Eq. 7.31 was contained in the top-left corner of

$$\langle \mathcal{A}_{\mathbf{z}_1 \mathbf{z}_2 \mathbf{z}_3; \mathbf{z}_1 \mathbf{z}_2 \mathbf{z}_3}^{(3)} \rangle(Y) = \left\langle \begin{bmatrix} A_{11}^{(3)} \text{ (diagram)} & 0 & 0 & 0 & 0 & 0 \\ 0 & A_{22}^{(3)} \text{ (diagram)} & 0 & 0 & 0 & 0 \\ 0 & 0 & A_{33}^{(3)} \text{ (diagram)} & 0 & 0 & 0 \\ 0 & 0 & 0 & A_{44}^{(3)} \text{ (diagram)} & 0 & 0 \\ 0 & 0 & 0 & 0 & A_{55}^{(3)} \text{ (diagram)} & A_{56}^{(3)} \text{ (diagram)} \\ 0 & 0 & 0 & 0 & A_{65}^{(3)} \text{ (diagram)} & A_{66}^{(3)} \text{ (diagram)} \end{bmatrix} \right\rangle(Y). \quad (7.32)$$

$1 \oplus (g^2)^{\oplus 3} \oplus g^3$

In this section we shall write

$$\langle \mathcal{A}_{ij}^{(3)} \rangle(Y) := [\langle \mathcal{A}_{z_1 z_2 z_3; z_1 z_2 z_3}^{(3)} \rangle(Y)]_{ij}, \quad (7.33)$$

for the sake of notational brevity, remembering that three coincidence limits have been taken. In terms of Wilson-lines, the g^2 correlator given by

$$\langle \mathcal{A}_{22}^{(3)} \rangle(Y) = \left\langle \frac{1}{d_A} \tilde{U}_{z_1}^{ab} \tilde{U}_{z_2}^{ab} \right\rangle(Y), \quad (7.34)$$

is manifestly real since $[\tilde{U}_{z_1}^{ab} \tilde{U}_{z_2}^{ab}]^\dagger = \tilde{U}_{z_1}^{ba} \tilde{U}_{z_2}^{ba} = \tilde{U}_{z_1}^{ab} \tilde{U}_{z_2}^{ab}$. Using the shorthand of Eq. 7.33, the JIMWLK equation of the g^2 correlator can be compactly written as

$$\frac{d}{dY} \langle \mathcal{A}_{22}^{(3)} \rangle(Y) = \frac{\alpha_s C_A}{\pi^2} \int_{z_3} \tilde{\mathcal{K}}_{z_1 z_3 z_2} [\langle \mathcal{A}_{55}^{(3)} \rangle(Y) - \langle \mathcal{A}_{22}^{(3)} \rangle(Y)]. \quad (7.35)$$

The 3-point truncation of $\langle \mathcal{A}_{22}^{(3)} \rangle(Y)$ is easily computed by setting \mathbf{y}_1 and \mathbf{x}_1 to \mathbf{z}_1 in Eq. 7.30, the result of which is given by

$$\langle \mathcal{A}_{22}^{(3)} \rangle_3(Y) = \exp[-C_A \mathcal{P}_{z_1 z_2}(Y, Y_0)] \langle \mathcal{A}_{22}^{(3)} \rangle(Y_0), \quad (7.36)$$

where \mathcal{P} is defined in Eq. 7.7a. Given a real initial condition $\langle \mathcal{A}_{22}^{(3)} \rangle(Y_0)$, Eq. 7.36 remains real for all Y since \mathcal{P} is real.

The 3-point truncation of $\langle \mathcal{A}_{55}^{(3)} \rangle(Y)$ requires a little more work to compute since it is part of the bottom-right 2×2 , g^3 block inside Eq. 7.32. Let us denote this 2×2 , g^3 block by

$$\langle \mathcal{A}^{(g^3)} \rangle(Y) = \left\langle \begin{bmatrix} A_{55}^{(3)} & A_{56}^{(3)} \\ A_{65}^{(3)} & A_{66}^{(3)} \end{bmatrix} \right\rangle(Y), \quad (7.37)$$

such that $\langle \mathcal{A}_{55}^{(3)} \rangle(Y) = \langle \mathcal{A}_{11}^{(g^3)} \rangle(Y)$. It is easy to check that the diagonal elements of $\langle \mathcal{A}^{(g^3)} \rangle(Y)$ are purely real while its off-diagonal elements are purely imaginary. For simplicity let us write the symmetric and anti-symmetric components of $\langle \mathcal{A}^{(g^3)} \rangle(Y)$ as

$$\langle \mathcal{A}_{(1)}^{(g^3)} \rangle(Y) = \begin{bmatrix} a_{11}^{(1)}(Y) & ia_{12}^{(1)}(Y) \\ ia_{12}^{(1)}(Y) & a_{22}^{(1)}(Y) \end{bmatrix}, \quad \langle \mathcal{A}_{(2)}^{(g^3)} \rangle(Y) = \begin{bmatrix} 0 & ia_{12}^{(2)}(Y) \\ -ia_{12}^{(2)}(Y) & 0 \end{bmatrix}, \quad (7.38)$$

where $a_{11}^{(1)}, a_{12}^{(1)}, a_{22}^{(1)}$ and $a_{12}^{(2)}$ are all real-valued functions. The 3-point truncation of Eq. 7.37 has as its exponentiating matrices

$$\mathcal{M}_{(\alpha)}^{[3]}(Y) = \begin{bmatrix} m_{11}^{(\alpha)}(Y) & im_{12}^{(\alpha)}(Y) \\ im_{12}^{(\alpha)}(Y) & m_{11}^{(\alpha)}(Y) \end{bmatrix}, \quad (7.39)$$

for $\alpha = 1, 2$ where

$$m_{11}^{(\alpha)}(Y) = \frac{C_A}{2} \left[G_{(\alpha)z_1z_3}^{(2;\delta)} + G_{(\alpha)z_3z_2}^{(2;\delta)} + G_{(\alpha)z_1z_2}^{(2;\delta)} \right] (Y), \quad (7.40a)$$

$$m_{12}^{(\alpha)}(Y) = i \frac{C_A}{2} \sqrt{N_c^2 - 4} \left[G_{(\alpha)(z_1z_3)}^{(3;d)} + G_{(\alpha)(z_3z_2)}^{(3;d)} - G_{(\alpha)(z_1z_2)}^{(3;d)} \right] (Y). \quad (7.40b)$$

From Sec. 7.1, we know that the entries of Eq. 7.40 are real-valued functions only for $\alpha = 1$; for $\alpha = 2$ these entries are a priori complex-valued. Eq. 7.39 is diagonalizable with

$$\mathcal{M}_{(\alpha)}^{[3]}(Y) = \frac{1}{\sqrt{2}} \begin{bmatrix} -1 & 1 \\ 1 & 1 \end{bmatrix} \cdot \begin{bmatrix} m_{11}^{(\alpha)}(Y) - im_{12}^{(\alpha)}(Y) & 0 \\ 0 & m_{11}^{(\alpha)}(Y) + im_{12}^{(\alpha)}(Y) \end{bmatrix} \cdot \frac{1}{\sqrt{2}} \begin{bmatrix} -1 & 1 \\ 1 & 1 \end{bmatrix}, \quad (7.41)$$

from which one can write down the evolution operators as

$$\begin{aligned} \mathcal{E}_{(\alpha)}^{[3]}(Y, Y_0) &= P \exp \left[-\frac{1}{2} \int_{Y_0}^Y dY' \mathcal{M}_{(\alpha)}^{[3]}(Y') \right] \\ &= e^{-\frac{1}{2} \tilde{m}_{11}^{(\alpha)}(Y, Y_0)} \begin{bmatrix} \cos \left(\frac{1}{2} \tilde{m}_{12}^{(\alpha)}(Y, Y_0) \right) & -i \sin \left(\frac{1}{2} \tilde{m}_{12}^{(\alpha)}(Y, Y_0) \right) \\ -i \sin \left(\frac{1}{2} \tilde{m}_{12}^{(\alpha)}(Y, Y_0) \right) & \cos \left(\frac{1}{2} \tilde{m}_{12}^{(\alpha)}(Y, Y_0) \right) \end{bmatrix}, \end{aligned} \quad (7.42)$$

where

$$\tilde{m}_{11}^{(\alpha)}(Y, Y_0) = \int_{Y_0}^Y dY' m_{11}^{(\alpha)}(Y') = \frac{C_A}{2} [\mathcal{P}_{z_1z_3} + \mathcal{P}_{z_3z_2} + \mathcal{P}_{z_1z_2}] (Y, Y_0), \quad (7.43a)$$

$$\tilde{m}_{12}^{(\alpha)}(Y, Y_0) = \int_{Y_0}^Y dY' m_{12}^{(\alpha)}(Y') = -\frac{C_A}{2} \sqrt{\frac{N_c}{C_d}} [\mathcal{O}_{z_1z_3} + \mathcal{O}_{z_3z_2} - \mathcal{O}_{z_1z_2}] (Y, Y_0). \quad (7.43b)$$

Again, for $\alpha = 1$ the entries of Eq. 7.43 are real-valued functions, following the discussion from Sec. 7.1. Finally, the 3-point truncation of $\langle \mathcal{A}_{55}^{(3)} \rangle(Y)$ is given by

$$\begin{aligned} \langle \mathcal{A}_{55}^{(3)} \rangle_3(Y) &= \frac{1}{2} e^{-\tilde{m}_{11}^{(1)}(Y, Y_0)} \left[2 \sin(\tilde{m}_{12}^{(1)}(Y, Y_0)) a_{12}^{(1)}(Y_0) \right. \\ &\quad \left. + (\cos(\tilde{m}_{12}^{(1)}(Y, Y_0)) + 1) a_{11}^{(1)}(Y_0) + (\cos(\tilde{m}_{12}^{(1)}(Y, Y_0)) - 1) a_{22}^{(1)}(Y_0) \right]. \end{aligned} \quad (7.44)$$

Notice that the left-hand-side of Eq. 7.44 is purely real as required.

Having calculated Eq. 7.44 and Eq. 7.36, we are now able to express Eq. 7.35 in terms of the 3-point truncation which reads

$$\begin{aligned} \frac{d}{dY} \mathcal{P}_{z_1 z_2}(Y, Y_0) = & \frac{\alpha_2}{\pi^2} \int_{z_3} \tilde{\mathcal{K}}_{z_1 z_3 z_2} \left[1 - \frac{1}{2} \exp \left[-\frac{C_A}{2} [\mathcal{P}_{z_1 z_3} + \mathcal{P}_{z_3 z_2} - \mathcal{P}_{z_1 z_2}](Y, Y_0) \right] \right] \{ \\ & - i \sin \left[\frac{C_A}{2} \sqrt{\frac{N_c}{C_d}} [\mathcal{O}_{z_1 z_3} + \mathcal{O}_{z_3 z_2} - \mathcal{O}_{z_1 z_2}](Y, Y_0) \right] \left(\langle \mathcal{A}_{56}^{(3)} \rangle(Y_0) + \langle \mathcal{A}_{65}^{(3)} \rangle(Y_0) \right) \\ & + \left(\cos \left[\frac{C_A}{2} \sqrt{\frac{N_c}{C_d}} [\mathcal{O}_{z_1 z_3} + \mathcal{O}_{z_3 z_2} - \mathcal{O}_{z_1 z_2}](Y, Y_0) \right] + 1 \right) \langle \mathcal{A}_{55}^{(3)} \rangle(Y_0) \\ & + \left(\cos \left[\frac{C_A}{2} \sqrt{\frac{N_c}{C_d}} [\mathcal{O}_{z_1 z_3} + \mathcal{O}_{z_3 z_2} - \mathcal{O}_{z_1 z_2}](Y, Y_0) \right] - 1 \right) \langle \mathcal{A}_{66}^{(3)} \rangle(Y_0) \} \langle \mathcal{A}_{22}^{(3)} \rangle^{-1}(Y_0), \end{aligned} \quad (7.45)$$

where we recall that $\langle \mathcal{A}_{ij}^{(3)} \rangle(Y)$ is defined through Eq. 7.33. For convenience of reference, let me quote the result of Eq. 7.14a replacing $\mathbf{x}, \mathbf{y}, \mathbf{z}$ with z_1, z_2, z_3 :

$$\begin{aligned} \frac{d}{dY} \mathcal{P}_{z_1 z_2}(Y, Y_0) = & \frac{\alpha_s}{\pi^2} \int_{z_3} \tilde{\mathcal{K}}_{z_1 z_3 z_2} \left[1 - \exp \left[-\frac{C_A}{2} [\mathcal{P}_{z_1 z_3} + \mathcal{P}_{z_3 z_2} - \mathcal{P}_{z_1 z_2}](Y, Y_0) \right] \right] \\ & \times \cos \left[\frac{C_A}{2} [\mathcal{O}_{z_1 z_3} + \mathcal{O}_{z_3 z_2} - \mathcal{O}_{z_1 z_2}](Y, Y_0) - \theta_{z_1 z_2; z_3}^{(1+g)}(Y_0) + \theta_{z_1 z_2}^{(1)}(Y_0) \right] r_{z_1 z_2; z_3}^{(1+g)}(Y_0) \\ & \times \left(r_{z_1 z_2}^{(1)}(Y_0) \right)^{-1}. \end{aligned} \quad (7.46)$$

Certainly in the 2-point truncation (in the absence of Odderon terms), Eq. 7.45 and Eq. 7.46 can be made to coincide if the initial conditions are chosen such that

$$\langle \mathcal{A}_{55}^{(3)} \rangle(Y_0) \langle \mathcal{A}_{22}^{(3)} \rangle^{-1}(Y_0) = r_{z_1 z_2; z_3}^{(1+g)}(Y_0) \left(r_{z_1 z_2}^{(1)}(Y_0) \right)^{-1}. \quad (7.47)$$

However, in the 3-point truncation where the Odderon terms are kept, Eq. 7.45 cannot be made to coincide with Eq. 7.46 without setting all initial conditions to zero. Notice that the pre-factors in front of the Odderon terms inside the sine and cosine functions differ between Eq. 7.45 and Eq. 7.46; the pre-factors in the latter equation differ with those of the former equation by a factor of

$$\sqrt{\frac{N_c}{C_d}} = \sqrt{\frac{N_c^2}{N_c^2 - 4}}. \quad (7.48)$$

Interestingly, in the large N_c limit Eq. 7.48 tends to 1. In this limit, Eq. 7.45 can be reconciled with Eq. 7.46 by enforcing Eq. 7.47 and setting the other initial conditions of Eq. 7.45 ($\langle \mathcal{A}_{56}^{(3)} \rangle(Y)$, $\langle \mathcal{A}_{66}^{(3)} \rangle(Y)$ and $\langle \mathcal{A}_{65}^{(3)} \rangle(Y)$) to zero. However, in order to reconcile these equations at finite N_c (i.e. $N_c = 3$), one clearly needs a higher order truncation of the $q^2 \bar{q}^2$ correlator matrix. That we need a higher order truncation is not wholly unreasonable, because we are trying to satisfy *three* equations — the real and imaginary parts of Eq. 7.1 as well as Eq. 7.35 (which is

purely real) — with only *two* degrees of freedom, the Pomeron and Odderon 2-point functions.

Chapter 8

Conclusion

I begin this chapter by summarizing the main results derived in this thesis in Sec. 8.1. Then, in Sec. 8.2 I provide an outlook for promising future cross-pollination between the work presented in this thesis and other closely related branches of theoretical high-energy physics research.

8.1 Thesis summary

In high-energy hadronic scattering experiments — experiments which involve a high-energy dilute projectile (a lepton or a hadron) scattering off some hadronic target — the gluon density of the hadronic wave-function rises steeply with decreasing Bjorken x_{bj} and eventually saturates. In this saturation regime, the parton model no longer provides a valid description for the process since the quondam assumption that partons in the hadronic wave-function scatter independently is bygone. Instead, these partons scatter coherently which precipitates important non-linear effects.

The CGC is an effective description of QCD in the Regge-Gribov limit which accounts for these non-linearities. In the CGC formalism, the gluon-saturated hadron is represented by a large (background) classical colour field. This background field is Lorentz contracted, with delta-function-like support in the direction of the collision axis and time dilated such that it appears static on the natural timescales of the strong interaction. Interactions with this background field are then mediated by virtual, coloured probes. Being highly energetic, they pierce the (almost) infinitely Lorentz contracted target without being displaced from their original trajectories: this is known as the eikonal approximation. Despite not being displaced, the coloured probes undergo multiple soft gluon interactions with the background field which when resummed generate Wilson-lines.

These Wilson-lines are the appropriate collective degrees of freedom for describing scattering in the saturation formalism. They enter the description of observables, like the cross-section, through rapidity-dependent averages called Wilson-line correlators. The averaging procedure (see Eq. 5.1) is rapidity-dependent because the isolation of the background field is a rapidity-dependent (factorization) definition: as the rapidity separation between the projectile and the target increases, soft gluonic modes which were previously regarded as quantum fluctuations atop the background field become subsumed into a redefinition of the background field through the aforementioned special relativistic effects of Lorentz contraction and time dilation.

The JIMWLK equation is a functional renormalization group (RG) equation for the rapidity evolution of Wilson-line correlators in the CGC formalism. Although written as a single (functional) equation, the JIMWLK equation generates an infinite tower of coupled integro-differential equations known as the Balitsky hierarchy¹. At leading-logarithm, the JIMWLK equation is also a functional Fokker-Planck equation which means that it can be recast as a Langevin problem and solved numerically. However, at next-to-leading logarithm this ceases to be so, in which case one requires a scheme for truncating the Balitsky hierarchy in order to obtain a solution (if only an approximate one).

One of the chief outputs of this thesis is a gauge-invariant and symmetry-preserving truncation of the Balitsky hierarchy. In particular, the latter “symmetry-preserving” property is an original contribution of mine. The truncation follows from a peculiar parameterization for the rapidity evolution of Wilson-line correlator matrices. The parameterization, which I methodically formulated in Sec. 6.1, is expressed in terms of rapidity evolution operators which evolve the symmetric and anti-symmetric parts of Wilson-line correlator matrices separately in a manner akin to the time evolution of Hermitian operators in the Heisenberg picture of quantum mechanics. Moreover, the independent parameterization of symmetric and anti-symmetric parts is manifestly symmetric and anti-symmetric, respectively, and in this sense is “symmetry-preserving”. The rapidity evolution operators are expressed as path-ordered exponentials where the exponent is an integral of a rapidity-dependent matrix (which we called the exponentiating matrix) which can be decomposed into a complete sum over contributions from linearly independent colour structures and colour structure functions.

In addition to establishing the “symmetry-preserving” property of the above truncation, I was also able to disentangle (some of) its systematic features. In Sec. 6.2 I explained in general how for colour structures constructed as eigenstates of special symmetry projection operators (see Sec. 4.2.3) the symmetry features of these colour structures are imprinted onto their associated colour structure functions. This idea, although originally my supervisor’s, was one whose details he and I ironed out together. Then, in Sec. 6.3 I scrutinized (some of) the properties of contributions to the exponentiating matrix emanating from each term in the complete sum.

¹Historically, this hierarchy is independent from the JIMWLK equation.

There I proved two original results. The first result gave a sufficient condition for when a contribution to the exponentiating matrix will be purely symmetric or anti-symmetric (Thm 6.1). This result was proved independent of the Wilson-line correlator matrix being parameterized. The second result (Thm 6.2) pertained to the behaviour of exponentiating matrix contributions under a simultaneous pairwise swap of quark–anti-quark pair transverse coordinate labels.

The requirement that our parameterization/truncation be “symmetry-preserving” followed from an observation I made in Sec. 5.2.2 where I calculated the JIMWLK equation for a general Wilson-line correlator matrix; this is recorded in Eq. 5.98. From Eq. 5.98 I noticed that the evolution of the symmetric part of the Wilson-line correlator matrix was driven only by the symmetric parts of a slightly larger Wilson-line correlator matrix of which the original Wilson-line correlator matrix is a sub-block. Similarly, the evolution of the anti-symmetric part was driven only by the anti-symmetric parts of this slightly larger matrix. In particular, symmetric and anti-symmetric parts evolve separately. This is not wholly surprising since the target average is linear and operates component-wise for Wilson-line correlator matrices and these matrices can always be decomposed into a sum of their symmetric and anti-symmetric pieces.

Another advantage of the form of the JIMWLK equation given in Eq. 5.98 is that it shows precisely how the JIMWLK equation couples the distinct sub-blocks within the slightly larger Wilson-line correlator matrix mentioned above. In Sec. 4.4, I showed, in general, how the $q^m \bar{q}^m$ correlator matrix (for $m \in \mathbb{N}^+$) can be embedded inside the $q^{(m+1)} \bar{q}^{(m+1)}$ correlator matrix when the latter is constructed in an embedding basis. The Fierz bases are all examples of embedding bases. In the limit that the transverse coordinates on the last quark–anti-quark pair of Wilson-lines become coincident, the $q^{(m+1)} \bar{q}^{(m+1)}$ correlator matrix block-diagonalizes into two sub-blocks. The top-left sub-block is the original $q^m \bar{q}^m$ correlator matrix while the bottom-right sub-block is the $q^m \bar{q}^m g$ correlator matrix and it is precisely these two sub-blocks that are coupled by the JIMWLK equation which I highlighted in Eq. 5.98.

Finally, in Sec. 7.2 I computed the (full) 3-point truncation of the $q^2 \bar{q}^2$ correlator matrix — an original calculation — which I showed was the smallest correlator matrix capable of accessing all colour structure functions available at the third order. The 3-point truncation is necessary in order to parameterize, for instance, the JIMWLK evolution of the argument of the $q\bar{q}$ correlator where the $q\bar{q}$ correlator is embedded inside the $q^2 \bar{q}^2$ correlator matrix in the manner described in the previous paragraph. Another new result appears in Sec. 7.3; here I demonstrated that the 3-point truncation of the $q^2 \bar{q}^2$ correlator matrix, and consequently the 2-point truncation given in [19], cannot consistently parameterize the JIMWLK evolution of the $q^2 \bar{q}^2$ correlator. Consequently a higher order truncation is required; this will be the topic of future research.

8.2 Outlook

It is now well established that in gauge theories like QED and QCD (as well as in perturbative quantum gravity) the infrared (IR) divergent contributions to scattering amplitudes *factorize*. For a scattering amplitude $i\mathcal{M}$ producing L outgoing hard particles, this factorization has the following schematic structure (see [7, 46–53])

$$i\mathcal{M} \sim \mathcal{H} \cdot \mathcal{S} \cdot \left[\prod_{i=1}^L \frac{J_i}{\mathcal{J}_i} \right], \quad (8.1)$$

where it is assumed that the renormalization of ultraviolet (UV) divergences has already been performed. The *hard function* \mathcal{H} can be thought of as the “tree-level” (no loops) amplitude for the scattering process which is finite in four space-time dimensions with no IR singularities. The *soft function* \mathcal{S} contains all *soft singularities* associated with the exchange of virtual particles (photons in QED and gluons in QCD) which are soft in the sense that their four-momenta tend to zero. For each $i = 1, \dots, L$, the factor J_i is called a *jet function* which contains all *collinear singularities* associated with the i^{th} outgoing hard particle. Since particles emitted co-linearly can also be soft, the associated singularities are doubly accounted for in the soft function as well as in the jet functions. This double counting is then corrected by dividing each jet function J_i by a corresponding *eikonal jet function* \mathcal{J}_i which may be regarded as the soft limit evaluation of the jet function J_i .

Eq. 8.1 follows from a systematic analysis of all possible IR (both soft and collinear) singularities that can arise in loop diagrams (in Minkowski space) with a fixed number of incoming and outgoing hard particles. IR singularities may materialize in loop integrals when poles in the integrand coalesce; in this case the contour is said to be *pinched* since it cannot be deformed away from the poles. These *pinches* or *pinch surfaces* are given by solutions to the *Landau equations* [54], but they only provide a necessary condition for when IR singularities may materialize. However, from the Landau equations and *infrared power counting* [54] one is able to write down Eq. 8.1.

Of particular interest to us is the soft function and we now restrict our discussion to QCD dominated processes. Having an infinite Compton wavelength, the soft gluons which constitute the soft function cannot resolve the internal structure of the jets; all they can see is the overall colour charge of each jet [53]. Conveniently, this means that the soft function has a Feynman diagram interpretation of its own in terms of *eikonal Feynman rules*. One builds up the soft function perturbatively by considering the exchange of multiple soft gluons between hard particle lines. For example, consider the one-loop diagram given in Fig. 8.1 which consists of a single soft gluon being exchanged between an outgoing quark and anti-quark, both emanating from a common vertex. This diagram represents the following integral

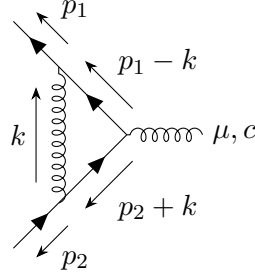


FIGURE 8.1: A single gluon exchanged between an outgoing quark and anti-quark emanating from a common vertex. Time runs from right to left.

$$i\mathcal{M}_{g \rightarrow q\bar{q}(+g)}^{\mu c} = \int \frac{d^d k}{(2\pi)^d} \frac{-i\eta_{\alpha\beta}\delta^{ab}}{k^2 - i\varepsilon} \times \bar{u}(p_1)(ig\gamma^\alpha t^a) \frac{\not{p}_1 - \not{k}}{(p_1 - k)^2 - m^2 + i\varepsilon} (ig\gamma^\mu t^c) \frac{\not{p}_2 + \not{k}}{(p_2 + k)^2 - m^2 + i\varepsilon} (ig\gamma^\beta t^b)v(p_2), \quad (8.2)$$

which, in $d = 4$ space-time dimensions, is logarithmically divergent in the IR as well as in the UV. The latter divergence can be removed by renormalizing the QCD coupling g such that Eq. 8.2 is UV finite in $d = 4$ space-time dimensions. In the *soft- or eikonal-limit* ($k \rightarrow 0$), Eq. 8.2 becomes

$$\begin{aligned} i\mathcal{M}_{g \rightarrow q\bar{q}(+g)}^{\mu c} &\xrightarrow{k \rightarrow 0} \underbrace{[\bar{u}(p_1)ig\gamma^\mu t^c v(p_2)]}_{=i\mathcal{M}_{g \rightarrow q\bar{q}}^{\mu c}} \frac{g^2}{2N_c} \int \frac{d^d k}{(2\pi)^d} \left[\frac{p_2^\beta}{p_2 \cdot k} \right] \left[-\frac{p_1^\alpha}{p_1 \cdot k} \right] \left[\frac{-i\eta_{\alpha\beta}}{k^2} \right] \\ &= i\mathcal{M}_{g \rightarrow q\bar{q}}^{\mu c} \frac{ig^2}{2N_c} \int \frac{d^d k}{(2\pi)^d} \frac{p_1 \cdot p_2}{k^2 p_1 \cdot k p_2 \cdot k}, \end{aligned} \quad (8.3)$$

where we ignored factors of \not{k} in the numerator and linearized the denominators of the fermion propagators, dropping $\mathcal{O}(k^2)$ terms. Eq. 8.3 is still logarithmically IR divergent in $d = 4$ space-time dimensions (the same logarithmic IR divergence that was present in Eq. 8.2). However, in taking the eikonal-limit we have introduced an additional, artificial UV singularity that is not accounted for in renormalized perturbation theory. Explicitly evaluating the integral in Eq. 8.3, one finds that the IR and UV singular contributions precisely cancel each other, producing zero. This cancellation or one-to-one correspondence between IR and UV singularities is true in general for the eikonal-limit. For a fixed number of fermion legs, resumming all eikonal diagrams (diagrams involving only the exchange of multiple soft gluons) produces Wilson-line operators which dress each fermion leg. Given the above discussion, it is not difficult to see that the UV singularities of these Wilson-line operators are in one-to-one correspondence with the IR singularities of scattering amplitudes.

For this reason we seek to isolate the UV singularities of Wilson-line operators which we do by replacing the usual QCD Wilson-line operators [7]

$$U_{n_i}[A] := P \exp \left[ig \int_0^\infty dt n_i^\mu A_\mu(tn_i) \right]. \quad (8.4)$$

by

$$U_{n_i}^{(m)}[A] := P \exp \left[ig\mu^\epsilon \int_0^\infty dt n_i^\mu A_\mu(tn_i) e^{-imt\sqrt{n_i^2 - i\epsilon}} \right]. \quad (8.5)$$

where m is an IR regulator (additional to the one already present in dimensional regularization) which smoothly cuts off the IR singularity of Eq. 8.4 such that only UV poles in ϵ are left. In the limit that $m \rightarrow 0$, Eq. 8.5 reduces to Eq. 8.4. Eq. 8.5 denotes the Wilson-line operator dressing the i^{th} outgoing hard particle whose trajectory is given by $x_i^\mu(t) = tn_i^\mu$ where n_i^μ is a constant four-vector proportional to the particle's four-momentum p_i^μ .

The soft function in Eq. 8.1 can be written as a *vacuum expectation value* (VEV) of L Wilson-lines operators (of the form given in Eq. 8.5)

$$\mathcal{S}_B \left(\gamma_{ij}, \alpha_s(\mu^2), \epsilon, \frac{m}{\mu} \right) := \langle 0 | U_{n_1}^{(m)}[A] \otimes \cdots \otimes U_{n_L}^{(m)}[A] | 0 \rangle, \quad (8.6)$$

where γ_{ij} is proportional to the normalized inner-product between n_i^μ and n_j^μ

$$\gamma_{ij} = 2\hat{n}_i \cdot \hat{n}_j, \quad (8.7)$$

and μ is the dimensional regularization scale. With this definition, the soft function is finite in $d = 4 - 2\epsilon$ space-time dimensions for $\epsilon > 0$. Eq. 8.6 can be multiplicatively renormalized (see [55–59]) where the renormalized soft function is defined by

$$\mathcal{S}_R \left(\gamma_{ij}, \alpha_s(\mu^2), \epsilon, \frac{m}{\mu} \right) := \mathcal{S}_B \left(\gamma_{ij}, \alpha_s(\mu^2), \epsilon, \frac{m}{\mu} \right) Z \left(\gamma_{ij}, \alpha_s(\mu^2), \epsilon \right), \quad (8.8)$$

and is finite in the limit that $\epsilon \rightarrow 0$. The multiplicative factor² Z collects all UV counter-terms and satisfies the following RG equation

$$\frac{d}{d \ln(\mu)} Z \left(\gamma_{ij}, \alpha_s(\mu^2), \epsilon \right) = -Z \left(\gamma_{ij}, \alpha_s(\mu^2), \epsilon \right) \Gamma \left(\gamma_{ij}, \alpha_s(\mu^2), \epsilon \right), \quad (8.9)$$

where Γ is the *soft anomalous dimension* and is finite in $d = 4$ space-time dimensions. Like Z , Γ is a matrix in colour space.

²This is a matrix in colour space.

Eq. 8.9 is intriguing to us because it bears some resemblance to our novel parameterization for the JIMWLK evolution of Wilson-line correlator matrices in the CGC context. In fact, if we had not required our parameterization to be symmetry-preserving (only gauge-invariant) then we could easily have written

$$\frac{d}{d \ln(x_{\text{bj}})} \langle \mathcal{A} \rangle(x_{\text{bj}}) = \overbrace{\langle \mathcal{A} \rangle(x_{\text{bj}}) \langle \mathcal{A} \rangle^{-1}(x_{\text{bj}})}^{\mathbb{1}} \underbrace{\frac{d}{d \ln(x_{\text{bj}})} \langle \mathcal{A} \rangle(x_{\text{bj}})}_{=:-\mathcal{N}(x_{\text{bj}})} = -\langle \mathcal{A} \rangle(x_{\text{bj}}) \mathcal{N}(x_{\text{bj}}), \quad (8.10)$$

where $\ln(x_{\text{bj}}) = Y$. Note that Eq. 8.10 can be mapped onto our original parameterization given in Eq. 6.15 if $\mathcal{M}_{(1)}(Y) = \mathcal{M}_{(2)}(Y)$.³ Comparing Eq. 8.10 with Eq. 8.9 one is tempted to interpret $\mathcal{N}(x_{\text{bj}})$ as the anomalous dimension for the Wilson-line correlator matrix $\langle \mathcal{A} \rangle(x_{\text{bj}})$. Both equations Eq. 8.9 and Eq. 8.10 admit a path-order exponential solution; the solution to the former equation is given by

$$Z(\gamma_{ij}, \alpha_s(\mu^2), \epsilon) = Z(\gamma_{ij}, \alpha_s(\mu_0^2), \epsilon) \bar{P} \exp \left[- \int_{\ln(\mu_0)}^{\ln(\mu)} d \ln(\mu') \Gamma(\gamma_{ij}, \alpha_s(\mu'^2), \epsilon) \right], \quad (8.11)$$

while the latter equation's solution is given by

$$\langle \mathcal{A} \rangle(x_{\text{bj}}) = \langle \mathcal{A} \rangle(x_{\text{bj}0}) \bar{P} \exp \left[- \int_{\ln(x_{\text{bj}0})}^{\ln(x_{\text{bj}})} d \ln(x_{\text{bj}}') \mathcal{N}(x_{\text{bj}}') \right]. \quad (8.12)$$

\bar{P} denotes the anti-path-ordering symbol with respect to the variable of integration. The path-ordered exponential in Eq. 8.11 can be written as an ordinary (matrix) exponential (see Eq. (2.5) of [55] as well as Eq. (2.11) of [60]) using the *Magnus expansion* [61] where the exponent of the ordinary matrix exponential is written in terms of matrices $\Gamma^{(n)}$ which are the coefficients of Γ in an expansion in α_s . These coefficient matrices $\Gamma^{(n)}$ can be computed directly in terms of *webs* (see Eq. (2.15) of [60]).

Why is this useful to us? Given the striking similarity between Eq. 8.10 (which can be mapped onto Eq. 6.15) and Eq. 8.9, it seems natural to ask to what extent the formalisms around these two equations can be linked and contrasted. Can the machinery of webs be employed in the context of the CGC to compute and give physical interpretation to contributions to the exponentiating matrix? Correspondingly, can the results that we prove in this thesis about contributions to the exponentiating matrix be applied in the context of webs and the *mixing matrix formalism*? (see [7] for a review.)

These tantalizing questions, although outside the scope of this thesis, suggest that the original work presented herein may have application beyond the JIMWLK context, and may eventually lead to a (more) unified formalism for the evolution of Wilson-line correlators.

³This mapping can be easily derived by expressing the Wilson-line correlator matrix $\langle \mathcal{A} \rangle(Y = \ln(x))$ as a column vector and then rewriting both Eq. 8.10 and Eq. 6.15 as linear matrix equations for this vector.

Appendix A

Standard pQFT results

A.1 Radiating a soft and co-linear, on-shell gluon from a hard quark



(A) No gluon radiated.

(B) One gluon radiated.

FIGURE A.1: The factorized production (represented by the blob) of an outgoing hard quark with momentum p , spin s and colour i accompanied (right) and un-accompanied (left) by the emission of an on-shell gluon with momentum k , adjoint colour index a , and transverse polarization λ . Time runs from right to left.

In this section, we demonstrate the claim made in the introduction to this thesis that the emission of a single soft gluon produces Sudakov logarithm in energy.

Consider the process depicted in Fig. A.1a. Let us define its matrix element to be

$$\text{Fig. A.1a} = i\mathcal{M}_q(p, s, i) = \bar{u}_i^s(p)[i\mathcal{M}_q(p)]_i, \quad (\text{A.1})$$

where $[i\mathcal{M}(p)]_i$ represents the factorized production of a hard quark with momentum p and colour i . In this section, repeated colour indices such as those in Eq. A.1 are not to be assumed implicitly summed over; any sum over colour indices shall be made explicit. In order to compute the cross-section for this process, one needs to take the square of the modulus of Eq. A.1 and

sum over final spins s and colours i [6] which yields

$$\sum_s \left| \sum_{i=1}^3 i\mathcal{M}_q(p, s, i) \right|^2 = \sum_{i,j=1}^3 \sum_s [i\mathcal{M}_q(p)]_i^* u_i^s(p) \bar{u}_j^s(p) [i\mathcal{M}_q(p)]_j = \sum_{i=1}^3 |[i\mathcal{M}_q(p)]_i|^2 (\not{p} + m_q), \quad (\text{A.2})$$

where in going to the last equality we used the spinor identity

$$\sum_s u_i^s(p) \bar{u}_j^s(p) = \delta_{ij} (\not{p} + m_q). \quad (\text{A.3})$$

Since the outgoing quark is “hard”, its momentum is approximately light-like and one may ignore its mass m_q in Eq. A.3 and therefore in Eq. A.2 too.

Now suppose the outgoing hard quark emits a soft and co-linear, on-shell gluon as in Fig. A.1b. Then the invariant matrix element is modified from Eq. A.1 as follows

$$\text{Fig. A.1b} = i\mathcal{M}_{q+g}(p, s, i; k, a, \lambda) = \sum_{j=1}^3 \bar{u}_i^s(p) (igt_{ij}^a \gamma^\mu) \frac{i(\not{p} + \not{k} + m_q)}{(p+k)^2 - m_q^2 + i\varepsilon} [i\mathcal{M}_q(p)]_j \epsilon_\mu^\lambda(k)^*, \quad (\text{A.4})$$

Working in the limit that the outgoing quark effectively has zero mass, the magnitude of the quark’s 3-momentum $|\vec{p}|$ is equal to the quark’s energy E_p . Consequently, the denominator of the propagator in Eq. A.4 becomes

$$2p \cdot k = 2(E_p E_k - \vec{p} \cdot \vec{k}) = 2E_p E_k (1 - \cos \theta_{pk}), \quad (\text{A.5})$$

where θ_{pk} is defined to be the angle between the 3-momenta \vec{p} and \vec{k} . Eq. A.5 vanishes when the gluon is radiated either softly ($E_k \rightarrow 0$) or co-linearly to the quark ($\theta_{pk} \rightarrow 0$). In the soft limit one may neglect the \not{k} term in the numerator of the propagator in Eq. A.4. Using the defining anti-commutator relation for Dirac matrices

$$\{\gamma^\mu, \gamma^\nu\} = 2g^{\mu\nu} \mathbb{1}_{4 \times 4}, \quad (\text{A.6})$$

and the Dirac equation for $\bar{u}(p)$

$$0 = \bar{u}(p)(\not{p} + m_q) = \bar{u}(p)\not{p} + \mathcal{O}(m_q), \quad (\text{A.7})$$

Eq. A.4 becomes

$$i\mathcal{M}_{q+g}(p, s, i; k, a, \lambda) = \bar{u}_i^s(p) [J_{q+g}(p; k, a, \lambda)]_{ij} [i\mathcal{M}_q(p)]_j, \quad (\text{A.8})$$

where

$$[J_{q+g}(p; k, a, \lambda)]_{ij} = -gt_{ij}^a \frac{p \cdot \epsilon^\lambda(k)^*}{p \cdot k + i\varepsilon}, \quad (\text{A.9})$$

is called the eikonal current. Taking the square of the modulus of Eq. A.8 and summing over final spins s , fundamental colours i , adjoint colours a and transverse polarizations λ , one obtains

$$\sum_s \sum_{a=1}^8 \sum_{\lambda=1}^2 \left| \sum_{i=1}^2 3i \mathcal{M}_{q+g}(p, s, i; k, a, \lambda) \right|^2 = g^2 C_f \sum_{\lambda=1}^2 \left| \frac{p \cdot \epsilon^\lambda(k)^*}{p \cdot k} \right|^2 \sum_s |[i \mathcal{M}_q(p)]_i|^2 (\not{p} + m_q), \quad (\text{A.10})$$

where we again used Eq. A.3 and the definition of the quadratic Casimir in the fundamental representation

$$\sum_{a=1}^8 t^a t^a = C_f \mathbb{1} \quad \text{where} \quad C_f = \frac{4}{3}. \quad (\text{A.11})$$

Comparing Eq. A.10 and Eq. A.2, one sees that the net effect of radiating a soft on-shell gluon is to multiply Eq. A.2 by the factor

$$g^2 C_f \sum_{\lambda=1}^2 \left| \frac{p \cdot \epsilon^\lambda(k)^*}{p \cdot k} \right|^2. \quad (\text{A.12})$$

This means that for any cross-section associated with Eq. A.2, the emission of a single soft gluon leads to a modification by a factor Eq. A.12 integrated over the Lorentz invariant phase space (LIPS) measure of the radiated gluon.

In order to compute this modification explicitly, let us introduce explicit 4-vectors for the momenta p and k as well as the polarization vector ϵ . Suppose that the intermediate (off-mass-shell) quark had a light-cone energy E^+ and no transverse momentum, i.e.

$$p^\mu + k^\mu = [E^+, p^- + k^-, \mathbf{0}_\perp]^\mu, \quad (\text{A.13})$$

where the square brackets $[\dots]$ represent a 4-vector in light-cone coordinates¹. Suppose also that the radiated gluon carries a small fraction $x_{\text{bj}} \ll 1$ (since it is soft) of the light-cone energy away. Using energy-momentum conservation and the (effective) massless of the outgoing quark and gluon, one obtains

$$k^\mu = [xE^+, \frac{k_\perp^2}{2xE^+}, \mathbf{k}_\perp]^\mu, \quad (\text{A.14a})$$

$$p^\mu = [(1-x)E^+, \frac{k_\perp^2}{2(1-x)E^+}, -\mathbf{k}_\perp]^\mu. \quad (\text{A.14b})$$

¹Given a 4-vector $v^\mu = (v^0, \vec{v})^\mu$ in standard coordinates, its light-cone representation is defined as $v^\mu = [v^+, v^-, \mathbf{v}_\perp]^\mu$ where $v^\pm := \frac{1}{\sqrt{2}}(v^0 \pm v^3)$ and $\mathbf{v}_\perp = (v^1, v^2)$.

The polarization vector must satisfy $g^{\mu\nu}\epsilon_\mu^\lambda(k)\epsilon_\nu^{\lambda'}(k) = -\delta^{\lambda\lambda'}$ and $k.\epsilon^\lambda(k) = 0$ for all $\lambda, \lambda' = 1, 2$ [1]. Choosing the axial gauge $\epsilon^{\lambda-}(k) = \epsilon_+^\lambda(k) = 0$, the polarization vector is given by

$$\epsilon_\mu^\lambda(k) = [0, \frac{\epsilon_\perp^\lambda \cdot k_\perp}{xE^+}, \epsilon_\perp^\lambda]^\mu, \quad \text{where} \quad \epsilon_\perp^\lambda = \hat{e}_\perp^\lambda = \begin{cases} (1, 0) & \text{if } \lambda = 1 \\ (0, 1) & \text{if } \lambda = 2 \end{cases}. \quad (\text{A.14c})$$

Using Eq. A.14, Eq. A.12 evaluates to

$$g^2 C_f \sum_{\lambda=1}^2 \left| \frac{p.\epsilon^\lambda(k)^*}{p.k} \right|^2 = \frac{4g^2 C_f}{k_\perp^2} (1-x) \stackrel{x \ll 1}{\approx} \frac{4g^2 C_f}{k_\perp^2}. \quad (\text{A.15})$$

Finally, the integrating Eq. A.15 over the LIPS measure of the radiated gluon yields

$$\begin{aligned} & \int \frac{d^4 k}{(2\pi)^4} (2\pi) \delta(k^2) \theta(k^0) \frac{4g^2 C_f}{k_\perp^2} \\ &= 4g^2 C_f \int \frac{dk^+ dk^- d^2 k_\perp}{(2\pi)^3} \delta(2k^+ k^- - k_\perp^2) \theta\left(\frac{1}{\sqrt{2}}(k^+ + k^-)\right) \frac{1}{k_\perp^2} \\ &= 4g^2 C_f \frac{1}{(2\pi)^2} \frac{1}{4} \int_{-\infty}^{\infty} \frac{dk^+}{k^+} \int_0^{\infty} \frac{dk_\perp^2}{k_\perp^2} \theta\left(\frac{k^+}{\sqrt{2}} \left(1 + \frac{k_\perp^2}{2(k^+)^2}\right)\right) \\ &= \frac{\alpha_s C_f}{\pi} \int_0^{\infty} \frac{dk^+}{k^+} \int_0^{\infty} \frac{dk_\perp^2}{k_\perp^2}, \end{aligned} \quad (\text{A.16})$$

where in going to the third line we used the integral over k^- to eliminate the Dirac delta function and we recast $\int d^2 k_\perp$ in polar coordinates as $\int_0^\infty dk_\perp k_\perp \int_0^{2\pi} d\phi = 2\pi \int_0^\infty dk_\perp k_\perp = \pi \int_0^\infty dk_\perp^2$, and in going to the last line we used the fact that the argument of the theta function is always positive provided k^+ is always positive in order to restrict the lower bound on the k^+ integral to zero. Ignoring the co-linear singularity associated with the integral over k_\perp^2 for a moment, one sees that there is a soft singularity associated with the k^+ integral. By restricting the range of the k^+ integral to be between physical limits such as the minimum energy that the detector can resolve k_{res}^+ and the factorization scale μ of the processes depicted in Fig. A.1, one obtains a SSL

$$\int_{k_{\text{res}}^+}^{\mu} \frac{dk^+}{k^+} = \ln(\mu/k_{\text{res}}^+), \quad (\text{A.17})$$

as promised which is large for $\mu \gg k_{\text{res}}^+$.

Appendix B

Propagators in the presence of a large background field

In this chapter, I compute the propagators for fermions and gluons in the presence of the target background field via the spectral method. The fermion propagator is used to compute the total cross-section for DIS given in Sec. 3.2. The gluon propagator is used extensively in Sec. 5.1 to derive the JIMWLK Hamiltonian at leading logarithmic accuracy. Since the gluon propagator is written in terms of the propagator for a scalar, I shall begin by deriving the scalar propagator in the presence of the target background field. For convenience I recall that the target background field is given by

$$b^\mu(x^+, x^-, \mathbf{x}) = g^{\mu-} \delta(x^-) \beta(\mathbf{x}) = g^{\mu-} \delta(x^-) \beta^a(\mathbf{x}) t^a, \quad (\text{B.1})$$

where x^+ is assumed to be zero unless otherwise stated.

B.1 The Scalar Propagator

Consider a massless complex-valued scalar field $\phi : \mathbb{R}^{1,3} \rightarrow \mathbb{C}^{N_c}; x \mapsto \phi(x) = \phi_i(x) \hat{e}_i$ whose dynamics are governed by the Lagrangian

$$\mathcal{L}_{\text{scalar}}[\phi, b](x) := -\frac{1}{2} \phi^\dagger(x) D_x [b]^2 \phi(x) = -\frac{1}{2} \phi_i^\dagger(x) D_\mu^x [b]_{ij} D_x^\mu [b]_{jk} \phi_k(x), \quad (\text{B.2})$$

where the covariant derivative in the fundamental representation is defined as

$$D_\mu^x [b]_{ij} := (\partial_\mu^x - ig b_\mu(x))_{ij} = \partial_\mu^x \delta_{ij} - ig b_\mu^a(x) t_{ij}^a. \quad (\text{B.3})$$

The square¹ of Eq. B.3

$$(-iD_x[b])^2 = -D_x[b]^2 = -2\partial^+\partial^- + \partial_\perp^2 + 2igb^+(x)\partial^-, \quad (\text{B.4})$$

can be inverted using the spectral method: if there exists a complete set of eigenfunctions $\{\phi(x; k) = \}_{k \in \mathbb{R}^{1,3}}$ such that

$$-D_x[b]^2 \phi(x; k) = k^2 \phi(x; k), \quad \int \frac{d^4 k}{(2\pi)^4} |\phi(x; k)|^2 = \delta^{(4)}(x - y) \mathbb{1}, \quad (\text{B.5})$$

then the inverse of Eq. B.4 can be computed as

$$\begin{aligned} \left[\frac{i}{-D[b]^2} \right] (x, y) &:= \langle x | \frac{i}{-D[b]^2 + i\varepsilon} | y \rangle \\ &= \langle x | \frac{i}{-D[b]^2 + i\varepsilon} \left(\int \frac{d^4 k}{(2\pi)^2} |k\rangle \langle k| \right) | y \rangle \\ &= \int \frac{d^4 k}{(2\pi)^4} \frac{i}{k^2 + i\varepsilon} \phi(x; k) \phi^\dagger(y; k), \end{aligned} \quad (\text{B.6})$$

where we have specified the Feynman pole prescription. This inverse is the propagator for the scalar field in the presence of Eq. B.1 which we shall sometimes write as

$$\left[\frac{i}{-D[b]^2} \right] (x, y) = \langle \phi(x) \phi(y) \rangle [b] = . \quad (\text{B.7})$$

Consider the following ansatz for the eigenfunctions

$$\phi(x; k) := \int d^2 p_\perp e^{-ip \cdot x} \int \frac{d^2 z_\perp}{(2\pi)^2} e^{-i(\mathbf{p}-\mathbf{k}) \cdot \mathbf{z}} U_{\mathbf{z}; x^-, -\infty}, \quad (\text{B.8})$$

where

$$p^- = k^-, \quad p^+ = \frac{p_\perp^2 + k^2}{2k^-}, \quad (\text{B.9})$$

and

$$U_{\mathbf{z}; x^-, -\infty} := P \exp \left[ig \int_{-\infty}^{x^-} dz^- b^+(z) \right] = \exp[ig\theta(x^-)\beta(\mathbf{z})]. \quad (\text{B.10})$$

Notice that for $x^- < 0$ or $\beta(\mathbf{x}) = 0$, Eq. B.8 can be regarded as a free particle, because Eq. B.10 reduces to the identity matrix, Eq. B.8 reduces to the plane-wave ansatz

$$\phi(x; k) = \exp \left[-i \left(\left(\frac{k_\perp^2 + k^2}{2k^-} \right) x^- + k^- x^+ - \mathbf{k} \cdot \mathbf{x} \right) \right], \quad (\text{B.11})$$

¹I include the factor of $(-i)^2$ in the definition of the differential operator in Eq. B.4 to connect with square of the covariant momentum operator.

which, for all $k \in \mathbb{R}^{1,3}$, forms a complete set of eigenfunctions for the Klein-Gordon operator $-D_x[0]^2 = -2\partial^+\partial^- + \partial_\perp^2$. However, one needs to confirm that Eq. B.8 satisfies Eq. B.5. To this end, using the fact that $p^2 = k^2$, which follows from Eq. B.9, one easily obtains

$$\begin{aligned} -D_x[b]^2\phi_k(x) &= k^2\phi(x; k) \\ &+ 2gk^-\delta(x^-) \int d^2p_\perp e^{-ip \cdot x} \int \frac{d^2z_\perp}{(2\pi)^2} e^{-i(\mathbf{p}-\mathbf{k}) \cdot \mathbf{z}} (\beta(\mathbf{x}) - \beta(\mathbf{z})) U_{\mathbf{z}; x^-, -\infty}. \end{aligned} \quad (\text{B.12})$$

The latter term involving $\delta(x^-)$ vanishes because

$$\begin{aligned} &\delta(x^-) \int d^2p_\perp e^{-ip \cdot x} \int \frac{d^2z_\perp}{(2\pi)^2} e^{-i(\mathbf{p}-\mathbf{k}) \cdot \mathbf{z}} (\beta(\mathbf{x}) - \beta(\mathbf{z})) U_{\mathbf{z}; x^-, -\infty} \\ &= \delta(x^-) \int d^2p_\perp e^{-i(k^-x^+ - \mathbf{p} \cdot \mathbf{x})} \int \frac{d^2z_\perp}{(2\pi)^2} e^{-i(\mathbf{p}-\mathbf{k}) \cdot \mathbf{z}} (\beta(\mathbf{x}) - \beta(\mathbf{z})) U_{\mathbf{z}; x^-, -\infty} \\ &= \delta(x^-) \int d^2z_\perp e^{-i(k^-x^+ - \mathbf{k} \cdot \mathbf{z})} \delta^{(2)}(\mathbf{x} - \mathbf{z}) (\beta(\mathbf{x}) - \beta(\mathbf{z})) U_{\mathbf{z}; x^-, -\infty} = 0. \end{aligned} \quad (\text{B.13})$$

Consequently, Eq. B.8 is indeed an eigenfunction of the differential operator $-D_x[b]^2$. To confirm the completeness relation, one uses

$$\begin{aligned} &\int dk^+ dk^- d^2p_\perp d^2q_\perp \exp \left[-i \left(\left(\frac{p_\perp^2 - k_\perp^2}{2k^-} \right) x^- - \left(\frac{q_\perp^2 - k_\perp^2}{2k^-} \right) y^- \right. \right. \\ &\quad \left. \left. + k^+(x^- - y^-) + k^-(x^+ - y^+) - \mathbf{p} \cdot \mathbf{x} + \mathbf{q} \cdot \mathbf{y} \right) \right] = 2\pi \delta(x^- - y^-) \int dk^- d^2p_\perp d^2q_\perp \\ &\quad \times \exp \left[-i \left(\left(\frac{p_\perp^2 - q_\perp^2}{2k^-} \right) x^- + k^-(x^+ - y^+) - \mathbf{p} \cdot \mathbf{x} + \mathbf{q} \cdot \mathbf{y} \right) \right], \end{aligned} \quad (\text{B.14})$$

to show that

$$\begin{aligned} &\int \frac{d^4k}{(2\pi)^4} \phi(x; k) \phi^\dagger(y; k) \\ &= \int \frac{d^4k}{(2\pi)^4} d^2p_\perp d^2q_\perp e^{-i(p \cdot x - q \cdot y)} \int \frac{d^2z_{1\perp}}{(2\pi)^2} \frac{d^2z_{2\perp}}{(2\pi)^2} e^{-i(\mathbf{p}-\mathbf{k}) \cdot \mathbf{z}_1} e^{i(\mathbf{q}-\mathbf{k}) \cdot \mathbf{z}_2} U_{\mathbf{z}_1; x^-, -\infty} U_{\mathbf{z}_2; y^-, -\infty}^\dagger \\ &= \delta(x^- - y^-) \delta^{(2)}(\mathbf{x} - \mathbf{y}) \int \frac{dk^-}{2\pi} \exp \left[-ik^-(x^+ - y^+) \right] = \delta^{(4)}(x - y). \end{aligned} \quad (\text{B.15})$$

Substituting Eq. B.8 into Eq. B.6, one obtains

$$\begin{aligned} \left[\frac{i}{-D[b]^2} \right] (x, y) &= \int \frac{d^4k}{(2\pi)^4} \frac{i}{k^2 + i\varepsilon} \int d^2p_\perp d^2q_\perp e^{-i(p \cdot x - q \cdot y)} \int \frac{d^2z_{1\perp}}{(2\pi)^2} \frac{d^2z_{2\perp}}{(2\pi)^2} \\ &\quad \times e^{-i(\mathbf{p}-\mathbf{k}) \cdot \mathbf{z}_1} e^{i(\mathbf{q}-\mathbf{k}) \cdot \mathbf{z}_2} U_{\mathbf{z}_1; x^-, -\infty} U_{\mathbf{z}_2; y^-, -\infty}^\dagger, \end{aligned} \quad (\text{B.16})$$

where

$$p^- = q^- = k^-, \quad p^+ = \frac{\mathbf{p}^2 + k^2}{2k^-}, \quad p^+ = \frac{\mathbf{q}^2 + k^2}{2k^-}. \quad (\text{B.17})$$

To simplify Eq. B.16, one evaluates the k^+ integral according to the Feynman prescription. With a pole located at $k^+ = \frac{k^2 - i\varepsilon}{2k^-}$, $e^{-ik^+(x^- - y^-)}$ has a vanishing contribution from the integral along the contour at infinity if and only if $k^- > 0$ and $x^- > y^-$, or $k^- < 0$ and $x^- < y^-$ which yields

$$\begin{aligned} \left[\frac{i}{-D[b]^2} \right] (x, y) &= \int \frac{dk^-}{(2\pi)^3 (2k^-)} [\theta(x^- - y^-) \theta(k^-) - \theta(y^- - x^-) \theta(-k^-)] \\ &\times \int d^2 p_\perp d^2 q_\perp e^{-i(p \cdot x - q \cdot y)} \int \frac{d^2 z_\perp}{(2\pi)^2} e^{-i(\mathbf{p} - \mathbf{q}) \cdot \mathbf{z}} U_{\mathbf{z}; x^-, y^-}, \end{aligned} \quad (\text{B.18})$$

where

$$p^- = q^- = k^-, \quad p^+ = \frac{\mathbf{p}^2}{2k^-}, \quad p^+ = \frac{\mathbf{q}^2}{2k^-}. \quad (\text{B.19})$$

One can repeat the above derivation for a massless scalar field. Adding a mass term of the form $\frac{1}{2}m^2|\phi(x)|^2$ to the Lagrangian in Eq. B.2 simply results in a modification of p^+ and p^- in Eq. B.19 to

$$p^- = q^- = k^-, \quad p^+ = \frac{\mathbf{p}^2 + m^2}{2k^-}, \quad p^+ = \frac{\mathbf{q}^2 + m^2}{2k^-}. \quad (\text{B.20})$$

B.2 The Quark Propagator

Consider a spinor $\psi : \mathbb{R}^{1,3} \rightarrow \mathbb{C}_{\text{spin}}^4 \otimes \mathbb{C}_{\text{colour}}^{N_c}; x \mapsto \psi(x) = \psi(x)_{ai} \hat{e}_a \otimes \hat{e}_i$ whose dynamics is governed by the Lagrangian

$$\mathcal{L}_{\text{Dirac}}[\psi, \bar{\psi}, b](x) := \bar{\psi}(x)(i\not{D}_x[b] - m)\psi(x) = \bar{\psi}(x)_{ai}(i\gamma_{ab}^\mu D_\mu^x[b]_{ij} - m\delta_{ab}\delta_{ij})\psi(x)_{bj}, \quad (\text{B.21})$$

where

$$D_\mu^x[b]_{ij} := (\partial_\mu^x - igb^\mu(x))_{ij} = \partial_\mu^x \delta_{ij} - igb^{a\mu}(x)t_{ij}^a. \quad (\text{B.22})$$

In order to compute the fermion propagator, examine

$$\begin{aligned}
\mathcal{D}_x[b]^2 &= \gamma^\mu \gamma^\nu D_\mu^x[b] D_\nu^x[b] \\
&= \frac{1}{2} \left(\{\gamma^\mu, \gamma^\nu\} + [\gamma^\mu, \gamma^\nu] \right) D_\mu^x[b] D_\nu^x[b] \\
&= (g^{\mu\nu} - i\sigma^{\mu\nu}) D_\mu^x[b] D_\nu^x[b] \\
&= D_x[b]^2 - i\sigma^{\mu\nu} [D_\mu^x[b], D_\nu^x[b]] \\
&= D_x[b]^2 - g\sigma^{\mu\nu} F_{\mu\nu}[b](x),
\end{aligned} \tag{B.23}$$

which means that

$$(i\mathcal{D}_x[b] - m)(i\mathcal{D}_x[b] + m) = -D_x[b]^2 + g\sigma^{\mu\nu} F_{\mu\nu}[b](x) - m^2. \tag{B.24}$$

The fermion propagator is defined as

$$\langle \bar{\psi}(x) \psi(y) \rangle [b] := (i\mathcal{D}_x[b] + m) \langle x | i[-D_x[b]^2 + g\sigma^{\mu\nu} F_{\mu\nu}[b](x) - m^2 + i\varepsilon]^{-1} | y \rangle. \tag{B.25}$$

The difference between Eq. B.6 and Eq. B.25, in terms of the content sandwiched between $\langle x | \cdots | y \rangle$ is the inclusion of the additional term $g\sigma^{\mu\nu} F_{\mu\nu}[b](x)$. After some thought, one can immediately write down the fermion propagator as

$$\begin{aligned}
\langle \bar{\psi}(x) \psi(y) \rangle [b] &= (i\mathcal{D}_x[b] + m) \int \frac{dk^-}{(2\pi)^3 (2k^-)} [\theta(x^- - y^-) \theta(k^-) - \theta(y^- - x^-) \theta(-k^-)] \\
&\times \int d^2 p_\perp d^2 q_\perp e^{-i(p \cdot x - q \cdot y)} \int \frac{dz_\perp^2}{(2\pi)^2} e^{-i(p - q) \cdot z} P \exp \left[ig \int_{y^-}^{x^-} dz^- \left(b^+ + \frac{\sigma^{\mu\nu} F_{\mu\nu}[b]}{2k^-} \right) (z) \right],
\end{aligned} \tag{B.26}$$

which can be constructed via the spectral method using the eigenfunctions in Eq. B.8 and suitably modifying the path-ordered exponentials. Note that the momenta are interrelated as in the previous section. Given the particular form of Eq. B.1, the field strength tensor has the form

$$F^{\mu\nu}[b](x) = \delta^{\mu i} \delta^{\nu +} \partial^i b^+(x), \tag{B.27}$$

which means that $\sigma^{\mu\nu} F_{\mu\nu}[b](x) = \sigma^{-i} F^{+i}[b](x)$ where $\sigma^{-i} = \frac{i}{2} [\gamma^-, \gamma^i]$. Using the defining anti-commutator relation for the Dirac matrices given in Eq. A.6, one can easily show that $(\gamma^-)^2 = 0$ and thus $\sigma^{-i} \sigma^{-j} = 0$. This last observation allows one to simplify² the path-ordered exponential

²Using the identity $\int_a^b dx \int_x^b dy f(x, y) = \int_a^b dy \int_a^y dx f(x, y)$ it is relatively straightforward to prove Eq. B.28.

in Eq. B.26

$$\begin{aligned}
P \exp \left[ig \int_{y^-}^{x^-} dz^- \left(b^+ + \frac{\sigma^{\mu\nu} F_{\mu\nu}[b]}{2k^-} \right) (z) \right] \\
= U_{z;x^-,y^-} + \frac{ig}{2k^-} \int_{y^-}^{x^-} dz^- U_{z;x^-,z^-} \sigma^{-i} F^{+i}[b](z) U_{z;z^-,y^-}.
\end{aligned} \tag{B.28}$$

One can show that the second term in Eq. B.28 does not contribute to the total cross-section for DIS. Consequently, the second term in Eq. B.28 can be omitted and the fermion propagator written as

$$\begin{aligned}
\langle \bar{\psi}(x) \psi(y) \rangle [b] &= (i \not{D}_x[b] + m) \int \frac{dk^-}{(2\pi)^3 (2k^-)} [\theta(x^- - y^-) \theta(k^-) - \theta(y^- - x^-) \theta(-k^-)] \\
&\quad \times \int d^2 p_\perp d^2 q_\perp e^{-i(p \cdot x - q \cdot y)} \int \frac{d^2 z_\perp}{(2\pi)^2} e^{-i(p-q) \cdot z} U_{z;x^-,y^-} \\
&= \int \frac{dk^-}{(2\pi)^3 (2k^-)} [\theta(x^- - y^-) \theta(k^-) - \theta(y^- - x^-) \theta(-k^-)] \int d^2 p_\perp d^2 q_\perp e^{-i(p \cdot x - q \cdot y)} (\not{p} + m) \\
&\quad \times \int \frac{d^2 z_\perp}{(2\pi)^2} e^{-i(p-q) \cdot z} U_{z;x^-,y^-} + \frac{1}{4} \gamma^- \delta(x^- - y^-) \delta^{(2)}(\mathbf{x} - \mathbf{y}) \text{sign}(x^+ - y^+),
\end{aligned} \tag{B.29}$$

where in going to the last line we used Eq. B.13 as well as the identity

$$\int_{-\infty}^{\infty} \frac{dk^-}{k^-} e^{-ik^-(x^+ - y^+)} = -i\pi \text{sign}(x^+ - y^+). \tag{B.30}$$

We shall represent the fermion propagator given in Eq. B.29 pictorially by

$$x \longleftarrow \textcircled{b} \longleftarrow y = \langle \bar{\psi}(x) \psi(y) \rangle [b]. \tag{B.31}$$

B.3 The Gluon Propagator

Following the procedure of Faddeev and Popov, the quantized QCD Lagrangian is given by

$$\begin{aligned}
\mathcal{L}_{QCD}[\psi, \bar{\psi}, c, \bar{c}, A](x) &:= \mathcal{L}_{YM}[A](x) + \mathcal{L}_{\text{Dirac}}[\psi, \bar{\psi}, A](x) + \mathcal{L}_{\text{ghost}}[c, \bar{c}, A](x) + \mathcal{L}_{\text{fix}}[A](x) \\
&= -\frac{1}{4} F_{\mu\nu}^a[A](x) F^{a\mu\nu}[A](x) + \bar{\psi}(x) (i \not{D}_x[A] - m) \psi(x) \\
&\quad + \partial_\mu^x \bar{c}^a(x) (\partial_x^\mu c^a(x) + g f^{abc} c^b(x) A^{c\mu}(x)) - \frac{1}{2\xi} (e_\mu A^{a\mu}(x)) (e_\nu A^{a\nu}(x)).
\end{aligned} \tag{B.32}$$

In order to obtain the gluon propagator in the presence of the shock-wave background b , one needs to expand $\mathcal{L}_{QCD}[\psi, \bar{\psi}, c, \bar{c}, b + \delta A]$ around b to quadratic order in the fluctuations δA . To

this end, recall

$$F_{\mu\nu}^a[A](x) = \partial_\mu^x A_\nu^a(x) - \partial_\nu^x A_\mu^a(x) + g f^{abc} A_\mu^b(x) A_\nu^c(x) \quad (\text{B.33})$$

which means that

$$\begin{aligned} F_{\mu\nu}^a[b + \delta A](x) &= F_{\mu\nu}^a[b](x) + (\partial_\mu^x \delta^{ac} + g b_\mu^b(x) f^{abc}) \delta A_\nu^c(x) - (\partial_\nu^x \delta^{ac} + g b_\nu^b(x) f^{abc}) \delta A_\mu^c(x) \\ &\quad + g f^{abc} \delta A_\mu^b(x) \delta A_\nu^c(x) \\ &= F_{\mu\nu}^a[b](x) + (D_\mu^x[b] \delta A_\nu(x))^a - (D_\nu^x[b] \delta A_\mu(x))^a + g f^{abc} \delta A_\mu^b(x) \delta A_\nu^c(x), \end{aligned} \quad (\text{B.34})$$

where the covariant derivative in the adjoint representation is defined as

$$D_\mu^x[b]^{ac} = \partial_\mu^x \delta^{ac} - i g b_\mu^b(x) [T^b]^{ac} = \partial_\mu^x \delta^{ac} + g b_\mu^b(x) f^{abc}. \quad (\text{B.35})$$

Using Eq. B.34, the term in $\mathcal{L}_{QCD}[\psi, \bar{\psi}, c, \bar{c}, b + \delta A]$ quadratic δA is

$$\begin{aligned} \mathcal{L}_{QCD}^{(2)}[\psi, \bar{\psi}, c, \bar{c}, b + \delta A](x) &= -\frac{1}{2} \left\{ g F_{\mu\nu}^a[b](x) f^{abc} \delta A^{b\mu}(x) \delta A^{c\nu}(x) - \frac{1}{\xi} (e_\mu A^{a\mu}(x)) (e_\nu A^{a\nu}(x)) \right. \\ &\quad \left. + (D_\mu^x[b] \delta A_\nu(x))^a (D_x^\mu[b] \delta A^\nu(x))^a - (D_\mu^x[b] \delta A_\nu(x))^a (D_x^\nu[b] \delta A^\mu(x))^a \right\}. \end{aligned} \quad (\text{B.36})$$

Examine

$$\begin{aligned} (D_\mu^x[b] \delta A_\nu(x))^a (D_x^\mu[b] \delta A^\nu(x))^a &= (\partial_\mu^x \delta^{ac} + g b_\mu^b(x) f^{abc}) \delta A_\nu^c(x) D_x^\mu[b]^{ab} \delta A^{b\nu}(x) \\ &= \delta A_\nu^c(x) (\partial_\mu^x \delta^{ac} - g b_\mu^b(x) f^{abc}) D_x^\mu[b]^{ab} \delta A^{b\nu}(x) \\ &= \delta A_\nu^c(x) (\partial_\mu^x \delta^{ac} + g b_\mu^b(x) f^{cba}) D_x^\mu[b]^{ab} \delta A^{b\nu}(x) = \delta A_\nu^c(x) (D_x[b]^2)^{cb} \delta A^{b\nu}(x), \end{aligned} \quad (\text{B.37})$$

where in the second line we dropped a total derivative term, and similarly³

$$\begin{aligned} (D_\mu^x[b] \delta A_\nu(x))^a (D_x^\nu[b] \delta A^\mu(x))^a &= -\delta A_\nu^c(x) (D_x^\mu[b] D_x^\nu[b])^{cb} \delta A_\mu^b(x) \\ &= -\delta A_\nu^c(x) (D_x^\nu[b] D_x^\mu[b])^{cb} \delta A_\mu^b(x) - g \delta A_\nu^c(x) F^{a\nu\mu}[b](x) f^{cba} \delta A_\mu^b(x), \end{aligned} \quad (\text{B.38})$$

where in the first line we dropped a total derivative term. Inserting Eq. B.37 and Eq. B.38 into Eq. B.36 yields

$$\begin{aligned} \mathcal{L}_{QCD}^{(2)}[\psi, \bar{\psi}, c, \bar{c}, b + \delta A](x) &= \frac{1}{2} \delta A_\mu^a(x) \left\{ \frac{1}{\xi} e^\mu e^\nu \delta^{ab} + (D_x[b]^2)^{ab} g^{\mu\nu} - (D_x^\mu[b] D_x^\nu[b])^{ab} \right. \\ &\quad \left. - 2g F^{c\mu\nu}[b](x) f^{cab} \right\} \delta A_\nu^b(x). \end{aligned} \quad (\text{B.39})$$

³Remember $[D_\mu^x[b], D_\mu^x[b]] = -ig F_{\mu\nu}[b](x)$.

Appendix C

The size of the Fierz-permutation basis

In this chapter, I show that the size of the Fierz-permutation basis for the colour space of $W^{\otimes m}$ (for $m \in \mathbb{N}^+$) is equal to $m!$. I proved this result together with Dr Stefan Keppeler from the University of Tübingen one evening during my attending the [QCD Master Class 2017](#).

Recall that the *Fierz-permutation basis* for the colour space of $W^{\otimes m}$ (for $m \in \mathbb{N}^+$), introduced in Sec. 4.3.2, is given by

$$\mathfrak{B}_{\text{Fierz-perm.}}(W^{\otimes m}) = \bigcup_{i=0}^m \bigcup_{\sigma \in S_{i, m-i}} \bigcup_{k=1}^{!i} \{ \sqrt{2^i} |1\rangle_{\sigma(1)} \otimes \cdots \otimes |1\rangle_{\sigma(m-i)} \otimes |t^{a_1}\rangle_{\sigma(m-i+1)} \otimes \cdots \otimes |t^{a_i}\rangle_{\sigma(m)} \mathcal{C}^{(i;k)a_1 \cdots a_i} \}, \quad (\text{C.1})$$

where, for $i = 2, \dots, m$

$$\mathfrak{B}_{\text{Tr.}}(A^{\otimes i}) = \{ \mathcal{C}^{(i;k)a_1 \cdots a_i} \}_{k=1}^{!i}, \quad (\text{C.2})$$

is the normalized *trace basis* for the colour space of $A^{\otimes i}$, introduced in Sec. 4.2.2. The subfactorial of i , denoted $!i$, which we use in Eq. C.1 and Eq. C.2, is given in Eq. 4.59 by

$$!i = i! \sum_{k=0}^i \frac{(-1)^k}{k!}. \quad (\text{C.3})$$

We want to calculate the number of elements in $\mathfrak{B}_{\text{Fierz-perm.}}(W^{\otimes m})$ and show that it is equal to $m!$. This must be the case since, for $m \leq N_c$, we know that there the colour space of $W^{\otimes m}$ is $m!$ -dimensional [34].

The size of $\mathfrak{B}_{\text{Fierz-perm.}}(W^{\otimes m})$ is calculated as

$$\begin{aligned} |\mathfrak{B}_{\text{Fierz-perm.}}(W^{\otimes m})| &\stackrel{\text{Eq. C.1}}{=} \sum_{i=0}^m |S_{i,m-1}|! i \stackrel{|S_{i,m-1}| = \binom{m}{i}}{=} \sum_{i=0}^m \binom{m}{i}! i \\ &\stackrel{\text{Eq. C.3}}{=} \sum_{i=0}^m \frac{m!}{i!(m-i)!} i! \sum_{k=0}^i \frac{(-1)^k}{k!} = m! \sum_{i=0}^m \frac{1}{(m-i)!} \sum_{k=0}^i \frac{(-1)^k}{k!}, \end{aligned} \quad (\text{C.4})$$

where the first equality follows from Eq. C.1, in the second equality $\binom{m}{i}$ gives the size of the set of $(i, m-i)$ shuffles, in the third equality we expressed $\binom{m}{i}$ as $\frac{m!}{i!(m-i)!}$ as well as used Eq. C.3, and in the last equality we canceled the factors of $i!$ and factored $m!$ out front. To show that Eq. C.4 is equal to $m!$, we need to show that

$$\sum_{i=0}^m \frac{1}{(m-i)!} \sum_{k=0}^i \frac{(-1)^k}{k!} = 1, \quad (\text{C.5})$$

which we shall do by induction. For $m = 1$,

$$\text{LHS}(\text{C.5})_{m=1} = \frac{1}{1!} \frac{(-1)^0}{0!} + \frac{1}{0!} \left(\frac{(-1)^0}{0!} + \frac{(-1)^1}{1!} \right) = 1 = \text{RHS}(\text{C.5})_{m=1}. \quad (\text{C.6})$$

Suppose Eq. C.5 is true for some $m = n \in \mathbb{N}^+$. For $m = n + 1$

$$\begin{aligned} \text{LHS}(\text{C.5})_{m=n+1} &= \sum_{i=0}^{n+1} \frac{1}{(n+1-i)!} \sum_{k=0}^i \frac{(-1)^k}{k!} = \sum_{i=-1}^n \frac{1}{(n-i)!} \sum_{k=0}^{i+1} \frac{(-1)^k}{k!} \\ &= \frac{1}{(n+1)!} + \sum_{i=0}^n \frac{(-1)^{i+1}}{(n-i)!(i+1)!} + \underbrace{\sum_{i=0}^n \frac{1}{(n-i)!} \sum_{k=0}^i \frac{(-1)^k}{k!}}_{=1(\text{induction hypothesis})} \\ &= 1 + \frac{1}{(n+1)!} + \frac{1}{(n+1)!} \sum_{i=0}^n (-1)^{i+1} \binom{n+1}{i+1} \\ &= 1 + \frac{1}{(n+1)!} + \frac{1}{(n+1)!} \sum_{i=1}^{n+1} (-1)^i \binom{n+1}{i} \\ &= 1 + \frac{1}{(n+1)!} \sum_{i=0}^{n+1} (-1)^i \binom{n+1}{i} \\ &= 1 + \frac{1}{(n+1)!} (1-1)^{n+1} = 1 = \text{RHS}(\text{C.5})_{m=n+1}. \end{aligned} \quad (\text{C.7})$$

Therefore, by induction, Eq. C.5 is true for all $m \in \mathbb{N}^+$ and

$$|\mathfrak{B}_{\text{Fierz-perm.}}(W^{\otimes m})| = m!. \quad (\text{C.8})$$

Bibliography

- [1] M. D. Schwartz, *Quantum field theory and the standard model*. Cambridge University Press, 2014.
- [2] **Particle Data Group** Collaboration, C. Patrignani *et al.*, “Review of Particle Physics,” *Chin. Phys.* **C40** no. 10, (2016) 100001.
- [3] R. Placakyte, “Parton Distribution Functions,” in *Proceedings, 31st International Conference on Physics in collisions (PIC 2011): Vancouver, Canada, August 28-September 1, 2011*. 2011. [arXiv:1111.5452 \[hep-ph\]](#).
<https://inspirehep.net/record/954990/files/arXiv:1111.5452.pdf>.
- [4] F. Gelis, E. Iancu, J. Jalilian-Marian, and R. Venugopalan, “The Color Glass Condensate,” *Ann. Rev. Nucl. Part. Sci.* **60** (2010) 463–489, [arXiv:1002.0333 \[hep-ph\]](#).
- [5] H. Fritzsch, M. Gell-Mann, and H. Leutwyler, “Advantages of the Color Octet Gluon Picture,” *Phys. Lett.* **47B** (1973) 365–368.
- [6] M. Peskin and D. Schroeder, “An introduction to quantum field theory,”
- [7] C. D. White, “An Introduction to Webs,” *J. Phys.* **G43** no. 3, (2016) 033002, [arXiv:1507.02167 \[hep-ph\]](#).
- [8] M. Froissart, “Asymptotic behavior and subtractions in the Mandelstam representation,” *Phys. Rev.* **123** (1961) 1053–1057.
- [9] H. Weigert, “Evolution at small $x(bj)$: The Color glass condensate,” *Prog. Part. Nucl. Phys.* **55** (2005) 461–565, [arXiv:hep-ph/0501087 \[hep-ph\]](#).
- [10] E. Iancu, A. Leonidov, and L. D. McLerran, “Nonlinear gluon evolution in the color glass condensate. 1.,” *Nucl. Phys.* **A692** (2001) 583–645, [arXiv:hep-ph/0011241 \[hep-ph\]](#).
- [11] T. J. Hobbs, *The Nonperturbative Structure of Hadrons*. PhD thesis, Indiana U., 2014-08. [arXiv:1408.5463 \[hep-ph\]](#).
<http://inspirehep.net/record/1312182/files/arXiv:1408.5463.pdf>.

- [12] A. Bacchetta, “Probing the transverse spin of quarks in deep inelastic scattering,” *arXiv preprint hep-ph/0212025* (2002) .
- [13] V. Barone, “An introduction to the transverse structure of hadrons,”
www.fe.infn.it/cabeo_school/2010/cabeo_school_2010.pdf.
- [14] I. O. Cherednikov, T. Mertens, and F. F. Van der Veken, *Wilson lines in quantum field theory*, vol. 24. Walter de Gruyter GmbH & Co KG, 2014.
- [15] R. Rivers, *Path integral methods in quantum field theory*. Cambridge University Press, 1988.
- [16] D. Bailin and A. Love, *Introduction to Gauge Field Theory Revised Edition*. CRC Press, 1993.
- [17] H. Weigert. in conversation.
- [18] M. Hentschinski, *Exclusive methods in QCD at high energies*. PhD thesis, University of Regensburg, 2015.
- [19] C. Marquet and H. Weigert, “New observables to test the Color Glass Condensate beyond the large- N_c limit,” *Nucl. Phys.* **A843** (2010) 68–97, [arXiv:1003.0813](https://arxiv.org/abs/1003.0813) [hep-ph].
- [20] T. Lappi, “Gluon spectrum in the glasma from JIMWLK evolution,” *Phys. Lett.* **B703** (2011) 325–330, [arXiv:1105.5511](https://arxiv.org/abs/1105.5511) [hep-ph].
- [21] G. Sterman, *An introduction to quantum field theory*. Cambridge University Press, 1993.
- [22] J. D. Bjorken and S. D. Drell, “Relativistic quantum mechanics,”.
- [23] R. P. Feynman, “Very high-energy collisions of hadrons,” *Phys. Rev. Lett.* **23** (1969) 1415–1417.
- [24] R. P. Feynman, “The behavior of hadron collisions at extreme energies,” *Conf. Proc.* **C690905** (1969) 237–258.
- [25] **CTEQ** Collaboration, R. Brock *et al.*, “Handbook of perturbative QCD: Version 1.0,” *Rev. Mod. Phys.* **67** (1995) 157–248.
- [26] Florence HEP, “Collider Physics - M. Peskin - lecture 3/6.”
https://youtu.be/qVew5SN_FEE.
- [27] H. Haber, “Polarization sum for massless spin-one particles.”
scipp.ucsc.edu/~haber/ph218/polsum.pdf, 2016. Accessed: 2018-01-18.
- [28] G. Soyez, “The DGLAP Evolution Equation.”
www.lpthe.jussieu.fr/~soyez/data/gsoyez_master.ps.gz.

- [29] M. Mézard, G. Parisi, and M. Virasoro, *Spin glass theory and beyond: An Introduction to the Replica Method and Its Applications*, vol. 9. World Scientific Publishing Co Inc, 1987.
- [30] F. Dominguez, C. Marquet, B.-W. Xiao, and F. Yuan, “Universality of Unintegrated Gluon Distributions at small x ,” *Phys. Rev.* **D83** (2011) 105005, [arXiv:1101.0715 \[hep-ph\]](#).
- [31] S. Munier, S. Peigné, and E. Petreska, “Medium-induced gluon radiation in hard forward parton scattering in the saturation formalism,” *Phys. Rev.* **D95** no. 1, (2017) 014014, [arXiv:1603.01028 \[hep-ph\]](#).
- [32] T. Lappi, A. Ramnath, K. Rummukainen, and H. Weigert, “JIMWLK evolution of the odderon,” [arXiv:1606.00551 \[hep-ph\]](#).
- [33] P. Cvitanovic, *Group theory: Birdtracks, Lie’s and exceptional groups*. 2008. <http://press.princeton.edu/titles/8839.html>.
- [34] J. Alcock-Zeilinger and H. Weigert, “Singlets.” in preparation.
- [35] S. Keppeler and M. Sjödal, “Orthogonal multiplet bases in $SU(N_c)$ color space,” *JHEP* **09** (2012) 124, [arXiv:1207.0609 \[hep-ph\]](#).
- [36] I. Goulden and D. Jackson, “Combinatorial enumeration, a wiley-interscience series in discrete mathematics,” 1983.
- [37] R. L. Graham, *Handbook of combinatorics*, vol. 1. Elsevier, 1995.
- [38] J. Rayner, “Reps for JIMWLK: Applications of representation theory to a novel approach to the JIMWLK equation.” 2017.
- [39] J. Alcock-Zeilinger and H. Weigert, “Compact Hermitian Young Projection Operators,” [arXiv:1610.10088 \[math-ph\]](#).
- [40] J. Alcock-Zeilinger and H. Weigert, “Transition Operators,” [arXiv:1610.08802 \[math-ph\]](#).
- [41] J. Rayner. in conversation.
- [42] H. Weigert, “Unitarity at small Bjorken x ,” *Nucl. Phys.* **A703** (2002) 823–860, [arXiv:hep-ph/0004044 \[hep-ph\]](#).
- [43] A. Kovner, M. Lublinsky, and Y. Mulian, “Jalilian-Marian, Iancu, McLerran, Weigert, Leonidov, Kovner evolution at next to leading order,” *Phys. Rev.* **D89** no. 6, (2014) 061704, [arXiv:1310.0378 \[hep-ph\]](#).
- [44] A. Kovner, M. Lublinsky, and Y. Mulian, “NLO JIMWLK evolution unabridged,” *JHEP* **08** (2014) 114, [arXiv:1405.0418 \[hep-ph\]](#).

- [45] S. Caron-Huot, “Resummation of non-global logarithms and the BFKL equation,” [arXiv:1501.03754 \[hep-ph\]](#).
- [46] A. H. Mueller, “On the Asymptotic Behavior of the Sudakov Form-factor,” *Phys. Rev.* **D20** (1979) 2037.
- [47] J. C. Collins, “Algorithm to Compute Corrections to the Sudakov Form-factor,” *Phys. Rev.* **D22** (1980) 1478.
- [48] A. Sen, “Asymptotic Behavior of the Sudakov Form-Factor in QCD,” *Phys. Rev.* **D24** (1981) 3281.
- [49] G. P. Korchemsky, “Double Logarithmic Asymptotics in QCD,” *Phys. Lett.* **B217** (1989) 330–334.
- [50] J. C. Collins, “Sudakov form-factors,” *Adv. Ser. Direct. High Energy Phys.* **5** (1989) 573–614, [arXiv:hep-ph/0312336 \[hep-ph\]](#).
- [51] L. Magnea and G. F. Sterman, “Analytic continuation of the Sudakov form-factor in QCD,” *Phys. Rev.* **D42** (1990) 4222–4227.
- [52] L. J. Dixon, L. Magnea, and G. F. Sterman, “Universal structure of subleading infrared poles in gauge theory amplitudes,” *JHEP* **08** (2008) 022, [arXiv:0805.3515 \[hep-ph\]](#).
- [53] L. J. Dixon, “Scattering amplitudes: the most perfect microscopic structures in the universe,” *J. Phys.* **A44** (2011) 454001, [arXiv:1105.0771 \[hep-th\]](#).
- [54] G. F. Sterman, “Partons, factorization and resummation, TASI 95,” in *QCD and beyond. Proceedings, Theoretical Advanced Study Institute in Elementary Particle Physics, TASI-95, Boulder, USA, June 4-30, 1995*, pp. 327–408. 1995. [arXiv:hep-ph/9606312 \[hep-ph\]](#).
- [55] G. Falcioni, E. Gardi, M. Harley, L. Magnea, and C. D. White, “Multiple Gluon Exchange Webs,” *JHEP* **10** (2014) 10, [arXiv:1407.3477 \[hep-ph\]](#).
- [56] A. M. Polyakov, “Gauge Fields as Rings of Glue,” *Nucl. Phys.* **B164** (1980) 171–188.
- [57] I. Ya. Arefeva, “QUANTUM CONTOUR FIELD EQUATIONS,” *Phys. Lett.* **93B** (1980) 347–353.
- [58] V. S. Dotsenko and S. N. Vergeles, “Renormalizability of Phase Factors in the Nonabelian Gauge Theory,” *Nucl. Phys.* **B169** (1980) 527–546.
- [59] R. A. Brandt, F. Neri, and M.-a. Sato, “Renormalization of Loop Functions for All Loops,” *Phys. Rev.* **D24** (1981) 879.

-
- [60] E. Gardi, J. M. Smillie, and C. D. White, “On the renormalization of multiparton webs,” *JHEP* **09** (2011) 114, [arXiv:1108.1357 \[hep-ph\]](#).
- [61] S. Blanes, F. Casas, J. Oteo, and J. Ros, “The magnus expansion and some of its applications,” *Physics Reports* **470** no. 5, (2009) 151–238, [arXiv:0810.5488 \[math-ph\]](#).

Turnitin Report

ORIGINALITY REPORT

8%

SIMILARITY INDEX

6%

INTERNET SOURCES

5%

PUBLICATIONS

2%

STUDENT PAPERS

PRIMARY SOURCES

1

www.wawparts.com

Internet Source

<1%

2

core.ac.uk

Internet Source

<1%

3

Weigert, H.. "Evolution at small x"^bj: The color glass condensate", Progress in Particle and Nuclear Physics, 200510

Publication

<1%

4

archiv.ub.uni-heidelberg.de

Internet Source

<1%

5

Submitted to University of Cape Town

Student Paper

<1%

6

arxiv.org

Internet Source

<1%

7

White, C D. "An introduction to webs", Journal of Physics G Nuclear and Particle Physics, 2016.

Publication

<1%

www.nikhef.nl

8	Internet Source	<1 %
9	pure.uva.nl Internet Source	<1 %
10	archive.org Internet Source	<1 %
11	www.hep.man.ac.uk Internet Source	<1 %
12	esc.fnwi.uva.nl Internet Source	<1 %
13	www.bighamster.co.uk Internet Source	<1 %
14	www.archive.org Internet Source	<1 %
15	Belitsky, A.V.. "Unraveling hadron structure with generalized parton distributions", Physics Reports, 200510 Publication	<1 %
16	Balitsky, I., and A. Tarasov. "Rapidity evolution of gluon TMD from low to moderate x", Journal of High Energy Physics, 2015. Publication	<1 %
17	lambda.gsfc.nasa.gov Internet Source	<1 %

18	repository.kulib.kyoto-u.ac.jp Internet Source	<1 %
19	Grahl, Martin. "The O(N=2) model in polar coordinates at nonzero temperature", Publikationsserver der Goethe-Universität Frankfurt am Main, 2011. Publication	<1 %
20	docslide.us Internet Source	<1 %
21	Iancu, E., and D.N. Triantafyllopoulos. "JIMWLK evolution for multi-particle production in Langevin form", Journal of High Energy Physics, 2013. Publication	<1 %
22	www.sachverstaendigenrat-wirtschaft.de Internet Source	<1 %
23	pos.sissa.it Internet Source	<1 %
24	www.research-collection.ethz.ch Internet Source	<1 %
25	open.uct.ac.za Internet Source	<1 %
26	Gelis, F.. "How particles emerge from decaying classical fields in heavy ion collisions: Towards a kinetic description of the Glasma", Nuclear	<1 %

Physics, Section A, 20090201

Publication

27	Jalilian-Marian, J.. "Saturation physics and deuteron-gold collisions at RHIC", Progress in Particle and Nuclear Physics, 200601 Publication	<1 %
28	Weidemann, Christian. "Preparations for the Spin-Filtering Experiments at COSY/Jülich", Kölner UniversitätsPublikationsServer, 2012. Publication	<1 %
29	qmro.qmul.ac.uk Internet Source	<1 %
30	ipht.cea.fr Internet Source	<1 %
31	Radim Bělohlávek. "Algebras with Fuzzy Equalities", Studies in Fuzziness and Soft Computing, 2005 Publication	<1 %
32	dare.ubvu.vu.nl Internet Source	<1 %
33	www.canoe-england.org.uk Internet Source	<1 %
34	www.nature-ic.am Internet Source	<1 %
35	utdallas.edu Internet Source	

		<1 %
36	edoc.hu-berlin.de Internet Source	<1 %
37	Vittorio Duca. "The infrared structure of gauge theory amplitudes in the high-energy limit", Journal of High Energy Physics, 12/2011 Publication	<1 %
38	pub.uni-bielefeld.de Internet Source	<1 %
39	Grabovsky, A. V.. "On the low-x NLO evolution of 4 point colorless operators", Journal of High Energy Physics, 2015. Publication	<1 %
40	www-pdg.lbl.gov Internet Source	<1 %
41	Lecture Notes in Physics, 2015. Publication	<1 %
42	www-pnp.physics.ox.ac.uk Internet Source	<1 %
43	Caron-Huot, Simon. "When does the gluon reggeize?", Journal of High Energy Physics, 2015. Publication	<1 %
publications.ub.uni-mainz.de		

44	Internet Source	<1 %
45	www.iexp.uni-hamburg.de Internet Source	<1 %
46	eprints.gla.ac.uk Internet Source	<1 %
47	dpnc.unige.ch Internet Source	<1 %
48	Dirk Graudenz. "Heavy-Quark Production in the Target Fragmentation Region", Fortschritte der Physik/Progress of Physics, 1997 Publication	<1 %
49	Lautemann, Sven-Eric. "Schemaevolution in objektorientierten Datenbanksystemen auf der Basis von Versionierungskonzepten", Publikationsserver der Goethe-Universität Frankfurt am Main, 2003. Publication	<1 %
50	www.thep.physik.uni-mainz.de Internet Source	<1 %
51	skladowanie.pgi.gov.pl Internet Source	<1 %
52	www.rmu.edu Internet Source	<1 %

Lohmayer, Robert. "Eigenvalue distributions of

53	Wilson loops", Publikationsserver der Universität Regensburg, 2010. Publication	<1 %
54	tel.archives-ouvertes.fr Internet Source	<1 %
55	Weigert, H.. "Non-global jet evolution at finite N ^c ", Nuclear Physics, Section B, 20040503 Publication	<1 %
56	www.wheel.gr.jp Internet Source	<1 %
57	opus.bibliothek.uni-wuerzburg.de Internet Source	<1 %
58	int12.itp.phys.ethz.ch Internet Source	<1 %
59	home.thep.lu.se Internet Source	<1 %
60	Submitted to King's College Student Paper	<1 %
61	www.imsc.res.in Internet Source	<1 %
62	Marquet, C.. "New observables to test the Color Glass Condensate beyond the large-N ^c limit", Nuclear Physics, Section A, 20101030 Publication	<1 %

63	Kovchegov, Yu.V.. "Triumvirate of running couplings in small-x evolution", Nuclear Physics, Section A, 20070301 Publication	<1 %
64	helda.helsinki.fi Internet Source	<1 %
65	hal.archives-ouvertes.fr Internet Source	<1 %
66	Del Duca, Vittorio, Giulio Falcioni, Lorenzo Magnea, and Leonardo Vernazza. "Analyzing high-energy factorization beyond next-to-leading logarithmic accuracy", Journal of High Energy Physics, 2015. Publication	<1 %
67	Lu, Shaojun(II. Physikalisches Institut). "Measurement of the strange quark contribution to the proton spin using neutral kaons at HERMES", Justus-Liebig-Universität Gießen, 2007. Publication	<1 %
68	cbbp.thep.lu.se Internet Source	<1 %
69	jyx.jyu.fi Internet Source	<1 %
70	Submitted to University of Durham Student Paper	<1 %

71	Kuokkanen, J.. "HERA-data in the light of small x evolution with state of the art NLO input", Nuclear Physics, Section A, 20120201 Publication	<1 %
72	matematicas.uniandes.edu.co Internet Source	<1 %
73	Gutzwiller, Simone. "Scattering phase shift for elastic two pion scattering and the rho resonance in lattice QCD", Publikationsserver der Universität Regensburg, 2012. Publication	<1 %
74	Submitted to The University of Manchester Student Paper	<1 %
75	Iancu, E., and J. Laidet. "Gluon splitting in a shockwave", Nuclear Physics A, 2013. Publication	<1 %
76	hal.in2p3.fr Internet Source	<1 %
77	Kovchegov, Yuri V., Daniel Pitonyak, and Matthew D. Sievert. "Helicity evolution at small x", Journal of High Energy Physics, 2016. Publication	<1 %
78	Alday, L.F.. "Scattering amplitudes, Wilson loops and the string/gauge theory correspondence", Physics Reports, 200811 Publication	<1 %

79	Winter, Frank. "Investigation of hadron matter using lattice QCD and implementation of lattice QCD applications on heterogeneous multicore acceleration processors", Publikationsserver der Universität Regensburg, 2012. Publication	<1 %
80	theses.gla.ac.uk Internet Source	<1 %
81	www.ideals.illinois.edu Internet Source	<1 %
82	Oxburgh, S., and C. D. White. "BCJ duality and the double copy in the soft limit", Journal of High Energy Physics, 2013. Publication	<1 %
83	th.physik.uni-frankfurt.de Internet Source	<1 %
84	Krattenthaler, C.. "Advanced determinant calculus: A complement", Linear Algebra and its Applications, 2005. Publication	<1 %
85	modular.math.washington.edu Internet Source	<1 %
86	www.ba.infn.it Internet Source	<1 %
87	inspirehep.net	

	Internet Source	<1 %
88	hal-cea.archives-ouvertes.fr Internet Source	<1 %
89	Submitted to Imperial College of Science, Technology and Medicine Student Paper	<1 %
90	bristol.ac.uk Internet Source	<1 %
91	Einan Gardi. "General properties of multiparton webs: proofs from combinatorics", Journal of High Energy Physics, 03/2011 Publication	<1 %
92	repositorio.uam.es Internet Source	<1 %
93	resources.aims.ac.za Internet Source	<1 %
94	Aicher, Matthias. "Threshold resummation effects on the parton distribution function of the pion and time-reversal-odd single-spin asymmetries", Publikationsserver der Universität Regensburg, 2011. Publication	<1 %
95	www.signal.uu.se Internet Source	<1 %

96	Huber, Max. "Radiative corrections to the neutral-current Drell-Yan process", Universität Freiburg, 2010. Publication	<1 %
97	svmo.mrsu.ru Internet Source	<1 %
98	Wang, Liang Wang, Yu Li, Yan. "Mining experiential patterns from game-logs of board game.(Research Article)(Report)", International Journal of Computer Games , Annual 2015 Issue Publication	<1 %
99	www.snge.co.jp Internet Source	<1 %
100	Böhme, Thomas. "Investigations of Microstructural Changes in Lead-Free Solder Alloys by Means of Phase Field Theories", Technische Universität Berlin, 2008. Publication	<1 %
101	www.ece.umd.edu Internet Source	<1 %
102	Submitted to University of Edinburgh Student Paper	<1 %
103	mgbsmadeinaustralia.org Internet Source	<1 %

104	Submitted to Middle East Technical University Student Paper	<1 %
105	www-irma.u-strasbg.fr Internet Source	<1 %
106	transborder.bts.gov Internet Source	<1 %
107	pubman.mpg.de Internet Source	<1 %
108	www3.nd.edu Internet Source	<1 %
109	Submitted to Universiteit van Amsterdam Student Paper	<1 %
110	Submitted to KTH - The Royal Institute of Technology Student Paper	<1 %
111	es.slideshare.net Internet Source	<1 %
112	Submitted to Higher Education Commission Pakistan Student Paper	<1 %
113	Herrmann, Florian. "Development and verification of a high performance electronic readout framework for high energy physics", Universität Freiburg, 2011. Publication	<1 %

114	euclid.trentu.ca Internet Source	<1 %
115	Ye, Jane J.. "Necessary optimality conditions for multiobjective bilevel programs.(Formula (Report))", Mathematics of Operations Research, Feb 2011 Issue Publication	<1 %
116	Drummond, J.M.. "Hexagon Wilson loop = six-gluon MHV amplitude", Nuclear Physics, Section B, 20090701 Publication	<1 %
117	Submitted to University of Newcastle upon Tyne Student Paper	<1 %
118	hans.math.upenn.edu Internet Source	<1 %
119	souravsengupta.com Internet Source	<1 %
120	www.scribd.com Internet Source	<1 %
121	aos.acornserver.com Internet Source	<1 %
122	Dinter, Simon(Göckeler, Meinulf, Jansen, Karl and Müller-Preußker, Michael). "Nucleon structure from lattice QCD", Mathematisch-	<1 %

Naturwissenschaftliche Fakultät I, 2012.

Publication

123	Schmidt, Thomas. "A Common Readout Driver for the COMPASS Experiment", Universität Freiburg, 2002. Publication	<1 %
124	www.hep.fsu.edu Internet Source	<1 %
125	ethesys.nuk.edu.tw Internet Source	<1 %
126	www.weizmann.ac.il Internet Source	<1 %
127	whisper.cse.ucsc.edu Internet Source	<1 %
128	Liu, Hong. "Optimal Consumption and Investment with Transaction Costs and Multiple Risky Assets", The Journal of Finance, 2004. Publication	<1 %
129	pefmath.etf.rs Internet Source	<1 %
130	pds1.egloos.com Internet Source	<1 %
131	Brandt, Bastian Benjamin. "Chiral properties of two-flavour QCD at zero and non-zero temperature", 08: Physik, Mathematik und	<1 %

Informatik. 08: Physik, Mathematik und
Informatik, 2012.

Publication

-
- | | | |
|------------|---|----------------|
| 132 | Kubocz, Michael. "Higgs production via gluon fusion in association with two or three jets in supersymmetric models", Universität Karlsruhe, 2009.
<small>Publication</small> | <1 % |
|------------|---|----------------|
-
- | | | |
|------------|---|----------------|
| 133 | www.orica.co.nz
<small>Internet Source</small> | <1 % |
|------------|---|----------------|
-
- | | | |
|------------|--|----------------|
| 134 | R. Rennie. "Geometry and topology of chiral anomalies in gauge theories", Advances In Physics, 11/1/1990
<small>Publication</small> | <1 % |
|------------|--|----------------|
-
- | | | |
|------------|--|----------------|
| 135 | www.lohnt-nicht.de
<small>Internet Source</small> | <1 % |
|------------|--|----------------|
-
- | | | |
|------------|--|----------------|
| 136 | phobos.physics.uiowa.edu
<small>Internet Source</small> | <1 % |
|------------|--|----------------|
-
- | | | |
|------------|---|----------------|
| 137 | www.ssnd.info
<small>Internet Source</small> | <1 % |
|------------|---|----------------|
-
- | | | |
|------------|--|----------------|
| 138 | Einan Gardi. "On the renormalization of multiparton webs", Journal of High Energy Physics, 09/2011
<small>Publication</small> | <1 % |
|------------|--|----------------|
-
- | | | |
|------------|---|----------------|
| 139 | E. Iancu. "Higher-point correlations from the JIMWLK evolution", Journal of High Energy | <1 % |
|------------|---|----------------|
-
- 195

Physics, 11/2011

Publication

140	E. Iancu. "JIMWLK evolution in the Gaussian approximation", Journal of High Energy Physics, 04/2012	<1 %
-----	---	------

Publication

141	Zvyagin, V.G. Ratiner, N.M.. "Oriented degree of Fredholm maps: finite-dimensional reduction method.(p. 543-590)", Journal of Mathematical Sciences, Feb 1 2015 Issue	<1 %
-----	---	------

Publication

142	contact.ics.uci.edu	<1 %
-----	---------------------	------

Internet Source

143	Krylov, P.A. Tuganbaev, A.A.. "Formal matrices and their determinants.", Journal of Mathematical Sciences, Dec 1 2015 Issue	<1 %
-----	---	------

Publication

144	dspace-unipr.cineca.it	<1 %
-----	------------------------	------

Internet Source

145	Schaefer, Stefan. "Chiral symmetry and hadronic measurements on the lattice", Publikationsserver der Universität Regensburg, 2003.	<1 %
-----	--	------

Publication

146	www.bloomfield.lib.in.us	<1 %
-----	--------------------------	------

Internet Source

147	www.wittenberg.edu Internet Source	<1 %
148	Uhlemann, Christoph Frank. "Holographic Description of Curved-Space Quantum Field Theory and Gravity", Universität Würzburg, 2013. Publication	<1 %
149	www.slideshare.net Internet Source	<1 %
150	www.hitachi-koki.com Internet Source	<1 %
151	Dunkel, Jörn. "Relativistic Brownian Motion and Diffusion Processes", University of Augsburg, GERMANY, OPUS, 2008. Publication	<1 %
152	cp3.phys.ucl.ac.be Internet Source	<1 %
153	www-a10.sjsu.edu Internet Source	<1 %
154	zippy.physics.niu.edu Internet Source	<1 %
155	insubriaspace.cineca.it Internet Source	<1 %
156	www.strings.ph.qmul.ac.uk Internet Source	<1 %

157	www-library.desy.de Internet Source	<1 %
158	Hedicke, Sonja. "Determination of the gluon polarisation in the nucleon using hadron pairs with high transverse momentum at COMPASS", Universität Freiburg, 2007. Publication	<1 %
159	ubm.opus.hbz-nrw.de Internet Source	<1 %
160	www-ttp.particle.uni-karlsruhe.de Internet Source	<1 %
161	Bindi, Marcello <1981>(Basile, prof. Maurizio). "Measurement of the charm production cross section in DIS events at HERA", Alma Mater Studiorum - Università di Bologna, 2011. Publication	<1 %
162	Kovchegov, Yuri V., and Douglas E. Wertheppny. "Long-range rapidity correlations in heavy-light ion collisions", Nuclear Physics A, 2013. Publication	<1 %
163	martin-ellis.net Internet Source	<1 %
164	authors.library.caltech.edu Internet Source	<1 %

Ternick, Marko. "Efficient calculation of gluon

165 amplitudes with n legs and an implementation of parton showers using the dipole formalism", 08: Physik, Mathematik und Informatik. 08: Physik, Mathematik und Informatik, 2011. <1 %
Publication

166 DOVIER, AGOSTINO, ENRICO PONTELLI, and GIANFRANCO ROSSI. "Set unification", Theory and Practice of Logic Programming, 2006. <1 %
Publication

167 Bähr, Manuel. "Underlying Event Simulation in the Herwig++ Event Generator", Universität Karlsruhe, 2008. <1 %
Publication

168 Scherer Daniel David(Bartosch, Lorenz, Fischer, Christian and Gies, Holger). "Low-dimensional chiral physics : gross-neveu universality and magnetic catalysis", Digitale Bibliothek Thüringen, 2012. <1 %
Publication

169 Kießlich, Gerold. "Nonlinear transport properties of quantum dot systems", Technische Universität Berlin, 2005. <1 %
Publication

170 Gardi, Einan. "From webs to polylogarithms", Journal of High Energy Physics, 2014. <1 %
Publication

Einan Gardi. "Webs in multiparton scattering

171 using the replica trick", Journal of High Energy Physics, 11/2010 **<1 %**
Publication

172 Yakov Berkovich, Zvonimir Janko. "§95 Nonabelian 2-groups of exponent 2e which have no minimal nonabelian subgroups of exponent 2e", Walter de Gruyter GmbH, 2011 **<1 %**
Publication

173 DJELLOUL, KHALIL, THI-BICH-HANH DAO, and THOM FRÜHWIRTH. "Theory of finite or infinite trees revisited", Theory and Practice of Logic Programming, 2008. **<1 %**
Publication

174 Gaigalas, Gediminas, Tomas alandauskas, and Zenonas Rudzikas. "LSjj transformation matrices for a shell of equivalent electrons", Atomic Data and Nuclear Data Tables, 2003. **<1 %**
Publication

175 Oellers, Dieter Gerd Christian. "Polarizing a Stored Proton Beam by Spin-Flip?", Kölner UniversitätsPublikationsServer, 2011. **<1 %**
Publication

176 Kang, Donghee. "Longitudinal lambda and anti-lambda polarization at the COMPASS experiment", Universität Freiburg, 2007. **<1 %**
Publication

Aouane, Rafik(Fischer, Christian, Ilgenfritz,

177 Ernst-Michael and Müller-Preußker, Michael). $<1\%$
"Gluon and ghost propagator studies in lattice
QCD at finite temperature", Mathematisch-
Naturwissenschaftliche Fakultät I, 2013.
Publication

178 Hristova, Ivana(Kolanoski, Hermann, Kowalski, $<1\%$
Marek and Ryckbosch, Dirk). "Transverse-
target single-spin azimuthal asymmetry in hard
exclusive electroproduction of single pions at
HERMES", Mathematisch-
Naturwissenschaftliche Fakultät I, 2008.
Publication

179 Wollny, Heiner. "Measuring azimuthal $<1\%$
asymmetries in semi-inclusive deep-inelastic
scattering off transversely polarized protons",
Universität Freiburg, 2010.
Publication

Exclude quotes On
Exclude bibliography On

Exclude matches Off

Signed